AN INVESTIGATION OF GLIAL CELL SIGNALLING IN THE RAT CEREBELLUM.

BY

RACHEL ELIZABETH ANNE CURRAN

A THESIS SUMITTED FOR THE DEGREE OF DOCTOR OF PHILOSOPHY IN THE UNIVERSITY OF LONDON.

SUPERVISOR DR. DAVID OGDEN

DIVISION OF NEUROPHYSIOLOGY

NATIONAL INSTITUTE OF MEDICAL RESEARCH

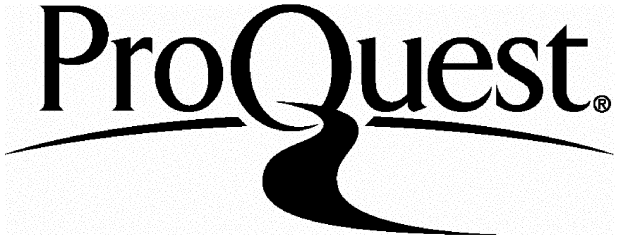

This investigation focuses on the physiological role of glial cell signalling by examining $InsP_3$ induced calcium release from the stores of cerebellar astrocytes.

1. $InsP_3$ type 3 receptor protein was identified in rat cerebellar type 1 astrocytes *in vitro* by immunohistochemical techniques. Cultured astrocytes do not appear to express detectable levels of type 1 but expression of $InsP_3$ subtype 2 receptor protein was detected at a low density. Protoplasmic astrocytes in the molecular layer expressed type 3 receptor but no expression of type 3 was found in the Bergmann glial cells. Receptor protein was located in and around the nuclear envelope within protoplasmic astrocytes.

2. The kinetic properties of calcium release by $InsP_3$ in single astrocytes were studied with the whole cell patch clamp technique, combined with microspectrofluorimetry of a low affinity calcium indicator furaptra and flash photolysis of caged $InsP_3$. $InsP_3$ concentrations (0.1-25μM) evoked $[Ca^{2+}]i$ rises in type 1 astrocytes *in vitro* and *in situ*. The $[Ca^{2+}]i$ responses comprised an initial delay, a fast rise of free $[Ca^{2+}]i$, a $[Ca^{2+}]i$ peak where net flux is zero and a slow declining phase. $InsP_3$ evoked Ca^{2+} flux was measured as the rate of change of free $[Ca^{2+}]i$ ($d[Ca^{2+}]i/dt$) in units of moles/litre of cytosol/second (μMs^{-1}).

3. The initial delay to the $[Ca^{2+}]i$ rise decreased with increasing $InsP_3$ concentrations from 111±15ms at high to 267±66ms at low. The rate of change of free $[Ca^{2+}]i$ and peak free $[Ca^{2+}]i$ appeared to be unrelated to concentration of $InsP_3$ released. The termination of the $InsP_3$ induced $[Ca^{2+}]i$ rise was not due to the metabolism of $InsP_3$. The rate of termination of $InsP_3$ evoked $[Ca^{2+}]i$ rise was linearly related to the Ca^{2+} flux through the $InsP_3$ receptor channel in both *in vitro* and *in situ* experiments, in agreement with previous studies. This result implies a common mechanism for the termination of Ca^{2+} flux for all $InsP_3$ receptor isoforms, possibly by calcium inhibition of the receptor or store depletion.

4. Furaptra injected into coupled astrocytes diffused from the patched cell into adjacent cells, presumably via gap junctions. U.V. illumination evoked a rapid calcium rise in adjacent cells, indicating that caged $InsP_3$ had also diffused from the patched cell loaded with caged $InsP_3$. This result would suggest that $InsP_3$ itself could act as a diffusible messenger between neighbouring cells during astrocytic $[Ca^{2+}]i$ wave propagation.

5. Whole cell patched type 1 astrocytes did not respond consistently to bath applied agonists such as glutamate and ATP, in contrast to ester loaded astrocytes *in vitro*.

6. Calcium release in glial cells was examined in physiological conditions, using rat cerebellar slices (P12). Glial cells were selectively loaded with acetoxy methyl ester form of a low affinity calcium indicator furaptra.

7. During neuronal stimulation the fluorescence signal from Bergmann glial cells was recorded using an imaging system. Preliminary results suggest that $[Ca^{2+}]i$ did not change in somal or filamentous regions of furaptra loaded Bergmann glial cells (with a $[Ca^{2+}]i$ range sensitive >0.5μM) as a result of Purkinje neurone climbing fibre stimulation.

To Kenny and my Mother and Father,
for all their love and support.

CONTENTS

LIST OF FIGURES

CHAPTER 2

CHAPTER 3

CHAPTER 4

LIST OF TABLES

GLOSSARY

A: AM-acetoxy methyl

AMPA-(S)-α-amino-3-hydroxy-5-methy-4-isoxazole propionic acid.

ATP-adenosine trisphosphate

A2B5-anti ganglioside epitope

B: BAPTA-1,2-bis(2-aminophenoxy)ethane-N,N,N',N',tetraacetic acid

BME-basal medium with Earles salts

BBB-blood brain barrier

BSA-bovine serum albumin

C: c*-caged *

$[Ca^{2+}]i$ -intracellular calcium concentration

Ca^{2+}-calcium ions

CCD-charged couple device

CNS-central nervous system

D: D-Dalton

DAG-diacylglycerol

DIV-days *in vitro*

DMSO-dimethylsulfoxide

E: E*-embryonic day *

EGTA-ethylene glycol-bis(β-aminoethyl ether) N,N,N,N,-tetraacetic acid sigma

ECF-extra cellular fluid

EAA-excitatory amino acid

EAAC- excitatory amino acid carrier

EPSP-excitatory post synaptic potentials

F: FCS-foetal calf serum

FITC-fluorescein Isothiocyanate

G Gal-C-galactocerebroside

GFAP-glial fibrillary acidic protein

GLAST-glial specific L-glutamate/L-aspartate transporter

gcm-glial cell missing (gene)

GLUT*-glucose transporter.

H: HEPES-hydroxlethylpiperazine ethane sulphonic acid

Hz-hertz

HPLC-high pressure liquid chromatography

HPTS-8-hydroxypyrene-1,3,6-trissulfonic acid, trisodium salt (pyranine)

I: IgG-immuno gamma globulin

$InsP_3$- inositol 1,4,5 trisphosphate

J J-joules

K: K^+-potassium ions

Kd-dissociation constant

k=kilo

L: l-litre

LTD-long term depression

LTP-long term potentiation

M: M*-mega 10^6

*M-molar

MEM-HEPES-minimum essential medium containing HEPES buffer

Mg^{2+}- magnesium ions

m*- milli 10^{-3}

μ-micro 10^{-6}

*m-metre

N: Na^+-sodium ions

n=*-number *

n-nano-10^{-9}

NIMR-National Institute for Medical Research

NA-numerical aperture

NMDA-N-methly-D-aspartate acid

O O2A progenitor-cell line that becomes type 2 astrocytes or oligodendrocytes.

O4-antiglycolipid antibody

Ω-ohms

P: P(number)- postnatal day (number) i.e age of animal

PBS-phosphate buffered saline

PMT-photomultiplier tube

PIP_2-phosphatidylinositol 4,5-bisphosphate

PTI-Photon Technology Instruments

PKC-protein kinase C

PLC-protein lipase C

p-pico 10^{-12}

Q: Qp-quantum yields

R: ROI-regions of interest

rpm-revolutions per minute

RT-PCR-reverse transcriptase polymerase chain reaction

RyR-ryanodine receptor protein

S: s-seconds

SEM-standard error of the mean

T: (5-Thio-$InsP_3$)-1-D-myo-inositol 1,4-bisphosphate 5-phosphorothioate

TRITC-tetramethylrhodamine isothiocyanate

U: U.V-ultra violet light

V: V-volts

X X-times

ACKNOWLEDGEMENTS

I would like to thank my supervisor Dr. David Ogden, for all his help and support throughout my research time at the Institute. I am especially grateful to him for his suggestions, patience and encouragement in experimental techniques and for showing me there is more to neurophysiology than just neurones. I especially thank him for all his advice and useful comments in the writing of this thesis.

I also owe a great deal to the "chaps" in the Lab for all their support and guidance over the last few years, Muriel Bouvier, Thierry Capiod, Tom Carter, Igor Chizhmakov, Nikolai Kiskin, Chris Magnus, Nancy Mulrine, Abdul Sesay, and Chris Watkins who I would also like to thank for reading this thesis. I express my graditude to them all for encouraging my research on glial cells and providing a friendly ambience in which to work.

For the immunohistochemistry studies I would like to thank Dr Anthony Lai for donating the antibody specific for the type 1 $InsP_3$ receptor protein; Dr. Tomoyasu Sugiyama for kindly sending me the KM1082 and KM1083 antibodies from Japan; Mick Errington and Dr. Myrna Dent for their assistance in tissue preparations; the Division of Neurobiology who allowed me the use of their equipment, particularly Dr. Peter Woodhams and John Atkinson; for their assistance with confocal microscopy I thank Dr. Nigel Empatage and Dr. Tom Carter. I am grateful to Dr. David Trentham and Dr. John Corrie for producing the caged compounds that were used in this study.

On a practical note I thank Eileen Clark for ordering equipment; Dr. Sulkvinder Dhanjal for his advice on electronic matters; Photographics at the institute for producing the colour pictures; and the Engineering workshop for their assistance with creating some experimental equipment. I also appreciate Dr. Rod King who as the Director of Studies helped me with student life at the institute and with the submission of this thesis.

I am grateful to all my friends and colleagues in the Division of Neurophysiology for encouraging my research and making my time at the institute interesting and enjoyable.

This work was supported by a M.R.C studentship.

On a more personal note I am extremely grateful to all my friends. I would also like to thank my brother and sister for all their encouragement. My parents, Des and Blanche, for always being there throughout all of my studies. I thank them for their guidance and I appreciate all their love and faith and will forever be indebted to them.

Finally to my partner Kenny, I am deeply grateful to him for all his patience and emotional support. I appreciate his understanding when things were difficult, and for having faith in me that one day I would finish my studies.

CHAPTER 1

INTRODUCTION

1. INTRODUCTION

The central nervous system (CNS) consists of two main kinds of cells. Neurones are excitable, they conduct action potentials and have synaptic connections. Glial cells are non-excitable, do not have synaptic connections or propagating action potentials. However, glia are able to respond to external stimuli by a rise in intracellular calcium concentration ($[Ca^{2+}]i$) which can spread to adjacent cells via a syncytium. Cellular $[Ca^{2+}]i$ rises are important in many metabolic events in peripheral non-excitable cells hence glia may be involved indirectly in regulating neuronal activity within the CNS. This thesis presents a study of glial cell calcium signalling in the rat cerebellum.

1.1 Neuro-glial interactions during synaptogenesis.

Glial cells interact with neurones to influence synaptic patterning. During CNS development there is an intimate relationship between glial development and synaptogenesis. For example, E12 (embryonic day twelve) rat retinal ganglion axons have begun to extend from the retina (neurogenesis site) to the superior colliculus but do not form synaptic connections until P21 (postnatal stage 21 days after birth) when the astrocytes have also differentiated (Skoff-R.P. 1990). Studies using tissue culture have shown that formation of functional synapses only occurs in the presence of neuroglia. O'Lague-P.H. *et al* (1978) examined sympathetic neurones grown in the presence or absence of glial cells in culture and found that glial cells were required for cholinergic synaptic development. Furthermore glial cells have also been shown to be involved in maintaining spontaneous neuronal synaptic activity by releasing growth factors which may be required for survival of retinal ganglion neurones (Meyer-Franke-A. *et al* 1995).

A *Drosophilia* mutant deficient in glial cells has been developed. The gene glial cell missing (gcm) is responsible for the promotion of bipotential precursor cells into either glial or neuronal cells (Jones-B.W. *et al* 1995). Mutation of gcm results in an absence of dendrites and a re-routing of longitudinal axonal pathways.

1.1.1 Glial cell ion channels

Schwann cells cultured from rabbit sciatic nerve were found to possess both voltage gated Na^+, K^+ channels (Chiu-S.Y. *et al* 1984), and Cl^- channels (Bevan-S. *et al* 1985). Subsequently it became evident that glial cells activated from the CNS also possess voltage activated Na^+, K^+, Ca^{2+} and Cl^- channels. More recent studies show that glia can also respond to neurotransmitters via ligand gated channels (Barres-B.A. 1991:Verkharatsky & Kettenmann 1996; Murphy-S. & Pearce-B. 1987; Sontheimer-H. 1994).

Recordings from slice preparations have allowed unambiguous identification of receptors free of any possible artefacts due to tissue culture. Thus, for example, mouse Bergmann glial cells in the cerebellum express glutamate, $GABA_A$, H1- histamine, α1-adrenergic, P_{2Y}-purinergic and endothelin ET_B receptors, but not receptors for ACh, aspartate, bradykinin, dopamine, glycine, oxytocin, serotonin, somatostatin, substance P, taurine, or vasopressin (Verkharatsky & Kettenmann 1996). It appears that the main ligand gated channels expressed in Bergmann glial cells match the neurotransmitters released from synapses of the cerebellar molecular layer. However, how Bergmann glial cells respond during synaptic activity is unclear.

1.1.2 Regulation of neurotransmitters in the synaptic cleft

Glial cells may modify levels of neurotransmitters after release from presynaptic terminals into the cleft. Excess glutamate is thought to be neurotoxic as it activates glutamate receptors excessively causing an internal rise in Ca^{2+} and Na^+ (Olney-J.W. & Sharpe-L.G. 1969). The increased ion entry causes the cells to swell and lyse. Increases in $[Ca^{2+}]i$ can cause an increased activation of internal cellular events with the up regulation of enzymes such as proteases, endonucleases and lipases. Under physiological

conditions the synaptic cleft extracellular fluid (ECF) concentration of glutamate is thought to be regulated by uptake carriers located on the membranes of glial cells and neurones.

GLAST (glial specific, L-glutamate/L-aspartate transporter, Storck-T. *et al* 1992) and GLT-1 (rat L-glutamate transporter 1, Pines-G. *et al* 1992) have been shown to be concentrated around astrocytic end feet which project into the synaptic cleft. The EAAC (excitatory amino acid carrier) glutamate uptake carrier (Kanai-Y. & Hediger-M.A. 1992) are neural glutamate transporters and are located on membranes of post-synaptic cells (Rothstein-J.D. *et al* 1994). Rothstein *et al* down regulated single subtypes of neuronal or glial glutamate transporters within the synaptic cleft with antisense oligonucleotides and showed that only when all glial transporters (not neuronal) were removed did glutamate concentrations in the ECF increase to neurotoxic levels (Rothstein-J.D. *et al* 1996).

Inside glial cells, glutamate is converted to inactive glutamine by an astrocyte-specific (Norenberg-M.D. & Martinez-Hernandez-A. 1979) enzyme glutamine synthetase in brain (Berl-S. *et al* 1961; van den Berg-C.J. & Garfinkel-D. 1971). Interestingly immunocytochemical studies has shown there to be a close correlation in the expression of GLAST and glutamine synthetase (Derouiche-A. & Rauen-T. 1995) in rat retinal glial cells.

Glial cells have been shown to be involved in the process of replenishing neurotransmitters by supplying neurones with glutamine. Glutamine is released by glial cells into the ECF and taken up by adjacent neurones. In neurones glutamine can be converted to glutamate or GABA. If glutamine synthetase is inhibited there is a reduction in the amount of release of GABA and glutamate from neurones (Paulsen-R.E. & Fonnum-F. 1989; Rothstein-J.D. & Tabakoff-B. 1984). There appears to be a "shuttle" system between neurones and glial cells such that glutamate is regenerated from glutamine in nerve terminals when needed by glutaminase (Erecinska-M. & Silver-I.A. 1990; Fonnum-F. 1993). If glial glutamine synthetase is inhibited pharmacologically (in hippocampal organotypics) there is a reduction in glial cell glutamine immunoreactivity and an increase in glutamate concentration these cells (Laake-J.H. *et al* 1995). Concurrently the glutamate content in neurones decreased by 50%. When glutamine was applied into the ECF the glutamate concentration in neurones increased. These

experiments on organotypic hippocampal slices imply that some of the neuronal glutamate synthesis is dependent on glial production and release of glutamine.

1.1.3 Glial cell metabolites provide the energy supply for neurones.

The close relationship between the brain microvasculature system and glial cells has been called the blood brain barrier (BBB). The BBB is a notional junction between the circulatory system (endothelial cells) and the brain tissue (glial cells). The BBB acts as a barrier preventing noxious metabolites that may be present in the blood from entering the brain. In addition the BBB is thought to be involved in regulating other essential metabolites from entering the brain. Energy is required for synaptic transmission and is supplied to the ECF in the form of glucose. In fact a fall in blood glucose levels, and hence a reduction in nervous tissue supply, results in severe disturbances of brain function and ultimately death (Sieber-F.E. & Traystman-R.J. 1992). Recent studies (discussed below) have provided some evidence that glia may play an intrinsic part in supplying neurones with essential nutrients such as glucose.

Astrocytes have integral membrane protein glucose transporters such as GLUT1 (45kDa) and GLUT5 (glucose/fructose transporter, Payne-J. *et al* 1997 ; see also Pessin-J.E. & Bell-G.I. 1992). Glucose transporters allow the passage of glucose into the glial cytoplasm (Vannucci-S.J. *et al* 1997). Studies in Müller cells of the guinea pig retina show that once in the glial cell, glucose undergoes anaerobic glycolysis to produce lactate (Poitry-Yamate-C. *et al* 1995). Lactate is then released into the ECF. The photoreceptors take up lactate and use it to produce energy. In cortical astrocytes a lactate uptake and metabolic processing system has been demonstrated to exist in pure neuronal cultures (Dringen-R. *et al* 1993a). Lactate is taken up and converted to pyruvate by lactate dehydrogenase. The pyruvate is used at mitochondrial sites in the tricarboxylic acid cycle to generate ATP (an energy source).

Glial cells may also serve as an energy store for adjacent neurones, since they have been shown to contain high levels of glycogen (Cataldo-A.M. & Broadwell-R.D. 1986a). Glycogen found specifically in glial cells of the brain can be broken down very rapidly. It is unclear whether the glycogen is broken down as purely an energy store for glial cells or whether the glycosyl units (mobilised from glycogenolysis) produce lactate

for adjacent neurones (Dringen-R. *et al* 1993a). In cortical astrocytic cultures exogenously applied glycogen does not cause astrocytes to release glucose (Dringen-R. *et al* 1993a). The degree of glycogenolysis in glia can be regulated by neurotransmitter activity. For example glutamate stimulates glucose uptake and release of lactate in cultured astrocytes (Pellerin-L. & Magistretti-P.J. 1994) as well as glycogen production (Swanson-R.A. *et al* 1990). This means that during increased neuronal activity the energy demand can be met by glial lactate production. A wide variety of monoamine neurotransmitters, such as noradrenaline, serotonin and histamine, can mobilise glucose by activating the break down of glycogen stores in glia (Tsacopoulos-M. & Magistretti-P.J. 1996), as well as adenosine, ATP, and arachidonic acid (Wiesinger-H. *et al* 1997). Glial glycogenolysis is mediated by an increase in cytosolic $[Ca^{2+}]i$ (Ververken-D. *et al* 1982).

Interestingly other blood components have been shown to interact with glial cells, particularly astrocytes. When astrocytes come into contact with blood derivatives, such as albumin (Nadal-A. *et al* 1995; Nadal-A. *et al* 1997) thrombin (Ubl-J.J. & Reiser-G. 1997) endothelin (ET-1 ; Zhang-W *et al* 1990; Stanimirovic-D.B. *et al* 1997) , bradykinin (Bernstein-M., *et al* 1996; Reetz-G. & Reiser-G. 1996), histamine (Kirischuk-S.,*et al* 1996; Inagaki-N; & Wada-H 1994) and cytokines (Merrill-J.E. & Benveniste-E.N. 1996) during pathological conditions of stress and injury, they respond with an increase in $[Ca^{2+}]i$. This rise in glial cell calcium can pass to adjacent cells, and so could be a means by which glial cells react during injury to the microvasculature, to form plaques and protect nervous tissue.

1.1.4 Glia and neurological disease

Astrocytes participate not only in normal CNS physiological behaviour but also have been shown to respond vigorously during neurological injury. The astroglial response, or astrocytosis, is characterised by an increase in glial cell number or size, with an increase in expression of GFAP (glial fibrillary acidic protein) a glial specific structural protein (Bignami-A. & Dahl-D. 1976). In vivo, these changes occur in astrocytes within the trauma area to form a "glial scar". Reactive astrocytosis occurs within one hour of damage and is thought to form protective boundaries around regions of the damaged

CNS to protect against spreading necrosis. Neurological disorders known to have astrocytic responses include AIDS dementia (De La Monte-S.M. *et al* 1987), viral infections (Zlotnik-I. 1968), prion associated spongiform encephalopathies (Gajdusek-D.C. 1990) inflammatory demyelinating disease such as multiple sclerosis (Merrill-J.E. & Benveniste-E.N. 1996), acute brain injury e.g. stroke , and neurodegeneration such as experienced in Alzheimer's disease and Huntington's chorea (Tomimoto-H. *et al* 1996).

Under pathological conditions where the BBB breaks down, as in brain disease or injury, the CNS may be exposed to environmental fluctuations. During BBB break down glial cells may come into contact with blood proteins, leukocytes, macrophages, endothelial cell metabolites, or blood based enzymes. Under normal conditions the brain would not come into contact with the immune system, and [T-cells] in the CNS as a result are low. Only activated T cells, resulting from chemotactic stimulus by infection can cross the BBB. Once in the CNS only T cells that recognise a CNS antigen remain.

Cytokines (such as interleukins, interferon, and growth factors), proteins (albumin, thrombin), or endothelin induce a rise in $[Ca^{2+}]i$ in glial cells which is linked to inositol 1,4,5-trisphosphate ($InsP_3$) production. The induced $[Ca^{2+}]i$ rise in glia spreads throughout the syncytium via gap junctions *in vitro*. This $[Ca^{2+}]i$ signalling could be a means by which glial cells communicate during pathological conditions to induce astrocytosis. The reactive astrocytes can affect neuronal function which may be symptomatic to a diseased or injured state.

1.1.5 Neuro-glial synaptic interactions

Glial cells are ideally located to influence synaptic behaviour and thus influence function. In the cerebellum for example, Bergmann glial cells have a close anatomical connection with the synapses of Purkinje cells (Palay-S. L. & Chan-Palay-V. 1974). However a functional relevance remains unclear. Glial cells are involved in the regulation of the ionic composition of the ECF surrounding neurones. Glial cells have a resting membrane potential of about -90mV, which is predominantly due to K^+ permeability. The normal $[K^+]$ of ECF is between 2-4mM (Moody-W.J.Jr. *et al* 1974). Resting intra or extracellular $[K^+]$ is maintained by Na^+/K^+ ATPases (Frank-G. *et al* 1983), activation of K^+/Cl^- cotransporters (Winter-Wolpaw E. & Martin-D.L. 1984),

general diffusion into the ECF. However during neuronal activity, $[K^+]$ increases in the ECF around the synapse. Glial cells help to remove K^+ ions from ECF in areas of high neuronal activity and dissipate it in regions of low $[K^+]$, thus maintaining resting $[K^+]$. This phenomenon is known as spatial buffering (Orkand-R.K. *et al* 1966).

Recent studies have shown that glial cells can respond to neuronal stimulation by producing slowly propagating calcium wave in hippocampal organotypic slice cultures, (Dani-JW & Smith-S.J. 1992) and *in situ* slice preparations (Duffy-S. & MacVicar-B.A. 1995; Pasti-L. *et al* 1997). Clark *et al* have shown in cerebellar slices that glutamate released from adjacent synapses induces glial cell currents and stimulated an electrogenic uptake of glutamate (Clark-B. A. & Borbour-B. 1997). They concluded that a large fraction of the glial current was mediated by AMPA/Kainate receptors, as a result of glutamate release from parallel fibre synapses. It was not possible to resolve the electrogenic uptake current in Bergmann glial cells associated with individual parallel fibre stimulation, because the ionotropic current was so much greater than the uptake current.

1.2 Glial calcium

Glial cells, as described previously, may affect synaptic function. Calcium has important cellular functions within glial cells. For example changes in $[Ca^{2+}]i$ can modulate structure within glial cells. When calcium binds to specific internal structural proteins, such as S-100 or GFAP, it affects microtubule assembly and hence glial cell morphology. Glial cell GFAP modifications are involved in neuronal synaptic plasticity and as a result development (Yang-Z.W.& Kong-C.F. 1988). These structural changes are also evident during trauma and injury (section 1.1.4). Glial kinases, such as Ca^{2+}/CaM kinase and PKC are affected by cytosolic $[Ca^{2+}]i$ changes to modulate DNA synthesis (Meader-Woodruff-JH, *et al* 1984 ; Saunders-R.D. & DeVries-G.H. 1988). Elevated $[Ca^{2+}]i$ levels within glial cells are also responsible for mobilising glycogen stores (Magistretti-P.J. *et al* 1986) providing metabolites for neurones (section 1.1.3) and are also involved in cellular mitotic behaviour and gene expression (Supattapone-S. *et al* 1989)

Views about glial calcium have changed drastically over the last few decades with the discovery that these cells respond to neurotransmitter, neuropeptides, electrical and mechanical stimulation with spatial and temporal $[Ca^{2+}]i$ changes. An induced rise in astrocytic $[Ca^{2+}]i$ is propagated throughout the syncytium in the form of characteristic waves or oscillations (Cornell-Bell-A. H. *et al* 1990; McNaughton-L.A. *et al* 1990a; McNaughton-L.A. *et al* 1990b; for a review see Finkbeiner-SM 1993;Verkharatsky & Kettenmann 1996). Glial calcium waves can be triggered as a result of neuronal activity in hippocampal organotypics (Dani-JW & Smith-S.J., 1992) and in acute hippocampal slice preparations (Porter-J.T. & McCarthy-K.D. 1996). Thus the glial cell can no longer be thought of as the passive element of the nervous system as they are capable of eliciting complex $[Ca^{2+}]i$ changes which may be used as a communication system. Although there have been many studies of astrocytic $[Ca^{2+}]i$ signalling little is known about the physiological relevance of such a system. There are some theories that it is the amplitude and frequency of the $[Ca^{2+}]i$ signalling that relays information from one brain region to another (Pasti-L., *et al* 1995; Andrea-P. & Grohovaz-F. 1995 ; Pasti-L. *et al* 1997). Conversely it has been shown that glial cell $[Ca^{2+}]i$ changes may directly influence neuronal excitability *in vitro* (Nedergaard-M. 1994; Parpura-V. *et al* 1994).

1.2.1 Plasma membrane bound channels

Glial cells although electrically inexcitable do express voltage gated Ca^{2+} channels in culture. The type of Ca^{2+} channel expressed in glia appears to be determined by their different locations. Cortical astrocytes appear to posses L-type "like" channels (MacVicar-B.A. & Tse-F.W. 1988), whereas hippocampal astrocytes *in situ* have T and N "like" channels (Akopian-G. *et al* 1996). Some neurotransmitters, for example glutamate, when released at the synapse can bind to ionotropic receptors, to cause ligand-gated channels to open and hence produce an increase in $[Ca^{2+}]i$ (Airaksinen *et al* 1997). As previously discussed glial cells possess many of the neuronal neurotransmitter operated channels which cause an increase in $[Ca^{2+}]i$ (Verkhratsky-A. *et al* 1998).

However signalling to the interior of the cell is not necessary for neurotransmitter or hormone release but may be required for other cellular functions such as transcription (Bading-H. *et al* 1993), mitochondrial metabolism (Mitchell-P. 1961 ; Rizzuto-R. *et al*

1993) and phosphoinositide turnover (Mangoura-D., *et al* 1995). Ca^{2+} diffusion in neurones is slow (Hodgkin-A.L. & Keynes-R.D. 1957 ; Allbritton-N.L. *et al* 1992) due to binding to endogenous buffers. A secondary system of internal calcium release is a means by which the cell can regulate $[Ca^{2+}]i$ more efficiently. This role could be performed by intracellularly located calcium release pores, such as ryanodine or inositol 1,4,5-trisphosphate gated channels.

1.2.2 Ryanodine receptors and calcium induced calcium release (CICR)

The ryanodine receptor (RyR) family of intracellular release Ca^{2+} channels can be identified by the fact that they bind the plant alkaloid ryanodine. Caffeine and ryanodine (at concentrations less than 10μM) selectively activate the channel whereas ryanodine greater than 10μM, ruthenium red are selective inhibitors and are used as pharmacological tools. The RyRs are also sensitive to Ca^{2+} and are thought to be involved in CICR (Bezprozvanny-I. *et al* 1991). Studies of RyR location has shown there to be at least three isoforms located in CNS tissue(Sorrentino-V. & Volpe-P. 1993).

Work by Langley and Pearce on reactive cultured cortical astrocytes suggests that astrocytes may express RyR type 3, as they respond to ryanodine but are insensitive to caffeine (Giannini-G. *et al* 1992; Langley-D. & Pearce-B. 1994). This aspect of astrocytic $[Ca^{2+}]i$ signalling was not studied in this work.

1.2.3 Inositol 1,4,5 trisphosphate induced calcium release

The inositol 1,4,5 trisphosphate receptor releases Ca^{2+} from the endoplasmic reticulum in response to binding of the second messenger $InsP_3$ (Berridge-MJ 1993). $InsP_3$ is formed by the activation of numerous metabotropic receptors (e.g glutamate, ATP, noradrenaline, histamine, bradykinin, endothelin, thrombin). On binding agonists, phospholipase C (PLC) hydrolyses membrane-bound lipid phosphatidylinositol 4,5-bisphosphate (PIP_2) to give soluble $InsP_3$ and insoluble membrane-bound diacylglycerol (DAG). DAG can, in turn, activate protein kinase C (PKC ; Nishizuka-Y. 1988).

$InsP_3$ receptors are large structural proteins (313 kDa) consisting of a ligand binding domain (N-terminal), a modulatory domain that transduces the signal, and transmembrane sections (M1-6) towards the C-terminal end of the molecule. The $InsP_3$ receptor channel protein exist as functional homotetramers forming a central Ca^{2+} pore. Three main types of $InsP_3$ receptor have been cloned and characterised. High amounts of subtype 1 have been localised to Purkinje cells and other neurones (Furuichi-T. *et al* 1989; Supattapone-S. *et al* 1988). Type 2 (Sudhof-T.C. *et al* 1991) and type 3 (Maranto-A.T. 1994) $InsP_3$ receptors have also been characterised. The $InsP_3$ binding domain of the receptor is the most conserved region, within the three subtypes, whereas the coupling region is the least conserved. The coupling domain has binding sites for ATP, Ca^{2+} , calmodulin, and several kinases. The differences in this region suggest that the subtypes are modulated to a different extent by neuroactive substances (Mignery-G.A. & Sudhof-T.C. 1990).

$InsP_3$ has advantages over Ca^{2+} as a second messenger, especially in that (unlike Ca^{2+}) it diffuses readily throughout the interior of the cell (Allbritton-N.L. *et al* 1992). The intracellular Ca^{2+} inflow depends upon other endogenous molecules. These endogenous Ca^{2+} binding molecules include buffering proteins (Baimbridge-K. G. *et al* 1992) such as calmodulin, and Ca^{2+} transporters which remove cytoplasmic Ca^{2+}. The location, mobility, affinity and kinetics of these binding molecules all affect $[Ca^{2+}]i$ (Clapham-DE, 1995). The break down of $InsP_3$ to $InsP_2$ (inositol 1,4, bisphosphate) by $InsP_3$ 5-phosphatase is slower (seconds) compared to Ca^{2+} binding to endogenous buffers .

Despite this $InsP_3$ molecules and Ca^{2+} ions closely integrate to regulate intracellular Ca^{2+} release from stores. When $InsP_3$ receptors are reconstituted into bilayers and the $InsP_3$ concentrations remains constant, varying $[Ca^{2+}]$ produces a bell-shaped $[Ca^{2+}]$-probability open relation. High $[Ca^{2+}]i$ causes the channel to inactivate (Bezprozvanny-I. *et al* 1991). Thus the $InsP_3$ receptor proteins interacts directly with Ca^{2+} ions.

1.3 Aims.

This thesis describes the identification of $InsP_3$ subtypes in astrocytes and characterises the properties of $InsP_3$-evoked Ca^{2+} release from these cells. The studies were performed using cerebellar tissue. The cerebellum has a relatively simple well characterised structure of repeating units based around Purkinje neurones. This anatomy makes cerebellar slices relatively robust and easy to manipulate when performing experiments, so facilitating the study of central synaptic neuro-glial interactions (Ito-M. 1984; Palay-S. L. & Chan-Palay-V. 1974).

Chapter 2 in this thesis describes the methods used to study the $InsP_3$ induced $[Ca^{2+}]i$ rises in astrocytes *in vitro* and *in situ*. Glia *in situ* are small and have a complex morphology, thus are difficult to identify, hence Chapter 2 describes a novel method for loading glia in cerebellar slices.

The immunohistochemical studies in Chapter 3 identify the $InsP_3$ receptor subtype protein of cerebellar astrocytes *in vitro*, and confirms (previous studies Yamamoto-Hino *et al* 1995) the isoform *in situ*. Chapter 3 also characterises the glial cell type used in the electrophysiological experiments as being "type 1" astrocytes.

The kinetic characteristics of the $InsP_3$ induced change in $[Ca^{2+}]i$ over a range of $InsP_3$ concentrations were examined in chapter 4. *In vitro* astro-astrocytic interactions involving $[Ca^{2+}]i$ rises were studied. The kinetics of $InsP_3$ evoked $[Ca^{2+}]i$ rises *in vitro* and *in situ* astrocytes were compared.

Chapter 5 describes experiments designed to investigate how astrocytic $[Ca^{2+}]i$ levels change during Purkinje cell activity. These experiments would provide information on how neuro-glia cells interact to influence synaptic activity.

Chapter 6 compares the results presented in the previous chapters to published data on glial cell calcium kinetics. The relevance of glial cell calcium signalling is discussed with respect to the neurophysiology of the cerebellum.

CHAPTER 2

MATERIALS AND METHODS

2. Primary cultures of cerebellar astrocytes.

Astrocyte cell cultures were prepared according to the method described by (Gallo-V. *et al* 1989). Wistar rats post natal day seven (P7) were anaesthetised, decapitated and cerebella dissected into cold filtered Basal Medium with Earles salts, (BME, Gibco) supplemented with 2 mM L-glutamine and 10% foetal calf serum (FCS). To prevent bacterial infection antibiotics gentamycin (100μg/ml), or penicillin and streptomycin (50μg/ml, Gibco) were used. The meninges other tissue debris were removed. Cerebella were chopped finely and placed in modified Krebs solution (mM NaCl 120, KCl 4.5, KH_2PO_4 1.2, $NaHCO_3$ 25, glucose 15 $MgSO_4$ 1.2, bovine serum albumin (BSA 3mg/ml) and spun for one minute at 2000rpm in a Labofuge 200 centrifuge (Haraeus Sepatech). The supernatant was removed, the pellet resuspended in Krebs solution containing 0.025% trypsin and placed in a shaking water bath (Grant model ss 30 220-240, 60 strokes/min) at 37°C for 15 minutes. After incubation 80μg/ml soybean trypsin inhibitor and 12.5 μg/ml DNase were added and the suspension spun for 1 minute at 2000rpm. The supernatant was aspirated and the pellet trituated in 520μg/ml soybean trypsin inhibitor and 80μg/ml DNase until a cloudy mixture remained. Care was taken not to generate air bubbles, which have a deleterious effect on cell membranes. The resulting suspension was then added to Krebs solution containing 1mM $CaCl_2$ and centrifuged for 5 minutes at 2500rpm. The supernatant was removed and the pellet resuspended in 0.2μm filtered BME. Sterile glass coverslips (30mm diameter) were immersed in 70% ethanol, washed with filtered distilled water and allowed to air dry in a microbiological safety hood. Coverslips were coated with poly-L-lysine (10μg/ml) and cells plated at a density of $2.5x10^6$ cells per 60mm sterile petri dish and incubated at 37°C in a humidified air incubator, gassed with 5% CO_2. The medium was changed the following day. The medium was replaced every two or three days depending on cell condition.

For flash photolysis experiments glass coverslips have poor optical properties, due to a prolonged phosphorescence after the flash. For this reason cells were grown on quartz coverslips. Glial cells would not grow well on poly-L-lysine coated quartz coverslips. Several coatings were tried to optimise the conditions for cell survival in culture:-Cell Tak (Collaborative Biomedical Products) 3.5μg/ml, poly-D-lysine (Sigma) 10μg/ml, surgical glue (Braunmelsungen Histoacrly blau) applied directly, collagen (Vitrogen 100, 0.012N HCl Celtrix labs) applied directly, laminin 4μg/ml (Sigma) and bovine fibronectin 4μg/ml (Sigma).

2.1 Preparation of cerebellar slices.

Wistar rats (P12-16) were anaesthetised with Metofane C-Vet and after cervical dislocation decapitated. The whole brain was removed and placed in 20 ml of ice cold slicing solution of composition , (mM) NaCl 120, KCl 2.5, $CaCl_2$ 0.5, $MgSO_4$ 2, $NaHCO_3$ 26, NaH_2PO_4 1.25, HEPES 5, Glucose 25, pH 7.25, osmolarity 305-315 mosmol/kg (table 2). The solution was pre-cooled for 4-5 hours at -20°C, the resulting ice was crushed to give a thick consistency ice slurry. The solution placed in the vibratome chamber (modified Oxford) was continually gassed (5% CO_2, 95% O_2). A thick block (approximately 5mm by 3mm) was cut from the middle vermis region of the cerebellum, either in a saggital or transverse orientation, and glued with cyanoacrylate adhesive (RS) to a cold aluminium metal block. Cerebellar slices of 200-250μm were cut. This thickness was optimal for cell survival and ease of cell visualisation at the surface level of the slices, which were illuminated from below. Once cut the slices were transferred into a holding chamber based on a design by Edwards F.A. *et al* (1989).

The holding chamber consists of a nylon mesh tray suspended in a beaker of slicing solution, which was continually gassed in such a way as to circulate the solution. The chamber containing the slices was incubated for 10-20 minutes at 34°C to allow cut or damaged cellular processes to seal up and repair. (Edwards-F.A, & Konnerth-A.,1992; Edwards-F.A, & Gibb-A.J.,1994). A short period of incubation allowed certain metabolic processes to equilibrate (Whittingham *et al* 1984). For example, the slicing

process could trigger various phosphorylation, dephosphorylation cascades, and stress related protein synthesis that could alter physiological responses (Aitken *et al* 1995).

2.2 Immunohistochemistry

For electrophysiological investigation rat cerebellar type 1 astrocytes were visually identified on the basis of a characteristic morphology determined in the immunocytochemical studies.

A number of specific monoclonal antibodies were used to distinguish glial cell types present in culture and acute slices. Glial fibrillary acidic protein (GFAP) is a structural molecule specific to astrocytes types 1 and 2 (Bignami-A., & Dahl-D., 1974). A2B5 (Eisenbarth *et al* 1979) is a anti ganglioside epitope marker for type 2 astrocytes and oligodendrocyte cells of the O2A progenitor lineage (Raff *et al* 1983a). However A2B5 gangliosides are also expressed on plasma membranes of other cell types such as neurones, neuroendocrine cells, and neurofibrillary tangles associated with Alzheimer's disease.

The antiglycolipid antibody 04 (Sommer & Schnanchner 1981) and myelin specific galactocerebroside (Gal-C) can be used as specific markers to identify oligodendrocytes (Raff *et al* 1978 ; Raff *et al* 1979) *in vitro*. From immunohistochemical studies using a combination of these antibodies glial cell types can be identified within rat cerebellar cultures. However this does not make the identification of the various types of glial cells in culture straight forward, one has to distinguish glia from degenerating neurones, unidentified progenitor cells, and other glial subtypes like oligodendrocytes.

Table1: Summary of some glial cell identification antibodies.

	GFAP	*A2B5*	*O4*	*GALC*
ASTROCYTE TYPE 1	+	-	-	-
ASTROCYTE TYPE2	+	+	-	-
OLIGODENDROCYTE	-	+	+	+
O2A-PROGENTOTOR	-	+	-	-
NEURONES	-	+	-	-

2.2.1 Immunohistochemistry using Gal C, 04 and A2B5

Glial cells grown on 13mm glass coverslips (No.1 or 0 thickness) were washed with MEM-HEPES (see table 2) and placed on pedestals within petri dishes. The cells were incubated with mouse monoclonal antibodies raised to the A2B5 antigen, or the Gal C antigen, or the 04 antigen for 30 minutes at room temperature (23°C). Antibodies were diluted in a solution which contained phosphate buffered saline (PBS) and 10% FCS, at dilution's A2B5 1:100, Gal C 1:100, and 04 1:1 respectively. Controls were performed by omitting the primary antibody. After washing the coverslips with MEM-HEPES three times, the secondary anti-mouse IgG (whole molecule) fluorescein isothiocyanate (FITC) conjugate or the tertramethylrhodamine isothiocyanate (TRITC) conjugate, both developed in goat, were incubated for 30 minutes in PBS plus 10% FCS solution (dilution of 1:100). Coverslips were then washed and cells fixed in 4% paraformaldehyde (made up in 0.1M PBS pH 7.4) for 20 minutes, before mounting on microscope slides with either mounting medium Vectashield (Vector Laboratories) or Uvinert (BDH).

2.2.2 Staining procedure for GFAP in cultured glial cells

Cells were fixed and permeabilised in 95% ethanol/5% acetic acid at -20°C for 15 minutes. The cells were incubated in 10% non fat skimmed milk powder (made up in 0.1M PBS pH7.4) to reduce non-specific binding of the antibody and 1% Triton-X100. This detergent was used to permeabilise the cell membrane to ensure the antibody reaches the internally located protein. The rabbit monoclonal (from IgG fraction of antiserum) anti GFAP antibody developed from goat was diluted 1:100 in PBS. Cultured glial cells on 13mm coverslips were submerged in 50µl of the anti-GFAP antibody and incubated with the cells for 30 minutes at room temperature (23°C). The anti-GFAP antibody solution was removed and the cultured cells washed thoroughly in PBS. The FITC conjugated anti rabbit IgG was applied to the cultured glial cells, at a dilution of 1:1000, for 30 minutes at room temperature (23°C). Once washed thoroughly in PBS the cells were mounted in a mounting medium Uvinert (BDH) or Vectashield (Vector Labs) onto microscope slides.

2.2.3 Identification of GFAP in cerebellum slices

The distribution of glial cells in the rat cerebellum was studied *in situ* in frozen sections. Wistar rats were perfused via cardiac catheter with either PBS (0.1M PBS pH7.4) or 4% paraformaldehyde (made up in the PBS) to preserve the brain tissue. The rat was deeply anaesthetised with intra-peritaneal urethane. A small incision was made just below the rib cage to expose the diaphragm. The torso which included the rib cage and skin was bisected directly along the mid line region to expose the beating heart. A needle attached to tubing was inserted and clamped into the left ventricle. A 20ml syringe was attached to the tubing and the 4% paraformaldehyde or PBS was perfused through the heart into the aorta to replace the blood. Perfusion was complete when the dead rigid animal took on a yellow colour. (This procedure was kindly performed by M.Errington).

The rat brain was removed and frozen in powdered dry ice. Slices of 10, 20, 25, 50 μm thickness were cut on a cryostat and placed on gelatine-coated microscope slides. Slices from PBS perfused animals were fixed in 95% ethanol/5% acetic acid at -20°C for 15 minutes prior to the staining procedure. Initially the slices were soaked in 10% non fat skimmed powdered milk (in 0.1M PBS pH7.4) to reduce non-specific binding of the antibody. To permeabilise glial cell membranes the slices were incubated with 1% Triton for 3 hours at room temperature (23°C). The rabbit monoclonal anti GFAP antibody was added, diluted 1:1000 in PBS, overnight in a humidified chamber at 4°C. After washing in PBS the secondary anti-rabbit IgG FITC conjugate was added at a dilution of 1:1000 in PBS. Slices were washed by immersion in PBS and mounted in a mounting medium Uvinert (BDH) covered with a coverslip.

2.2.4 Staining with rabbit polyclonal anti $InsP_3$ receptor protein antibody.

2.2.4.1 Cultured cells.

Cells grown on 13mm coverslips were fixed in 4% paraformaldehyde for 20 minutes at room temperature (23°C). After washing in PBS the cells were incubated in 10% non fat skimmed powdered milk (in 0.1M PBS pH 7.4) and 0.1% Triton X-100 for 1 hour. The polyclonal antibody raised in rabbit was specific to 19 amino acid sequence of the C-terminus, of mouse $InsP_3$ type 1 receptor protein (kindly provided by Dr Lai NIMR). This antibody was based on published sequence data by (Mignery *et al* 1989). The antibody was diluted 1:1000 in PBS and 0.1% milk for 1 hour at room temperature 23°C (Dent-M.R. *et al* 1996) and incubated with the tissue. After washing in PBS the cells were incubated with FITC conjugated anti rabbit IgG (1:100) for a further hour. Cells were mounted in Uvinert mounting medium on microscope slides after further washing in PBS.

Antibodies to $InsP_3$ type 2 (KM1083) and type 3 (KM1082) receptor proteins were raised against synthetic peptides in mouse. The epitope corresponded to C-terminal regions of specific amino acid sequences for each $InsP_3$ receptor protein of the human $InsP_3$ receptor, type 2 and type 3 were generously donated by Dr Sugiyama

(Sugiyama-T. *et al* 1994; Yamamoto-Hino *et al* 1995). These mouse monoclonal anti-$InsP_3$ type2 and $InsP_3$ type3 antibodies were used as described above at 1:500 dilution in PBS (23°C). The secondary antibody used was anti mouse conjugated FITC or rhodamine (TRITC).

2.2.4.2 Rat cerebellar slices

Cryostat sections of rat cerebella were prepared as described in Section 2.2.3. The $InsP_3$ receptor proteins were identified by either rabbit polyclonal anti $InsP_3$ type 1 antibody or by mouse monoclonal anti type 2 and anti type 3 antibody. The anti $InsP_3$ receptor protein subtype 1 antibody was applied at a dilution of 1:1000 in PBS (Dent-M.R. *et al* 1996). Anti-$InsP_3$ type 2 and anti-$InsP_3$ type 3 antibodies were used at 2μg ml^{-1} in PBS with 2% horse serum (Yamamoto-Hino *et al* 1995). To achieve adequate labelling of the anti-type 2 and -type 3 $InsP_3$ antibodies the slices had to be fixed for 15 minutes with 4% paraformaldehyde in PBS and treated with 0.3% H_2O_2 in methanol for 30 minutes.

2.2.5 Staining with rabbit polyclonal antibody against the connexin 43 protein

Cultured cells were washed in PBS and fixed with 70% ethanol at -20°C for 20 minutes. Glial cells were rinsed in PBS three times after fixing and incubated in mouse polyclonal anti-connexin 43 primary antibody for 1 hour at 37°C with a 1:30 dilution in PBS (Becker *et al* 1995). The cells were washed in PBS and the antibodies, secondary labelled with a Texas red conjugated anti mouse antibody for 2 hours at 1:100 dilution in PBS with 1% BSA at room temperature 23°C. Once rinsed in PBS the cells were mounted on slides with one drop of a mounting medium Vectasheild (Vector Labs).

2.2.6 Dual antibody labelling with anti-GFAP and anti-$InsP_3$ type 1 receptor protein in the rat cerebellum

In order to examine the relationship between Purkinje neurones and glia in the cerebellum double staining experiments were performed. The glial cells were identified by a specific probe mouse polyclonal anti-GFAP antibody and the Purkinje cells by rabbit polyclonal anti-$InsP_3$ type 1 receptor subtype antibody. The frozen cryostat rat cerebellar sections were incubated overnight in a humidified chamber 4°C with anti-GFAP (1:1000 in PBS) and anti-$InsP_3$ (1:1000 dilution in PBS). The sections were then washed in PBS. As the antibodies were raised in either mouse or rabbit, the antibodies were identified by complementary secondary anti mouse conjugated FITC (1:1000 dilution in PBS) and anti rabbit TRITC (1:1000 dilution in PBS) for 1 hour at 23°C. The sections were washed in PBS and mounted in mounting medium covered by a coverslip.

To identify the cell type which express the type 2 and type 3 $InsP_3$ receptor proteins dual antibody labelling experiments were performed (see above section). The co-expression of GFAP and $InsP_3$ type 2 or type 3 receptor proteins would verify which $InsP_3$ receptor protein subtypes are expressed in glia *in situ* (Yamamoto-Hino *et al* 1995).

2.2.7 Photographs

The photographs were taken with a Zeiss Axiophot Photomicroscope, using Kodak Ektachrome 400HC EL 35-36 mm film.

2.3 Whole cell voltage clamp recording

Single cultured type 1 like astrocytes were studied using the whole cell patch clamp technique (Hamill-O. *et al* 1981) after 2-5 days *in vitro* at room temperature 23 °C. Recordings were made using an Axopatch 200A or 1D amplifier with a CV 201A ß=1 or a C4 1/100 headstage. The circuit was completed using a bath ground comprised of a silver chloride pellet inside a syringe body containing bath solution, in contact with the bath via a polyethylene tube also containing bath solution. All surfaces close to input and the steel base-plate were earthed to input ground of the amplifier. Data were recorded on a Racal tape recorder at 3 ¾ inches per second filtered at 2.5kHz, and displayed on an oscilloscope.

In many experiments cultured cells were perfused continually with external solution, of composition in (mM), NaCl 150, KCl 2.8, $CaCl_2$ 2, $MgSO_4$ 2, HEPES 10, pH 7.25, osmolarity 305-315 mosmol (see table 2). The solution was removed by negative pressure from an aquarium pump connected to a collecting vessel. Bubble traps were located in the perfusion lines.

Cerebellar slice preparations were continually perfused with gassed (95% O_2 and 5% CO_2) external solution, mM composition, NaCl 120, KCl 2.5, $CaCl_2$ 2, $MgSO_4$ 2, $NaHCO_3$ 26, NaH_2PO_4 1.25, HEPES 5, Glucose 25, pH 7.25, osmolarity 305-315 mosmol/kg. In some experiments the bath solution was warmed by heating bath holder via a circulating water exchange system to 30 °C.

Internal solution used for all glial cell experiments had the following composition (mM), Kgluconate 153, HEPES 8, Na_2ATP 3, $MgSO_4$ 3 pH 7.25, osmolarity 295-305 mosmols/kg.

Table 2: Solutions used for electrophysiological studies

SOLUTIONS	KREBS	SLICE		ELECTROPHYSIOLOGY	
	GLIAL CULTURE	CEREBELLAR Slice	External	EXTERNAL Solution	INTERNAL Solution
	mM	mM	mM	mM	mM
SALTS					
NaCl	120	120	120	150	-
KCl	2.8	2.5	2.5	2.8	-
$CaCl_2$	-	0.5	2.0	2.0	-
$MgCl_2$	-	-	-	-	-
$MgSO_4$	1.2	2.0	2.0	2.0	3.0
$NaHCO_3$	25	26	26	-	-
NaH_2PO_4	-	1.25	1.25	-	-
KH_2PO_4	1.2	-	-	-	-
EGTA	-	-	-	-	-
Mg(ATP)	-	-	-	-	-
Na_2(ATP)	-	-	-	-	3.0
Glucose	15	25	25	-	-
BSA	3mg/ml	-	-	-	-
Kgluconate	-	-	-	-	153
HEPES		5	5	10	8
pH	7.2/7.3	7.2/7.3		7.25	7.2
WITH	1M HCl	gas (95% O_2,5%CO_2,)		1M NaOH	1MKOH

Micropipettes were made from borosilicate glass either thick wall (1.5 mm O.D X 0.86 mm I.D) or thin wall (1.5 mm O.D X 1.17 mm I.D) pulled on a Narishige puller and polished with a heating coil. Pipette resistances were between 10-15 MΩ after pulling. The morphology of the flat cells precluded the use of electrodes with large tip diameters. In order to get a tight seal, pipette tips were placed slightly off centre on the large cell soma of protoplasmic type 1 cells. The membranes of these cells appeared to be quite fluid and often the membrane would enter the end of the electrode to form a rod like structure before a seal would occur. The series resistance in these type1 astrocytes ranged from 10-50MΩ.

Another major problem with clamping these cells was their large size . The whole cell capacitances of these type 1 astrocytes range between 50-100pF. For non spherical cells (such as type 1 astrocytes and Bergmann glial cells) plasma membrane areas away from the cell-electrode junction can not be clamped accurately.

2.3.1 Liquid junction potentials

A potential forms at the junction of solution of different ionic compositions. When the electrode containing internal solution is placed in the bath containing external solution a junction potential difference exists which, at the start of the experiment, is compensated by setting the pipette potential to make the current zero. When the electrode seals on the cell the junction potential disappears, but the compensated voltage remains as an error in the pipette potential. The error can be measured prior to the experiment, and is a constant for the same two solutions, so can be corrected for at the end of the procedure.

To measure the junction potential in these experiments a patch pipette filled with internal solution was placed into the recording chamber which contained identical internal solution. The recording bath reference was a pipette containing 3M KCl. The amplifier output was set to zero. The bath solution was then replaced with external solution, which resulted in an offset potential due to the liquid junction potential. For the solutions (see table 2) Kgluconate internal and culture external solution there is liquid junction potential of -7.5mV bath-pipette, for slice external solution and Kgluconate

internal liquid junction is -3.6mV. The pipette potentials were not corrected for, within the data.

2.4 Fluorescent calcium indicators

Indicators that change their fluorescence as a consequence of calcium binding can be used to obtain quantitative estimates of intracellular calcium concentrations. This is because the fluorescent intensity of the calcium indicators represent the concentration of calcium bound (or calcium free) indicator molecules. These indicators were used in conjunction with the whole cell patch clamp technique to study the kinetics of astrocytic cytosolic calcium transients, giving information on the time course and amplitude of intracellular calcium fluxes.

For these experiments the low affinity calcium indicators furaptra (Raju *et al* 1989 ; Molecular Probes Eugene, Ore., USA) and fura-2-ff (London *et al* 1996) were used. For measuring the rates of change of $[Ca^{2+}]i$ low affinity indicators are more accurate than high affinity calcium indicators. High affinity calcium indicators have calcium dissociation constants Kd ($[Ca^{2+}]$ at 50% of the maximum binding) which are around resting levels of internal cytosolic calcium concentration e.g fluo-3 Kd=0.4μM. Previous experiments with $InsP_3$ induced calcium transients in Purkinje cells, hepatocytes and endothelial cells have shown that there are problems associated with these high affinity indicators in reporting accurately the large fast cytosolic calcium transients when compared to lower calcium affinity dyes (e.g furaptra Kd=48μM; Ogden-D. *et al* 1995). This is due to the hyperbolic, saturating, relationship between calcium bound indicator and free $[Ca^{2+}]$ hence between fluorescence and free $[Ca^{2+}]$. This underestimate of $[Ca^{2+}]$ is further exaggerated with high affinity indicators because cytosolic calcium changes are not uniform in cells. Thus Ca^{2+} efflux from stores causes localised high $[Ca^{2+}]i$ transients adjacent to the calcium channel proteins. These localised high calcium transients distort the spatially averaged signal because the fluorescence change is saturated at high $[Ca^{2+}]i$ close to stores but not at lower $[Ca^{2+}]$ further away. The overall result is that the calcium change measured from the recorded area is an underestimation of both the net $[Ca^{2+}]$ change, and, because the local $[Ca^{2+}]$ is higher initially than later, particularly the rate of calcium efflux measured by the change of fluorescence.

A further complication is that calcium indicators act as mobile buffers (Grynkiewicz-G. & Tsien-R.Y., 1985). Within the cytosol there are endogenous buffers, which bind calcium at physiological levels and are relatively immobile (Zhou-Z. & Neher-E. 1993). The calcium indicators however compete for calcium with the endogenous fixed buffers, dissipating [Ca^{2+}] gradients and affecting the cellular calcium regulating mechanisms that are normally activated at high localised calcium levels. This effect is greater with high affinity indicators. Thus, high affinity indicators can cause a change in the cellular processes that affect the calcium release channels that are examined in these experiments.

The rate of calcium dissociation is faster from low affinity than high affinity indicators (Hollingworth-S., *et al* 1992). Therefore low affinity indicators have a rapid response time of less than 1 millisecond and so can be used to estimate rapid calcium transients. The higher Kd values of the low affinity indicators also means that the fluorescence change is linear with higher [Ca^{2+}]i changes. The buffering effects are reduced because a smaller proportion of indicator is bound with calcium (Ogden-D. *et al* 1995).

The characterisation of furaptra binding calcium is Kd=48μM (22°C, ionic strength I=148mM, Konishi-M.,*et al* 1991; 16°C, Ogden-D. *et al* 1995) and for Mg^{2+} and furaptra Kd=3.6mM at 23°C, and 1.5mM at 37 °C Raju *et al* 1989 .

2.4.1 Characterisation of calcium indicator fura-2-FF

Another low affinity indicator that behaves like furaptra is fura2-FF (2-[2(5-carboxyethyl-oxazole)]-5-[2-(2-bis(carboxymethylmethyl)amino-5,6-difluorophenoxy)]ethoxy-6-bis(carboxymethyl-methyl)aminobenzofuran, London *et al* 1996 ; Texas Fluorescence Labs). The advantage of this indicator over furaptra is that its affinity for magnesium is much lower than that of furaptra. To test this the excitation and emission spectra for fura-2-FF were measured in Ca^{2+} and Mg^{2+} containing solutions using a spectrofluorimeter (See table 3). Calcium concentrations were buffered between 0-1.3mM using 40mM K-citrate buffer. The total magnesium and the fura-2-FF concentration were 20mM (free [Mg^{2+}]=1.85mM) and 10μM respectively. A 6ml solution containing the K-citrate, magnesium and dye was split into two aliquots of 2ml

and 4ml. Into the 2ml solution 19mM calcium was added, to give a free calcium ion concentration of 1280μM (pH 7.2) i.e High calcium. Free ion concentration estimates were taken from the stability constants of Ca^{2+} and Mg^{2+} binding to citrate (Dr K.Macleod $K_{ca}=2.99x10^{-4}$, $K_{Mg}=4.22x10^{-4}$ at 25°C, I=0.1M, pH 7.0 (see table 3). The second solution had low [Ca^{2+}] pH 7.2. However distilled water was found to contain 6μM calcium so 100μM EGTA was also added to the low [Ca^{2+}]. The excitation spectra were measured at an emission wavelength of 510nm for 500μl of zero [Ca^{2+}] solution in a cuvette with the spectrofluorimeter. This was repeated for high [Ca^{2+}] solution. To measure the emission spectrum the cuvette remained in the spectrofluorimeter and the test samples excited at a wavelength of 420nm. Initially 500μl of zero [Ca^{2+}] was placed into the cuvette and its emission fluorescence recorded. Then 250μl of the solution was removed and 250μl of high [Ca^{2+}] added, mixed thoroughly to give half the original (free [Ca^{2+}] 640μM) concentration by dilution. This procedure repeated until 1μM free [Ca^{2+}] remained. Finally all of the solution was removed and cuvette washed and air dried for final high (free [Ca^{2+}] 1280μM) calcium measurement.

To measure the Kd for Mg^{2+} and fura-2-FF binding a similar procedure was used. A 4ml solution contained 40mM K-citrate, 100μM EGTA, 10μM fura-2-FF, was split into two aliquots a 1ml and 3ml. One (3mls) contained no magnesium, and the other (1ml) had high [Mg^{2+}] of 60mM which was 20.8mM free [Mg^{2+}]. The solutions were periodically diluted to give a range of free [Mg^{2+}] from 0 through to 20.8mM.

All the fura-2-FF spectra characterisation experiments were conducted at room temperature 23 °C.

Table 3 Contents of solutions for spectral characterisation of fura-2-FF

10μM Fura-2-FF	*[Ca^{2+}] in Solution*		*[Mg^{2+}] in Solution*		*[K-citrate] in solution*	
	Total (mM)	*Free (mM)*	*Total (mM)*	*Free (mM)*	*Total (mM)*	*Free (mM)*
High [Ca^{2+}]	19	1.280	20	1.853	40	4.134
Low [Ca^{2+}]	0	0	20	0.405	40	20.41
High [Mg^{2+}]	0	0	60	20.8	40	0.796
Low [Mg^{2+}]	0	0	0	0	40	40

Free ion concentrations ([*]) are derived from

Tot=Total, F=free, Cit=Citrate $^{3-}$, Ca=Calcium ion $^{2+}$, Mg=Magnesium ion $^{2+}$
Stability Constants from The Chemical Soceity, Stability Constants of Metal Ion Complexes, Section II Ed. L.G. Sillen & A.E. Martell
(1) KCa=[Ca][Cit]/[Ca-Cit] =$2.99 \times 10^{4-}$,

(2) KMg=[Mg][Cit]/[Mg-Cit] = $4.22 \times 10^{4-}$

(3) [Ca.tot]=[Ca F]+ [Ca-Cit]

(4) [Mg.tot]=[Mg F]+[Mg-Cit]

(5) [Cit.tot]=[Cit -3]+[Mg-Cit]+[Ca-Cit]

figure 2.5.1 Fluorescence spectra of fura-2-FF and furaptra

Figure 2.5.1 A+B+C: Fluorescent Spectra of fura-2-FF to varying [Ca^{2+}].

Graph A shows the excitation spectra at 510nm emission for fura-2-FF in high and zero [Ca^{2+}]. At 420nm point (dashed line) in the excitation spectra the fluorescence intensity at zero [Ca^{2+}] is 20 fluorescence units whereas at high [Ca^{2+}] the fluorescence is near zero. Thus for microspectrofluorimetry experiments the indicator fura-2-FF was excited by light of wavelength 420nm with a 420 ± 20 nm band pass filter. At this wavelength the fluorescence signal is high for resting levels of free [Ca^{2+}]i. As [Ca^{2+}] increases the fluorescence signal decreases. This change in fluorescence can be measured by a PMT and a quantitative estimate of [Ca^{2+}] level calculated.

Graph B demonstrates the emission spectra of fura-2-FF in solutions with [Ca^{2+}] buffered between 0=1280μM range, when excited by light of 420nm wavelength. The fluorescence emission spectra of fura-2-FF peaks at wavelength 510nm (dashed line). The fluorescent response to varying [Ca^{2+}] is near linear so smaller changes in [Ca^{2+}]i can be distinguished as greater changes in fluorescence. At high [Ca^{2+}] the 420nm excited fluorescence signal is quenched almost to zero. Thus during an experiment F_{camax} can be determined by measuring intrinsic background fluorescence. The F_{camin} value was taken as the equilibrium peak of the indicators fluorescence after entry into a cell when [Ca^{2+}]i is low i.e resting [Ca^{2+}]i levels.(see figure 2.5.2).

Graph C shows normalised fluorescence plotted against free [Ca^{2+}]. The points are fitted by a 1:1 Ca^{2+} binding to fura-2-FF i.e indicator has a single binding site for Ca^{2+} ions. The Kd for Ca^{2+} binding to fura-2-FF is 29.8μM (K=29.8μM, 25°C, ionic strength I=100mM).

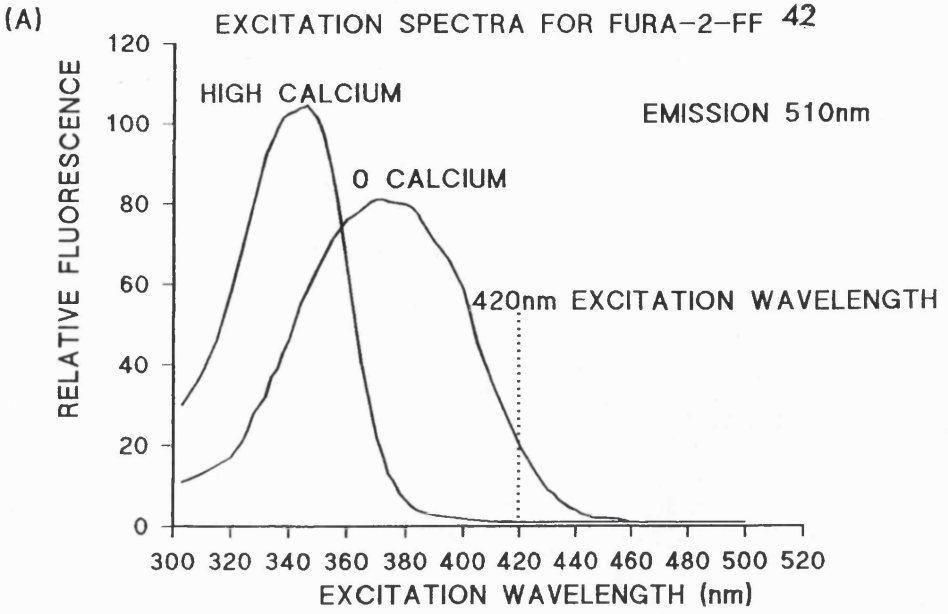
(A)
EXCITATION SPECTRA FOR FURA-2-FF
HIGH CALCIUM
EMISSION 510nm
0 CALCIUM
420nm EXCITATION WAVELENGTH
RELATIVE FLUORESCENCE
EXCITATION WAVELENGTH (nm)

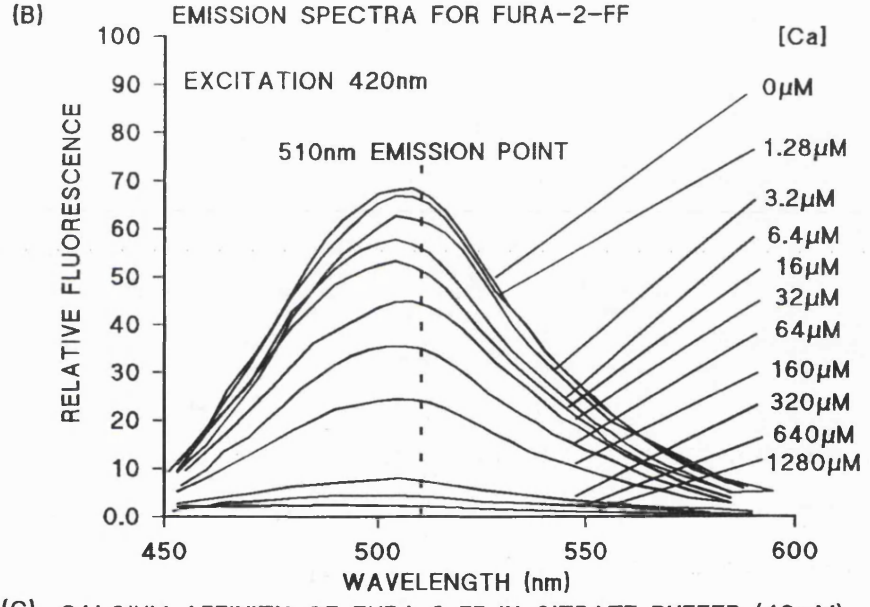
(B)
EMISSION SPECTRA FOR FURA-2-FF
EXCITATION 420nm
510nm EMISSION POINT
[Ca]
0μM
1.28μM
3.2μM
6.4μM
16μM
32μM
64μM
160μM
320μM
640μM
1280μM
RELATIVE FLUORESCENCE
WAVELENGTH (nm)

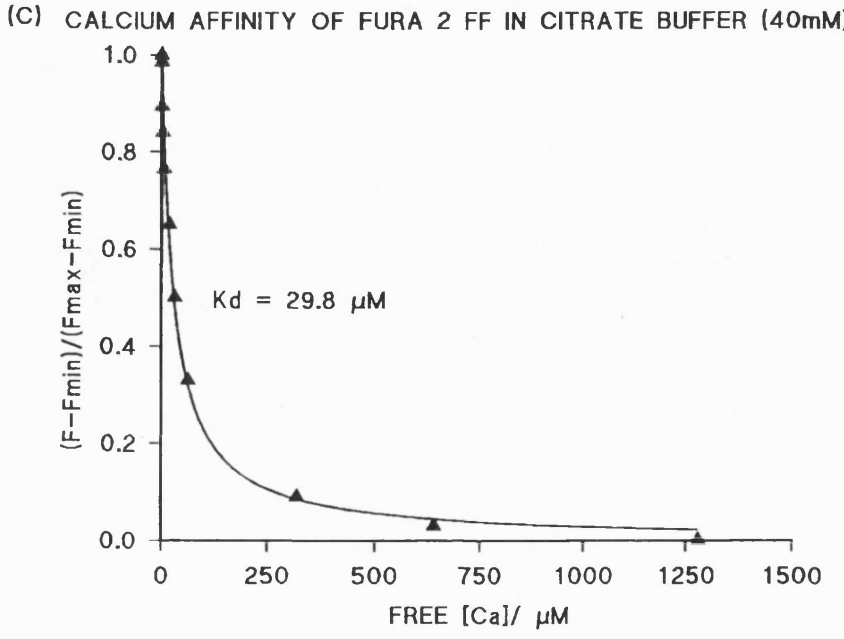
(C) CALCIUM AFFINITY OF FURA 2 FF IN CITRATE BUFFER (40mM)
Kd = 29.8 μM
(F-Fmin)/(Fmax-Fmin)
FREE [Ca]/ μM

Figure 2.5.1 D+E: Fluorescence spectra of fura-2-FF to varying [Mg^{2+}]

Figure D shows the emission spectra in for fura-2-FF in the presence of Mg^{2+} buffered between 0-20.8mM with citrate. Fura-2-FF was excited at 420nm wavelength of light and the emission light recorded between 450nm to 595nm. The graph shows the fluorescence measured in arbitrary units plotted against light wavelength in nm. The spectra peaks at 510nm. The changes in [Mg^{2+}] between 0 and 10.4 mM cause a 20 (arbitrary arb) units change in fluorescence.

Figure E displays the normalised fluorescence plotted against free [Mg^{2+}]. The points were fitted with a 1:1 binding of Mg^{2+} to fura-2-FF. The Kd is 18.40mM for fura-2-FF binding to Mg^{2+} (K=18.40 mM, 25°C, ionic strength I=100mM).

(D) Emission spectra for fura-2-FF

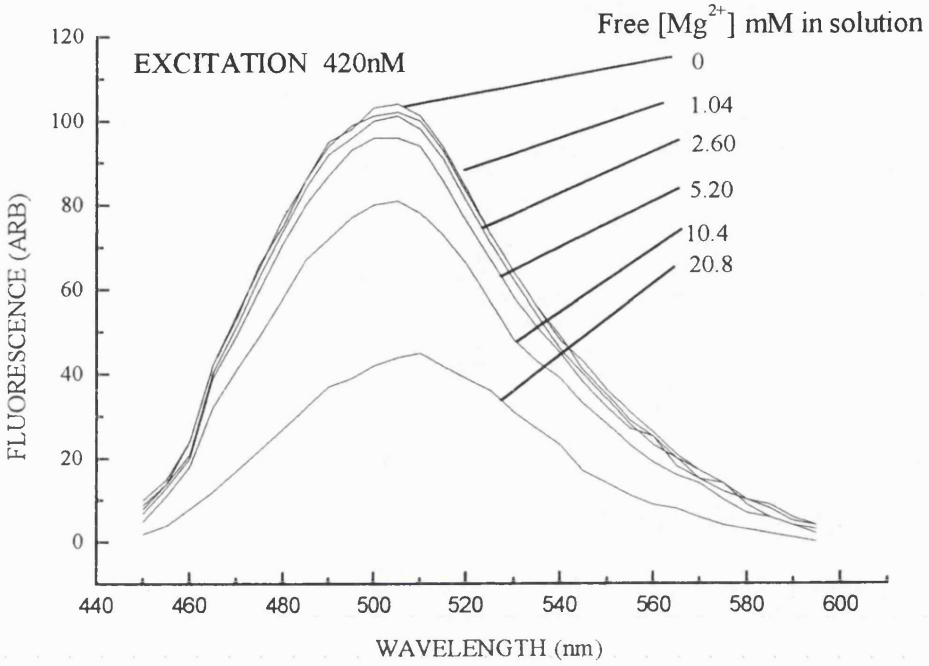

(E) Magnesium affinity of fura-2-FF in citrate buffer

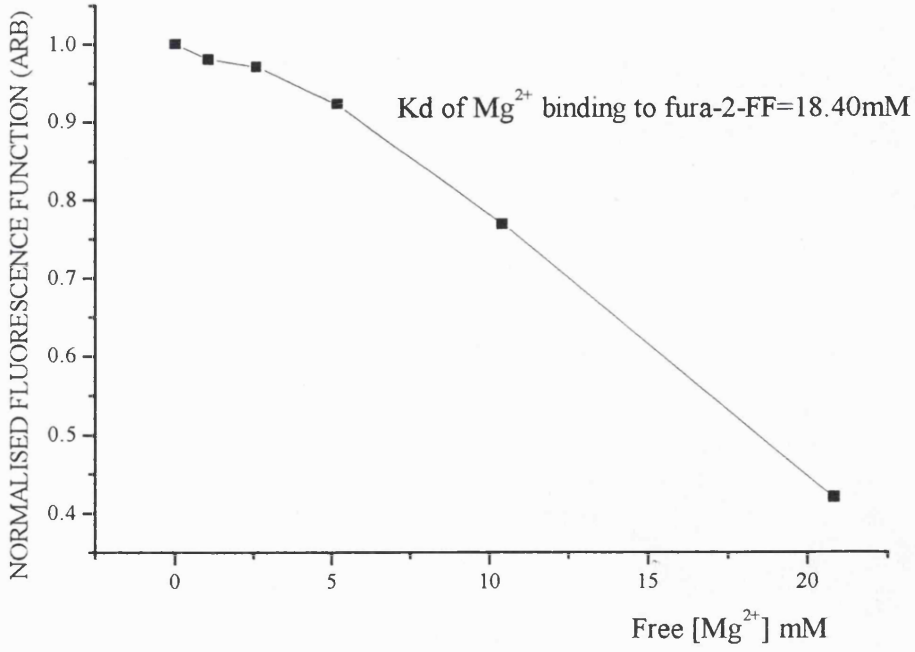

Figure 2.5.1 F, G, H Fluorescence spectra of furaptra to varying [Ca^{2+}].

from (Ogden-D. *et al* 1995)

Figure F: Excitation spectra of furaptra measured at 510nm emission. As with fura-2-ff at high [Ca^{2+}] the fluorescence is low, compared to high fluorescence at zero calcium.

Figure G :Emission spectra of furaptra, excited at 420nm wavelength of light to a range of [Ca^{2+}] 0-1000μM. This spectra is similar to the fura-2ff emission. At zero calcium fluorescence is high compared to 1mM calcium where fluorescence levels are low. The greatest fluorescence changes for varying [Ca^{2+}] occur at 510nm emission point.

Figure H : The calcium affinity of furaptra Kd =48μM using a citrate buffer.

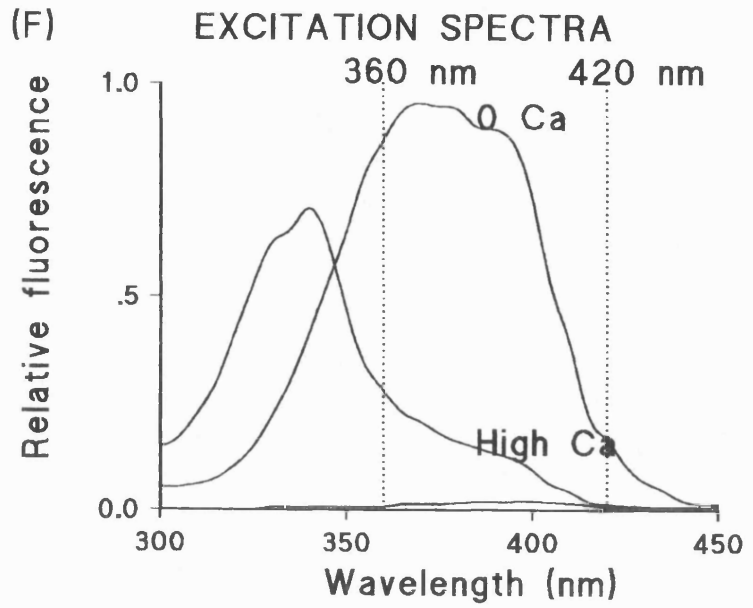
(F)
EXCITATION SPECTRA
360 nm
420 nm
0 Ca
High Ca
Relative fluorescence
1.0
.5
0.0
300
350
400
450
Wavelength (nm)

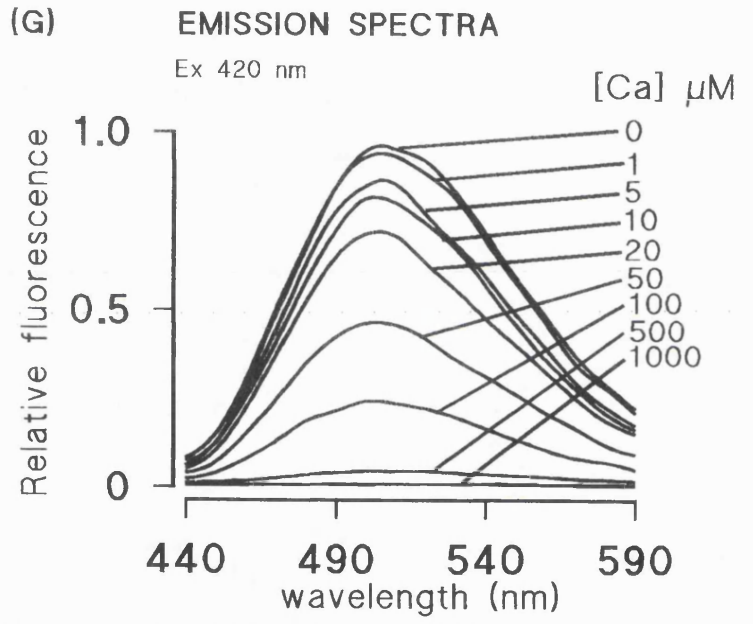
(G)
EMISSION SPECTRA
Ex 420 nm
[Ca] μM
0
1
5
10
20
50
100
500
1000
Relative fluorescence
1.0
0.5
0
440
490
540
590
wavelength (nm)

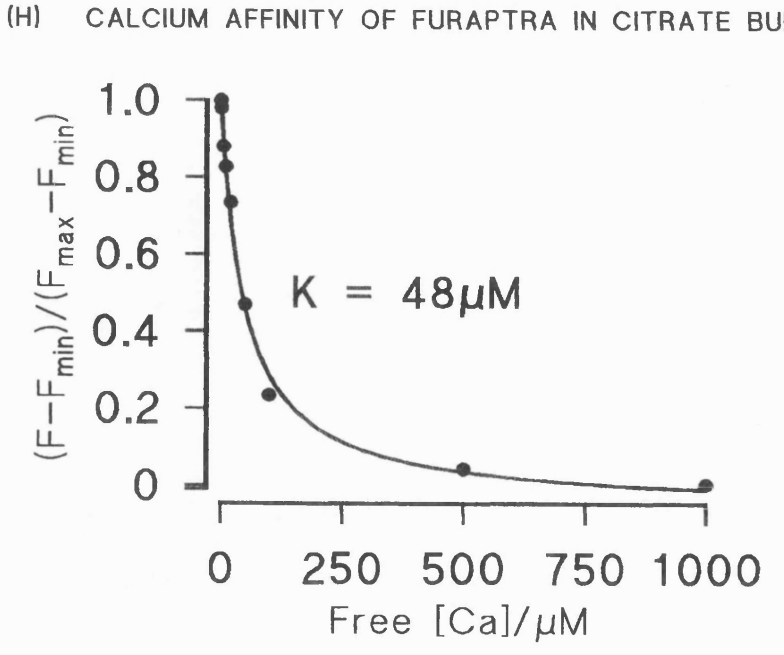
(H) CALCIUM AFFINITY OF FURAPTRA IN CITRATE BUFFER (40mM)
(F−Fmin)/(Fmax−Fmin)
1.0
0.8
0.6
0.4
0.2
0
K = 48μM
0
250
500
750
1000
Free [Ca]/μM

Fura-2-FF has a higher affinity for calcium ions (K_{ca}=29.8μM) than furaptra, (48μM) but a lower affinity for magnesium K_{mg}=18.4mM, furaptra 3.6mM. Fura-2-FF can be used to measure cytosolic free $[Ca^{2+}]i$ under the same excitation and emission conditions as furaptra.

Furaptra was excited at wavelength 420nm by light passed through a band pass filter 420±20nm and recorded at an emission of 510nm. Under these conditions the fluorescence of the indicator was quenched to almost zero for high calcium concentrations. The fluorescence recorded in the cell attached mode was taken as an estimate of fluorescence at saturating calcium concentration, F_{maxCa} (Ogden-D. *et al* 1995). During whole cell recording the indicator entered the cell and reached equilibrium in about 8 minutes (see figure 2.5.2). This plateau value of fluorescence was at resting $[Ca^{2+}]i$ taken as (F_{minCa}.). Free $[Ca^{2+}]i$ changes were calculated from the fluorescence measurements (F), in the relation below (equation 1), Kd is the dissociation constant for the calcium and dye interaction (see equation 8):

$$[Ca^{2+}]i = Kd \cdot (F_{minCa} - F) / (F - F_{maxCa}) \quad \ldots\ldots (1)$$

Figure 2.5.2 Fluorescence loading curve of a type 1 astrocyte *in vitro*

The curve shows a fluorescence trace of an astrocyte (*in vitro*) cell being loaded with furaptra during a whole cell patch clamp experiment. It shows fluorescence as photon counts (ΔF) against time in seconds. F_{maxCa} shows the background fluorescence as no indicator has entered the cell and is the fluorescence expected at high calcium under these conditions is almost zero (F_{maxCa}). F_{minCa} is the fluorescence at the resting calcium concentration of the cell. Furaptra and fura-2-FF have a low affinity for calcium so at resting the fluorescence is within 1% of fluorescence at zero calcium.

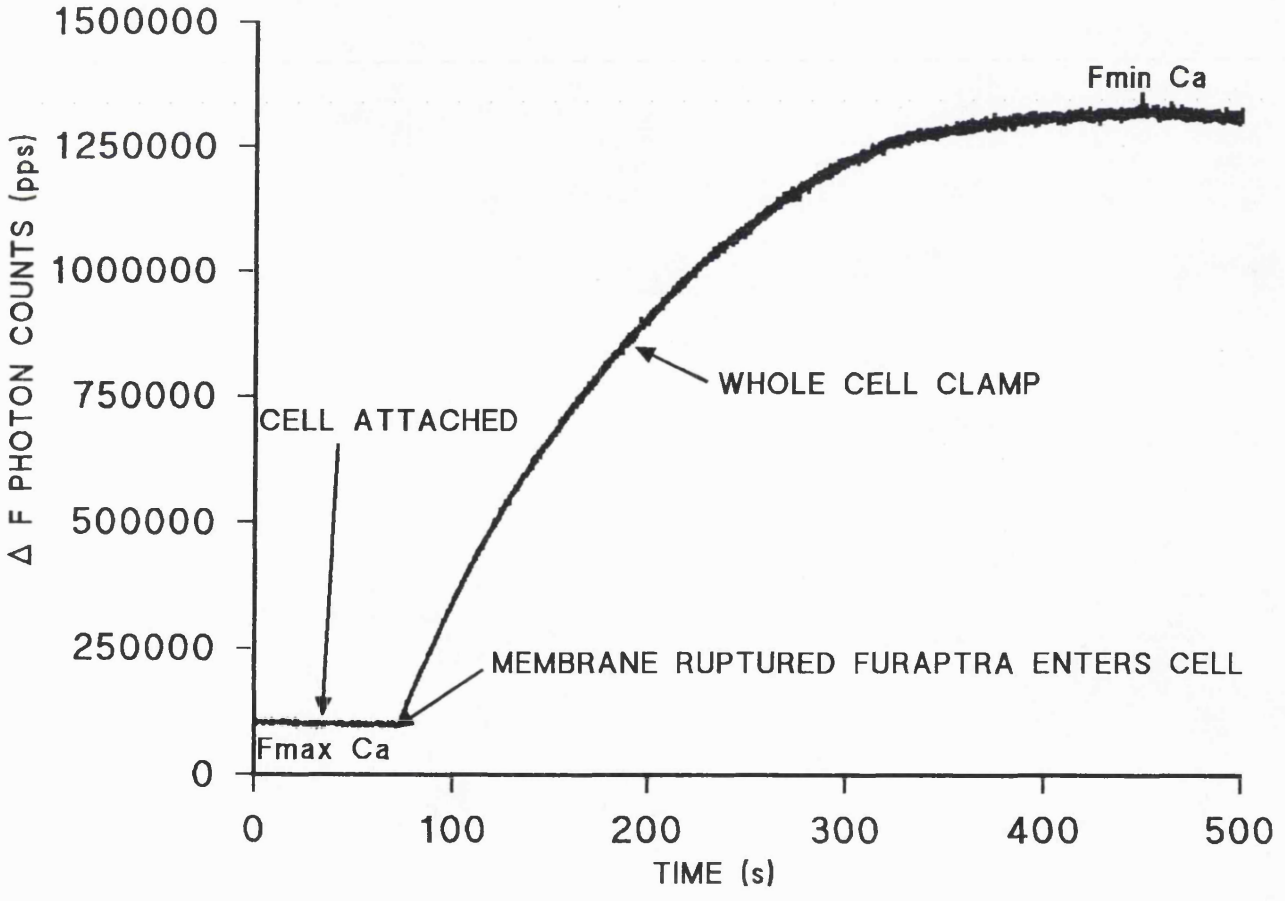

(i) Derivation of equation (1)

$[Ca^{2+}]i = Kd .(F_{minCa} - F) / (F - F_{maxCa})$.....(1)

Fluorescence (F_A) due to Ca Indicator complex concentration $[D_{ca}]$,

is $F_A = A.[D_{ca}]$

Fluorescence (F_B) at Free Indicator concentration $[D_F]$ is

$F_B = B.[D_F]$

Where A and B are constants.

So Total $F = F_A + F_B = A[D_{ca}] + B[D_F]$.....(2)

and total indicator concentration $[D_T] = [D_{ca}] + [D_F]$.....(3)

For F_{maxCa}, $[D_F] = 0$. and so $[D_{ca}] = [D_T]$

Thus $F_{maxCa} = A.[D_T]$, hence

$A = F_{maxCa}/[D_T]$.....(4)

Similarly for F_{minCa},

$[D_{ca}] = 0$ and so $[D_F] = [D_T]$

thus $F_{minCa} = B.[D_T]$,

$B = F_{minCa}/[D_T]$.....(5)

Substituting (4) and (5) into (2) ,

Total $F = (F_{maxCa}/[D_T]).[D_{ca}] + (F_{minCa}/[D_T]).[D_F]$.....(6)

$F.[D_T] = F_{maxCa}[D_{ca}] + F_{minCa}.[D_F]$

as in equation (3) $[D_T] = [D_{ca}] + [D_F]$,

substitute (3) into (6)

$F.([D_{ca}] + [D_F]) = F_{maxCa}[D_{ca}] + F_{minCa}.[D_F]$

$F.[D_{ca}] + F.[D_F] = F_{maxCa}.[D_{ca}] + F_{minCa}.[D_F]$

$F.[D_{ca}] - F_{maxCa}.[D_{ca}] = F_{minCa}.[D_F] - F.[D_F]$

$[D_{ca}].(F - F_{maxCa}) = [D_F] .(F_{minCa} - F)$

$[D_{ca}]/[D_F]=(F_{minCa}-F)/(F-F_{maxCa})$ .....(7)

as the reaction is $C+D_F \Leftrightarrow D_{Ca}$ where, free calcium concentration = C

then the equilibrium dissociation constant is $Kd=[C].[D_F]/[D_{ca}]$.....(8)

which rearranges to $[D_{ca}]/[D_F]=[C]/Kd$.....(9)

substituting (9) into (7) to give (1)

$[C]/Kd=(F_{minCa}-F)/(F-F_{maxCa})$

so $[C]=Kd\ (F_{minCa}-F)/(F-F_{maxCa})$.....(1)

2.4.2 Microspectrofluorimetry and calcium measurements

Microspectrofluorimetry combined with the whole cell clamp technique were used for the calcium measurements of the $[Ca^{2+}]i$ of glial cells. Furaptra and fura-2-FF were used at a single excitation wavelength 420nm as originally described by (Konishi-M.,*et al* 1991) and adapted to measure calcium kinetics in voltage clamped cells (Ogden-D. *et al* 1995). The cells were epi-illuminated by light from a quartz halogen 100 watt bulb on a Nikon inverted microscope. The light passed through a band pass filter (420±20nm) through 90° by a long pass 455 nm dichroic mirror to the objective. A 40X, 1.3NA oil immersion objective was used to view the cells. A rectangular diaphragm was used to isolate light from only the patched cell. The emitted light from the cells passed via the objective back through the 455nm dichroic mirror, a barrier filter (470nm) to the photomultiplier tube (PMT) for detection. Located in front of the PMT was a dichroic mirror that deflected light of wavelength greater than 780nm to a charged coupled device (CCD) video camera which displayed on a Hitachi monitor. The PMT operated in photon counting mode with a Tecmar interface and PTI software, and in conjunction with a Cairn Research photon counting board to produce a corrected analogue signal was recorded onto FM tape. The fluorescence analogue signal was recorded at 3¾ inches per second and filtered at 1.25kHz (see figure 2.5.3.A).

Figure 2.5.3 (A) Experimental apparatus setup for *in vitro* studies.

The diagram represents the experimental setup for recording from cultured cells, grown on quartz coverslips. The system is focused around an inverted Nikon microscope. The fluorescent changes were measured using a PMT Cairn research photon counting system. All data were recorded on computer using PTI software and a Racal tape recorder. The apparatus was encompassed by a Faraday cage.

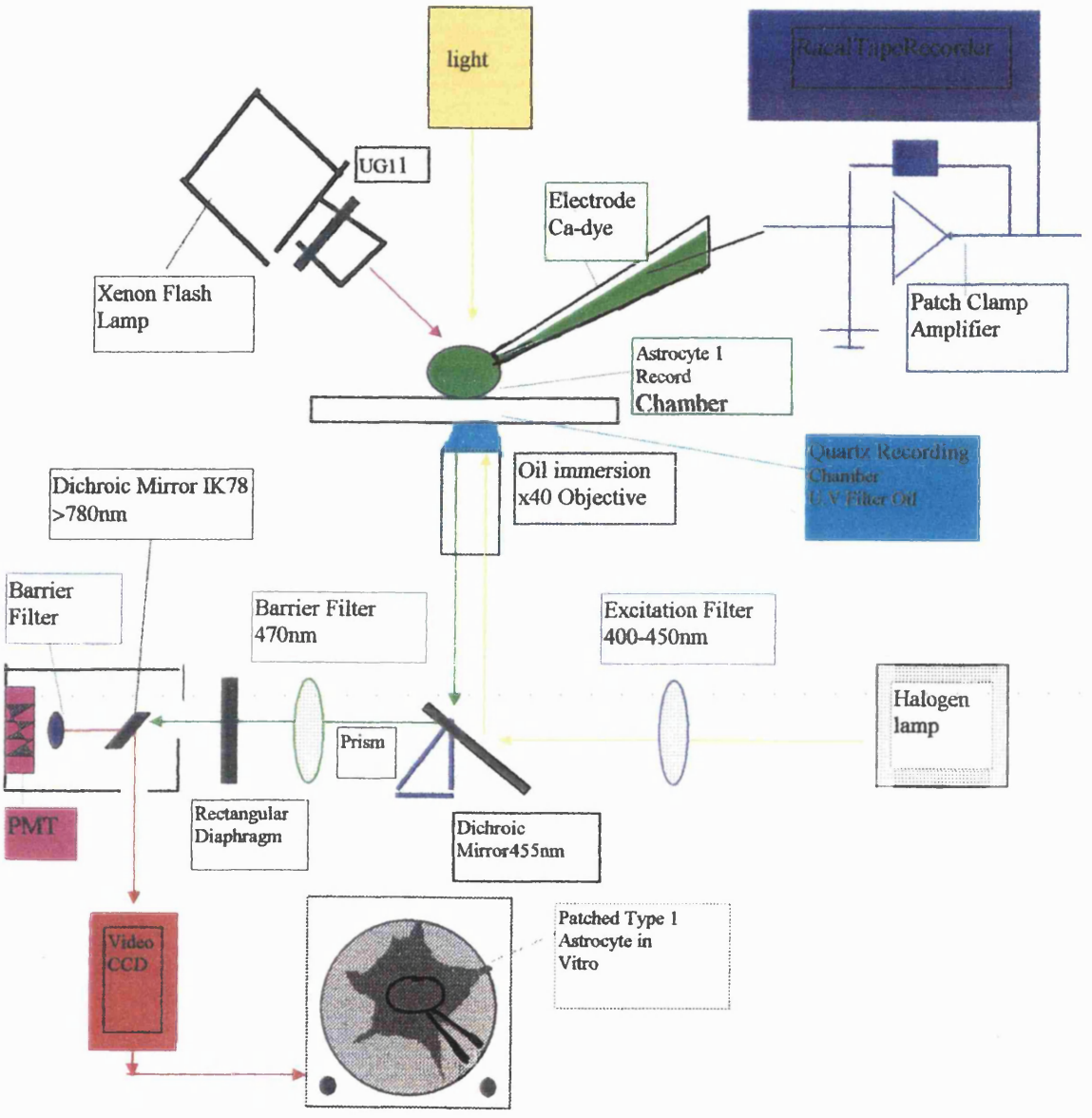
light
Racal TapeRecorder
UG11
Electrode
Ca-dye
Xenon Flash
Lamp
Patch Clamp
Amplifier
Astrocyte 1
Record
Chamber
Quartz Recording
Chamber
U.V Filter Oil
Oil immersion
x40 Objective
Dichroic Mirror IK78
>780nm
Barrier
Filter
Barrier Filter
470nm
Excitation Filter
400-450nm
Halogen
lamp
Prism
PMT
Rectangular
Diaphragm
Dichroic
Mirror455nm
Video
CCD
Patched Type 1
Astrocyte in
Vitro

For the slice experimental setup the recording system was similar (see figure 2.5.3 B). An upright Zeiss Axioskop was used to visualise the cells in a slice. For illumination, light from a 100 watt quartz halogen bulb was transmitted into the condenser. The slice was illuminated from below. By placing a UG1 filter in the light path, infra red illumination (650-800nm) was sometimes used to view the slice (Dodt-H. & Zieglgansberger-W. 1990). The fluorescence excitation was from a quartz halogen lamp located in the epi-illumination port of the microscope via a 400-440nm filter. A dichroic mirror (455nm) directed light shorter than 455nm down to the Zeiss water immersion objective, (X40 0.75NA). The light emitted from a single cell was isolated by a rectangular diaphragm. In cell attached mode, before the indicator had diffused into the cell, a fluorescence background reading was taken. Once in whole cell configuration the indicator diffused into the cell. Light of longer wavelength emitted from the cell passed through the dichroic mirror, a 470nm long pass barrier filter to a second dichroic mirror. This dichroic mirror directed light of wavelength less than 700nm, 90° to the photomultiplier which was located at the top of the microscope. The longer wavelengths of light passed through the mirror to the CCD video camera and were displayed on a monitor. The UG1 filter in the transmitted light path allowed the image to be illuminated by infra red light. The use of infra red illumination enhances cellular detail by reduced light scattering in the slice. The video also allowed the preparation to be viewed without having to use the eyepieces and thus keeping movement to a minimum. (see setup figure 2.5.3 B) .

Figure 2.5.3.(B): Experimental set up for recording from brain slices

Figure B demonstrates the arrangement of the apparatus needed for the experiments performed on brain slices using an upright Zeiss microscope. The microscope was mounted on an anti-vibration air table. The central panel of the diagram represents the equipment which was surrounded by a Faraday cage.

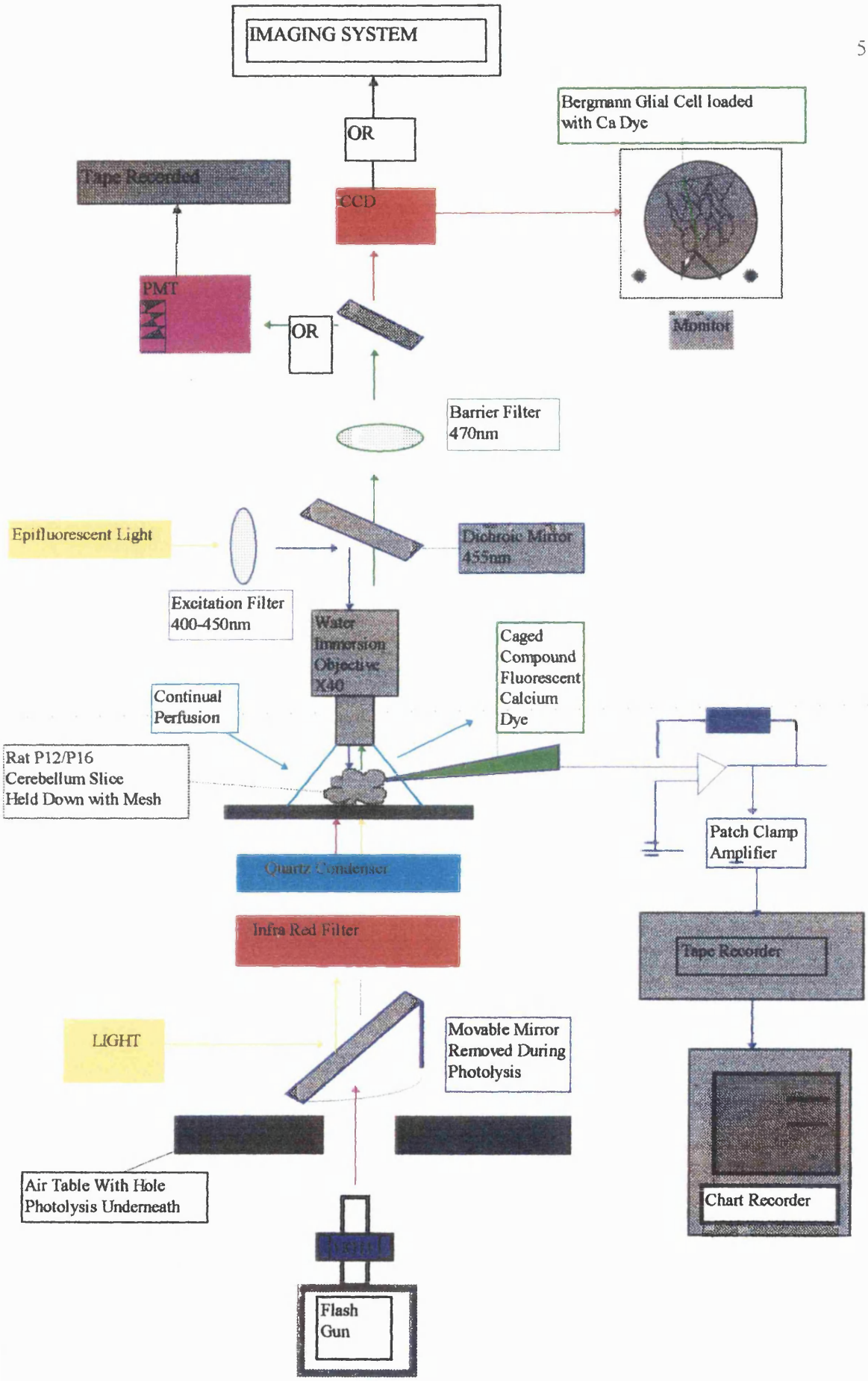
IMAGING SYSTEM
OR
Bergmann Glial Cell loaded with Ca Dye
Tape Recorded
CCD
PMT
OR
Monitor
Barrier Filter 470nm
Epifluorescent Light
Dichroic Mirror 455nm
Excitation Filter 400-450nm
Water Immersion Objective X40
Caged Compound Fluorescent Calcium Dye
Continual Perfusion
Rat P12/P16 Cerebellum Slice Held Down with Mesh
Patch Clamp Amplifier
Quartz Condenser
Infra Red Filter
Tape Recorder
LIGHT
Movable Mirror Removed During Photolysis
Air Table With Hole Photolysis Underneath
Chart Recorder
Flash Gun

2.5 Application of physiological agonists

The cells were grown on glass coverslips which were coated with poly-L-lysine. Pipettes were filled with Kgluconate internal and 500μM furaptra. A cell was patched and after the membrane ruptured in whole cell configuration, furaptra diffused into the cell until equilibrium was established between pipette and cells contents.

Either a U-tube perfusion system (Krishtal & Pidoplichko V.I. 1980) with a fine output point, or a pressure ejection "puffer" microelectrode were placed by micromanipulator to direct solution at the cell. In the case of pressure ejection the electrode holder was connected to a regulated oxygen cylinder via a twelve volt relay valve, which allowed the compound to be "puffed" out directly over the cell with a time course of 0.25 seconds. The time for application was measured by placing Lucifer yellow in the puffer pipette and measuring the time taken for the Lucifer yellow fluorescent signal to equilibrate. All fluorescence and membrane currents were recorded on FM tape and on the computer.

2.6 Caged myo-inositol 1,4,5-trisphosphate and 1-D-myo-inositol 1,4-bisphosphate 5-phosphorothioate

Caged $InsP_3$ has a 2-nitrophenylethyl group esterified on one of its phosphates (Walker *et al* 1989). The caged $InsP_3$ used in these studies was esterified at the 5' phosphate (P5). This compound was synthesised and generously provided by Dr D.R. Trentham (NIMR). The 5' isomer showed no calcium mobilising activity at concentrations up to 50μmol l^{-1} at the $InsP_3$ receptor site (Walker *et al* 1989 : Ogden-D.C., *et al* 1990).

Caged 1-D-myo-inositol 1,4-bisphosphate 5-phosphorothioate (5-thio-$InsP_3$) was used as a photolabile source of a stable analogue of $InsP_3$. The 5-thio-$InsP_3$ is resistant to break down by $InsP_3$ 5-phosphatase. 5-thio-$InsP_3$, when released from the cage is five times less potent than the $InsP_3$, released by photolysis from caged $InsP_3$ (Wootton-JF; *et al* 1995). Caged 5-thio-$InsP_3$ was kindly provided by Dr D.R. Trentham (NIMR). (Figures 2.7.0 A+B from Ogden-D. & Khodakhah-K. 1996).

Figure 2.7: Chemical structure of caged compounds

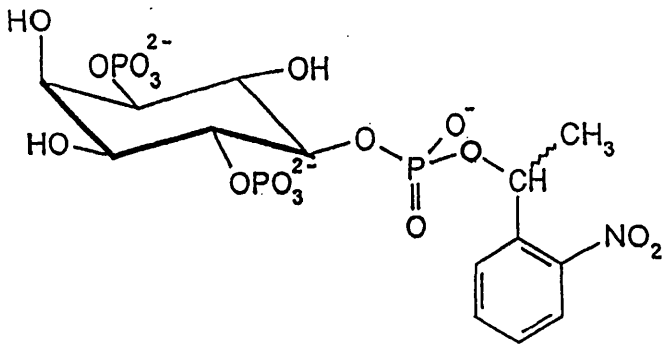

(A) Chemical structure of caged $InsP_3$

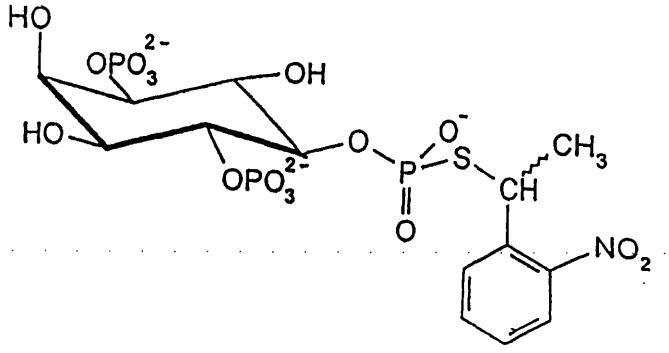

(B) Caged 5-Thio-$InsP_3$

2.6.1 Flash photolysis of caged compounds

Flash photolysis was produced by a 1ms pulse of U.V light from the arc of a xenon flash lamp (or gun, Rapp-G. & Guth-K. 1988). The gun was positioned an angle of 38°, at 4 cm from the preparation on the inverted microscope. The light passed through a UG11 filter (wavelength 280-360nm) and convex lens (63 P 25mm Comar working distance 4cm) focused to give a 0.5cm spot (see figure 2.5.3.A). For some of the experiments a Chadwick-Helmutt Strobex 238 gun and power supply was used, the maximum power output at 150watts/sec was 30mJ measured with a bolimeter in near ultra violet (U.V). For other photolysis experiments a Rapp gun and power supply was used. Maximum power for this gun was 90-110mJ output in near U.V (see figure 2.7.1 taken from Ogden-D. & Khodakhah-K., 1996, and McCray-J.A. & Trentham-D.R. 1989). The photolysis of caged $InsP_3$ is a two step process. First the absorption of a

photon from the U.V flash generates enough energy to form activated aci-nitro intermediates in a nanosecond time scale, followed by a slower dark phase (10-15ms) decay stage, of the intermediates, to release $InsP_3$. When photolysed caged $InsP_3$ releases $InsP_3$ molecules, protons and nitroso-aceto-phenone byproduct which has no toxic affect within cells at concentrations less than 50 μM.

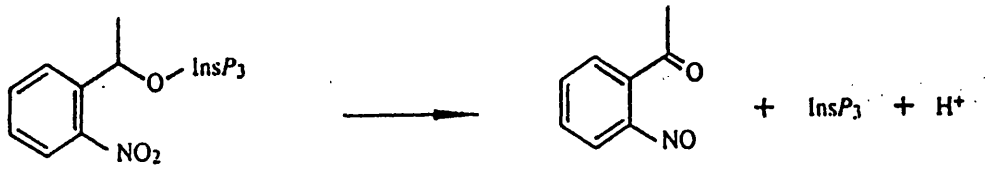

Figure 2.7.1 Photolysis of caged $InsP_3$

from (Ogden-D.C. *et al* 1993)

For slice experiments the Rapp flash gun was mounted underneath the air table and focused through the condenser. A 5 cm wide hole drilled in the table allowed the pulse of light through. The Zeiss Axiophot upright microscope was modified to allow the transmitted illumination mirror to be moved out of the light path of the flash lamp. The lens in the condenser was quartz to reduce the flash artefact. In these experiments the extent of photolysis was less due to the greater distance between the preparation and the flash lamp (see fig 2.5.3.B). An extinction coefficient for cerebellar slices of 10-12cm^{-1} at 320nm was measured giving 26% attenuation of the flash at the surface of a 300μm slice (Khodakhah-K. & Ogden-D.C. 1995).

2.6.2 Calibration of photolysis for experimental setups

Calibration of photolysis for the experimental setup was done by the photolysis of caged HPTS (8-(2-nitrophenylethyl)oxypyrene-1,3,6-trisulfonic acid trisodium salt) synthesised by Dr D.R. Trentham, which is a derivative of the fluorescent pH indicator HPTS (8-hydroxypyrene-1,3,6-trisulfonic acid, trisodium salt (pyranine), and quenched in its unphotolysed form. As the fluorescent emission peak of HPTS depends on the pH of the solution, the caged HPTS was made up in 100mM sodium borate pH 9. At pH 9 the change in fluorescence when caged HPTS is photolysed is at its highest, with an

excitation wavelength of 450nm and an emission wavelength of 510nm. A 450-490nm excitation filter, 510 dichroic mirror and high pass 520nm (FITC) filter were used. To calibrate the inverted microscope apparatus, a 2µl droplet of 10µM caged HPTS was placed under oil in a dish. The flash gun was set to maximum (in this case 150 watts/sec) and caged HPTS solution flashed approximately once every 30 seconds, when the fluorescence signal reached a plateau. This process was continued until the all the caged HPTS had been photolysed. When the fluorescent values were plotted as a function of flash number see figure 2.7.2, the resulting curve could be fitted with an exponential function of the form

$y=A[1-\exp^{(-k*x)}]+c$.....(i)

2.6.2.1 Derivation of calibration curve for flash photolysis

A = Initial Cage concentration

k =the % of photolysis per flash

c = y at x=0

x = number of flashes

y = concentration of HPTS

A→y where A=cage, y=product from cage, at a proportion k,

At start of experiment number of flashes x=0, A=A_0 where A_0=amount of cage present and y=c, where c is product.

After x number of flashes cage remaining =$A_0(1-k)^x$ .....(ii)

as $x\rightarrow\infty(1-k)^x$ =1-xk+ {x(x-1)k2}/2! -{x(x-1)(x-2)k3}/3!

This is an exponential function so $(1-k)^x\rightarrow e^{(-kx)}$.....(iii)

by substituting (iii) into (ii)

cage remaining after x flashes = $A_0e^{(-kx)}$.....(iv)

and product formed after x flashes =$A_0[1-e^{(-kx)}]$.....(v)

so for product=c, when x=0, then

$y=A[1-e^{(-kx)}]+c$ .....(i)

where k= proportion of photolysis per flash.

Figure 2.7.2; Calibration curve of photolysis for experimental setup

This figure illustrates an example of a typical calibration curve. Each data point represents a flash of U.V light from a Strobex flash gun plotted against fluorescence, (photon counts) of HPTS as it was released from it's cage. In this experiment the extent of photolysis with an inverted microscope and Strobex flash gun was 0.034. The fluorescence was measured using a PMT system and counting board and displayed as a digital signal with PTI software.

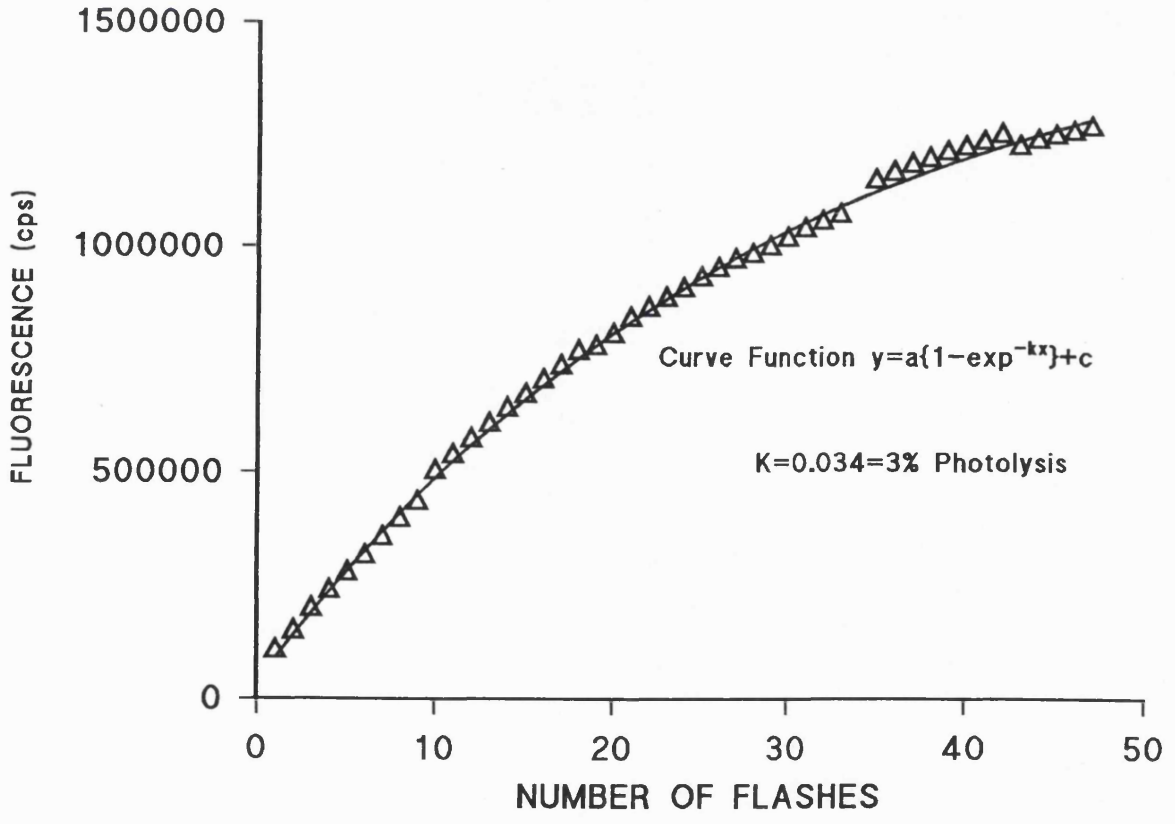

2.6.2.2 Results of calibration experiments

The Strobex 238 flash gun and inverted microscope the calibration of efficiency of photolysis i.e. what proportion of compound is released from its cage per flash, using cHPTS, was k = 0.0273 (n=3) approximately 3%.
For the Rapp and inverted microscope k= 0.158=15.8% ,
the Rapp and upright microscope with dichroic mirror, k =0.105 =10.5%.
For the Rapp upright microscope without mirror, k= 15.0%.

The efficiencies of caged ATP and caged $InsP_3$ photolysis have been shown to be similar under these experimental conditions with quantum yields (Q_p) for ATP from its cage at 0.63 and for $InsP_3$ from its cage Q_p=0.65 (Walker *et al* 1989). Photolysis of a droplet of 10 µl 0.4mM caged ATP was subjected to HPLC analysis. The amount of free ATP and caged ATP can be measured. This gives information on how much ATP was released by each flash (Walker-J.W *et al* 1989; Ogden-D.C., *et al* 1990).

The extent of photolysis of ATP was 30% on the inverted microscope using the Rapp gun full power (300V 7 capacitors 93mJ with UG11 filter 300-360nm). So under the same conditions the amount of HPTS and ATP photolysed are 15.8% and 30.0% respectively. As the extent of photolysis for caged ATP and caged $InsP_3$ is the same then full power of the inverted microscope and Rapp gun gave 30% photolysis of caged $InsP_3$.

As 15.8% caged HPTS is equal to 30% $InsP_3$ then as a ratio the upright 10.5% photolysis of HPTS is equivalent to 20% photolysis of $InsP_3$ full power. The rate of photolysis was estimated as $200s^{-1}$ corresponding to a half-time for $InsP_3$ formation of about 3 ms after the flash (Walker *et al* 1989).

Table 4: Summary of percentage photolysis with microscope/flash lamp:

	HPTS	cATP	$cInsP_3$
Inverted/Strobex	3%	6%	6%
Inverted/Rapp	16%	30%	30%
Upright/Rapp	11%	20%	20%

2.7 Simultaneous flash photolysis and calcium measurements

Combining flash photolysis with microspectrofluorimetry can allow estimates of the kinetics of the $InsP_3$ induced calcium release in type 1 astrocytes to be made. The cells were grown on quartz coverslips, to reduce the prolonged phosphorescent artefact that glass and plastic coverslips have as a result of a U.V flash. U.V transparent oil was also used on the oil immersion objectives. This combination (quartz and oil) are important as the initial rise phase of a response can be masked by this artefact, which with glass and lens oil can be up to 100 ms long compared to 5-10ms with quartz and U.V transparent oil.

The electrode tips were filled with 0.5µl of 500µM furaptra and various concentrations of caged $InsP_3$ made in internal solution, and back filled with the same internal solution without indicator or cage. After going into whole cell configuration, the indicator and caged compound diffused into the cell (see fig 2.52) until a stable fluorescent level was attained. After about 5 minutes when the concentration of indicator and cage in the pipette equilibrated with the cytosol. Cells were clamped at their resting membrane potential, where Im=0, to minimise ion fluxes which may interfere with the calcium changes being investigated. The flash gun gave a 1msec pulse of U.V light, causing $InsP_3$ to be photoreleased from its caged compound into the cytosol. The release of $InsP_3$ molecules into the cytosol caused a changed in cytosolic $[Ca^{2+}]i$. The change in $[Ca^{2+}]i$ was detected by the calcium indicator furaptra to cause the fluorescence of the indicator to change. This change in fluorescence was measured at the same time as the cell membrane current.

Control experiments were performed as described in the protocol above with the exception that the caged $InsP_3$ was omitted from the internal solution content.

2.7.1 Investigation of glial calcium kinetics

The techniques described above were used to study the kinetics of $[Ca^{2+}]i$ in cultured type 1 astrocytes to various $InsP_3$ concentration. The same changes $[Ca^{2+}]i$ kinetics were examined *in situ,* using cerebellar slices. Cerebellar slices were placed on a quartz recording chamber and held down with a mesh. Patched Bergmann glial cells were identified electrically by their resting membrane potentials between -80mV and -90mV, and that they do not fire action potentials on depolarisation. Once loaded with the calcium indicator a distinctive cellular morphology can be distinguished. Cell somas were located around the cell body of the larger more visible Purkinje cells, as flat tear shaped structures. The processes of the cells project to the pial surface ending in little end feet. The Bergmann glial cells have no projections into the granule layer. You can identify these cells by their characteristic shape compared to granule cells, stellate cells, basket cells, Lugaro cells and Purkinje cells.

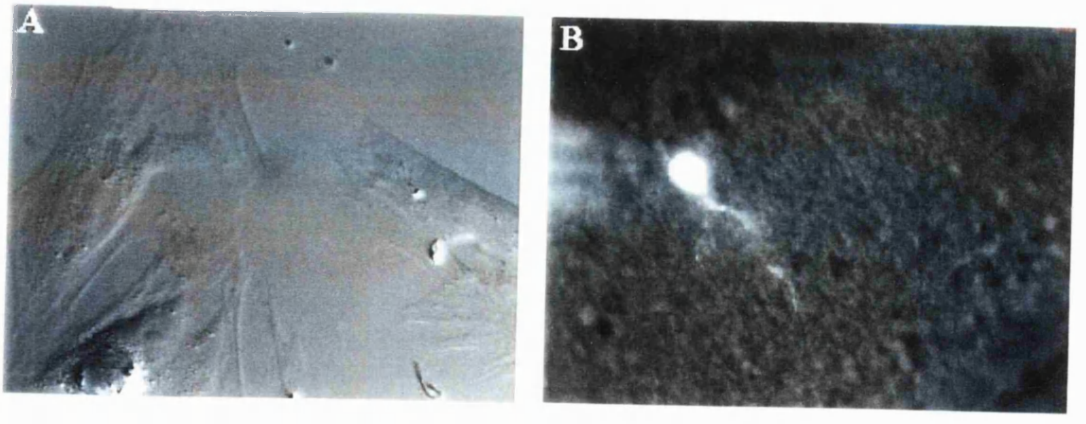

Figure 2.8.1 Comparison of astrocytes *in vitro* and *in situ*.

(A) Cultured type 1 rat cerebellar astrocytes grown on glass coverslips. (B) A single Bergmann glial cell loaded with a calcium sensitive indicator (furaptra) within a saggital section of the rat cerebellum.

2.8 Imaging system for fluorescent calcium measurements

□Figure 2.9: T.I.L.L Photonics Imaging System

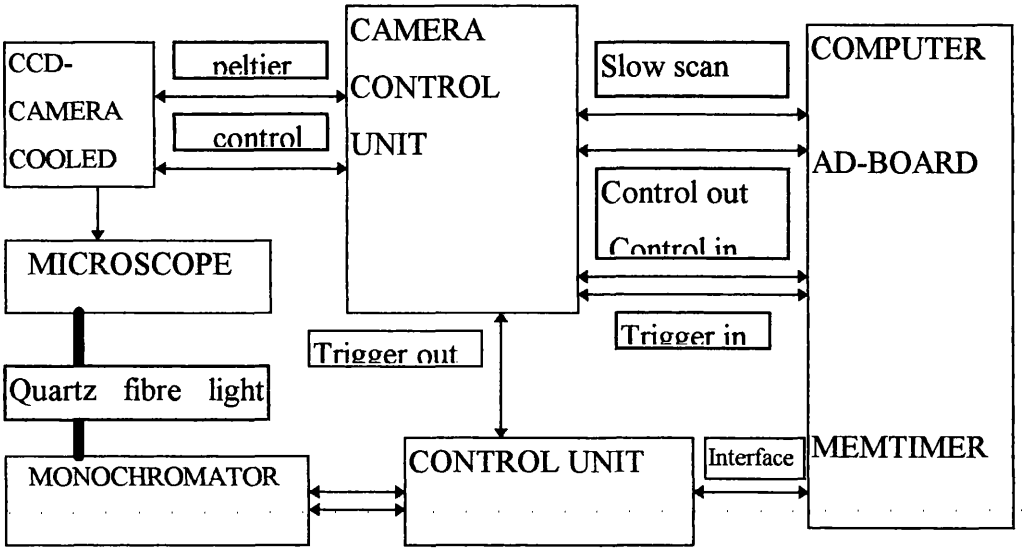

An imaging system was used to measure the fluorescence of the glial cells in slices (figure 2.9). This system has the advantage when identifying Bergmann glial cells *in situ* by their characteristic morphology. The imaging system comprised a fast switching monochromator for excitation and a cooled CCD camera (T.I.L.L Photonics). The monochromator comprised a xenon arc lamp, a rotating monochromator grating to produce the required wavelength directed to the microscope epifluorescent attachment port through a quartz optical fibre.

The camera used was either a water cooled CCD THETA camera, or a T.I.L.L IMAGO peltier cooled CCD (-15°C). The IMAGO CCD camera had 640X480 pixels, emptied consecutively at 12.5 MHz with 12 bits of resolution.

Three versions of the imaging software were used as the system was being developed.

(1) Fucal, a DOS based program (T.I.L.L Theta camera), images recorded in PIC format.

(2) IDEA a Windows 3.11 version (T.I.L.L IMAGO camera), images in IDE format.

(3) Vision a Windows NT based version (T.I.L.L IMAGO camera), images TIFF based format. (Tagged Image File Format).

Some analysis was done using the software supplied, but most was performed by measuring line plots and exporting data into either Microsoft Excel or Origin.

2.8.1 Real-time imaging.

Two problems related to timing were encountered. The files were very large and so caused storage problems for the computer. When the virtual disk became full the computer automatically downloaded its content. If this occurred during a series of frame acquisitions recordings were suspended. One way to overcome this problem was to record regions of interest (ROI, making each frame size smaller) thus allowing more images to be acquired. Another problem during image storage was the time interval required for recording and transferring information from the camera to the computer. The computer ran the acquisition system according to its processing time and not to the programmed experimental time. For this reason experiments were recorded for brief time intervals between 100-500ms and data plotted as frame numbers. Finally there was no analysis function to the software. Lines of fluorescence intensity profiles were taken for the series of images. Each reference line was exported as a ASCII file and imported into a spreadsheet program for analysis.

2.8.2 Imaging of calcium sensitive fluorescent indicators in cultured glial cells

Imaging was used to locate the $InsP_3$ induced calcium effects within cultured type 1 astrocytes. The acetoxymethyl (AM) ester form of the indicator is cell permeant and readily diffuses across cell membranes. When inside the cell the acetoxymethyl group is hydrolysed by cytosolic esterases to leave the active fluorescent indicator. The astrocytes were loaded with 5μM of the acetoxymethyl ester forms of the calcium indicators furaptra (Molecular probes Inc. Eugene O.R) or fluo-3 a rhodamine derivative Kd=0.37μM, (Minta-A. *et al* 1989a; Minta-A. *et al* 1989). The process of cell loading was helped if the cells were incubated with a pluronic acid and dimethylsulfoxide

(DMSO) mixture at 35°C for 20 minutes. Cells were cultured on glass and images taken, using the T.I.L.L photonic system through an upright Axioskop microscope with a 40X, 0.75NA water immersion objective. The monochromator was set at an excitation wavelength of 480nm for fluo-3 experiments. For furaptra experiments the monochromator was used at dual wavelengths of excitation at 420nm and 347nm (isoemissive point). Agonists were applied by pressure ejection. Images were taken at intervals of between 500ms-2s, with an exposure time of 200ms, for approximately 50-100 cycles.

2.8.3 Investigation of neuronal and glial interactions in cerebellar Slices

A technique for ester loading cells in slices (Regehr-W.G. & Tank-D.W. 1991) was adapted to load Bergmann glial cells. The dendrites of Purkinje cells at P12 are still growing and have not yet reached the pial surface of the molecular layer. Bergmann glial cells are the initial radial glial cells that form the network for developing nerve structures, such as Purkinje dendrites. The acetoxymethyl forms of the indicators (50μg) were made up in 20μl of 75% DMSO, 25% pluronic acid mixture and 400μl of external salt solution at concentrations of 110μM-160μM. Bergmann glial cells in saggital or transverse slices were selectively loaded via their pial projections with acetoxymethyl calcium indicators using two electrodes, placed 5μm apart in the pial region of the cerebellum fold. The first electrode (resistance 1MΩ) contained AM-indicator and was attached to a gas supply with a switch mechanism which expelled 1μl of the acetoxymethyl indicator over the area of the pial surface of a cerebellar fold. The second electrode was attached via tubing to a suction pump to remove excess indicator. The result was a small localised spot of indicator on the pial surface. After 15-20 minutes of loading, the main cell types to take up the indicator were glial cells whose end feet projected into this region, and granule cells which were migrating along them. In addition some parallel fibres also took up the dye. Indicators used were furaptra-AM, fura-2-AM, fluo-3-AM, fura-red-AM and indo-1-AM.

Figure 2.9.2 Selective Bergmann glial cell loading in cerebellar slices

Photograph A represents a phase bright photograph taken of a pair of electrodes placed in the folia junction of a saggital section of a P12 rat cerebellum. One electrode applied the calcium sensitive indicator furaptra-AM. The second electrode had negative pressure and removed the excess furaptra.

Photograph B shows the same framed image when illuminated by light at 420nm wavelength. The furaptra-AM pooled in the central area, which is seen as a bright spot in the middle region. The small spherical structures around the electrodes are probably granule cells. Radiating from the spots were fine linear structures. Due to the structure of the molecular layer of the cerebellum in saggital orientation these cells are likely to be Bergmann glial cells.

Panel C shows 9 consecutive panels of cerebellar Bergmann glial loading with furaptra-AM taken with the imaging system (excitation 420nm) using the THETA camera and IDEA software.

Photograph D depicts the region to the right of the loading spot. This picture demonstrates the loaded Bergmann glial cells in the molecular layer. The small spots are granule cells which are migrating to the granule cell layer. The region to the far right of the photograph shows the Purkinje cell soma layer. The arrow depicts an unloaded Purkinje cell soma which remains as a "black hole".

The images show the gradual filling with calcium indicator furaptra-AM of the glial cells via their end feet. Notice running diagonally (top right corner to bottom middle) the series of "black holes" that form the Purkinje cell somas. In addition the small white spots that are located around the holes are probably Bergmann glial cell somas. The loading process performed at 23° C takes 20 minutes. These images were taken over 30 minutes.

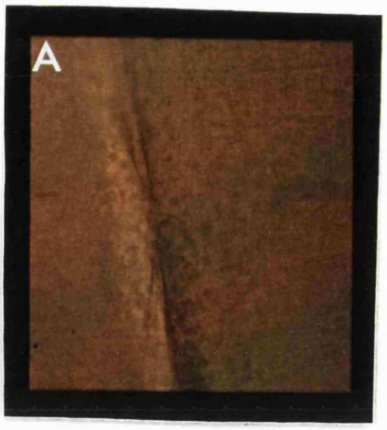
A

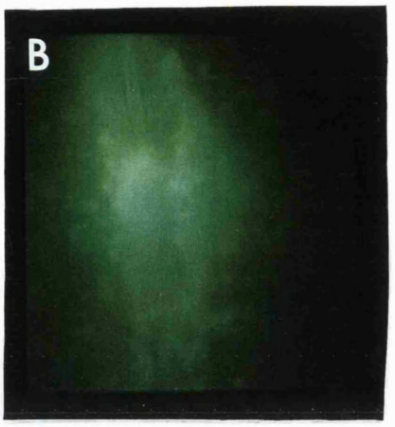
B

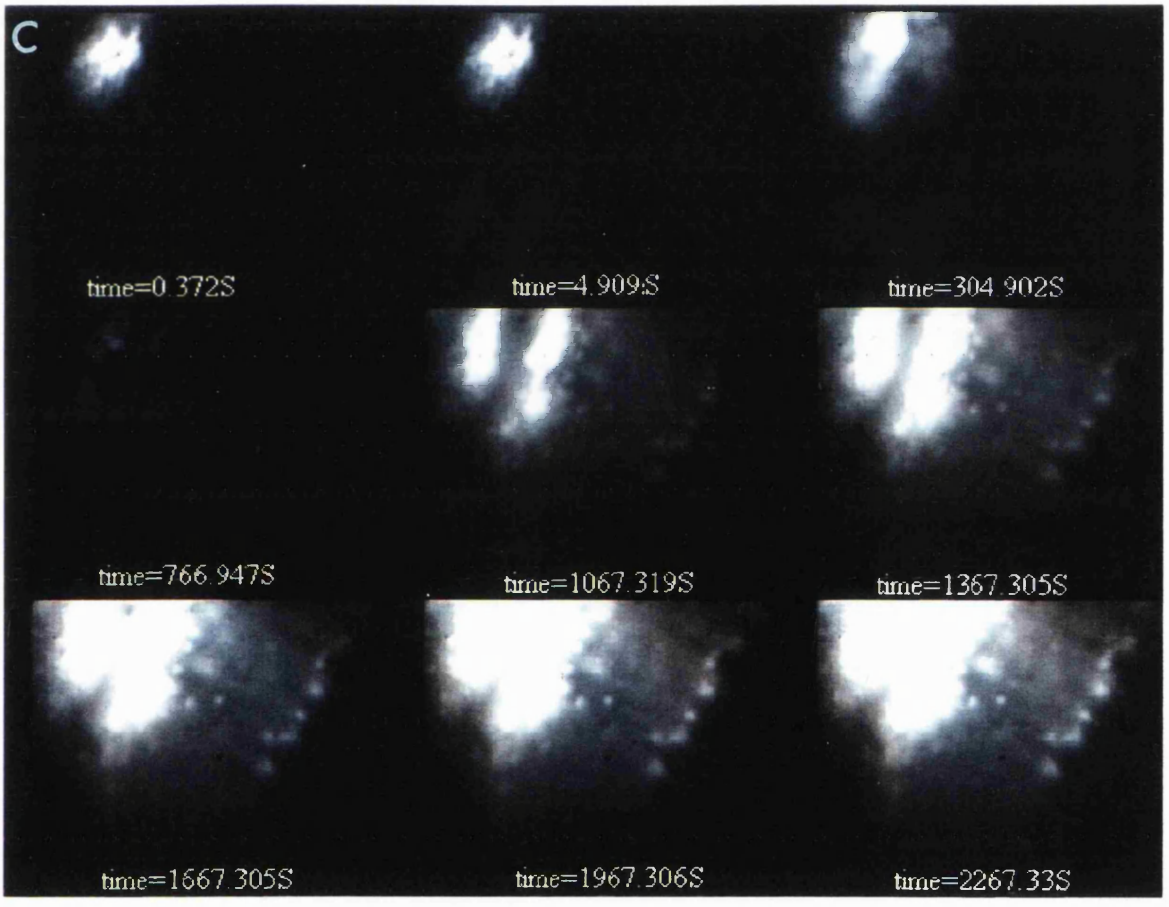
C
time=0.372S
time=4.909S
time=304.902S
time=766.947S
time=1067.319S
time=1367.305S
time=1667.305S
time=1967.306S
time=2267.33S

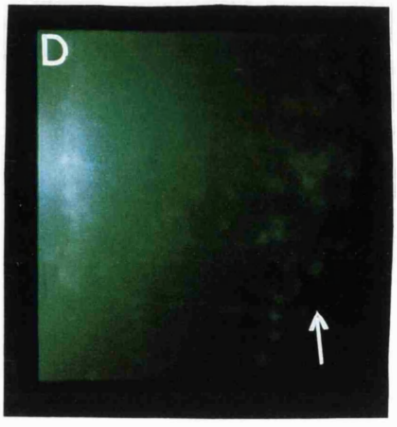
D

2.8.4 Stimulation of excitatory post synaptic potentials (epsps) in Purkinje cells

In order to investigate how glial cell calcium concentration might change during neuronal stimulation the localised glial cell loading method was combined with electrical stimulation of the cerebellar slice. The Purkinje cells were visualised using a Zeiss Axioskop microscope and 40X 0.75 NA water immersion objective in a continually perfused slice. A stimulating electrode was placed in the central region of the fold, halfway between the white matter area and the Purkinje cell body layer, activating the climbing fibres. Whole cell patch clamp recordings were made from the Purkinje cells that were located on or near the surface with an Axoclamp or an Axopatch 1D. Purkinje cells were clamped at -65 to -70mV, just below their firing threshold. Epsps were stimulated at 10μA at either 1, 3, 5, 10 Hz. Images were recorded using the T.I.L.L photonic system.

CHAPTER 3

THE CHARACTERISATION OF RAT GLIAL CELLS AND THEIR $InsP_3$ RECEPTOR SUBTYPES *IN VITRO* AND *IN SITU*.

3. Introduction

This chapter will describe the types of glial cell present in cultures of the rat cerebellum. Specific antibodies raised against glial antigens were used as immunocytochemical markers to characterise glial cells.

The histological studies were to identify;-

(i) the different types of macroglial cells in rat cerebellar cultures.

(ii) the presence of gap junction proteins.

(iii) the location of glial fibrillary acidic protein (GFAP) positive cells in the cerebellum and their relation to adjacent neurones.

(iv) the subtype of the $InsP_3$ receptor protein present in glial cells *in vitro* and *in situ.*

3.1 Immunohistochemical characterisation of glial cells present in rat cerebellar cultures

3.1.1 Astrocytes

Traditionally glial cells have been defined by their morphology, rather than physiology. Cajal used a method of gold chloride sublimate to stain and identify the different kinds of astrocytes. Cajal first showed astrocytes, originating from the ectoderm region of the brain, to be either fibrous or protoplasmic in appearance and found in the white or grey matter of the cerebral cortex (Cajal-R. Y. 1937). Fibrous astrocytes, as the name suggests, have many fine projections and small cell somas. The protoplasmic cells have smaller but more numerous projections and a larger cell soma compared to glial

fibrous cells (figure 3.1.1 A&B). Both types of astrocytes have fine projections which *in situ* encompass the surrounding neurones. The glia fine filaments have end-feet on blood vessels (see figure 3.1.1 C). It was apparent therefore that the glial cells formed cellular links between the neuronal system and the brain microvasculature.

The anti GFAP antibody is a specific label for a filamentous structural protein involved in astrocytic morphology (Bignami-A. *et al* 1972 ; Bignami & Dahl-D., 1974). This antibody was used to identify subtypes of astrocytes from other glial cells present in rat cerebellar cultures. Figure 3.1.1 A&B illustrates the two types of GFAP positive astrocytes present in the rat cerebellar cultures. There are large protoplasmic cell typical of the "type 1 like" astrocyte, and the smaller stellate cells of "type 2 like" astrocytes described by Raff *et al* in the rat optic nerve (Raff *et al* 1979 ; Raff *et al* 1983b) . Type 1 astrocytes have a larger cell soma in comparison to the type 2, and the GFAP radiates throughout the protoplasm which in the type 2's forms finer projections.

The monoclonal antibody A2B5 (Eisenbarth *et al* 1979) distinguishes between type 1 and type 2 astrocytes by identifying plasma membrane bound sialogangliosides and sulfatides. Figure 3.1.1 D shows how the fibrous "type 2 like" cells stain positive for this antibody. The A2B5 antibody was secondary labelled with a Texas Red fluorochrome. The A2B5 antibody was a label for plasma membrane molecules which are not only present in "type 2 like" astrocytes but also found on their O2A progenitor cells, oligodendrocytes, neurones, neuroexocrine cells, and neurofibrillary tangles associated with Alzheimer's disease. The A2B5 epitope was not often present in type 1 cells so can serve as a distinguishing feature between type 1 and 2 astrocytes. However, it has been shown that A2B5 can identify some type 1 astrocytes (Raff *et al* 1983a) so alone it may not be a definitive marker and should be used in conjunction with other glial antibodies.

For all experiments controls were performed whereby the primary antibody was omitted from the PBS 1% FCS solution.

Figure 3.1.1: Identification of cultured type 1 astrocytes

Photograph A: Shows a coverslip of cultured rat cerebellar glial cells 7 DIV. The astrocytes were identified with an antibody raised to an epitope specific for an interior structural protein GFAP. The GFAP antibody was raised in rabbit so was secondary labelled with an anti rabbit conjugated fluorescent fluorochrome fluorescein (FITC). When the cells were illuminated with light of wavelength 450-490nm positive cells appear green. The two central cells with small somas and fine filaments are typical examples of "type 2 like" astrocytes. Surrounding them are other examples of longitudinal shaped protoplasmic cells, with round somas of the "type 1 like" astrocytes. The calibration bar is 50μm.

Photograph B: This panel was also of GFAP positive astrocytes which were counter stained with fluorescien. The photograph (taken with light wavelength 450-490nm) consists mainly of the GFAP positive protoplasmic astrocyte cell type. These "type 1 like" protoplasmic astrocytes seem to have two forms. There are large circular cells which have small cell nucleolus that do not contain any GFAP filaments. An example of this large round astrocyte is located in the centre of the image. The other protoplasmic "type 1 like" astrocytes were small and longitudinal. These smaller astrocytes can be seen in the outskirts of the image. Calibration bar is 50μm.

Photograph C: Shows a single astrocyte in a cerebellar slice cut in the saggital orientation. The glial cell was identified with a mouse monoclonal antibody that specifically identifies the $InsP_3$ subtype 3 receptor protein. The antibody was raised against synthetic peptides which correspond to the amino acid sequence of the C-terminal end of human $InsP_3$ receptor protein. This antibody was then identified with an anti-mouse conjugated FITC marker. The picture demonstrates clearly the intimate relationship that glial cells have with the micro blood vessels of the cerebellum. The glial cell was small with fine filaments. This glial cell had a single projection which terminated in an end foot on the small blood vessel. The calibration bar is 20μm.

Photograph D: Cultured astrocytes 5 DIV grown on a glass coverslip stained with an antibody raised in mice to the A2B5 antigen. The A2B5 antibody was marked with an anti-mouse Texas Red flourochrome. The A2B5 antibody identified glial cells from the O2A progenitor cell lineage. These cells have small cell somas and fine filaments, typical of "type 2 like" astrocytes. Scale bar is 50μm.

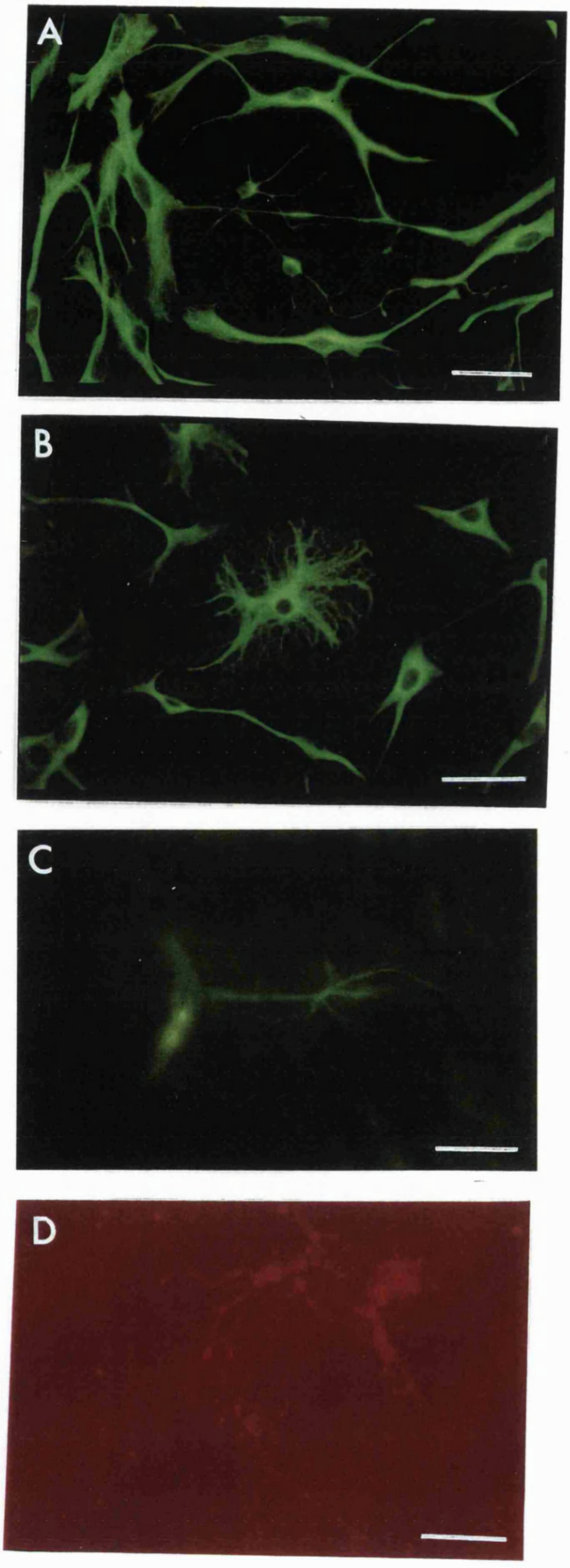
A
B
C
D

3.1.2 Oligodendrocytes

Oligodendrocytes are "web like" cells whose fibrous projections encompass bundles of nerve fibres. Oligodendrocytes are responsible for myelination of nerves within the CNS. The oligodendrocytes were identified by the monoclonal antibody 04 which recognises sulfatides and glycolipids specifically found on oligodendrocytes and some cells of the O2A progenitor lineage (Sommer & Schnanchner 1981). Oligodendrocytes were also identified by the presence of a surface antigen Galactocerebroside (Gal C ; Raff *et al* 1978). Gal C is the main glycolipid constituent of myelin a specific oligodendrocyte protein (Figure 3.1.2 A B C D). Gal C, 04 positive cells i.e those that express these oligodendrocyte proteins, do not express the astrocytic structural protein GFAP so do not react to the GFAP recognising antibodies. The cells that were identified as positive to 04, Gal C and negative to GFAP were oligodendrocytes (see table 1 Chapter 2).

Figure 3.1.2 Identification of oligodendrocytes.

Photograph A: show cultured (7 DIV) rat cerebellar glial cells grown on a glass coverslip. The antibody specific to the O4 antigen was raised in mice and counter labelled with anti mouse conjugated FITC. The image was taken in transmitted light and clearly shows that there are glial cells throughout the field.
Photograph B: shows 04 positive cells were labelled with FITC (and are illuminated with light of wavelength 450-490nm). Oligodendrocytes (green fibrous cells) were located in the central region of this image and had web styled filaments with small spherical somas. Notice that the cells in panel A top left are small and transparent, do not stain positive for O4 (panel B), these cells were astrocytes.

Photograph C shows a bright field image of cultured rat cerebellar glial cells (7 DIV). The central cell can be identified by its different morphology compared to the surrounding cells that were flat protoplasmic cells. The oligodendrocyte marker an antibody raised in mice to the antigen for Gal C, was secondary labelled with anti mouse conjugated FITC.

Photograph D illustrates (the same image as C) that the central cell had on its surface plasma membrane galactocerebroside making this cell an oligodendrocyte. The oligodendrocyte had circular filaments forming a web around a small nucleus. Notice that the astrocytes surrounding the oligodendrocyte did not posses this specific antigen and remain dark in the image which was photographed under 450-490nm wavelength light.

Calibration for panels A,B,C, &D is 50μm.

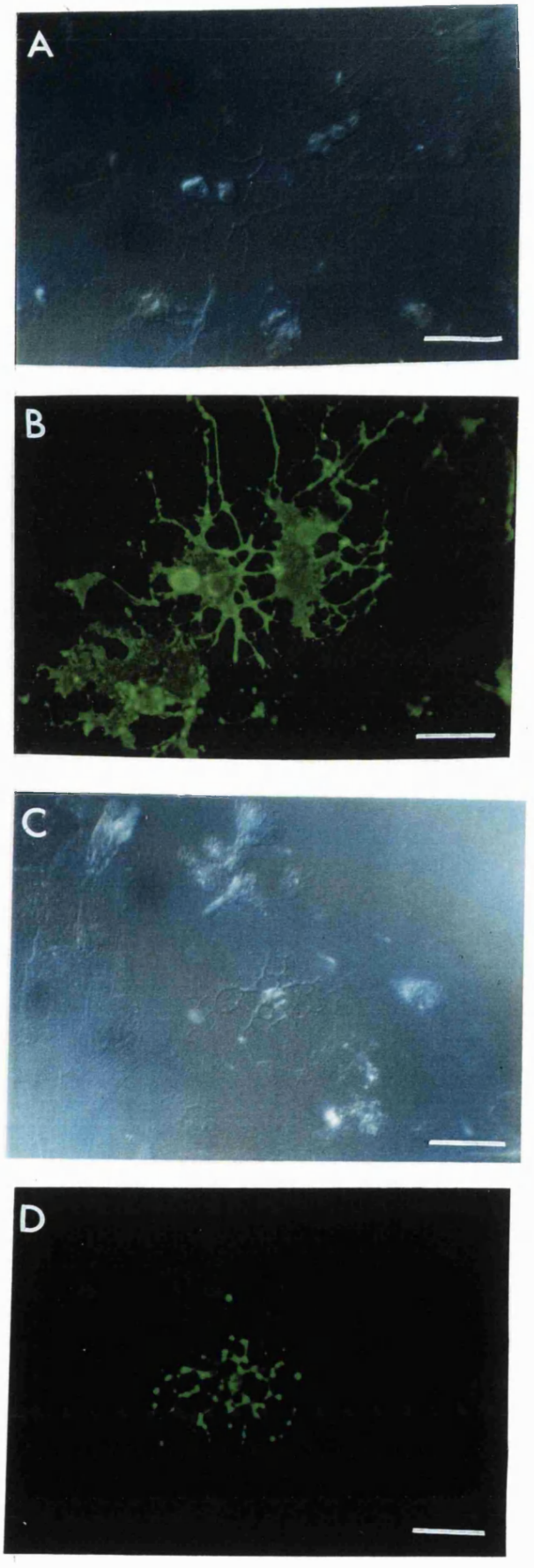
A
B
C
D

3.1.3 Progenitors and neurones

The progenitor cells have round cell bodies with bipolar projections. The O2A progenitor cells (>8 DIV) eventually differentiate into "type 2 like" astrocytes or oligodendrocytes depending on the medium conditions. The progenitor cells are visually difficult to distinguish from the degenerating granule cells because both had small central somas with dwindling dendrites (see figure 3.1.3). Type 2 astrocytes were visually difficult to identify for patch clamp recordings.

3.2 Gap junction proteins-connexin 43

An antibody raised to the gap junction protein connexin 43, was used to identify its presence in cerebellar astrocytes in culture. Figure 3.2 shows a cluster of "type 1 like" astrocytes. At this stage *in vitro* (5 days) the cells form clusters rather than monolayer sheets. The arrows indicates the staining for presence of the connexin 43 protein. This protein is known to form a homomeric structure generating a gap junction channel. The presence of connexin 43 in these cells means they are capable of making gap junction complexes between the other astrocytes (via plasma membrane) which could allow intercellular communication. However at this stage *in vitro* the staining for connexin 43 was faint and could be due to glia only producing the connexin when contact with other cells had been made. There were other clusters of cells which were not fluorescent, an indication that they did not express the connexin 43 protein.

Figure 3.1.3: Identification of neurones and progenitors

Photograph A was a bright field image of a rat cerebellar culture 5 DIV. The cells were dense and formed a cellular monolayer. Within the field are small round cells that have a phase bright ring around them. These small spherical cells would be either in small clusters or isolated. Some isolated small round cells had bipolar projections from the top and bottom areas of the soma (arrow). These cells were characteristic of O2A progenitor cells. The other groups of cells were degenerating granule neurones. The scale bar is 50μm.

Photograph B was a bright field image of glial cells *in vitro* (5 DIV). The large bundles of small round cells were contaminating neurones (granule cells). After 5-10 DIV the granule cells disappeared as the plasma membranes disintegrated as a result of the culture medium conditions. The large clump of tissue debris to the left of the panel was degenerated neuronal tissue. The small granule neurones had a similar morphological shape as the progenitor cells so were not used as part of this study. The scale bar is 50μm.

Figure 3.2: Localisation of gap junction proteins

This image (A) depicts a cluster of cultured cerebellar astrocytes 5 DIV. These cells were stained with an antibody raised to an antigenic epitope specific for connexin 43 raised in mice. The connexin 43 antibody was identified by a secondary fluorochrome marker anti mouse conjugated Texas red. The image was recorded at with a confocal microscope (Leitz) and pseudo coloured red. The arrows indicate the junctions of two cells. There was also positive staining through out the cytoplasm. The connexin 43 was present in clusters of cells at this stage of 5 DIV. Scale bar is 20 μm.

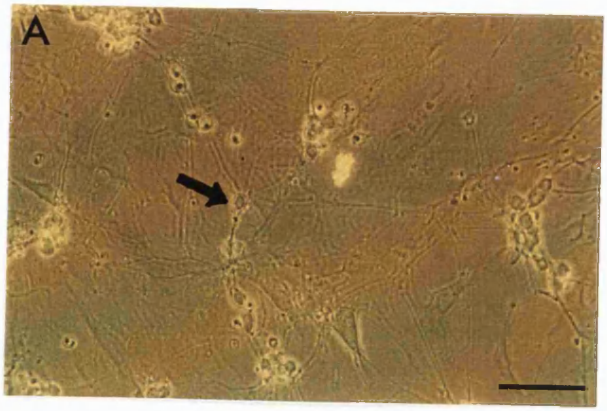
A

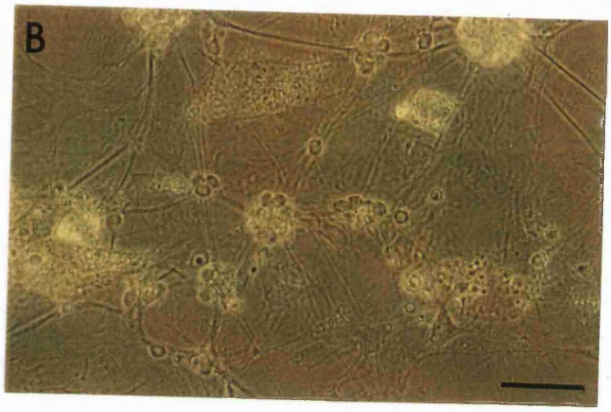
B

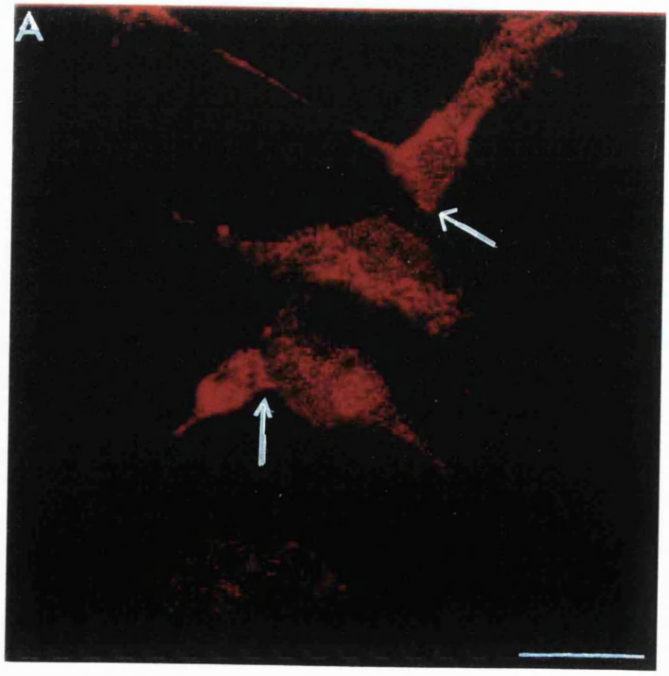
A

3.3 Identification of the protein subtype of inositol 1,4,5 trisphosphate receptor in cultured astrocytes

To localise the $InsP_3$ receptor protein that is present in cultured cerebellar astrocytes, antibodies for regions specific to the type 1, 2, or 3 $InsP_3$ receptor subtype proteins were used in immunohistochemical studies. The type 1 specific $InsP_3$ antibody was kindly provided by Dr Lai, and the antibodies specific for type 2 and type 3 $InsP_3$ receptor proteins by Dr Suigama (Sugiyama-T. *et al* 1994). As shown in figure 3.3.1 cerebellar cultured type 1 astrocytes have the $InsP_3$ type 3 subtype receptor protein. These pictures demonstrate the expression of subtype 3 $InsP_3$ receptor proteins in cultured type 1 astrocytes which has not been reported elsewhere.

Figure 3.3.1: Identification of the type 1 astrocytic $InsP_3$ receptor protein *in vitro*

All six panels were recorded on a confocal microscope and the fluorescence pseudo coloured. High expression of the $InsP_3$ receptor proteins attracted more fluorescent fluorochrome (FITC) and was shown as a black area, lower level fluorescence and hence expression as red. Yellow represented the lowest light levels.

Panel A,C,E are the results of control experiments which are displayed on the left hand side of the figure. The control experiments showed a lack of positive staining for any of the three protein subtypes. Background auto fluorescence from the cell was indicated by the yellow colour of the type 1 astrocytes.

Panel B shows that with the type 1 specific antibody there was little fluorescence detected (yellow) hence very low level $InsP_3$ subtype 1 receptor protein expressed in cerebellar cultured type 1 astrocytes.

Panel D depicted that the fluorescence due to the $InsP_3$ subtype 2 isoform was generally low. However some astrocytes had a higher fluorescent level that was speckled red. This light level region implies that some of the type 1 astrocytes expressed very low levels of $InsP_3$ subtype 2 receptor protein.

Panel F showed that the subtype 3 $InsP_3$ receptor protein was highly expressed (black) and was located around the central soma regions of the type 1 astrocyte in the cytoplasm. The receptor proteins tended to localise around the nucleus in fairly dense clusters. There appeared to be little or no staining in the outer cytoplasm area of the type 1 astrocytes.

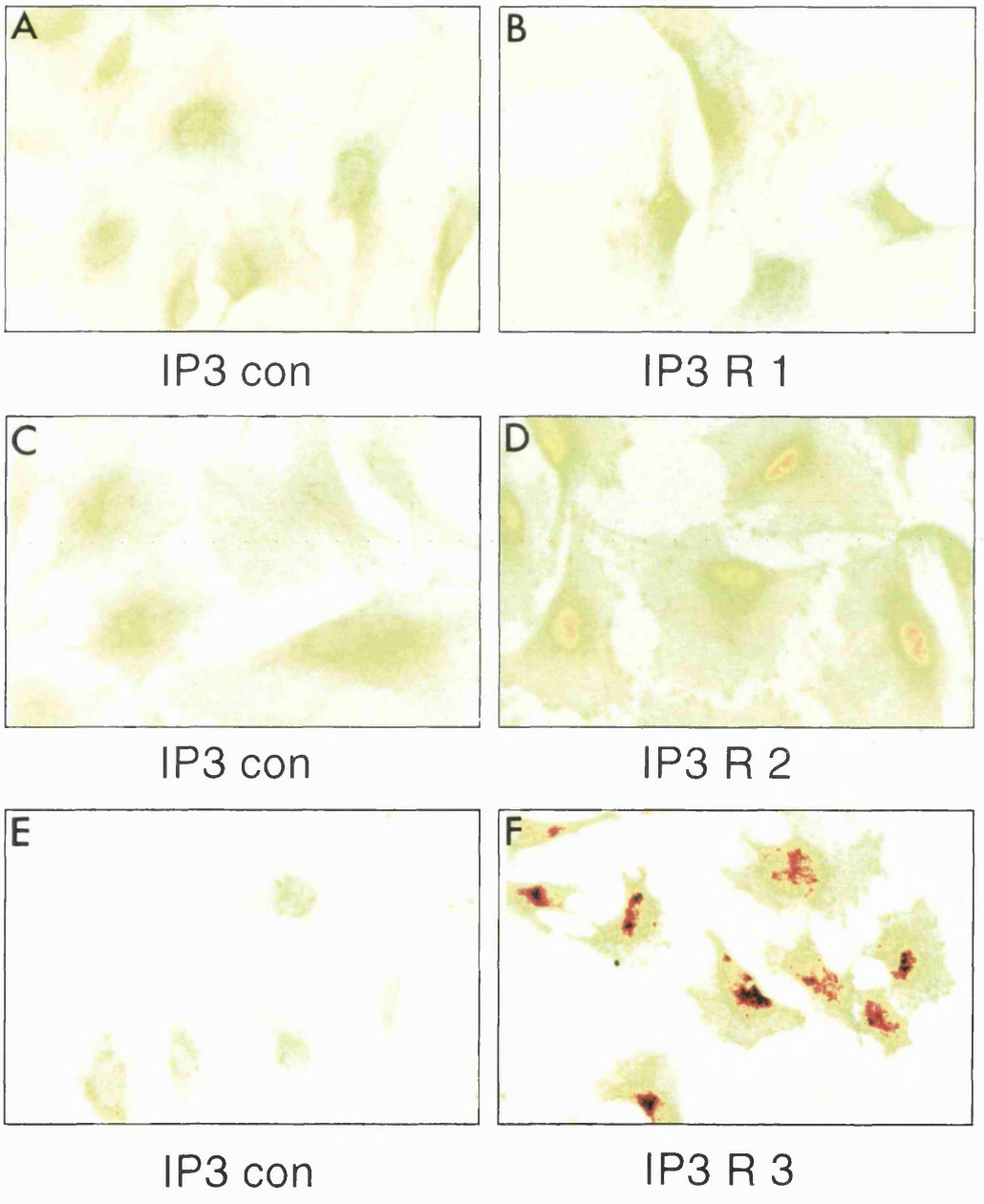
A
B
IP3 con
IP3 R 1
C
D
IP3 con
IP3 R 2
E
F
IP3 con
IP3 R 3

3.4 Location of astrocytes in acute slices of the rat cerebellum

3.4.1 Glial cells in slices

Cerebellar slices were cut in the saggital orientation. Astrocytes were identified with mouse monoclonal anti GFAP antibodies. GFAP positive labelling in saggital cerebellar slices revealed the architecture of the glial cells within the cerebellar folium (Figure 3.4.1 A, B). Within the central regions of the folium the granule cell layer has ring like structures that are GFAP positive (Figure 3.4.1 A) indicating that there are astrocytes surrounding granule cell bodies. These small protoplasmic astrocytes are present throughout the granule cell layer.

A second form of GFAP positive cells were identified (figure 3.4.1 B) in the molecular region of the rat cerebellum which are fine fibrous cells. These fibrous cells are Bergmann glial cells. Bergmann glial cells have a strikingly different morphology to other astrocytes, such as found in the granular layer, with small cell somas and long fine processes. The fine processes maintain their irregular shape in the same direction running to the pial surface of the slice (see figure 3.4.1.C).

Around the Purkinje cell layer, the somas of the Bergmann glial cells encapsulate the cell bodies of the neurones (see Figure 3.4.1.D). Their filamentous projections form a "candelabra" like structure which radiates to the pial surface through an extensive network of neuronal processes. This network consists of Purkinje cell dendrites, granule cell parallel fibres, stellate cell and basket cell dendrites (see Figure E). There is close contact between neurones and Bergmann glial astrocytes.

At the pial surface the Bergmann glial cells have what appear to be end feet. The end-feet project to the micro-vascular of the brain (see figure 3.1.1 C). This suggests that Bergmann glial cells may play a role in the transportation of blood metabolites to other brain regions.

At P12 stage of development each Bergmann glial cell has 4/5 fibrous projections to the pial surface. Bergmann glial cells have no anterior projection down into the granular layer. In the neonatal cerebellum, Bergmann glial cells form a radial glial network that allows neurones to migrate from their site of neurogenesis to their final

position. At birth most radial glia disappear but the Bergmann glial cells remain. The fine filaments of the Bergmann glial cells within the molecular layer diversify, thicken and in adulthood have a spiny appearance. At birth the anterior projection of the Bergmann glial cells disappears from the granule cell layer.

Figure 3.4.1 Location of astrocytes in acute slices of the rat cerebellum

Photograph A shows astrocytes that were positive to GFAP raised in rabbit, and counter labelled with anti rabbit conjugated FITC. The photograph of an adult rat cerebellar slice was taken when illuminated through light wavelength 450-490nm. The astrocytes were small with fine filaments that appear to encapsulate larger round structures of the granule cells. Scale bar is 50μm.

Photograph B is of a folium from a P12 rat cerebellar slice. The rabbit antibody was specific for the GFAP epitope. The anti rabbit conjugated TRITC fluorochrome identified the GFAP. The photograph was taken with light of wavelength 550-590nm. Within this region the astrocytes were linear Bergmann glial cells. Scale bar is 50μm.

The images C, D, E were recorded using a T.I.L.L Photonics imaging system with light of wavelength 420nm.

Panel C depicts an image of a single Bergmann glial cell in a live P12 rat cerebellar slice. A patch pipette filled with a calcium sensitive indicator furaptra, loaded the single Bergmann glial cell. The image clearly shows the small cell soma of Bergmann glia, the fine filaments (of which there are two in this instance) radiating in the same direction. Notice there was no projection towards the granule cell layer in the top left corner of the image.

Panel D shows the close relationship of glial and neuronal cells. This image was of a live rat cerebellar slice (P12). The larger cell with a round soma and bifurcating dendrites was a Purkinje neurone. The second smaller cell was a Bergmann glial cell. The same patch pipette filled the two cells with furaptra.

Panel E is an image of a live cerebellar slice selectively loaded with furaptra-AM. The picture shows fine neuronal dendrites forming a mesh with Bergmann glial filamentous projections. The larger spherical areas that appear black are the Purkinje cell bodies that have not been infiltrated with furaptra-AM (see chapter 5).
Scale bar represents 20μm for images C,D and E.

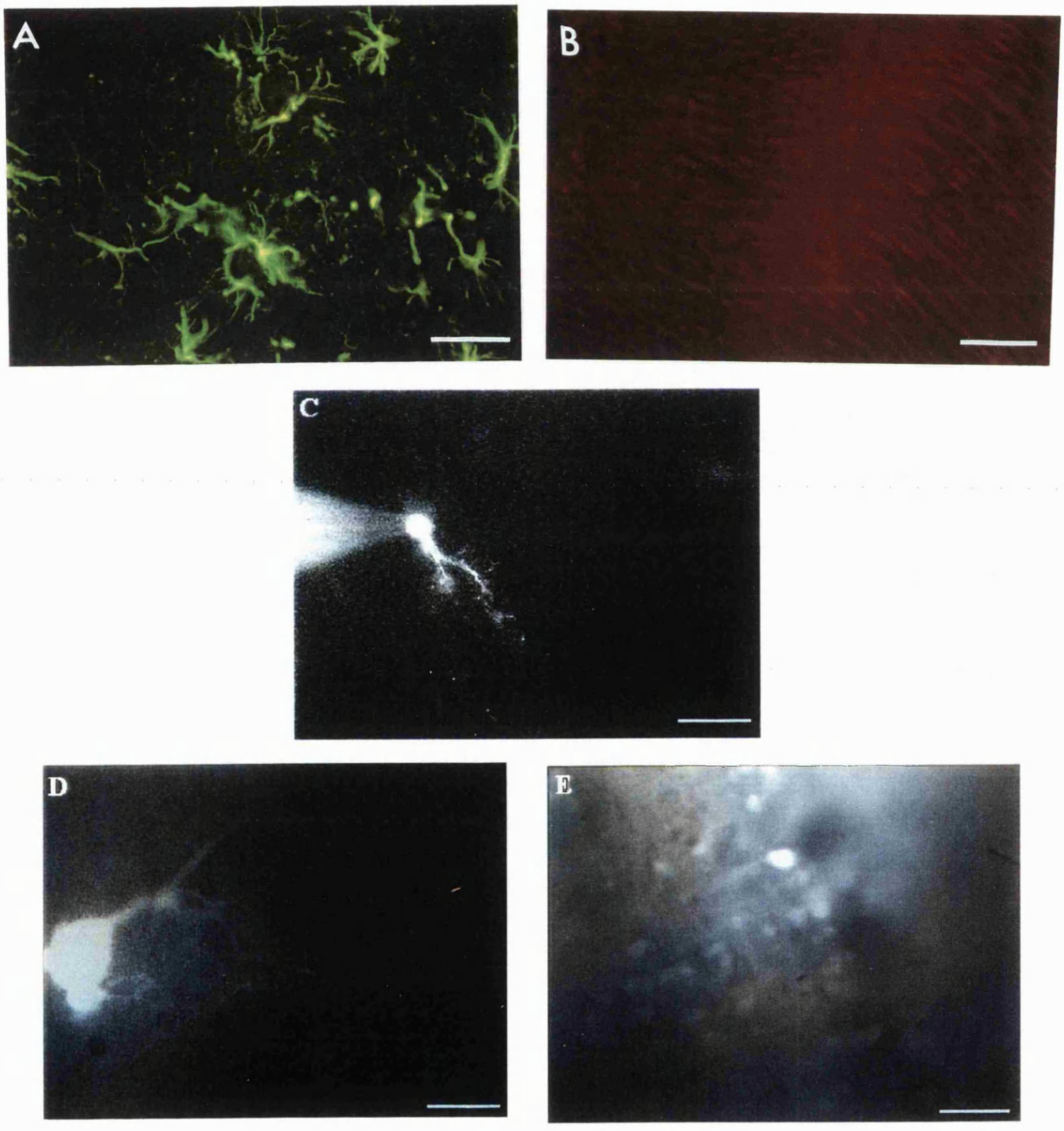
A
B
C
D
E

3.5 Which type of $InsP_3$ receptor is present in astrocytes *in situ*?

3.5.1 Inositol 1,4,5 trisphosphate type 1 receptor protein

There was strong expression of type 1 $InsP_3$ receptor proteins are within saggital sections of the rat cerebellum. Figure 3.5.1 shows that type 1 $InsP_3$ receptor proteins predominantly in the Purkinje cells (A). The receptor proteins were in the cytoplasm around the Purkinje cell nucleus of the soma and dendritic tree (B). Type 1 $InsP_3$ receptor proteins were also in the descending axon (C).

Figure 3.5.1 shows a set of photographs taken of a saggital section of rat cerebellum (P12). At this stage of development the Purkinje cell dendrites were still growing into the molecular layer but terminated part way up the region (Figure 3.5.1.A).

The labelling studies showed that there was no $InsP_3$ subtype1 receptor protein expression in the surrounding Bergmann glial cells of the molecular layer. GFAP (glial specific marker) verified the position of the Bergmann glial cells. In figure 3.5.2 there was no matched labelling between $InsP_3$ type 1 and GFAP in the granule or molecular layer. Neither the protoplasmic astrocytes nor the Bergmann glial cells expressed the type 1 $InsP_3$ receptor protein. This data is comparable with studies of cultured type 1 astrocytes, in that cerebellar glial cells do not express type 1 $InsP_3$ receptor proteins (see figure 3.3.1 A&B).

In the granule cell layer there appeared to be low level positive staining with the type 1 specific antibody. The subtype1 $InsP_3$ receptor protein expression was restricted within the granular layer to the Purkinje cell descending axon (see 3.5.1.C). Interestingly the granule cells appeared not to highly express this type 1 $InsP_3$ receptor protein. There was no $InsP_3$ type 1 receptor located in other cerebellar neurones such as basket cells, stellate cells and Lugaro cells. As the fluorescence of $InsP_3$ subtype 1 immunohistochemistry in Purkinje cells was very strong, it would be difficult to conclude for certain that there was no subtype 1 present in the other neurones. It is probable that the subtype 1 protein expression in these cells occurs but at a lower level than Purkinje cells and, due to the intensity of the signal is difficult to distinguish.

Figure 3.5.1 The Immunolocalisation of the $InsP_3$ subtype 1 receptor protein *in situ*

Photograph A shows the pial edge of a rat (P12) cerebellar section through a fluorescein filter. The rabbit developed antibody specific for subtype 1 region of $InsP_3$ receptor protein was secondary labelled with an anti rabbit conjugated FITC. The panel shows that there was strong localisation of the subtype 1 $InsP_3$ receptor protein in the Purkinje cell. There was a lack of fluorescent signal in the granular layer where the protoplasmic astrocytes would be. At the top edge of the section there was no fluorescent signal where you expect the Bergmann glial cells to be. The scale bar is 50μm.

Photograph B was of a single Purkinje cell at higher magnification. Anti rabbit conjugated TRITC labelled the subtype 1 $InsP_3$ receptor protein (immunolocalisation as above). There was no subtype 1 $InsP_3$ receptor proteins located in the nucleus of the Purkinje cell. The photograph shows the red fluorescence throughout the cell through a rhodamine filter of light wavelength 550-590nm. Calibration bar is 20μm.

Photograph C (Immunohistochemistry as above) was of the granular layer in the central region of a cerebellar folium. Within the granular layer the type 1 $InsP_3$ receptor proteins were in the descending axons of the Purkinje cells. The spherical regions to the left of the image were the Purkinje cell bodies. Scale bar is 50μm.

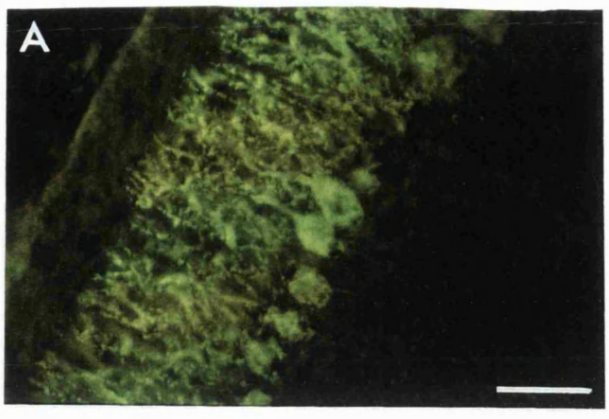
A

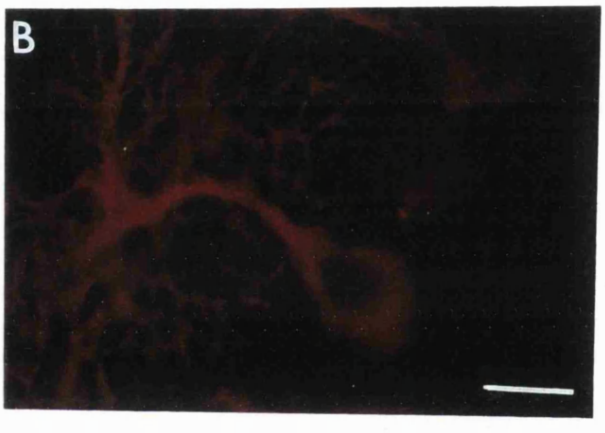
B


C

3.5.2 Neuronal and glial cell morphology was identified using double staining

Figure 3.5.2 shows clearly the double labelling within a cerebellar folium edge of a rat saggital section. GFAP was only expressed by the astrocytes and the neurones specifically express the type 1 $InsP_3$ receptor protein. The staining (to either GFAP or $InsP_3$ type 1) distinguished the morphology of the Bergmann glial cells from the neuronal Purkinje cells. The Bergmann glial cells radiate out to the pial surface, through the molecular layer of the Purkinje cell dendritic tree. Within the rat Purkinje cell dendritic tree there appears to be about 10-12 Bergmann glial cells. Figure 3.5.2 demonstrates just how closely the Bergmann glial cells were interspersed with Purkinje cells maintaining an anatomically close relationship. Figure 3.5.2 further demonstrates that the type 1 $InsP_3$ receptor protein was not present in Bergmann glial cells *in situ*.

The small size and fine projections of Bergmann glial cells makes them difficult to visually define and hence patch in acute slices. The technical difficulty in working with these cells *in situ*, means that their exact physiological role within the cerebellum remains undefined.

Figure 3.5.2 Immunolocalisation of Bergmann glial cells and Purkinje cells

The picture shows two images taken with a confocal microscope of the rat cerebellum (P12). *Panel A* depicts the astrocytic marker GFAP identified Bergmann glial cells. The fluorescence (FITC) was pseudo coloured blue. Notice how the astrocytes of the molecular layer are small thin linear structures that radiate to the edge.

Panel B shows, in the same section, the fluorescence image of rhodamine labelled Purkinje cells which were pseudo coloured blue (as above) to represent the $InsP_3$ type 1 antibody (TRITC). At P12 the dendritic tree of the Purkinje cells ends part way through the molecular layer. The section to the pial edge of the folium was predominantly glia (See Chapter 5).

Scale bar is 40μm for images A and B.

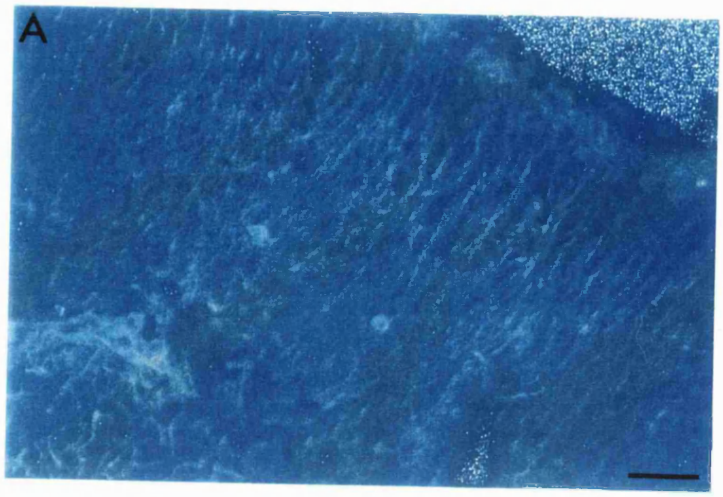
A

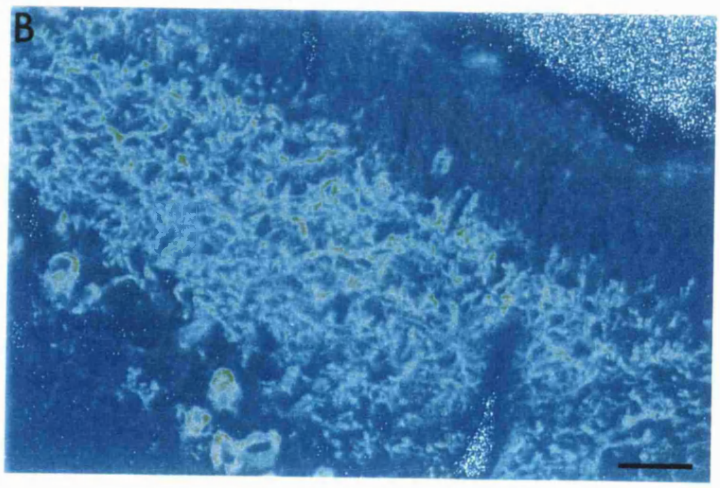
B

3.5.3 Inositol 1,4,5-trisphosphate type 2 receptor protein

Immunohistochemistry with mouse monoclonal antibodies specific for the $InsP_3$ type 2 receptor channel tried to determine the protein's location within the rat cerebellum. Figure 3.5.3 A&B depicts the result. There appeared to be some fluorescent labelling in the blood capillaries of the brain microvasculature. However this localisation in blood vessels was present in the control sections and was an artefact of the perfusion. Despite this there seemed to be no type 2 $InsP_3$ receptor proteins present in any other regions of the cerebellar slices. This data corroborates that of the cultured astrocytes (Figure 3.3.1 C&D).

3.5.4 Inositol 1,4,5-trisphosphate type 3 receptor protein

The subtype 3 $InsP_3$ receptor protein was present in the cerebellar slices. Small filamentous cells expressed the $InsP_3$ subtype 3 protein. Double immunohistochemistry (Figure 3.5.4 B) identified the $InsP_3$ type 3 positive cells as co-expressing GFAP and hence are granular layer astrocytes, a conclusion previously shown by Dr Sugiyama and his colleagues (Yamamoto-Hino-M., *et al* 1995). Yamamoto-Hino *et al* showed that Bergmann glial cells and granular layer astrocytes have the type 3 $InsP_3$ receptor protein *in situ*. However it was difficult to reproduce the quality of $InsP_3$ positive staining as seen by Yamamoto-Hino, in these sections the staining appeared to localise only around the granular region of the section. The fluorescence signals from the Bergmann glial cells were weak. However based on Yamamoto-Hino conclusions and the granular layer localisation of the antibody, these results corroborate that type 1 astrocytes *in vitro* and *in situ* express the $InsP_3$ subtype 3 receptor protein (Figure 3.3.1 E & F).

Figure 3.5.3 Type 2 $InsP_3$ receptor protein localisation *in situ*

Photograph A was illuminated with a fluorescein filter and identified the localisation of type 2 $InsP_3$ receptor protein. The blood micro-vessels had a positive fluorescent signal. However in control experiments this pattern of staining existed and was due to the perfusion technique used (4% Paraformaldehyde). There was no other fluorescent signal present in the cerebellum. Scale bar 200μm.

Photograph B shows the exact location of the fluorescent signal with higher magnification. No other brain regions demonstrated a fluorescent signal. This process was repeated n=5. All experiments showed the same pattern. Scale bar is 20μm.

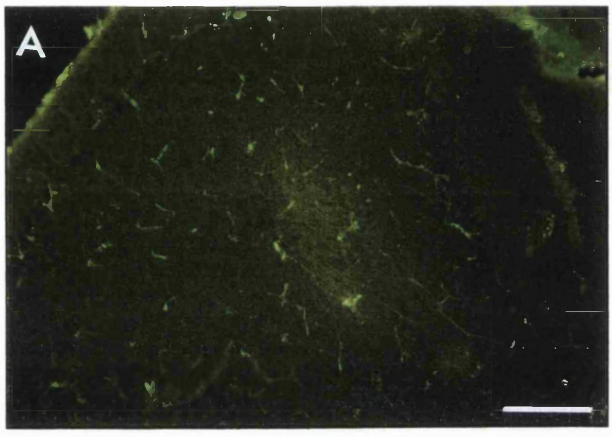
A

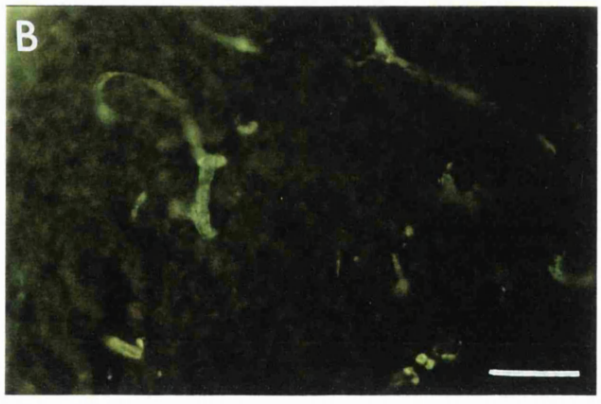
B

Figure 3.5.4 Type 3 $InsP_3$ receptor protein localisation *in situ*

Photograph A is a bright field image taken from the granular layer, comprising of a central folium region, within a saggital section of rat cerebellum. The picture represents both neurones and glial cells. The scale bar is 50μm.

Photograph B is of the same field illuminated with light of wavelength 450-490nm. The anti mouse conjugated FITC identified the antibody raised to the $InsP_3$ subtype 3 isoform. The positive cells appeared to have fine filaments, small somas, which was characteristic of the granular layer astrocytes. The scale bar is 50μm.

Photograph C shows the identical field to A and B illuminated with a rhodamine filter 550-590nm. The anti rabbit TRITC stained the GFAP antibody (raised in rabbit). This image shows that the labelling of the type 3 $InsP_3$ antibody was co-expressed with GFAP the astrocytic marker. This result confirms that *in situ* astrocytes appear to have low level $InsP_3$ type 3. The scale bar is 50μm.


A

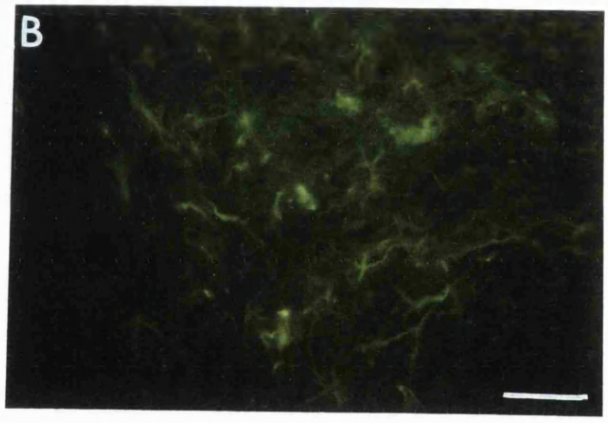
B

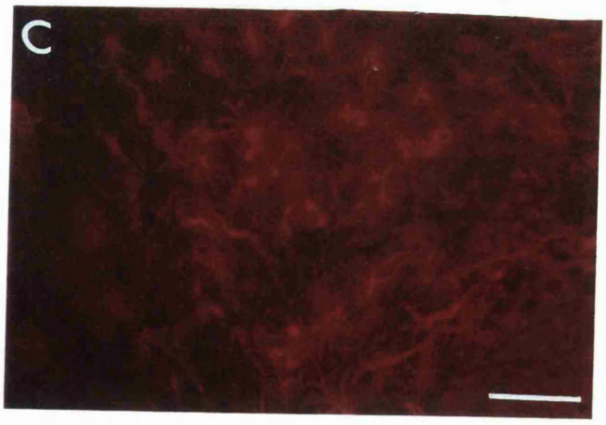
C

3.6 Summary

i) Type 1 astrocytes in culture have a characteristic morphology with a large cytoplasm and a raised cell soma. Type 1 astrocytes are GFAP positive, Gal C negative, 04 negative, and A2B5 negative. Type 1 astrocytes are transparent cells which in culture readily migrate and spread to make contact with other adjacent glial cells. Visually these astrocytes were easy to identify unlike other glia in culture (Figure 3.6.1 A).

ii) Fibrous "type 2 like" astrocytes are GFAP positive, A2B5 positive, 04 negative, and Gal C negative and were identified in the rat cerebellar cultures of >8 DIV. The fibrous "type 2 like" astrocytes have not been located *in vivo* (Miller-R.H. *et al* 1989) and are thought to be culture artefacts (Fulton-B.P. *et al* 1991). The small cell soma and filamentous morphology of the "type 2 like" astrocytes are difficult to visualise and characterise.

iii) Low levels of oligodendrocytes, which are positive to Gal C, 04, and negative to GFAP were identified in the cultures after 7 DIV. Before this stage *in vitro* the oligodendrocytes have not differentiated from the O2A progenitor cells. The cell culture medium used in these experiments (BME supplemented with 10% foetal calf serum) favours astrocytic development and as a result oligodendrocytes made up less than 5% of the cultures contents. O2A Progenitor cells are small bipolar cells and have a similar morphology to degenerating nerve cells in culture. O2A Progenitor cells can differentiate into oligodendrocytes or "type 2 like" astrocytes. Between 1-7 DIV it was difficult to visually distinguish the stage of O2A progenitor metamorphosis into oligodendrocytes or type 2 astrocytes making their exact phenotypic characterisation difficult.

iv) Cerebellar cultured type 1 astrocytes (5 DIV) have gap junction proteins, located in their plasma membrane consisting of connexin 43 units.

v) Rat cerebellar type 1 astrocytes express the $InsP_3$ subtype 3 receptor protein *in vitro* (Figure 3.2.1 F). These cultured astrocytes do not appear to express detectable levels of type 1 (figure 3.2.1 B) but may have a low density of $InsP_3$ subtype 2 receptor proteins (see figure 3.2.1 D).

vi) Bergmann glial cells and protoplasmic astrocytes express the $InsP_3$ type 3 receptor isoform (Yamamoto-Hino *et al* 1995) *in situ.* This study shows that the protoplasmic

"type 1 like" astrocytes in rat cerebellar slices express the type 3 $InsP_3$ receptor protein. However it was difficult to detect any $InsP_3$ type 3 positive staining in Bergmann glial cells within these saggital sections. Bergmann glia and granular layer astrocytes do not appear to express detectable levels of the subtype 1 or 2 receptor proteins.

vii) Within P12 rat cerebellar slices Bergmann glial cells radiate to the pial surface of the folium but the Purkinje cell dendritic tree at this stage does not (Figure 3.5.2). The separation of neuronal and glia projections at the pial surface is important in identifying glial cells *in situ* (see chapter 5).

Table 5: Summary of subtype $InsP_3$ receptor proteins.

(**X=Not** detectable amounts of $InsP_3$: **O**=$InsP_3$ isoform **is present**)

$InsP_3$ SUBTYPE	**TYPE 1**	**TYPE 2**	**TYPE 3**
IN VITRO			
GLIAL TYPE 1 ASTROCYTE	**X**	**X?**	**O**
IN SITU			
BERGMANN GLIA	**X**	**X**	**X**
GRANULAR LAYER ASTROCYTE	**X**	**X**	**O**
CEREBELLAR NEURONES			
PURKINJE	**O**	**X**	**X**
GRANULE	**X**	**X**	**X**
BASKET	**X**	**X**	**X**
STELLATE	**X**	**X**	**X**
LUGARO	**X**	**X**	**X**
VASCULAR			
PORCINE ENDOTHELIAL	**O**	**O**	**X**
BRAIN CAPILLARIES	**O**	—	—

CHAPTER 4

KINETIC CHARACTERISATION OF THE $InsP_3$ INDUCED CALCIUM RELEASE WITHIN ASTROCYTES.

4. Introduction

Glial cells respond to extracellular stimuli such as neurotransmitters, neuropeptides, blood plasma proteins and hormones by changes in intracellular calcium concentrations ($[Ca^{2+}]i$) within the glial cytosol (Verkhratsky-A. *et al* 1998). The agonists bind to specific membrane located, G-protein coupled receptors and cause the production of $InsP_3$ from a membrane bound phospholipid PIP_2. $InsP_3$ binds to specific $InsP_3$ receptors, located on the membranes of the endoplasmic reticulum which are known to be intracellular calcium stores, to release calcium into the cytosol (Berridge-MJ, & Irvine-R.F., 1989 ; Berridge-MJ 1993). This second messenger mechanism is present in glial cells *in vitro* (Khodakhah-K.& Ogden-D.C., 1993 ; Charles-A.C. *et al* 1993). Astrocytes also express the $InsP_3$ receptor isoform type 3 (see chapter 3) and it is possible that astrocytes uses Ca^{2+} as a second messenger in a slow signalling system, analogous to hormonal signalling in non-excitable peripheral cells.

The observations that glial cells possess neurotransmitter receptors, ion channels and are capable of stimulus-evoked calcium responses has led to the hypothesis that glial cells have a calcium based signalling system which can influence neuronal behaviour (Cornell-Bell-A. H., *et al* 1990 ; McNaughton-L.A., *et al* 1990 ; McNaughton-L.A., *et al* 1990 : Jensen-A.M., & Chiu-SY, 1990). There is strong evidence of a bi-directional Ca^{2+} signalling between neurones and glial cells. In rat optic nerve glial $[Ca^{2+}]i$ is increased by glutamate released from axons of stimulated nerves (Kriegler-S. & Chiu-S.Y. 1993). Glial $[Ca^{2+}]i$ can also influence neurotransmitter receptor activity directly in neurones. In co-cultures of rat cortical astrocytes and neurones, astrocytes release glutamate to directly excite adjacent neurones by causing NMDA receptor mediated rises in $[Ca^{2+}]i$ Parpura-V. *et al* (1994) and Nedergaard (1994) showed in a separate study that when astrocytic calcium waves were induced in co-cultures the neuronal cytosolic $[Ca^{2+}]i$

also increased. This neuronal increase in cytosolic [Ca^{2+}] can be attenuated by gap junction antagonists, suggesting there is a cytosolic connection between neurones and glial cells in culture.

The kinetics and regulation of $InsP_3$ evoked Ca^{2+} release have been examined in a number of preparations using a variety of techniques. It is necessary to gain access to receptors in the cytosol, to release $InsP_3$ in a controlled way and measure kinetic changes of [Ca^{2+}]i. Techniques used to study $InsP_3$ receptors are: channel reconstitution into lipid bilayers (Bezprozvanny-I. & Ehrlich-B. 1994), permeabilised cells (Iino-M, 1990), microsomal preparations (Combettes-L. *et al* 1994; Finch-E.A. *et al* 1991) and photolysis of caged $InsP_3$ (Ogden-DC, *et al* 1990; Khodakhah-K & Ogden-D.C. 1995; Ogden-D., & Capiod-T., 1997;Carter-T.D. & Ogden-D. 1997). These types of studies have shown that the $InsP_3$ evoked [Ca^{2+}]i rise is a fast event, regulated by free cytosolic [Ca^{2+}] as well as $InsP_3$.

The aim of the experiments in this chapter was to investigate the kinetics of $InsP_3$ induced Ca^{2+} release within cerebellar astrocytes *in vitro* and *in situ.* Flash photolysis of caged $InsP_3$ and microspectrofluorimetry were used to study the kinetics of [Ca^{2+}]i rises as a result of astrocytic $InsP_3$ receptor activation. The kinetic details gained can give information about the mechanisms regulating the astrocytic $InsP_3$ type 3 receptor during neurotransmitter stimulation and release of Ca^{2+} ions. The $InsP_3$ induced Ca^{2+} rise can be divided up into a number of components (see figure 4.0.1) which can be quantified. (1) An initial delay, (2) the fast rising phase which is due to Ca^{2+} flux into the cytosol. Rate of rise of [Ca^{2+}]i=d[Ca^{2+}]i/dt measures flux in moles/litre cytosol/second (3) peak free [Ca^{2+}]i where net flux d[Ca^{2+}]/dt is zero (4) a decline where d[Ca^{2+}]/dt is negative due to Ca^{2+} removal. These kinetic parameters were used to provide information about the glial $InsP_3$ receptor protein and its function. How do delays of Ca^{2+} flux and peak Ca^{2+} depend upon $InsP_3$ concentration? What mechanism is responsible for the abrupt cessation of the Ca^{2+} flux at peak [Ca^{2+}]i, is there evidence for regulation of $InsP_3$ evoked flux by [Ca^{2+}]? Therefore how does $InsP_3$ evoked [Ca^{2+}]i release in astrocytes (with type 3 receptor) compare to other peripheral non-excitable cells and Purkinje neurones?

The latter part of the chapter shows measurements of $InsP_3$ induced [Ca^{2+}]i rises in Bergmann glial cells from the rat cerebellar slice. This section of work attempted to characterise differences in astrocytes $InsP_3$ induced Ca^{2+} responses *in situ* compared to the *in vitro*.

4.1 Flash photolysis of caged $InsP_3$ combined with microfluorimetry.

In control experiments the caged $InsP_3$ was omitted from the internal solution. The type 1 astrocytes were patched, loaded with a Ca^{2+} sensitive indicator and flashed with a 1ms U.V. pulse from the flash gun. Figure 4.0.2 shows an example of a control response. U.V illumination of a whole cell patch clamped astrocyte without caged $InsP_3$ present in the pipette solution demonstrated no change in free $[Ca^{2+}]i$ levels (n=7 cells). The membrane current remained constant in response to the pulse of U.V. light (seen as a flash artefact in figure 4.0.2). All astrocytes in these experiments (chapter 4) were voltage clamped at their resting membrane potentials (I=0), to ensure that any changes in cytosolic free $[Ca^{2+}]i$ were as a result of release from intracellular stores by $InsP_3$. Membrane current records are not presented in further figures as they remained constant during the recordings.

Figure 4.0.1 An example of an $InsP_3$ induced $[Ca^{2+}]i$ rise in a type 1 like protoplasmic astrocyte.

(A) The figure shows a change in free $[Ca^{2+}]i$ in response to photolysis of caged $InsP_3$ in a single type 1 cerebellar astrocyte. For kinetic analysis the response has been divided into distinct sections which can be quantified. The arrow indicates the flash artefact and is the time of $InsP_3$ release (1) Delay between $InsP_3$ release and $[Ca^{2+}]i$ change (2) The net Ca^{2+} flux into the cytosol by measuring the rate of rise $d[Ca^{2+}]/dt$ as the linear fit to the rising phase (moles/litre of cytosol/second). (3) Peak $[Ca^{2+}]i$ is the point of the response where there was no net Ca^{2+} flux into the cytosol and so $d[Ca^{2+}]/dt=0$ (4) The initial rate of response decline, where $d[Ca^{2+}]/dt$ is negative.

The scale bar is represented bottom . horizontal at 2 seconds and vertical represents a rise of 5μM of $[Ca^{2+}]i$.

(B) Membrane current recorded simultaneously with the fluorescence trace. The artefact indicates the point of photolysis. The cell was whole cell voltage clamped at -37mV which was the resting membrane potential for this cell. The horizontal scale bar denotes 2 seconds and vertical represents a change in membrane current of 50pA.

Figure 4.0.2: A result from a control experiment.

(A) This figure shows an example of a control experiment with the calcium indicator furaptra (500μM). The figure shows no change in $[Ca^{2+}]i$, in a type 1 cerebellar astrocyte *in vitro* as a result of the U.V pulse. The flash artefact is indicated by the arrow. The horizontal scale bar shown is 2 seconds and the vertical bar is for a $[Ca^{2+}]i$ change of 10μM.

(B) Changes in membrane current during flash lamp pulse applied in a control experiment. The artefact indicates the lamp discharge. Same time scale as the fluorescence record. Type 1 astrocyte whole cell voltage clamped at -45mV (the resting membrane potential for this cell). Horizontal scale bar denotes 2 seconds, and vertical scale bar is 50 pA.

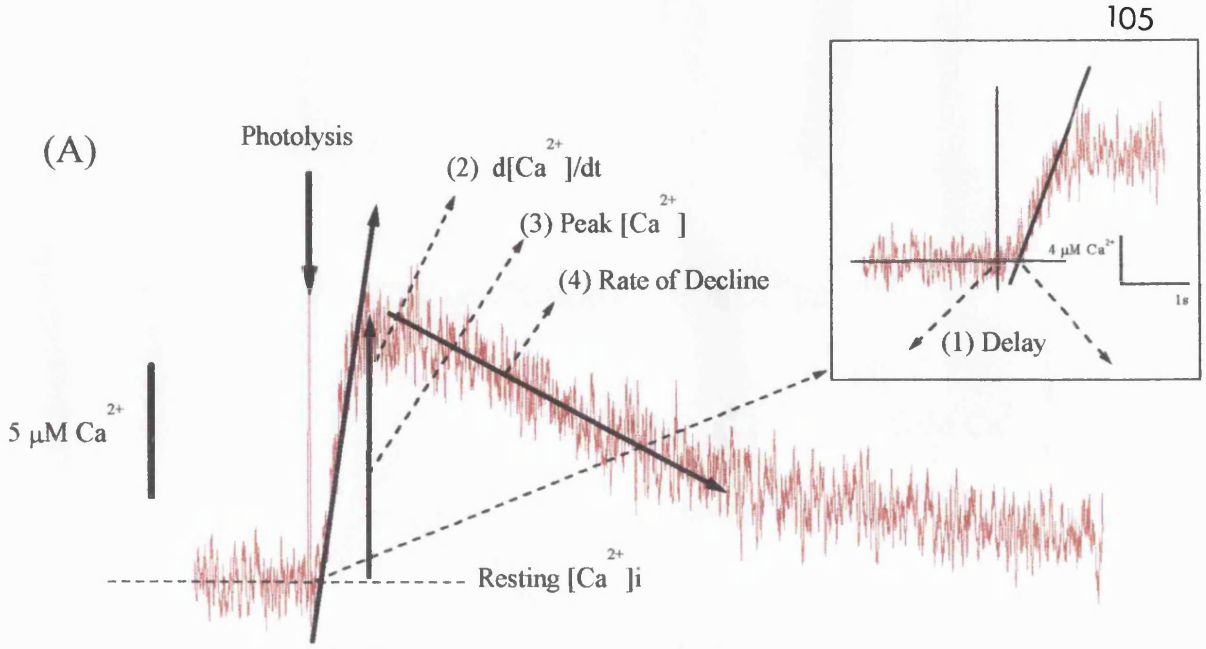
(A)
Photolysis
(2) d[Ca 2+]/dt
(3) Peak [Ca 2+]
(4) Rate of Decline
(1) Delay
4 μM Ca2+
1s
5 μM Ca 2+
Resting [Ca 2+]i

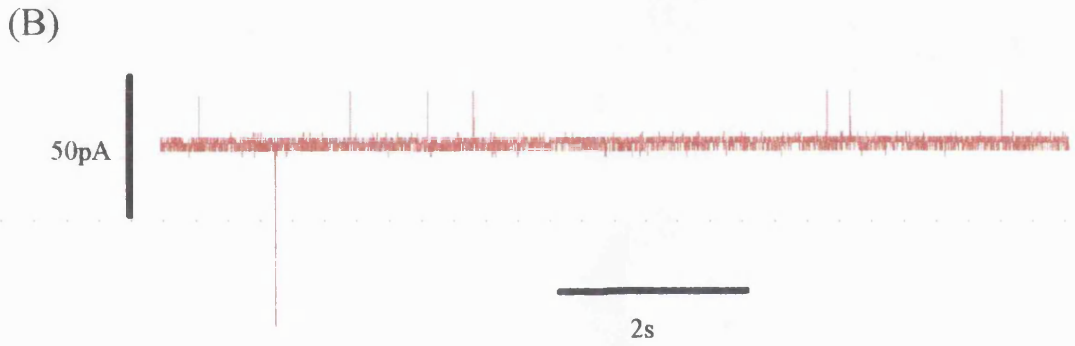
(B)
50pA
2s

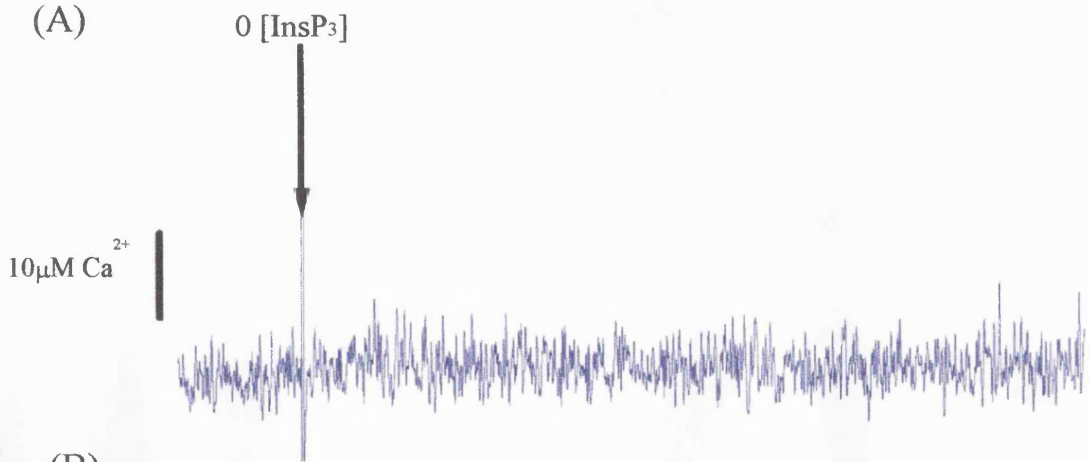
(A)
0 [InsP3]
10μM Ca 2+

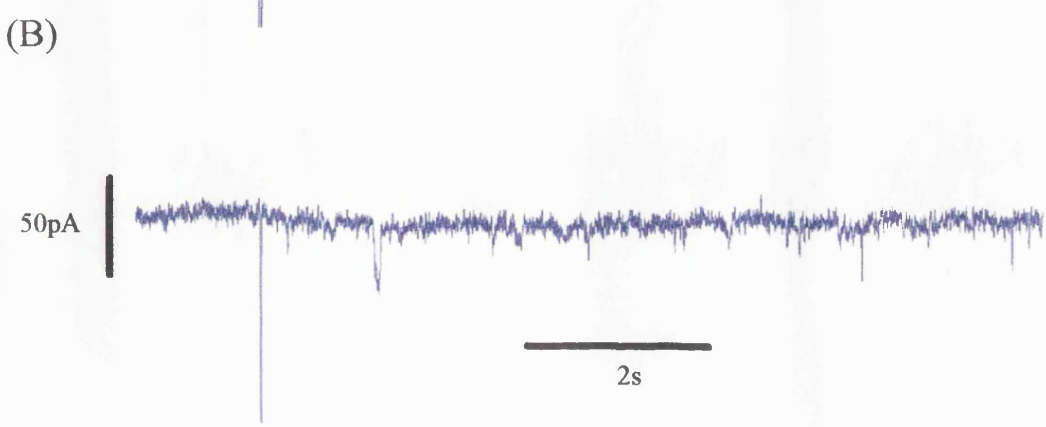
(B)
50pA
2s

$InsP_3$ evoked $[Ca^{2+}]i$ responses were analysed with respect to the four distinguishable components (figure 4.0.1) and quantified as follows:

4.1.1 Delay of $InsP_3$ induced $[Ca^{2+}]i$ response.

As in experiments by (Ogden-DC, *et al* 1990; Khodakhah-K & Ogden-D.C. 1995 ; Ogden-D.C. & Capiod-T, 1997 ; Carter-T.D. & Ogden-D. 1997) low $InsP_3$ concentrations activated $[Ca^{2+}]i$ responses in type 1 astrocytes after a delay. The initial delay in receptor activation was dependent on the $InsP_3$ concentration released (see figure 4.1.1 A B C). Figure 4.1.1 illustrates Ca^{2+} responses induced by three different $InsP_3$ concentrations in three separate type 1 astrocytes *in vitro*. The time interval between photoreleased $InsP_3$ (marked by the arrow at the artefact) and rise of $[Ca^{2+}]i$ is related to $InsP_3$ concentration.

Figure 4.1.2 is a summary of all data of delay times in milliseconds of initial responses plotted against $InsP_3$ concentration on a log scale (n=20 cells). The graph demonstrates that at low $InsP_3$ concentrations the delays of response initiation were longer compared to the higher $InsP_3$ concentration. At low $InsP_3$ concentration between (0.1-0.4 μM) the delays range from 95 to 520ms, whereas at high $InsP_3$ concentrations (10-25 μM) the delays were shorter from 71-200ms. The data in figure 4.1.2 shows at low $InsP_3$ concentration (less than 1μM) delays of mean 267 ±66ms occur (Mean±SEM, n=7 cells) whereas at higher $InsP_3$ concentrations 10-25μM the responses had average delays of 111ms (±15 ms, n=9 cells).

In some experiments the initial phase of the $[Ca^{2+}]i$ rise was obscured by the flash artefact so a delay time could not be measured (figure 4.1.3). During photolysis experiments a 1ms pulse of U.V light causes the glass or quartz to phosphoresce. Phosphorescence phase of glass can last for ≥50ms, so no emitted fluorescent light from the cell can be recorded. Quartz has an artefact of ≤ 20ms, so was more suited to these experiments. (See also section 4.6.1). The delay times for Ca^{2+} responses were only plotted when a clear latency was distinguishable.

Figure 4.1.1 Initial delays in time courses of evoked $[Ca^{2+}]i$ changes are dependent on different $InsP_3$ concentration

The photolysis of caged was $InsP_3$ was calibrated previously (results in chapter 2, section 2.7.2).

This figure shows a low (0.3μM) $InsP_3$ concentration evoked $[Ca^{2+}]i$ rise, a medium (3μM) and a high (24μM) in three separate type 1 astrocytes *in vitro*. The $[Ca^{2+}]i$ change was measured in whole cell voltage clamp mode held at resting membrane potential with 500μM furaptra in the three cells. The flash induced release of $InsP_3$ was indicated by an arrow and the resultant artefact. The time delay of response was estimated from the point of photolysis flash to the region where the fluorescence level rises above the baseline (see figure 4.0.1)

Panel A is an example of the low (0.3μM) $InsP_3$ induced $[Ca^{2+}]i$ and had an initial delay of 165ms. Holding potential =-20mV.

Panel B a medium (3μM) $InsP_3$ induced $[Ca^{2+}]i$ rise with a delay of 161ms. Holding potential=-40mV.

Panel C is a high (24μM) $InsP_3$ evoked $[Ca^{2+}]i$ rise which had a delay of 68ms. Holding potential=0mV.

Scale bars are the same for each cell at horizontal representing 0.25 seconds, vertical a change of $[Ca^{2+}]i$ of 5μM for A and B, and 10μM for figure C. All data summarised in figure 4.1.2.

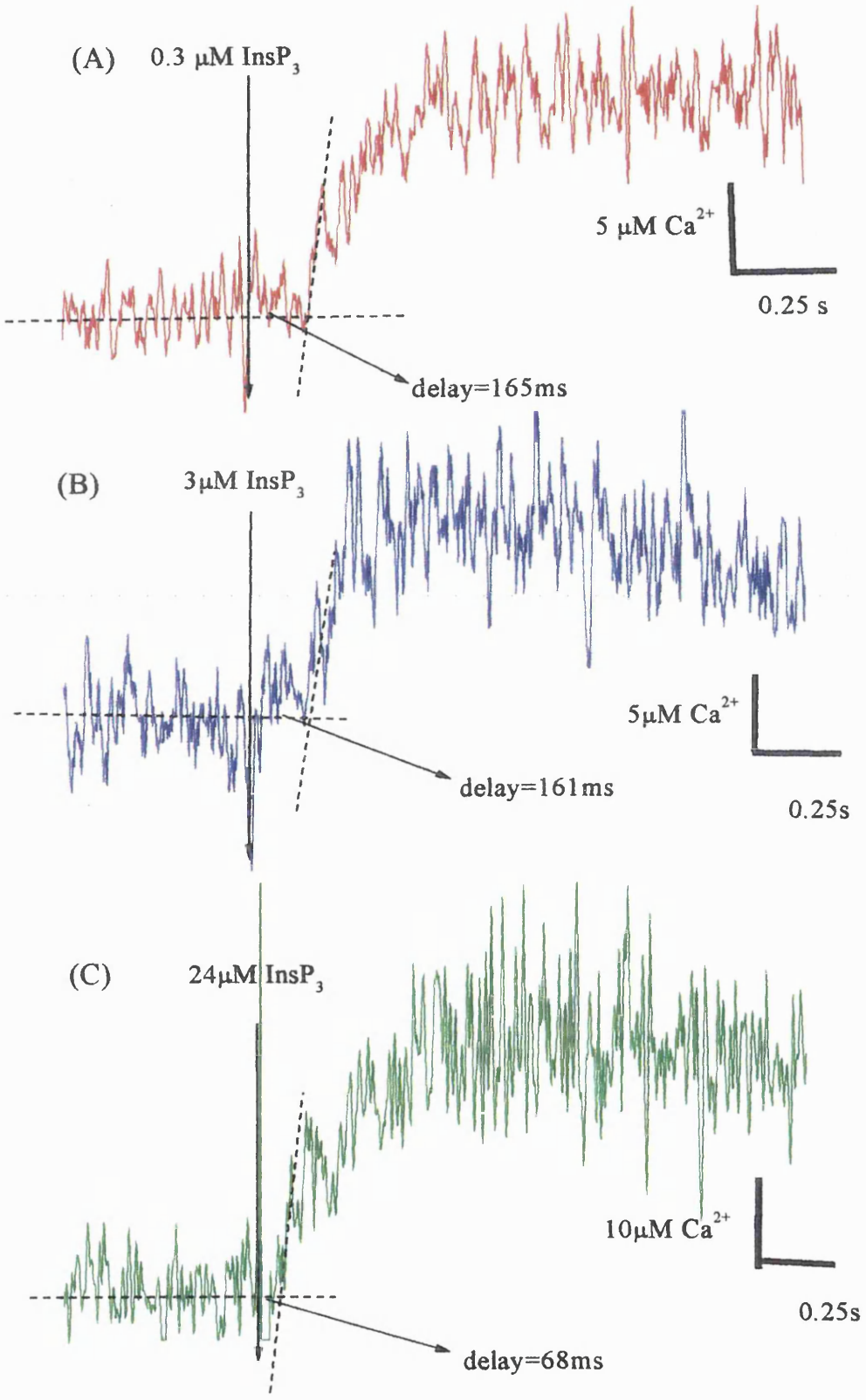
(A) 0.3 μM InsP3
5 μM Ca2+
0.25 s
delay=165ms
(B) 3μM InsP3
5μM Ca2+
delay=161ms
0.25s
(C) 24μM InsP3
10μM Ca2+
0.25s
delay=68ms

Figure 4.1.2 Delays of $InsP_3$ evoked $[Ca^{2+}]i$ responses in cerebellar cultured type 1 astrocytes.

This figure shows data from single astrocytes for the delay times (milliseconds) between $InsP_3$ release and initiation of Ca^{2+} flux into the cell cytosol (n=20 cells). The astrocytes $[Ca^{2+}]i$ rises were measured with 500μM furaptra and plotted against $InsP_3$ concentrations in μM on a log scale.

Low $InsP_3$ concentrations	0-1μM	267±66	n=7
Medium $InsP_3$ concentrations	1-10μM	132±25	n=4
High $InsP_3$ concentrations	10-25μM	111±15	n=9

Figure 4.1.3 Initial rising phase of $InsP_3$ induced $[Ca^{2+}]i$ response in a cell grown on a glass coverslip.

This figure shows a flash induced release of $InsP_3$ from a photolabile cage in a type 1 astrocyte that has been cultured on a glass coverslip. The fluorescence of the initial rising phase of the response is obscured by the phosphorescence of the glass coverslip.

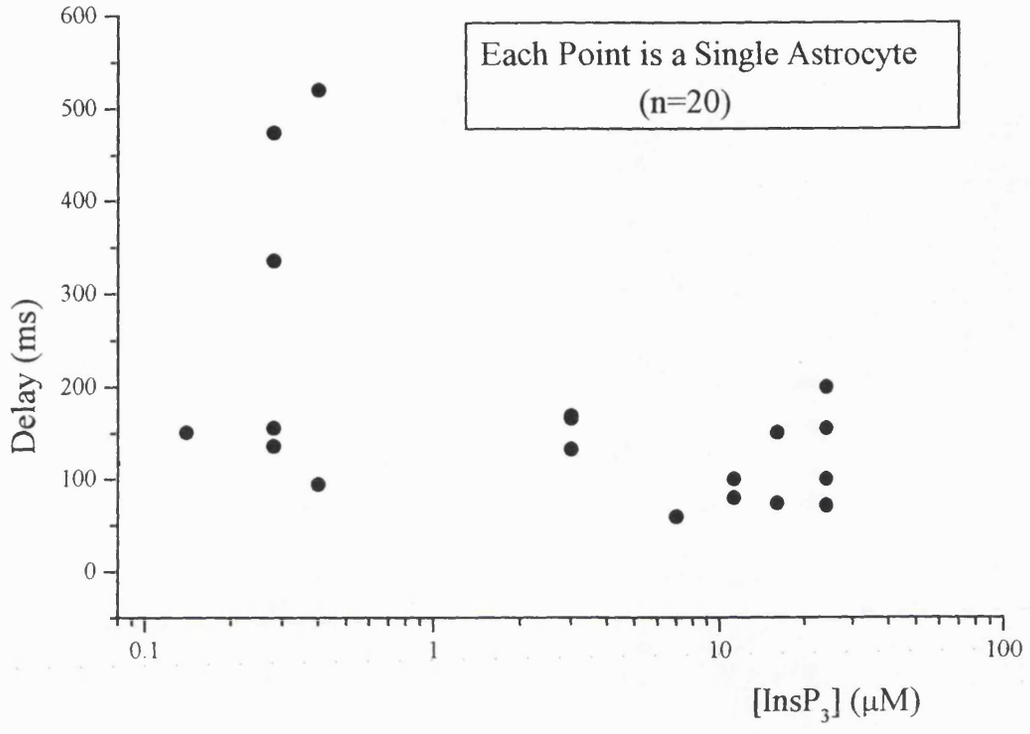
Each Point is a Single Astrocyte
(n=20)
Delay (ms)
600
500
400
300
200
100
0
0.1
1
10
100
[InsP3] (μM)

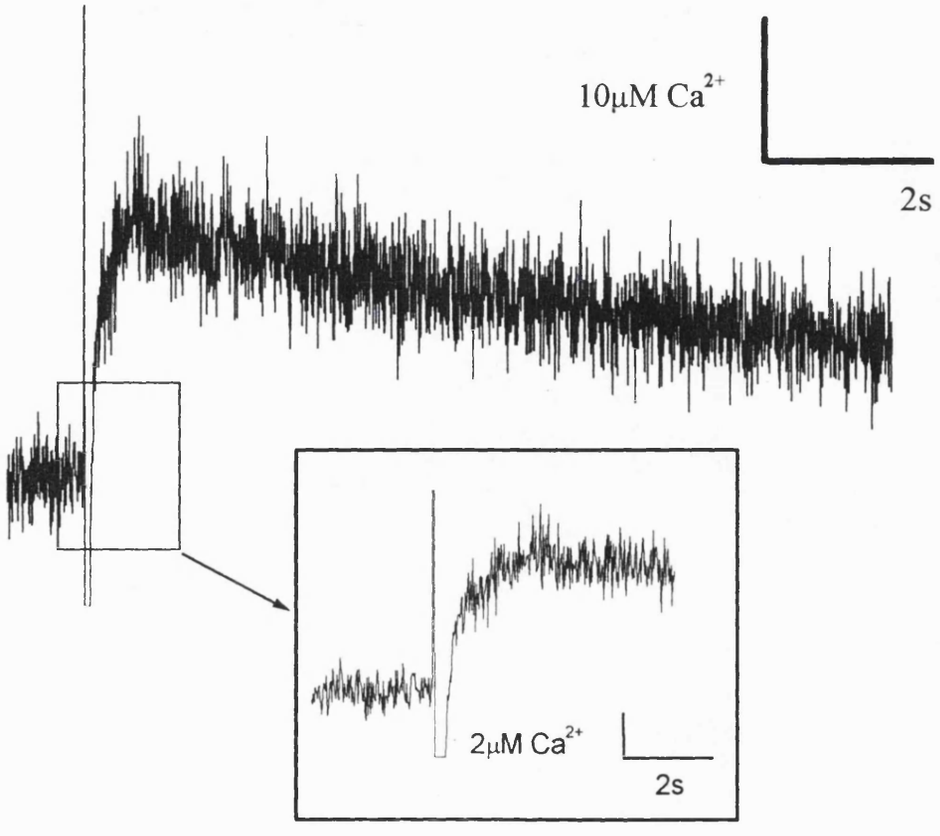
10μM Ca2+
2s
2μM Ca2+
2s

The initial delay times cannot be accounted for by the delay time of photolytic $InsP_3$ release. $InsP_3$ has a half time of release of 3 ms (Walker *et al* 1989). The shorter delays seen at higher $InsP_3$ concentrations are an indication that $InsP_3$ is capable of acting directly upon the receptor protein.

4.1.2 Rate of rise of $InsP_3$ evoked $[Ca^{2+}]i$ response measures Ca^{2+} flux into the cytosol.

The rate of free $[Ca^{2+}]i$ change ($d[Ca^{2+}]i/dt$) is used as a measure of Ca^{2+} flux from internal stores via the $InsP_3$ receptor into the cytosol (Ogden-DC, *et al* 1990). Free $[Ca^{2+}]i$ results from (i) the rate of flux of Ca^{2+} into the cytosol from internal stores (ii) rate of Ca^{2+} efflux from the cytosol (either out of the cell or back into internal stores) (iii) the amount of Ca^{2+} ions buffered within the cytosol by endogenous proteins and the Ca^{2+} indicator.

Reporting transient $[Ca^{2+}]i$ changes with high affinity indicators that have dissociation constants around resting $[Ca^{2+}]i$ underestimates the speed and amplitude of the response. Localised high $[Ca^{2+}]i$ that occur near receptor sites saturate the indicators so the spatial average fluorescence signal underestimates the average $[Ca^{2+}]i$. Due to the hyperbolic relationship of fluorescence and Ca^{2+} binding $d[Ca^{2+}]i/dt$ is not the same as the dF/dt (where F=fluorescence). With low affinity indicators (e.g furaptra) the relationship of F and binding is linear over a wide range up to high $[Ca^{2+}]i$ so the spatial average of F is proportional to $[Ca^{2+}]$ at all times during the response.

A comparison of fluo-3 and furaptra (Ogden-D., *et al* 1995) showed that furaptra provided better estimates of fast $[Ca^{2+}]i$ rises than fluo-3 in hepatocytes, Purkinje cells, and endothelial cells. Fluo-3 is a high affinity Ca^{2} indicator ($K=0.4\mu M$). Fluorescence traces of Ca^{2+} activated K^{+} conductances (with similar time scales) in cells loaded with furaptra and fluo-3 were compared. Cells loaded with fluo-3 had signals that were distorted by the non linearity of fluo-3 and Ca^{2+} binding at high $[Ca^{2+}]$ compared to furaptra traces which had a fast rise and decline time.

The peak Ca^{2+} flux was estimated from the maximum rate of rise of free $[Ca^{2+}]i$ by fitting a line to the linear region of the rise. The $d[Ca^{2+}]i/dt$ measures $[Ca^{2+}]i$ flux into the cells cytosol, in units of moles/litre of cytosol/second, and so is proportional to the $InsP_3$ channel density per unit volume times the channel open probability. This allows

the channel activity of the $InsP_3$ receptor to be measured and quantified. (figure 4.1.4). Furthermore Ca^{2+} indicators form a pool of mobile Ca^{2+}-buffering in the cytosol. The extent of buffering can be calculated from the indicator concentration, the K_{Ca} and the free $[Ca^{2+}]$. At free $[Ca^{2+}]i$=100nM buffering by 100μM fluo-3 (K_{Ca}=0.4μM) averages 200 Ca^{2+} ions bound for each free ion, and for 500μM furaptra (K_{Ca}=48μM) 10 bound Ca^{2+} for each free Ca^{2+} ion (Ogden-D. *et al* 1995).

Figure 4.1.4 Varying $InsP_3$ concentrations induces different $d[Ca^{2+}]/dt$ in a single type 1 astrocyte.

This figure shows two responses taken from the same cultured type 1 astrocyte during whole cell voltage clamp at -13mV, resting membrane potential for this cell (where I=0). The indicator (500μM) fura-2-ff and caged $InsP_3$ were applied to the inside of the cell via the patch pipette. The cells were grown on quartz coverslips for 4 DIV.

Panel A is a rise in $[Ca^{2+}]i$ derived from the fluorescence trace. 24μM $InsP_3$ evoked a Ca^{2+} response with a $d[Ca^{2+}]i/dt$ of 36.7μMs^{-1}.

Panel B illustrates the second $[Ca^{2+}]i$ rise recorded from the same cell under identical voltage clamp conditions. The 17μM photolytically released $InsP_3$ induced a $d[Ca^{2+}]i/dt$ of 27.9μMs^{-1}

Horizontal scale bar represents an $[Ca^{2+}]i$ change of 5μM, vertical represents a time interval of 0.5 seconds.

The recording of consecutive responses in the same cell maintains identical numbers of $InsP_3$ receptor proteins so $d[Ca^{2+}]i/dt$ can be compared. This data is an illustration of how $d[Ca^{2+}]i/dt$ of $InsP_3$ induced $[Ca^{2+}]i$ increases with $InsP_3$ concentration.

Panel C :Data from single cells for rate of Ca^{2+} release plotted against $InsP_3$ concentration

Panel C shows pooled data from 21 separate rat cerebellar type 1 astrocytes. Each cell was whole cell voltage clamped at resting membrane potential, and the $[Ca^{2+}]i$ measured with 500μM furaptra. The data shows rates of reaction $d[Ca^{2+}]i/dt$ (μMs^{-1}) plotted on a log scale against varying $InsP_3$ concentrations. The data shows that as $InsP_3$ concentration increases the $d[Ca^{2+}]i/dt$ remains fairly constant in individual cells.

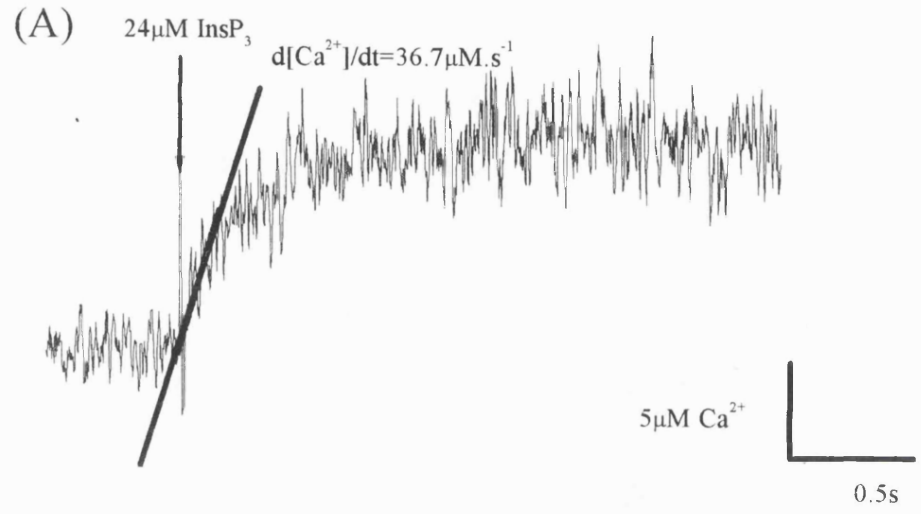
(A)
24μM InsP3
d[Ca2+]/dt=36.7μM.s-1
5μM Ca2+
0.5s

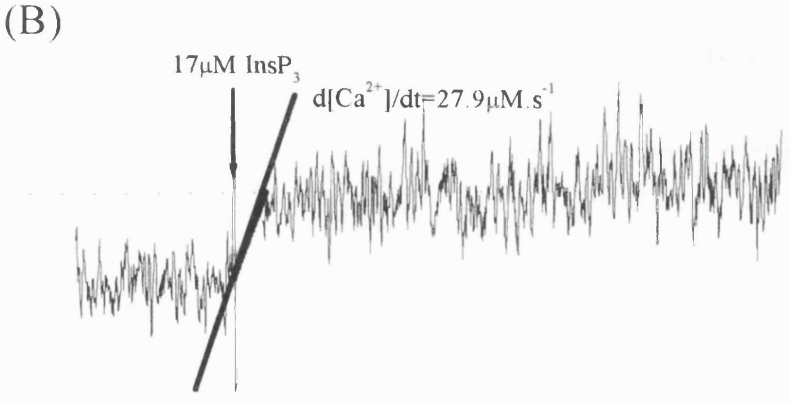
(B)
17μM InsP3
d[Ca2+]/dt=27.9μM.s-1

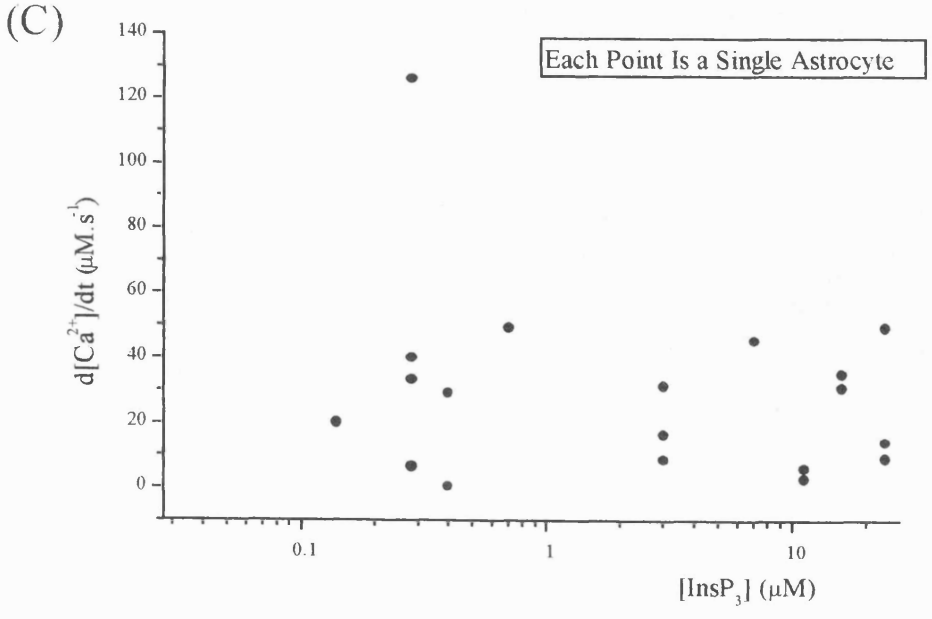
(C)
Each Point Is a Single Astrocyte
d[Ca2+]/dt (μM.s-1)
140
120
100
80
60
40
20
0
0.1
1
10
[InsP3] (μM)

Figure 4.1.4. illustrates that in the same cell, when the density of $InsP_3$ receptors are the same, the $d[Ca^{2+}]/dt$ was dependent on the $InsP_3$ concentration. Response (A) for 24μM $InsP_3$ has a rate of activation of 36.7μMs^{-1}, whereas the second (B) for 17μM $InsP_3$ has a lower rate 27.9μMs^{-1}. Data with two pulses in the same cell were not obtained often.

Figure 4.1.4.C shows pooled data for $d[Ca^{2+}]/dt$ plotted against $InsP_3$ concentrations from 21 cells. Figure 4.1.4.C shows that the $d[Ca^{2+}]/dt$ generally was not dependent on the $InsP_3$ concentration in separate cells. As the $InsP_3$ concentration increases the rate of change of $[Ca^{2+}]i$ remains constant. The maximum $[Ca^{2+}]i$ change for a cultured type 1 astrocytes was 126 μMs^{-1} (n=1); this was an exception.

It was evident (from figure 4.1.4.C) that there was considerable variation in Ca^{2+} flux $d[Ca^{2+}]/dt$ for the same $InsP_3$ concentrations in different cells. This could be interpreted by the fact that individual cells (i) have different $InsP_3$ receptor densities. (ii) The rate of Ca^{2+} flux may actually be constant with only the rate of endogenous buffering differing. (iii) The variability may also be due to heterogeneous receptor channel properties due to the presence of various $InsP_3$ receptor protein subtypes (Nakade-S., *et al* 1994; Monkawa-T. *et al* 1995).

4.1.3 Peak free $[Ca^{2+}]i$

Responses are shown as a rise from resting $[Ca^{2+}]i$ cellular levels and so were measured as changes and not absolute values. Maximum changes in peak $[Ca^{2+}]i$ were 25μM and minimum values around 2.5μM for photoreleased $InsP_3$ concentration 0.1-25μM.

There was also considerable cell to cell variation in the peak free $[Ca^{2+}]i$ from individual cultured type 1 astrocytes. The reason for the variation in peak $[Ca^{2+}]i$ maybe the same as those for $d[Ca^{2+}]i/dt$ as discussed above.

To test directly the effect of $InsP_3$ concentration on the flux and peak free $[Ca^{2+}]i$ it is necessary to release $InsP_3$ at different concentrations within the same cell. In hepatocytes (Ogden-D.C. & Capiod-T. 1997), endothelial cells (Carter-T. & Ogden-D.C. 1997) and Purkinje cells (Khodakhah-K. & Ogden-D.C. 1995) such experiments have shown a concentration dependence of both flux and peak free $[Ca^{2+}]i$ in response to varying $InsP_3$ concentrations. However, in the experiments described here, it was not routinely possible

to record more than one response to photolytic release of $InsP_3$. Thus data for flux rates and peak $[Ca^{2+}]i$ were derived from single responses in any particular cell. The reason for the rapid run down of responses was not clear, but may reflect loss of some essential cytosolic factor during whole cell recording.. Astrocytic peak free $[Ca^{2+}]i$ levels did not vary systematically with varied $InsP_3$ concentrations (0.1-25μM) in separate cells; however there was considerable variation in the size of $d[Ca^{2+}]i/dt$ and peak free $[Ca^{2+}]i$ in different cells for the same $InsP_3$ concentration. These differences are probably due to the $InsP_3$ receptor channel density being heterogeneous across a population of cells.

Figure 4.1.5 Peak free$[Ca^{2+}]i$ plotted against $InsP_3$ concentration.

The graph illustrates the peak free $[Ca^{2+}]i$ (μM) as a function of $InsP_3$ concentration (μM) (cells n=21). Each circle is a separate cell 3-7DIV. The *x* axis is on a log scale *y* is linear. The graph shows considerable cell to cell variation in the size of peak $[Ca^{2+}]i$.

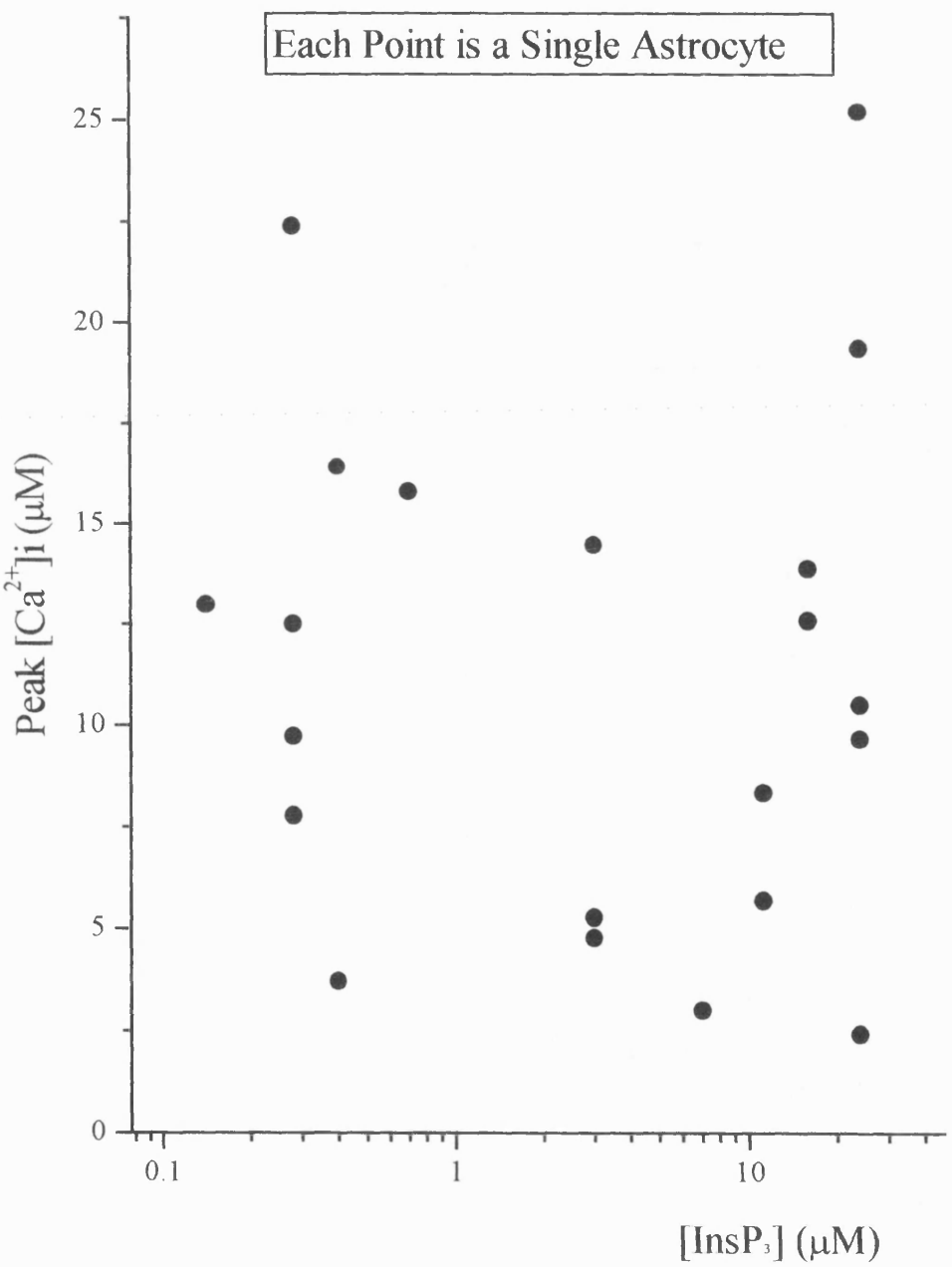

The peak free $[Ca^{2+}]i$ measurements are spatial averages of fluorescence from the entire recording area of the cell. The region of cytosol adjacent to the calcium stores has high initial localised $[Ca^{2+}]i$ changes due to flux through the $InsP_3$ R channel (Stern-M.D. 1992 ; Rizzuto-R. *et al* 1993 ; Roberts-W.M. 1994). Therefore if the localised $[Ca^{2+}]i$ is close to the dissociation constant for furaptra it is probable that the peak $[Ca^{2+}]i$ adjacent to the $InsP_3$ receptor proteins are actually higher than those recorded here due to local saturation of the furaptra. Consequentially the peak $[Ca^{2+}]i$ may be underestimated.

4.1.4 Termination and decline of $InsP_3$ evoked $[Ca^{2+}]i$ rise.

After the peak, $[Ca^{2+}]i$ levels decline due to net loss of Ca^{2+} from the cytosol. Generally, the rate of decline is much less than the rate of rise due to $InsP_3$ evoked Ca^{2+} flux. Figure 4.16 A shows initial rates of decline plotted against varying $InsP_3$ concentration for 20 cells (log scale). The figure shows that at high $InsP_3$ concentration (10-25μM) rates of decline were generally greater than low $InsP_3$ concentrations (0.1-1μM). This suggests that as $[Ca^{2+}]i$ rises the rate of Ca^{2+} efflux from the cytosol is greater. Figure 4.1.6.B shows this is the case. The data, rate of decline plotted as a function of peak $[Ca^{2+}]i$ levels (linear axis) showed an increased rate at high peak $[Ca^{2+}]i$ with less variation than the plot against $InsP_3$ concentration.

Figure 4.1.6 Pooled data of the initial decline rate of the $InsP_3$ induced $[Ca^{2+}]i$ rise.

Graph A shows decline rates measured as a linear fit to the initial decrease of the $[Ca^{2+}]i$, plotted against $InsP_3$ concentrations (μM). The data represents single measurements taken from separate astrocytes (n=20 cells).

Graph B illustrates initial rate of decline plotted as a function of peak free $[Ca^{2+}]i$. The graph shows that the initial rate of decline depends on the peak $[Ca^{2+}]i$. Data are single responses from individual astrocytes 3-7 DIV (n=20 cells).

(A)

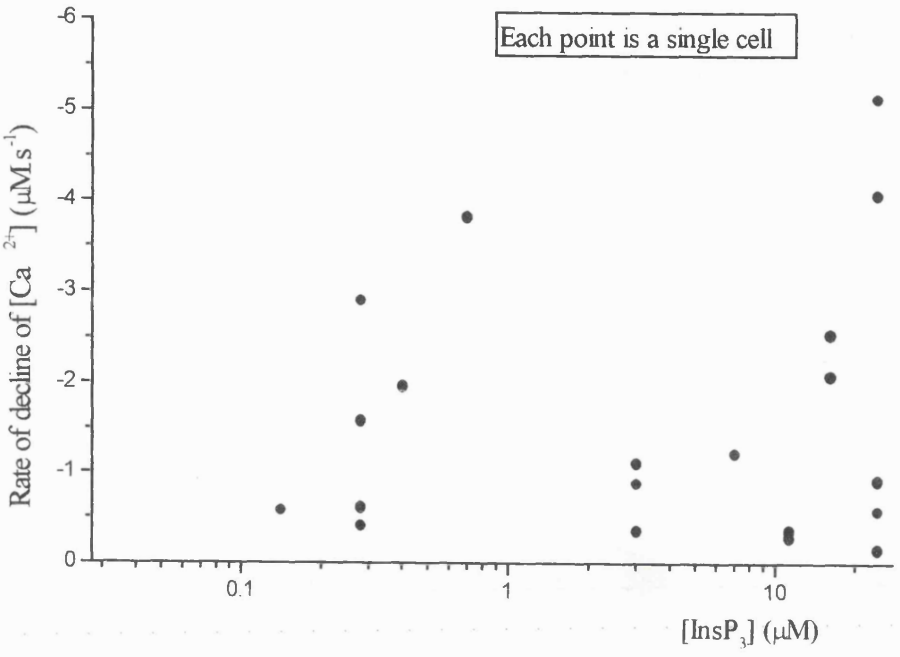
Each point is a single cell
Rate of decline of [Ca 2+] (μM.s-1)
-6
-5
-4
-3
-2
-1
0
0.1
1
10
[InsP3] (μM)

(B)

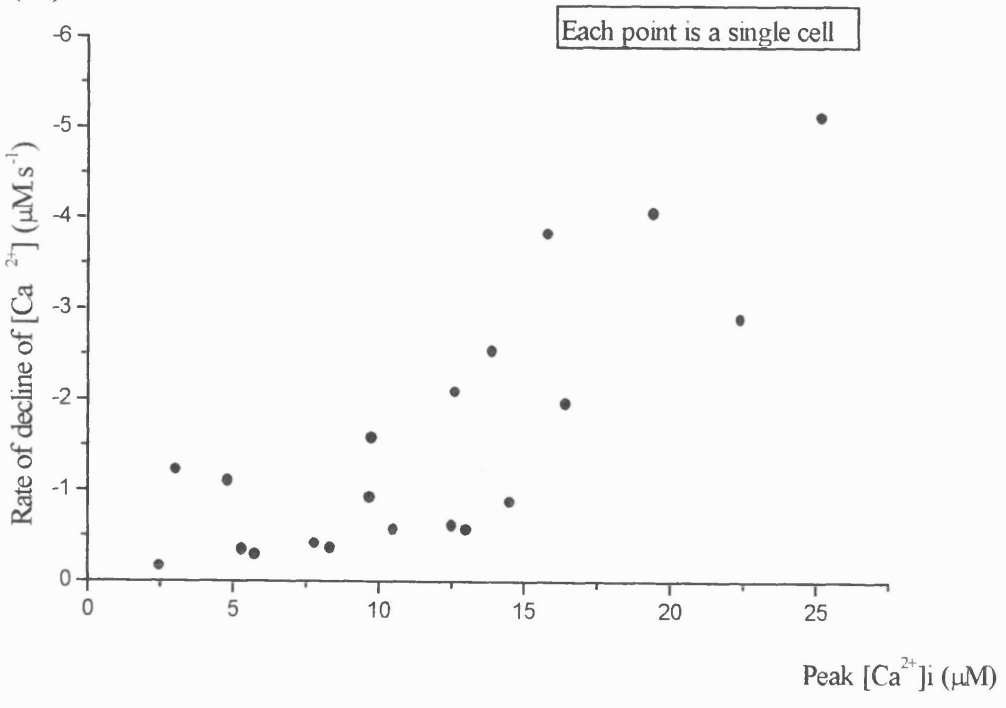
Each point is a single cell
Rate of decline of [Ca 2+] (μM.s-1)
-6
-5
-4
-3
-2
-1
0
0
5
10
15
20
25
Peak [Ca2+]i (μM)

4.2 Rate of termination of Ca^{2+} flux.

It was noted that when the magnitude of the $[Ca^{2+}]i$ flux, $d[Ca^{2+}]i/dt$ was high the duration of the rise time, measured from artefact to the peak of the Ca^{2+} response, was short. At the peak $[Ca^{2+}]i$, $d[Ca^{2+}]i/dt=0$, therefore the $InsP_3$ evoked Ca^{2+} efflux into the cytosol had declined to a low level. The idea that the rate of termination of $InsP_3$ evoked $[Ca^{2+}]i$ flux depends upon the size of $[Ca^{2+}]i$ flux was tested by plotting the reciprocal of the 10-90% rise time against $d[Ca^{2+}]i/dt$. If termination of Ca^{2+} flux is produced by Ca^{2+} binding to and inactivating channels then the termination rate should be proportional to local $[Ca^{2+}]i$. This local $[Ca^{2+}]$ is proportional to the Ca^{2+} flux through channels (Stern-M.D. 1992), thus in this case the termination rate should be linearly related to $d[Ca^{2+}]i/dt$.

Figure 4.2.1 illustrates the rate of termination plotted as a function of Ca^{2+} flux. The graph shows to a first approximation that the rate of termination {reciprocal 10-90% rise times; $(Duration)^{-1}$, s^{-1}} is proportional to Ca^{2+} flux. The linear rate of termination and flux are consistent with 1 free Ca^{2+} inhibiting each receptor.

The linear correlation between rate of termination of flux and flux into unit cytosolic volume could be explained by an accumulation of free Ca^{2+} close to the release sites. The free calcium inactivates the $InsP_3$ receptor protein by binding to a single site, producing a negative feedback mechanism; thus the rate of inactivation would be directly proportional to the flux (as is evident from figure 4.2.1). Other studies have shown that when cytosolic calcium levels are raised prior to $InsP_3$ release then the $InsP_3$ induced calcium flux is inhibited (Iino-M. 1990; Ogden-D.C. *et al* 1990; Finch-E. *et al* 1991; Bezprozvanny-I. *et al* 1994; Khodakhah-K. & Ogden-D.C. 1995; Ogden-D.C. & Capiod-T. 1997; Carter-T. & Ogden-D.C. 1997). Furthermore if the free calcium is buffered to resting levels termination is prevented (Ogden-D.C. & Capiod-T. 1997; Carter-T. & Ogden-D.C. 1997). Metabolism of $InsP_3$ or simply store depletion may also contribute to the inhibition of the $InsP_3$ evoked Ca^{2+} release. The possible role of $InsP_3$ metabolism is addressed in the next section 4.2.2. Figure 4.1.4 shows that two consecutive pulses of different $InsP_3$ concentrations, in the same cell, elicit different rates of flux and peak free $[Ca^{2+}]i$ levels. Peak $[Ca^{2+}]i$ is higher at high $InsP_3$ concentrations, indicating that there was calcium still present in the store after release of low $InsP_3$ although the flux terminated.

Similar observations have been made previously (Ilyin-V. & Parker-I. 1994; Ogden-D.C. & Capiod-T. 1997; Carter-T. & Ogden-D.C. 1997). Thus, whilst not tested directly in astrocytes, previous experiments have demonstrated a role for cytosolic calcium inhibition of the $InsP_3$ receptor in the termination of flux the extent of contribution of store depletion to the response remains unclear (discussed further in chapter 6).

Figure 4.2.1 Relation between rate of termination of Ca^{2+} flux and $d[Ca^{2+}]i/dt$ in astrocytes *in vitro.*

The graph A shows the relation between the rate of termination of Ca^{2+} flux measured as reciprocal of 10-90% rise time $(duration)^{-1}$ and $d[Ca^{2+}]i/dt$ ($\mu M.s^{-1}$) plotted on a linear scale for values of $d[Ca^{2+}]i/dt$ greater than 20 $\mu M.s^{-1}$.

Inset graph B shows the termination rate plotted as a function of $d[Ca^{2+}]i/dt$ rate on a linear scale (0-140$\mu M.s^{-1}$), which is fitted through zero (R=0.88) with ± 1.08s.d

At low $d[Ca^{2+}]i/dt$ (less than 20 $\mu M.s^{-1}$) there appeared to be a deviation from the linear correlation when (all data n=54) was fitted through zero (R=0.88). This suggests the flux is terminated more quickly at low $d[Ca^{2+}]i/dt$ than predicted from this linear model.

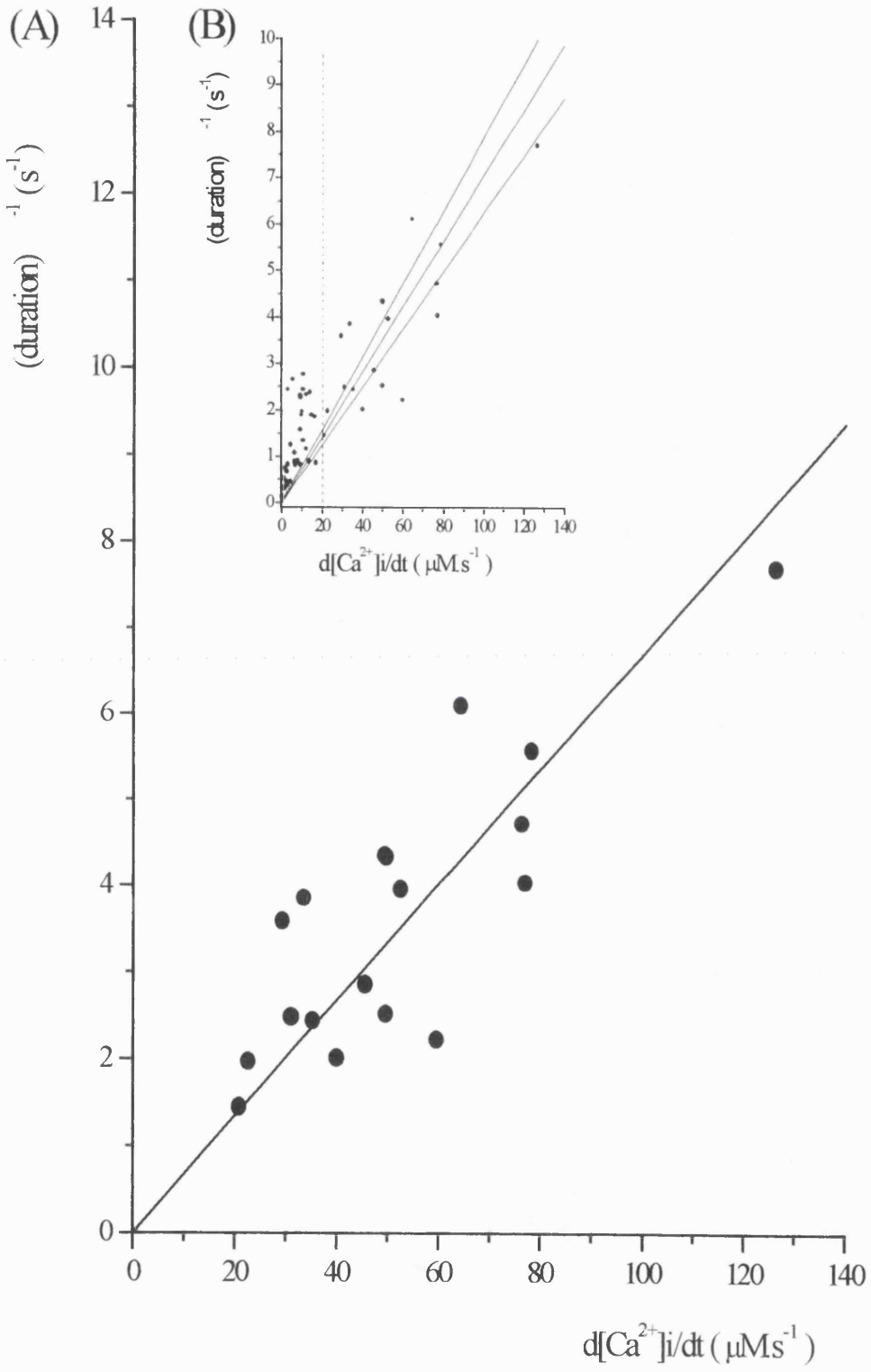
(A)
(B)
(duration) $^{-1}$ (s^{-1})
d[Ca^{2+}]i/dt (μM.s^{-1})
0
2
4
6
8
10
12
14
0
20
40
60
80
100
120
140

4.2.1 Comparison of the kinetics of Ca^{2+} flux in type 1 astrocytes with other cell types?

The data obtained in type 1 astrocytes can be compared with properties of Ca^{2+} flux in other cells possessing different $InsP_3$ receptor isoforms (see figure 4.2.2 A+B). Endothelial cells have type 1 and type 2 $InsP_3$ receptor proteins (unpublished data) whereas hepatocytes have mainly type 2 and a small fraction of type 1 (DeSmedt *et al* 1994). Purkinje cells express the type 1 isoform (splice variant $s1^-$,$s11B^+$, Nakagawa-T., *et al* 1991) and astrocytes express type 3 *in vitro* and *in situ* (Yamamoto-Hino *et al* 1995). Graph A shows rate of termination against Ca^{2+} flux for non-excitable endothelial cells and hepatocytes (Carter-T.D. & Ogden-D. 1997 ; Ogden-D.C. & Capiod-T. 1997). Graph B shows a plot for cerebellar astrocytes and Purkinje cells (Ogden-D.C. & Capiod-T. 1997).

Graph A shows that type 1 astrocytes (stars) are comparable with other non-excitable cell types porcine endothelium (triangles) and guinea pig hepatocytes (circles), in that the rates of termination are related in the same way to flux (correlation r=0.88 astrocytes, r=0.95 endothelial cells, r=0.91 hepatocytes) proportional on a linear plot. A comparison of Ca^{2+} fluxes ($d[Ca^{2+}]i/dt$) shows that the astrocyte data is similar to hepatocytes data ($< 50\mu M.s^{-1}$) and much less than the endothelial cells (flux range 100-$1000\mu M.s^{-1}$). Graph B illustrates that data from Purkinje cell somas also fit this linear relationship (r=0.91 on a linear scale) but at much faster Ca^{2+} flux rates. The $InsP_3$ receptor (subtype 1) of the Purkinje cells are activated for less time (10-20ms) at higher rates (maximum $1400\mu M.s^{-1}$) compared to the smaller cultured type 1 astrocytes (subtype 3, 10-1000ms, $126\mu M.s^{-1}$).

The magnitude of Ca^{2+} flux differs between the two cell types, $d[Ca^{2+}]i/dt$ measures the density of open channels per unit volume of cytosol Therefore a low density of receptors in hepatocytes and astrocytes would account for small values in Ca^{2+} flux compared to Purkinje and endothelial cells.

Despite the cell to cell variability that exists between cells and tissue types, the rate of termination is proportional to flux in all cases. This relationship appears to exist for all the $InsP_3$ receptor isoforms located in the cells of figure 4.2.2. These data supports the idea that the same mechanism of inactivation by Ca^{2+} binding may apply to all isoforms of the $InsP_3$ receptor. For detailed discussion see chapter 6.

Figure 4.2.2; Rate of termination as a function of $[Ca^{2+}]i$ flux.

Graph A shows the inverse duration $(duration)^{-1}$ plotted against rate of $[Ca^{2+}]i$ flux ($d[Ca^{2+}]i/dt$ $\mu M.s^{-1}$) on a log scale for non excitable cells using the same experimental protocol. The non excitable cells compared were hepatocytes (circles ; Ogden-D.C. & Capiod-T. 1997), endothelial cells (triangle ; Carter-T.D. & Ogden-D. 1997), astrocytes (stars) and Bergmann glial cells (semi-circles).

Graph B shows inverse duration (s^{-1}) as a function of $d[Ca^{2+}]i/dt$ ($\mu M.s^{-1}$) for other cerebellar cells plotted on log scales. Purkinje neurones (Khodakhah-K; & Ogden-D.C.; Ogden-D.C. & Capiod-T. 1997 ; squares), cerebellar astrocytes *in vitro* (stars) and *in situ* Bergmann glial cells (semi-circles).

Log scales are used to extend the range the range for comparison. Data on a linear scales is shown on figure 4.2.1.

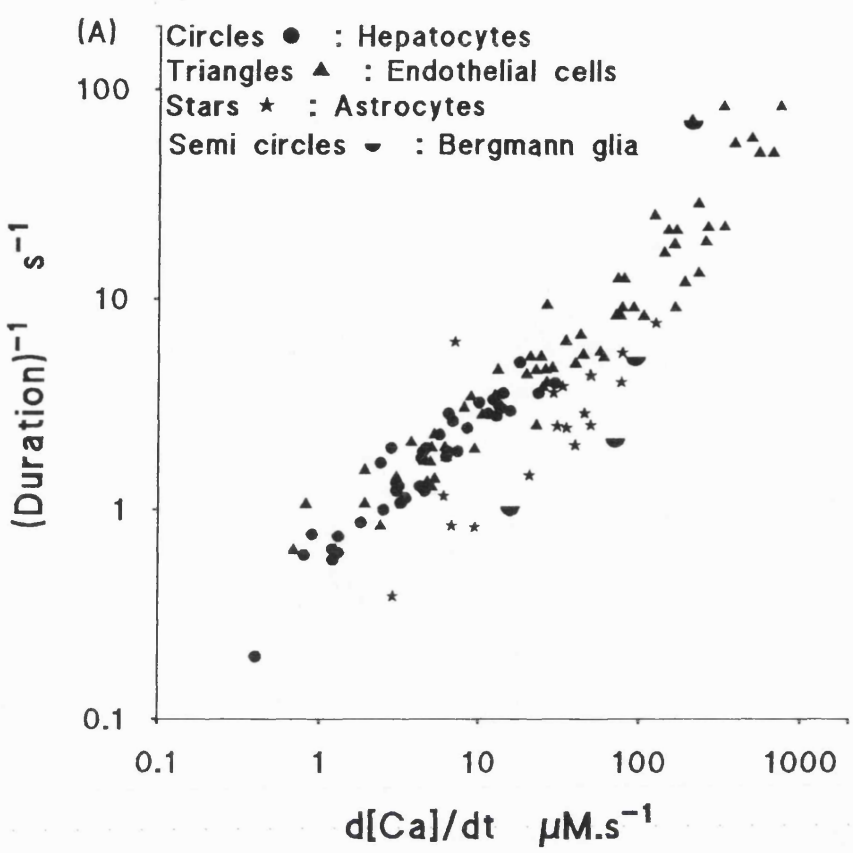
(A)
Circles ● : Hepatocytes
Triangles ▲ : Endothelial cells
Stars ★ : Astrocytes
Semi circles ◒ : Bergmann glia
100
10
1
0.1
(Duration)$^{-1}$ s^{-1}
0.1
1
10
100
1000
d[Ca]/dt μM.s^{-1}

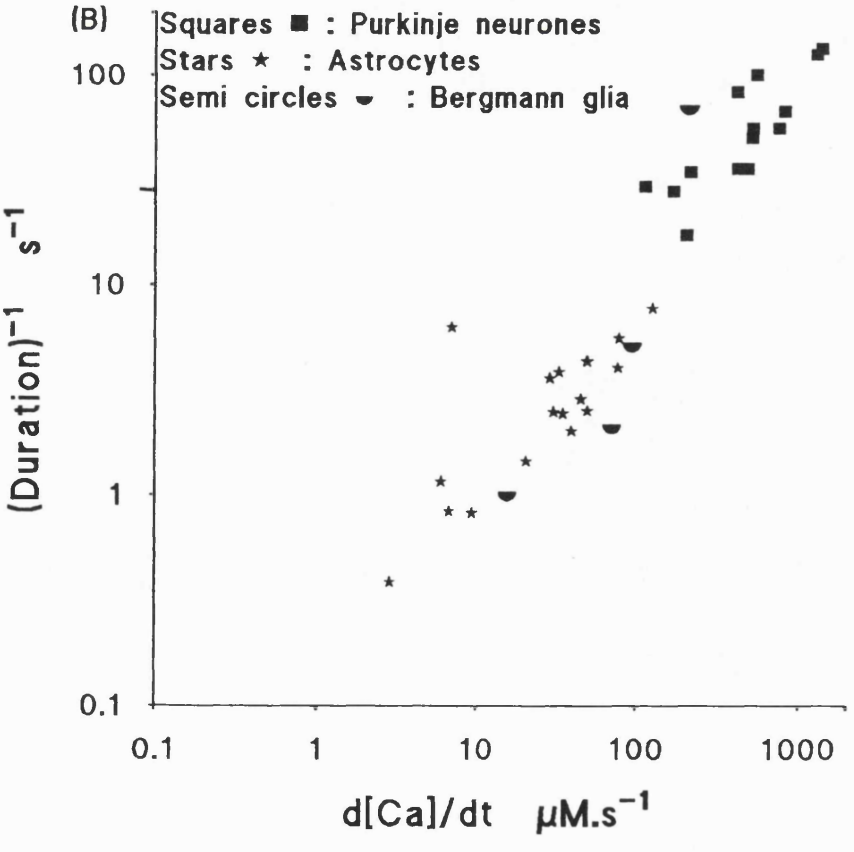
(B)
Squares ■ : Purkinje neurones
Stars ★ : Astrocytes
Semi circles ◒ : Bergmann glia
100
10
1
0.1
(Duration)$^{-1}$ s^{-1}
0.1
1
10
100
1000
d[Ca]/dt μM.s^{-1}

4.2.2 Role of $InsP_3$ metabolism.

Inositol 1,4,5-trisphosphate is hydrolysed to form inositol 1,4-bisphosphate ($InsP_2$) by the enzyme $InsP_3$ 5-phosphatase (Batty-I.R. *et al* 1985). A thio substituted analogue of $InsP_3$ 1-DL-myo-inositol 1,4-bisphosphate 5-phosphorothioate (DL-5-thio-$InsP_3$) resistant to 5-phosphatase was developed to produce maintained $InsP_3$ stimulation (Safrany-S.T. *et al* 1991). However unless the ligand is applied in a pulse the $InsP_3$ receptor desensitises before activation. To overcome this a caged form of this non-hydrolysable $InsP_3$ analogue the S-1-(2-nitrophenyl)ethyl thio ester of 5-thio-$InsP_3$ (D-myo-inositol 1,4,5-phosphorothioate was used, Wootton-JF; *et al* 1995). Photoreleased 5-thio-$InsP_3$ has a 5 fold lower affinity for the $InsP_3$ receptor protein than photolysis released $InsP_3$. Higher caged concentrations in the order of 160μM were used. In fact the reduced affinity of the $InsP_3$ receptor protein for 5-thio $InsP_3$ (Wootton-JF; *et al* 1995; Khodakhah-K; & Ogden-D.C., 1995) made the induction of responses in astrocytes difficult. In 6 out 9 of cells tested no $[Ca^{2+}]i$ rise was detected as a result of 5-thio-$InsP_3$. Consequentially the data shows initial observations n=3 cells.

Figure 4.2.3 Investigation into the termination mechanism of the $InsP_3$ induced $[Ca^{2+}]i$ response.

Panel A shows the flash photolysis of caged 5-thio-$InsP_3$ in a type 1 astrocyte 3DIV. The fluorescence trace depicts the $[Ca^{2+}]i$ rise in response to 48μM 5-thio-$InsP_3$. The type 1 astrocyte was filled with 500μM furaptra and whole voltage clamped at 0mV.

Panel B is an $InsP_3$ evoked $[Ca^{2+}]i$ response in a type 1 astrocyte 5 DIV. The rise in $[Ca^{2+}]i$ level was measured using furaptra (500μM) and the cell was whole cell voltage clamped at -40mV (resting membrane potential).

The scale bar for A and B is horizontal 10 seconds and vertical for a $[Ca^{2+}]i$ rise of 2μM.

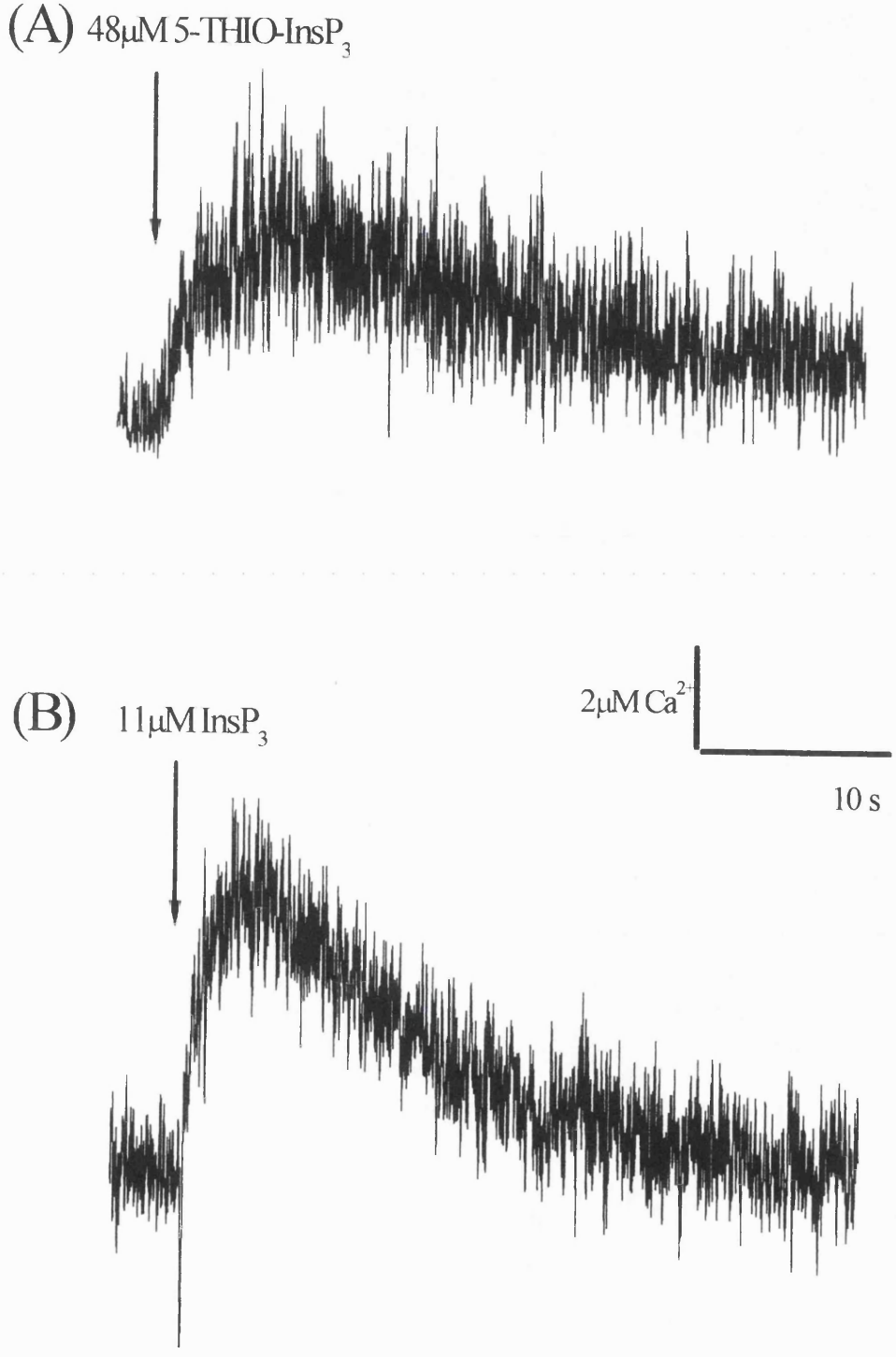
(A) 48μM 5-THIO-InsP3
(B) 11μM InsP3
2μM Ca2+
10 s

Figure 4.2.3 A shows a response induced by 48μM 5-thio-$InsP_3$. The figure demonstrates that the 5-thio-$InsP_3$ $[Ca^{2+}]i$ response has a similar time course to the $InsP_3$ evoked $[Ca^{2+}]i$ rise. The 5-thio-$InsP_3$ $[Ca^{2+}]i$ response had an initial rate of rise ($d[Ca^{2+}]i/dt$), a sharp peak and declined back to pre photolysis resting $[Ca^{2+}]i$ levels as $[Ca^{2+}]i$ is removed from the cytosol. Thus the response to 5-thio-$InsP_3$ shows that $InsP_3$ metabolism is not involved in the termination of the $InsP_3$ evoked response (n=3 cells). Figure 4.2.3 A&B shows a comparison between 48 μM 5-thio $InsP_3$ and 11μM $InsP_3$ induced $[Ca^{2+}]i$ responses in two individual cells. The figure shows that at equivalent concentrations 5-thio-$InsP_3$ and $InsP_3$ evoke $[Ca^{2+}]i$ rises with similar time courses.

4.3 Intercellular communication of type 1 astrocytes via gap junctions.

Type 1 astrocytes *in situ* and *in vitro* form a syncytium via gap junction complexes so have a communicating cytosol (Finkbeiner-S 1992). Type 1 astrocytes *in vitro* and *in situ* respond to a variety of stimuli, e.g. neurotransmitters, by an increase in $[Ca^{2+}]i$. The rise in $[Ca^{2+}]i$ appears to propagate from one cell to another within the syncytium forming Ca^{2+} waves travelling at 10-20μms^{-1} (Cornell-Bell-A. H. *et al* 1990; Dani-JW & Smith-S.J., 1992). Interestingly this form of signalling requires extracellular Ca^{2+}. Mechanical stimulation also causes a rise in $[Ca^{2+}]i$ which propagates between astrocytes, but this form of intercellular signalling was not dependent upon external $[Ca^{2+}]$ levels. Thus this form of communication is thought to involve second messenger systems such as $InsP_3$ (Charles-A.C. *et al* 1993; Charles-A.C. *et al* 1991).

Several models have been proposed to describe how this cellular based Ca^{2+} signalling occurs. As the intercellular signalling is fairly rapid there is some doubt whether diffusion of the mediator would be fast enough. If internal $[Ca^{2+}]$ is raised Ca^{2+} ions can diffuse through gap junctions into neighbouring cells (Dunlap-K. *et al* 1987). Cellular $[Ca^{2+}]i$ are tightly controlled by buffering and removal from the cytosol. In addition the process of Ca^{2+} diffusion is slow (Allbritton-N.L. *et al* 1992). The communicating agents could be other diffusible second messenger molecules such as $InsP_3$ (Bennett-M. V. L. *et al* 1991).

Carter *et al* have shown in porcine endothelial cells that gap junctions consisting of connexin 43 and 37 are permeable to caged $InsP_3$, which has similar size and valency as $InsP_3$ molecules (valency 5^-, Mr 635 Da , Carter-T.D. *et al* 1996).

Rat cerebellar glial cells at 5DIV (Chapter 3) have connexin 43 (Dermietzel-R. *et al* 1991; Massa-P.T. & Mugnaini-E. 1985; Mugnaini-E. 1986). The possibility that caged $InsP_3$ can pass through astrocytic gap junctions and induce a $[Ca^{2+}]i$ rise in the adjacent glial cells *in vitro* after photolysis was investigated. Paired type 1 astrocytes were loaded with 500μM furaptra and 40 or 80 μM caged $InsP_3$ as described above. The fluorescence from the patched cell was not recorded as it was shielded by the rectangular diaphragm from the PMT. The furaptra fluorescence signal took longer to equilibrate in paired cells than single cells, average loading time for single cells 419±63 n=10 cells, compared to 640±146, n=10.

Figure 4.3.1 An investigation into astrocytic intercellular communication.

Photograph A shows a pair of astrocytes 8 DIV. The cell on the left was whole cell clamped at resting membrane potential . The pipette contained 500μM furaptra and 40/80μM caged $InsP_3$.

Photograph B depicts the same frame as photograph A, when illuminated with light of wavelength 420nm. The picture shows that the cell on the right has been infiltrated with the furaptra, via the cell on the right.

Graph C illustrates the time taken to load the second astrocyte through the first. The fluorescent signal from the un-patched cell took over 20 minutes to equilibrate. The graph shows the fluorescence measured as photon counts plotted as a function of time in seconds.

Panel D is of a fluorescent trace of an $InsP_3$ induced $[Ca^{2+}]i$ change as a result of photolysis of caged $InsP_3$ loaded through a single adjacent cell initial $InsP_3$ concentration was 80μM. The response shows a 20μM increase in $[Ca^{2+}]i$ as a result of photolysis of caged $InsP_3$ in the un-patched cell.

Scale Bar vertical represents $[Ca^{2+}]i$ of 10μM, horizontal 2 seconds.

(A) PATCHED PAIRED ASTROCYTES *IN VITRO*

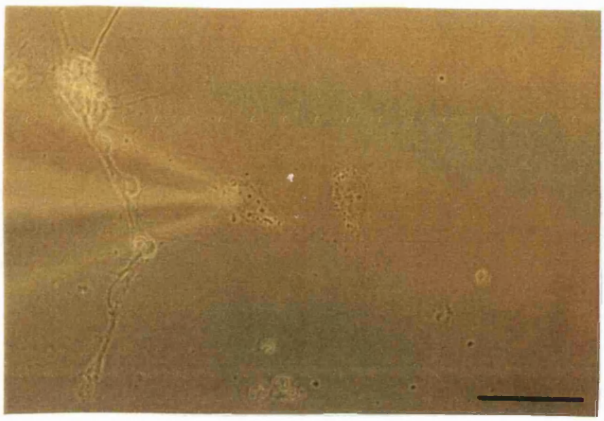

(B) PAIRED ASTROCYTE LOADED WITH 500μM FURAPTRA

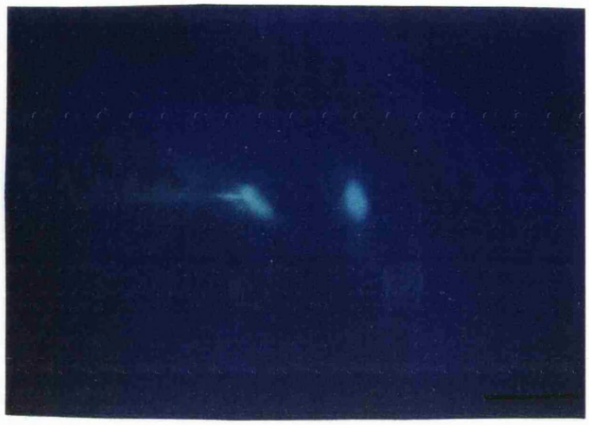

(C) LOADING TIME OF INDICATOR

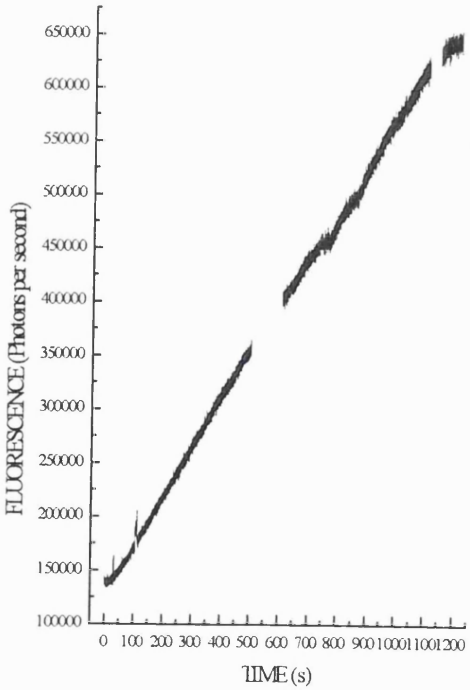

(D) $[Ca^{2+}]i$ RISE OF UN-PATCHED CELL

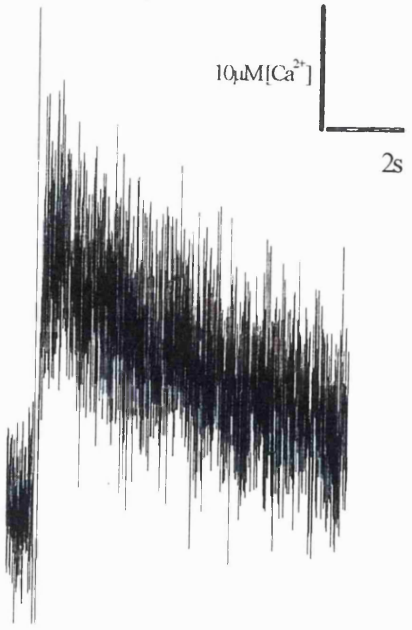

Figure 4.3.1 A shows a bright field photograph of a patched pair of type 1 cultured astrocytes. Figure 4.3.1.B shows the same pair of cells filled with 500μM of furaptra excited with light of 420nm and recorded at >490nm. The photographs were taken after the completion of the experiment and show clearly that the Ca^{2+} indicator furaptra diffused through into the second cell. Figure 4.3.1 C shows the loading profile for the cell pair used in figure D. Loading in paired cells took 1.5 times as long as the indicator loading time in single astrocytes. Figure 4.3.1.D shows a typical $InsP_3$ evoked $[Ca^{2+}]i$ rise. This type of result was seen in 7 out of the 10 pairs of type 1 astrocytes tested.

The diffusion of free $[Ca^{2+}]i$ is slow due to buffering (Allbritton-N.L. *et al* 1992), so at this time scale the $[Ca^{2+}]i$ rise is likely to be a result of $InsP_3$ released activity in the un-patched, coupled cell. However a better test would be to measure the delay times of the response in the coupled cell and compare it with single cells. This was difficult in these experiments as the cells were grown on glass coverslips, so the initial rising phase was obscured by the phosphorescence artefact. These experiments were difficult to perform on astrocytes cultured on quartz with poly-L-lysine, as they did not readily form healthy monolayers (see section 4.6.1).

In conclusion these experiments show that furaptra and caged $InsP_3$ can diffuse from one type 1 astrocyte via gap junction complexes, as photolysis elicits a $[Ca^{2+}]i$ rise in the adjacent cell. Thus it is possible that the endogenous $InsP_3$ molecules could pass between cells and so act as a diffusible second messenger involved in $[Ca^{2+}]i$ waves of interastrocytic communication.

4.4 Agonist induced Ca^{2+} responses in cultured type 1 astrocytes.

Many neurotransmitters and hormones induce the production of $InsP_3$ via a G-protein coupled mechanism to induce a rise $[Ca^{2+}]i$ from internal stores within glial cells (for review see Verkhratsky-A. *et al* 1998). Each type of mediator can induce individual patterns of $[Ca^{2+}]i$ signalling. The experiments in this section were designed to investigate whether $InsP_3$ induced $[Ca^{2+}]i$ responses were similar to agonist evoked $[Ca^{2+}]i$ rises in type 1 astrocytes.

Agonists were applied to induce an $[Ca^{2+}]i$ rise. Figure 4.4.1 A, B, shows two examples of responses taken from individual astrocytes grown on glass coverslips for 4-5 DIV. The agonists were applied via pressure ejection from a "puffer" pipette located above the cell (rate of $235\mu Ms^{-1}$). A variety of agonists were tested but inducing a rise $[Ca^{2+}]i$ was difficult in single voltage clamped astrocytes. It was apparent that whole cell patched cultured astrocytes did not respond to agonists routinely. However the two agonist that did evoke $[Ca^{2+}]i$ responses had slightly different characteristics.

Figure 4.4.1 Examples of agonist induced rises in $[Ca^{2+}]i$ in astrocytes *in vitro.*

Panel A shows a fluorescence trace from an astrocyte loaded with 500μM furaptra. The cell whole cell voltage clamped at -60mV. 100μM ATP was applied (approximately 1s) marked by the bar point. The response consisted of an initial rise, a $[Ca^{2+}]i$ peak, followed by a decline phase. The decline phase appeared to be biphasic with a slower secondary stage. The rapid initial response peaked and terminated but not quite to base $[Ca^{2+}]i$ level. These type of responses are thought to be characteristic of the P_{2Y} adenosine receptor which are coupled to the $InsP_3$ second messenger system (Kastritsis-C.H. *et al* 1992). This type of response was observed in 3 out of 5 cells.
Note scale bar vertical 10μM rise in $[Ca^{2+}]i$, horizontal 1 second.

Panel B depicts an example of a 30μM glutamate induced rise in $[Ca^{2+}]i$ measured with 500μM furaptra. This cell was whole cell voltage clamped at -80mV (resting membrane potential). Vertical scale 3μM rise in $[Ca^{2+}]i$ horizontal 10 seconds. The $[Ca^{2+}]i$ rise peaked and declined back to resting levels. The shape of $[Ca^{2+}]i$ rise appeared to be similar to the photolytically $InsP_3$ induced $[Ca^{2+}]i$ rise. Astrocytes are known to possess metabotropic glutamate receptors that operate through an $InsP_3$ induced $[Ca^{2+}]i$ release (Holzwarth-J.A. *et al* 1994). This type of response was seen in 5 out of 19 cells.

A) 100μM ATP

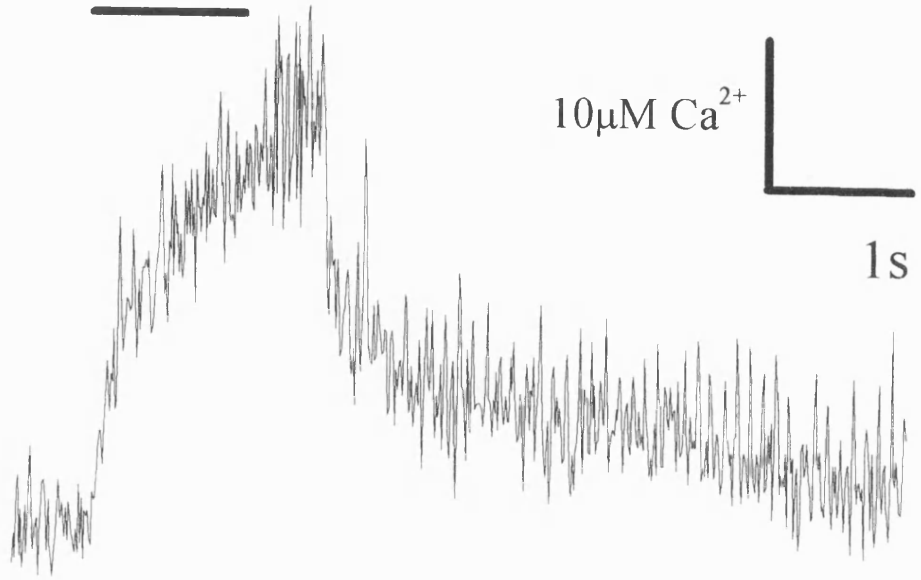

B) 30μM Glutamate

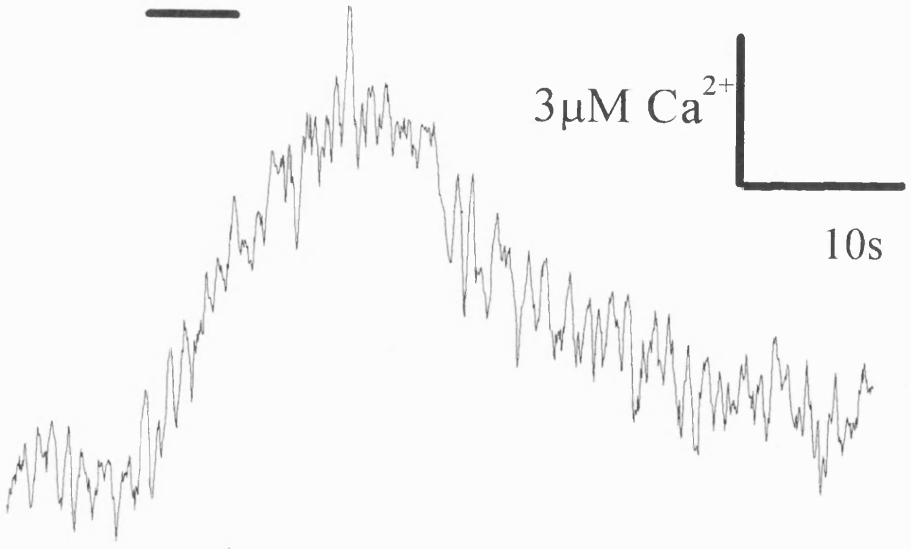

4.4.1 Image Analysis of Agonist evoked $[Ca^{2+}]i$ responses in cultured astrocytes.

To further investigate agonist induced $[Ca^{2+}]i$ in astrocytes an imaging system was used (see figure 4.4.2). Previous studies using imaging systems have shown that in response to bath applied agonists not all cells in the recording field respond. With a PMT measurement system the $[Ca^{2+}]i$ was only recorded from a single astrocyte. These experiments were designed to overcome the low percentage of responses recorded in individual astrocytes.

Type 1 astrocytes were loaded with the acetoxy methyl (AM) form of Ca^{2+} sensitive indicators and the $[Ca^{2+}]i$ rise within the cell recorded. For technical detail refer to chapter 2. The cultured cells were incubated with 5-10μM AM forms of either fluo-3, furaptra or fura-2. The cells cultured (3-7 DIV) on glass were viewed using the upright microscope and water immersion objectives. The cells at this stage of development were not yet confluent. On application of agonist the frame number was noted.

Figure 4.4.2; Characterisation of agonist evoked $[Ca^{2+}]i$ rises in type 1 astrocytes using an Imaging system.

(Part I)

Image A shows four cells A, B, C, D within the frame loaded with fluo-3-AM. The image was recorded with IDEA software with excitation wavelength 480nm. Each image was exposed for 200ms every 1second. Line profiles 1 and 2 (marked on image) were used to perform analysis. Fluorescence was measured along the line in each frame. $[Ca^{2+}]i$ was expressed as a function of time (consecutive frame number).

Panel B depicts two graphs which are the line profiles 1 and 2 taken from the image A. The figures represent a level of fluorescence measured in pixels expressed as length of the profile. The peaks in line 1 represent the fluorescence intensity of cells A and B. Line 2 shows the level of fluorescence for cells C and D. Once recorded the line profiles could be exported from the image software as ASCII files. The data was further analysed using a spreadsheet program. The fluorescence peaks, corresponding to cells, were plotted as a function of time (frame number). The line intensity profiles were tracked throughout all the recorded frames 0-100 and shown in Panel C (Part II).

(A)

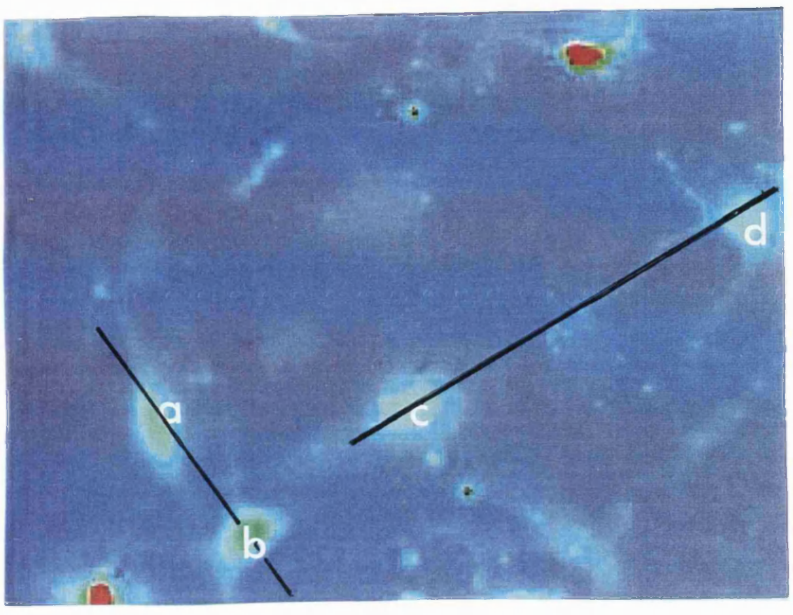

(B) Line Profile 1

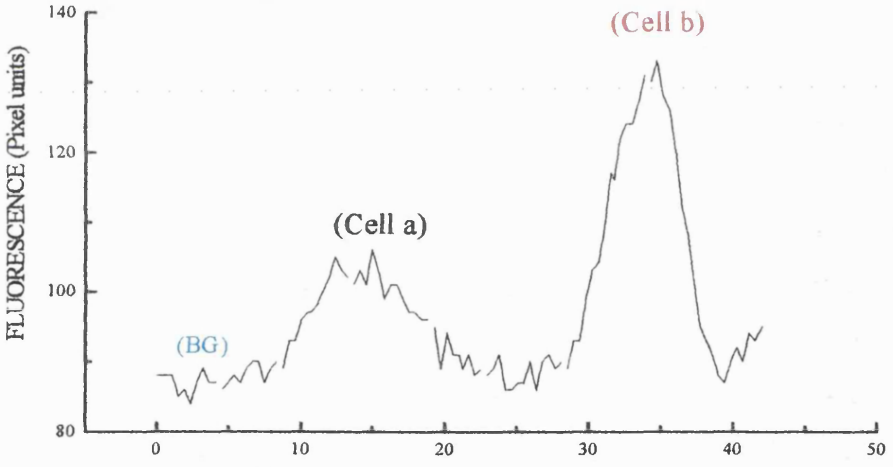

Line Profile 2

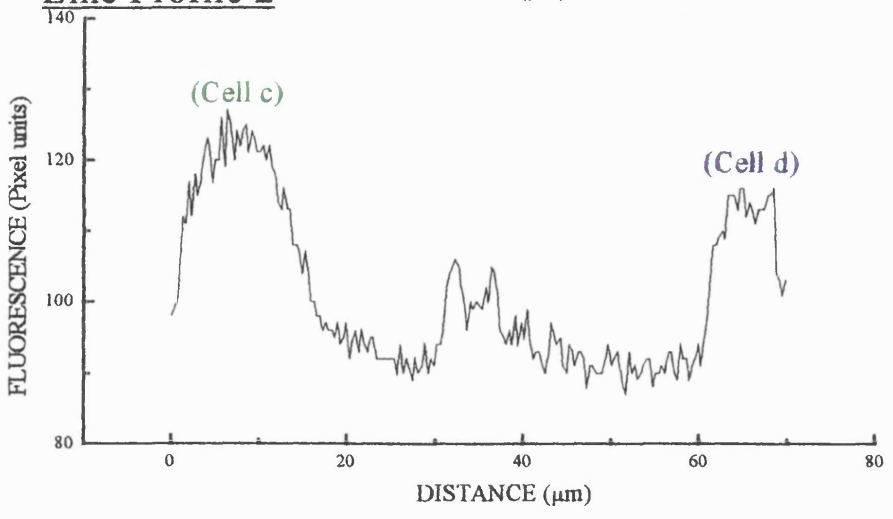

Figure 4.4.2 Part II

Graph C shows the fluorescence change measured with fluo-3, in astrocytes A,B,C,D. The cells are colour coded. The graph shows fluorescence plotted as a function of time in consecutive frames (seconds) . Each frame was recorded every 1 second exposure time of 200ms.. The background fluorescence represents the auto-fluorescence from the coverslip. Background fluorescence was constant. All experiments were conducted at 23°C. The bar indicates when 100μM ATP was applied (frame 14-30). The cells respond by an $[Ca^{2+}]i$ measured by a rise in fluorescence. The $[Ca^{2+}]i$ rise appears to oscillate throughout the four astrocytes.

Panel D depicts a selection of recorded images from the experiment in panel C. The images were recorded with IDEA software under excitation illumination of 480nm. The cells had been loaded with the Ca^{2+} sensitive indicator fluo-3. The arrow represents the point at which the 100μM ATP was applied. Note how cell C (green line) is the first astrocyte to respond, followed by B,A and finally D.

This type of experiment was repeated n=5. $[Ca^{2+}]i$ responses were recorded in 3 out of the 5 total with 11 astrocytes responding out of a possible 30 cells.

C)

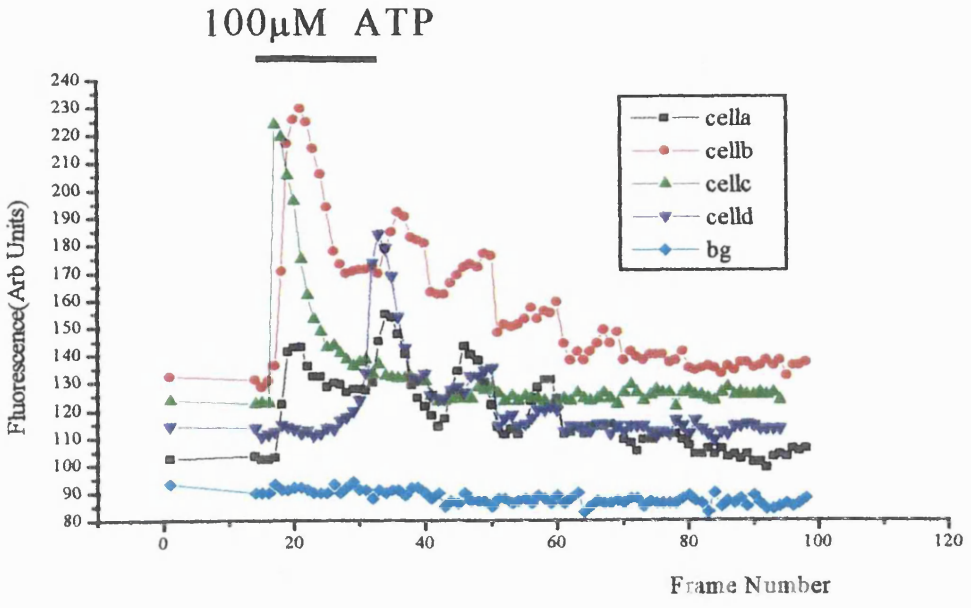
100μM ATP
Fluorescence(Arb Units)
Frame Number
cella
cellb
cellc
celld
bg
240
230
220
210
200
190
180
170
160
150
140
130
120
110
100
90
80
0
20
40
60
80
100
120

D)

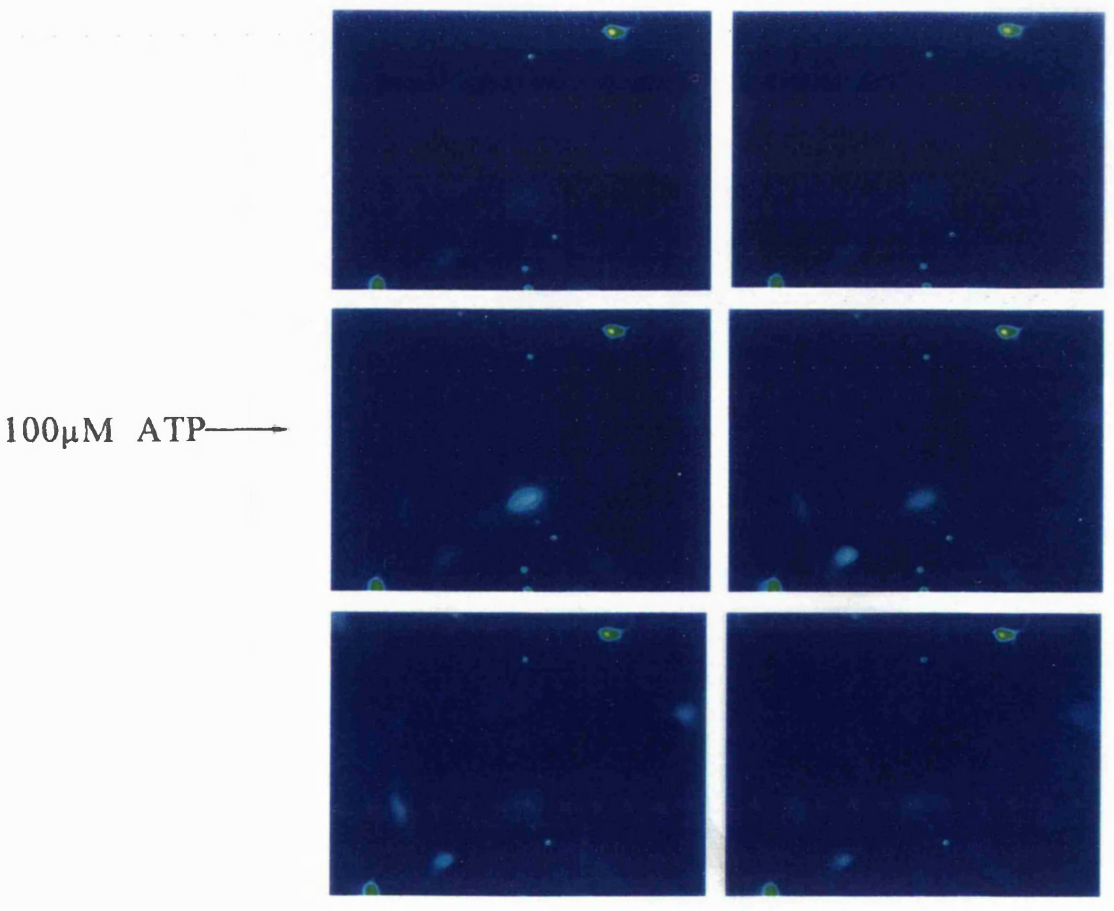
100μM ATP

Figure 4.4.2 A shows four type 1 astrocyte cells labelled a, b, c, d. In each frame line intensities were measured (1 and 2). The lines each encompassed two cells (profile figure 4.4.2. B) and were used to extract information from the frames in the form of ASCII files. Using a spreadsheet program the fluorescence was monitored throughout the experiment (see chapter 2 for details).

In figure 4.4.2.part II, four cells responded to 100μM ATP with periodic fluctuations in $[Ca^{2+}]i$. Figure C represents the rise in fluorescence plotted over time in seconds for cells a-d. An example of 6 of the frames tracked throughout the series can be seen in figure D. Increases in $[Ca^{2+}]i$ are seen as increases in fluorescence traces. Cell a (black squares) and cell d (blue inverse triangles) had a change in $[Ca^{2+}]i$ which peaked every 10 seconds and appeared to be synchronised. The synchronised behaviour of the cells implied there could be some form of communication between astrocytes in response to an externally applied agonist. Cell b (red circles) was located to the left of c and had a larger rise in $[Ca^{2+}]i$ than a or d. However the smaller protoplasmic cell b had a $[Ca^{2+}]i$ oscillation rate which was slower than that of a and d at approximately every 20s. Cell c was a large protoplasmic type 1 astrocyte. The response in cell c (triangles green) had an initial a fast $[Ca^{2+}]i$ peak which declined to base level, and within the time period seen no further $[Ca^{2+}]i$ changes. Cell d was small and had a central soma with spindle like projections, characteristic of "type 2 like" astrocytes. The differences in $[Ca^{2+}]i$ rises could be a result of different cell types. Note background fluorescence (turquoise diamonds) remained constant.

Interestingly the detection of agonist induced synchronised calcium waves in these studies is in contrast to the studies described in section 4.4., which showed that whole cell patch clamped astrocytes *in vitro* did not routinely respond to bath applied agonists (unlike the AM indicator loaded astrocytes described above). It is possible that the process of rupturing the membrane (to go whole cell) causes deleterious affects to the cell by physical stresses. After membrane rupture, the pipette solution diffuses into the cell and mixes with the cytosol, removing or greatly diluting second messenger molecules which might be essential for repetitive $InsP_3$ evoked Ca^{2+} rises in astrocytes to occur. One possible candidate is GTP, which is often required for G protein mediated signalling; this hypothesis could be tested by supplementing the pipette solution with 0.5-2mM Na_3GTP.

The lack of this or other, unknown, molecules internally may affect the way in which second messenger cascades are initiated, and so explain the lack of agonist induced calcium responses seen in whole cell voltage clamped astrocytes *in vitro*. The calcium affinity of the indicators used in the two sets of experiments differ. The *in vitro* data presented in section 4.4.1 were obtained from astrocytes which were AM loaded with the high affinity indicator fluo-3, whereas the whole cell voltage clamped astrocytes described here contained the low affinity indicator furaptra. It is possible that the agonist induced $[Ca^{2+}]i$ rises are too small to be discerned with furaptra, but are detectable by fluo-3. The disadvantage of using fluo-3 however in these kinetic studies is that the indicator will not report accurately rapid calcium fluxes (see chapter 2 section 2.4).

4.5 $InsP_3$ evoked $[Ca^{2+}]i$ in Bergmann glial cells.

The kinetics of the $InsP_3$ induced $[Ca^{2+}]i$ response were examined *in situ* in Bergmann glial cells of the rat cerebellum. The problem with studying astrocytes in slices is identification, as they are small and have complex morphology. The Bergmann glial cells were identified in three ways. Primarily the Bergmann glial cells when patched had a resting membrane potential of around -85mV which is more negative than adjacent neurones. Secondly when depolarised the Bergmann glial cells did not fire any action potentials. Finally once the cell was loaded with furaptra the characteristic cellular morphology was seen (figure 4.5.1 A and B).

The Bergmann glial cells had a tear shaped cell soma which was located on or in around the larger Purkinje cell somas. The Purkinje soma with the Bergmann glial cell soma form a characteristic line at the edge of the molecular layer of the saggital cerebellar slice. The fine filamentous projections of the Bergmann glial cell project only up to the pial surface of the slice. Bergmann glial cells have no fine projections into the granule cell layer at this stage (P12) of development.

Figure 4.5.1 A furaptra loaded Bergmann glial cell *in situ.*

Image A depicts the saggital section of a cerebellar slice viewed with transmitted light. The section shows the molecular layer (bottom right) of a 250μm thick slice.

Image B (same field as above) shows a single Bergmann glial cell loaded with 500μM furaptra. The image was recorded for 200ms with excitation light of 420nm wavelength. The picture shows the glial cell soma and the fine filaments running through the molecular layer. The patch electrode is seen to the left of the image.

Scale bar is 20μm, for both images.

A)

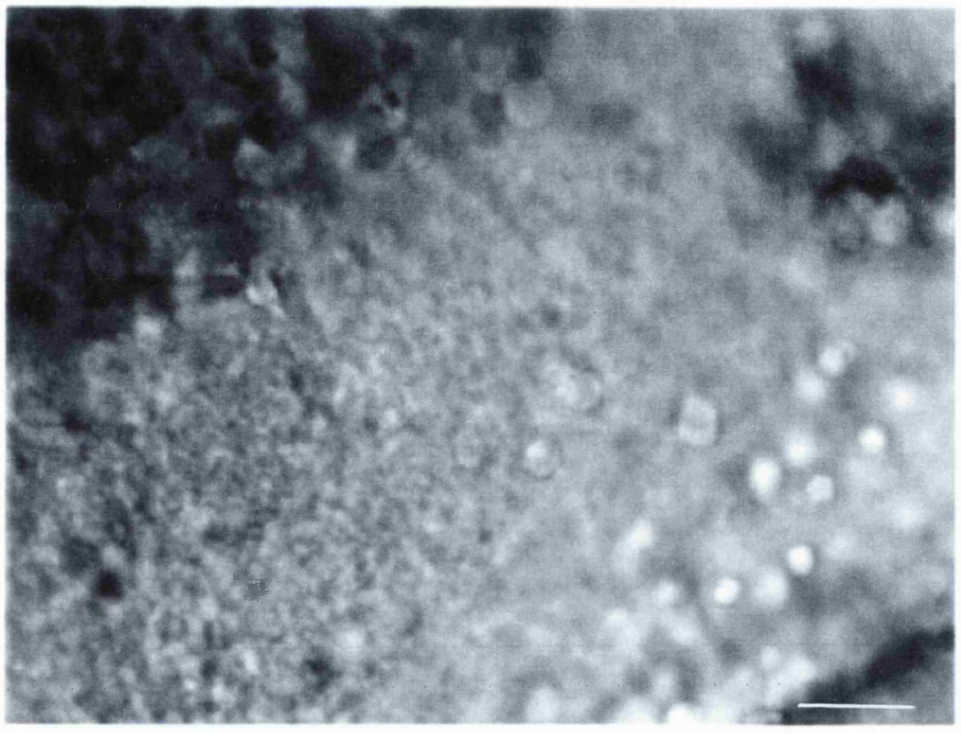

B)

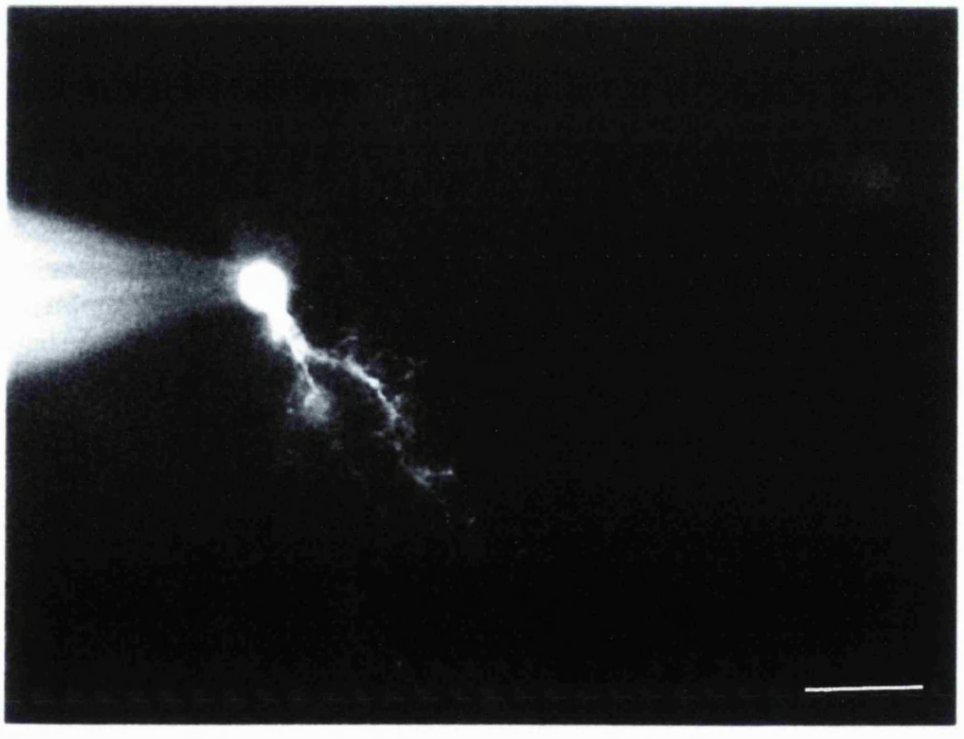

4.5.1 How do the kinetics *in situ* differ from the previous *in vitro* studies?

These experiments were difficult to perform so the results are based on few observations (responses n=4). In order to draw precise conclusions further work is required. In Bergmann glial cells the $InsP_3$ induced $[Ca^{2+}]i$ signal rises rapidly, peaks, and declines back to pre-stimulus resting $[Ca^{2+}]i$ levels. Figure 4.5.2 shows an example of a typical $InsP_3$ induced $[Ca^{2+}]i$ rise in a Bergmann glial cell *in situ*.

Figure 4.2.2 (A&B) shows the termination rate of $[Ca^{2+}]i$ rise as a function of $[Ca^{2+}]i$ flux for the Bergmann glial cells (semi-circles). Bergmann glial cells had larger $InsP_3$ induced $[Ca^{2+}]i$ fluxes, occurring, over a shorter time interval than cultured astrocytes, although these cells have the same $InsP_3$ receptor protein (subtype 3). These few observations show that differences in kinetic parameters may exist, in that the Bergmann glial cells had greater rises in $[Ca^{2+}]i$. If this is the case a reason may be due to tissue culture. Culturing techniques can influence the protein production which affects cell function (Juurlink-B.H.J. & Hertz-L. 1986 ; Barres-B.A. *et al* 1989). The $InsP_3$ receptor protein type 3 may be expressed in different densities and locations due to morphological differences within the two cell types. Figure 4.5.1 shows that Bergmann glial cells have fine filament projections with a smaller cell soma, compared to the cultured type 1 astrocytes. The cultured astrocytes were large round flat cells with a central cell soma. The endoplasmic reticulum membrane which contains the receptor proteins, would run through the length of the projections of the Bergmann glia so would be encompassed by smaller volumes of cytosol.

Figure 4.5.2 An $InsP_3$ evoked $[Ca^{2+}]i$ rise in a Bergmann glial cell *in situ*.

Panel A shows a fluorescence trace for a 20μM $InsP_3$ evoked $[Ca^{2+}]i$ response (arrow) in Bergmann glial cells. The cell was loaded with 500μM furaptra and whole cell clamped at -83mV (cells resting membrane potential). On depolarisation the cell did not fire action potentials. The cell was observed with excitation light of wavelength 420nm, and had the characteristic Bergmann glial cell morphology.

Vertical scale bars show a rise in $[Ca^{2+}]i$ of 10μM and horizontal 2 seconds.

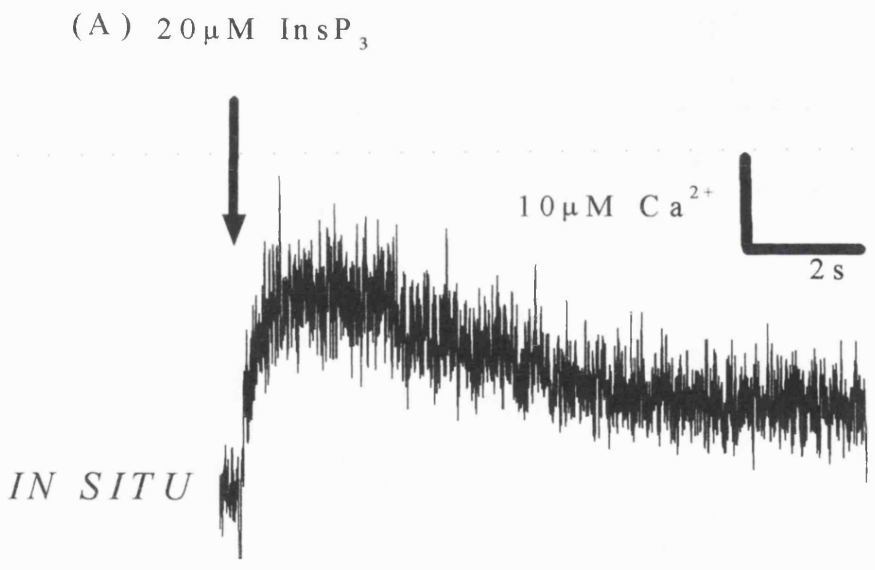

4.5.2 Imaging analysis of $[Ca^{2+}]i$ responses in Bergmann glial cells *in situ*.

There was some difficulty in inducing $[Ca^{2+}]i$ responses in these cells with the conventional "puffer" application method. When 100μM ATP was applied to the patched small Bergmann glial cell the image was difficult to record. The initial fluorescent intensities appeared to change in the cell soma region. However when samples of the cells were examined in detail and projected in a continuous sequence the intensity differences were shown to be due to cell movement artefacts. Within cerebellar slices Bergmann glial cells are very small and fine. The pressure of ATP being expelled onto the cell pushed the cell out of focus. During an image sweep no refocusing was possible. It was difficult to conclude whether $[Ca^{2+}]i$ changes occurred. The slice was fixed within the recording chamber to try and prevent movement, but the continual perfusion system made slight motion difficult to prevent. This was a problem with Bergmann glial cells as they are only a few microns in diameter. This procedure was repeated n=3.

Figure 4.5.3 Experimental protocol.

Figure 4.5.3 shows four panels depicting the experimental procedure.

Panel A shows a bright field image of a cerebellar slice, with a row of Purkinje cell bodies visible running diagonally left to right.

Panel B shows the patched Bergmann glial cell loading with 500μM furaptra, in the same field illuminated by 420nm excitation wavelength of light. The electrode is visible in the top left section of the image. The image was exposed for 200ms.

Panel C shows the "puffer" pipette in position containing 100μM ATP. This pipette was placed over the Bergmann glial cell.

Panel D was the first image taken from a series which recorded the changes in fluorescence and hence record $[Ca^{2+}]i$ changes. See Figure 4.5.3.E.

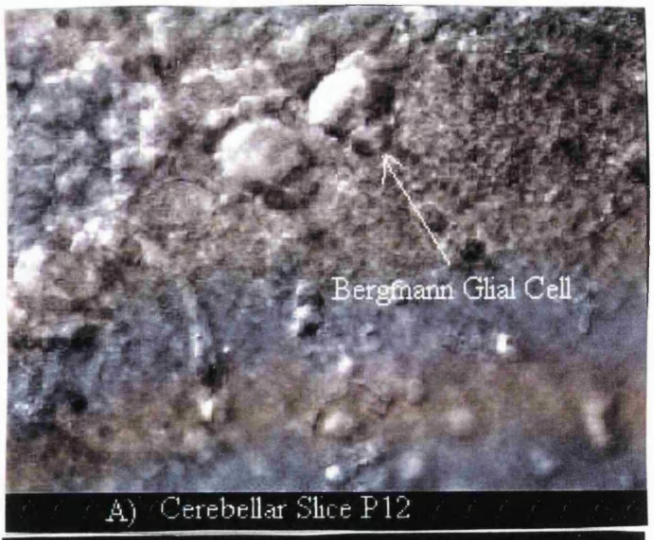

A) Cerebellar Slice P12

B) Patched Bergmann Glial Cell

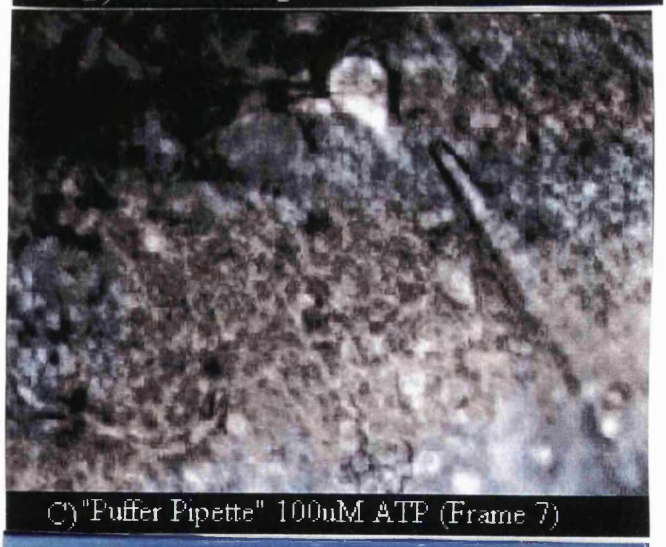

C) "Puffer Pipette" 100uM ATP (Frame 7)

D) Test Image Prior to Sequence

Figure 4.5.3.E Consecutive images from the experiment.

This figure shows six consecutive frames from the series recorded. When the images were played in real time it was evident that the patched cell moves out of focus. The images demonstrated that it was difficult to record $[Ca^{2+}]i$ changes in whole cell Bergmann glial cells. The software limitations prevented further analysis.

(E)

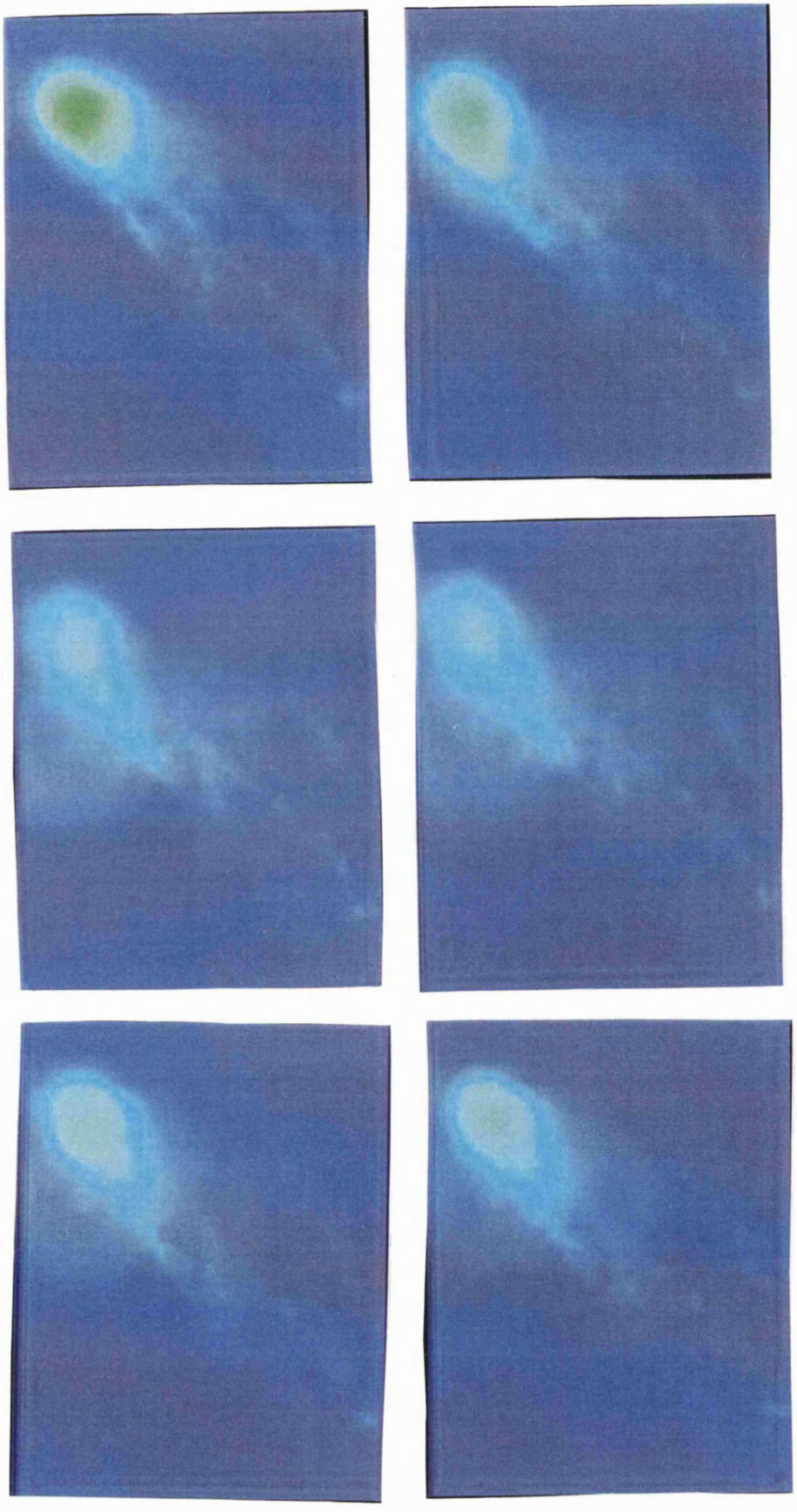

4.6 Practical assessment of Experimental Techniques.

4.6.1 Cultured astrocytes do not like quartz!

For microfluorimetry it was important to minimise the phosphorescence artefact generated in the glass coverslip and optics by the U.V. flash. Quartz coverslips have less phosphorescence. However type 1 astrocytes did not grow well on quartz. The experimental culture procedure was exactly the same as for glass. The major difference between the two types of coverslips was that the quartz were recycled. It is possible that the cleaning process had an effect on the surface of the coverslip which interacted with the new cells and their attachment mechanisms.

Various cell surface adhesion molecules were used to improve the condition of the astrocytes in culture. Cell Tak (Collaborative biomedical Products) 3.5μg/ml, Poly-D-lysine (Sigma) 10μg/ml, Surgical glue (Braunmelsungen Histoacrly blau) coated directly, collagen (Vitrogen 100, Celtrix labs) coated directly, laminin 4μg/ml (Sigma) and bovine Fibronectin 4μg/ml (Sigma) were all tested and the condition of the astrocytes assessed on quartz coverslips.

Figure 4.6.1: Photographs of the results of the tissue culture experiments.

Photograph A shows type 1 astrocytes cultured on glass coverslips coated with poly-L-lysine. The cells were large and readily interacted with adjacent cells. The cells plasma membranes spread to make connections with other cells. The large areas of cytoplasm were transparent and the membranes were intact. There was also an absence of small circular densely formed cells.

Photograph B shows the same batch of cultured cells on quartz coverslips coated with Poly-L-lysine. There was in this culture a lack of large protoplasmic cells. The few that can be seen were small dense cells that appear to have holes in their membranes. There was a distinctively high proportion of small circular phase bright cells, which could be either granule cells or progenitors which have not developed further.

Photograph C illustrates cultured astrocytes from the same procedure grown on quartz coverslips coated with Cell Tak. The cells appearance was very similar to cells in picture B. The overall condition was dull and granular, which was characteristic of unhealthy cells. This unhealthy appearance was also seen with the coating procedures of surgical glue, Poly-D-lysine and the laminin.

Photograph D shows the results of cells grown on collagen coated quartz coverslips. The astrocytes in this photograph had an improved condition similar to the cells grown on poly-L-lysine coated glass. In D there was large protoplasmic cells with very little contamination from other granular types of cells. However as collagen is not native to brain tissue, this process was not routinely used.

Photograph E shows glial cell cultures grown on quartz coated with bovine derived fibronectin. The cells in these cultures appeared healthy. The cells were large protoplasmic cells, that readily formed connections with other cells. There was a very low proportion of smaller dark cells. As fibronectin is found in neural tissue this was the substrate of choice.

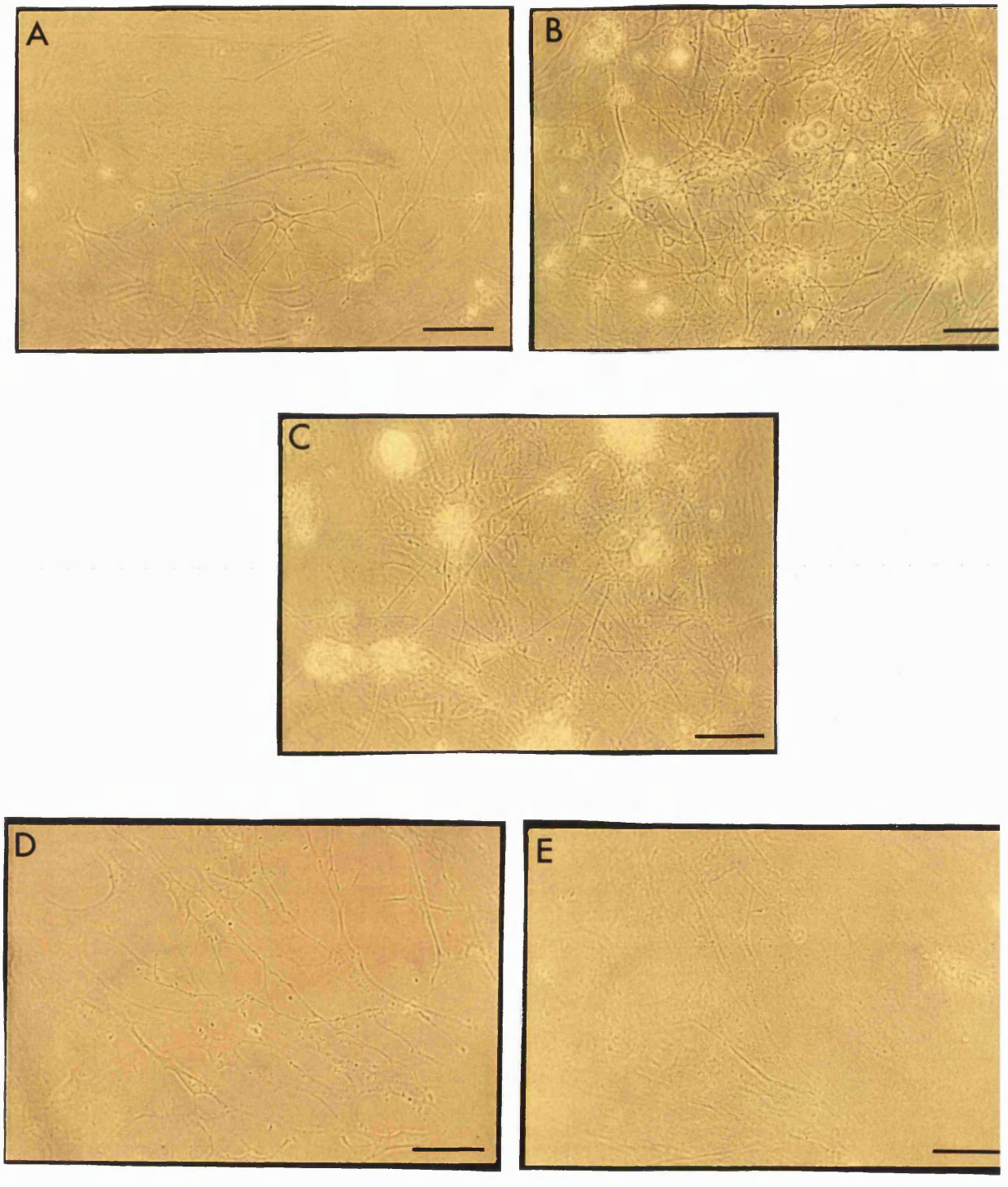
A
B
C
D
E

4.6.2 Furaptra is a magnesium sensitive indicator.

Furaptra has a large range for Ca^{2+} binding which is suitable for measuring high localised transient $[Ca^{2+}]i$ changes and the extent of Ca^{2+} buffering is minimised. However the indicator has an affinity for Mg^{2+} Kd≈1.5mM at 37°C (Raju *et al* 1989) and Kd≈5mM at 16°C (Konishi-M. *et al* 1991) which is in the physiological range. It is possible therefore that some $[Ca^{2+}]i$ changes measured were contaminated by small amounts of the furaptraMg^{2+} complex. Resting $[Mg^{2+}]$ is approximately 0.5mM which could give an under estimation of up to 10% for the F_{minCa} value which would mean an over estimation of large $[Ca^{2+}]i$ transient measurements. Fura-2-ff has a lower affinity for Mg^{2+}, Kd=18.4mM, compared to furaptra, Kd=3.6mM, although its affinity for Ca^{2+} is higher at Kd=29.8μM compared to 48μM.

4.6.3 Fura-2-FF measured responses compared to furaptra.

Photolytically released $InsP_3$ experiments in astrocytes were performed with fura-2-FF to compare with the furaptra measured $[Ca^{2+}]i$ changes. Figure 4.13.2. A.B shows identical 24μM $InsP_3$ concentration released on two separate type 1 astrocytes. The initial rise time phase were similar. In this instance the $[Ca^{2+}]i$ peaked and the response then declined.

Figure 4.6.2 Comparison of $InsP_3$ evoked $[Ca^{2+}]i$ response measured with furaptra and fura-2-FF.

Panel A shows a fluorescence trace measured with fura-2-ff to 24μM $InsP_3$ concentration. The astrocyte was loaded with 500μM fura-2-ff and whole cell voltage clamped.

Panel B illustrates the fluorescence trace in response to 24μM $InsP_3$ concentration measured with 500μM furaptra in a single astrocyte. The cell was whole cell voltage clamped and indicator applied via the pipette.

Vertical scale bar represents at rise in $[Ca^{2+}]i$ of 5μM, horizontal 2 seconds. Both cells holding potential =0mV.

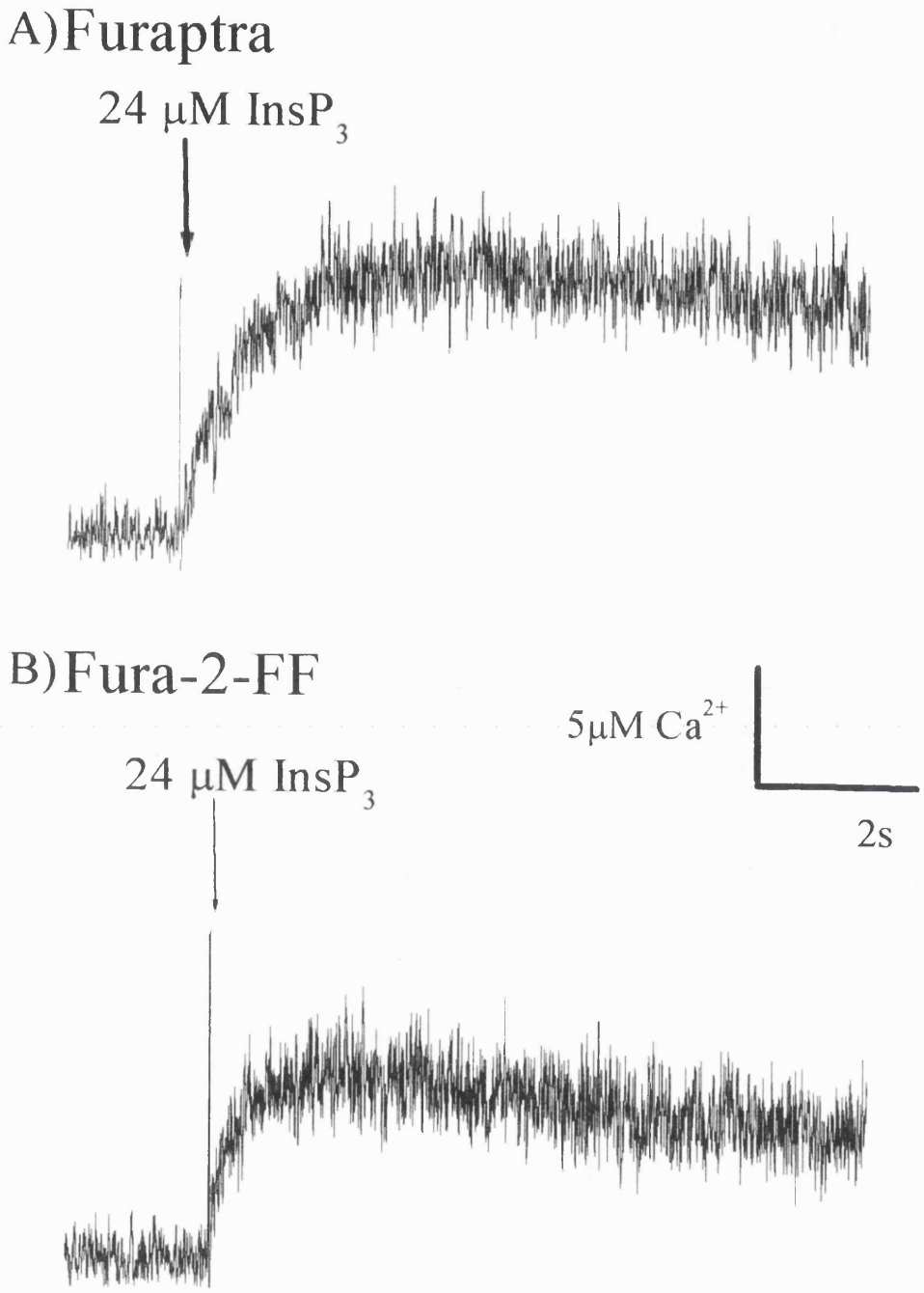
A)Furaptra
24 μM InsP3
B)Fura-2-FF
5μM Ca2+
24 μM InsP3
2s

4.7 Summary.

(i) $InsP_3$ concentrations (0.1-25μM) evoked $[Ca^{2+}]i$ rises in type 1 astrocytes *in vitro*.

(ii) The initial delay phase of the $[Ca^{2+}]i$ rise decreased with increasing $InsP_3$ concentrations.

(iii) The Ca^{2+}-flux, $d[Ca^{2+}]i/dt$ of $InsP_3$ induced $[Ca^{2+}]i$ rises were dependent on the $InsP_3$ concentration within the same type 1 astrocyte. Within different cells the extent of response varied. Astrocytes and hepatocytes had similar $d[Ca^{2+}]i/dt$ at 50-100$\mu M.s^{-1}$ which were considerably lower than endothelial and Purkinje cells at 1000-1400$\mu M.s^{-1}$.

(iv) The termination of the $InsP_3$ induced $[Ca^{2+}]i$ response was not due to the metabolism of $InsP_3$. In conditions where $InsP_3$ concentrations remained high the $[Ca^{2+}]i$ response returned to pre-photolysis $[Ca^{2+}]i$ levels.

(v) The rate of termination of $InsP_3$ evoked $[Ca^{2+}]i$ response was linearly related to the Ca^{2+} flux through the channel in both *in vitro* and *in situ* studies.

(vi) The linear relation of termination rate and Ca^{2+} flux in type 1 astrocytes was similar to other peripheral non-excitable cells (such as hepatocytes and endothelial cells) and Purkinje cells studied (Ogden-D.C. & Capiod-T. 1997 ; Carter-T.D. & Ogden-D. 1997). This suggests that the same mechanism of inactivation by Ca^{2+} binding may apply to all isoforms.

(vii) Paired astrocytes in culture were filled with furaptra and caged $InsP_3$. Within the un-patched cell an $InsP_3$ evoked $[Ca^{2+}]i$ rise was observed. Thus $InsP_3$ could act as a diffusible agent during astrocytic $[Ca^{2+}]i$ wave propagation.

(viii) Patched type 1 astrocytes (*in vitro*) did not respond well to bath applied agonist.

(ix) More studies are required before definite conclusions can be made about the kinetic parameters of $InsP_3$ evoked $[Ca^{2+}]i$ in Bergmann glial cells. Bergmann glial cells were difficult to identify *in situ* thus the process of patching single Bergmann glial cells was difficult.

CHAPTER 5

GLIAL CELL CALCIUM SIGNALS DURING NEURONAL ACTIVITY.

5. Introduction

This chapter examines astrocytic Ca^{2+} signalling in acute cerebellar slices in an attempt to identify a role for glial $InsP_3$ evoked $[Ca^{2+}]i$ rises. Previous studies examined glial cell $[Ca^{2+}]i$ levels and wave propagation patterns (Kriegler-S. & Chiu-S.Y. 1993; Verkhratsky-A., & Kettenman-H. 1996) in co-cultures and in organotypic slice preparations (Dani-JW & Smith-S.J., 1992). Their studies show that neuronal activity *in vitro* directly influences $[Ca^{2+}]i$ in adjacent astrocytes. Conversely work by two groups Nedergaard-M. (1994) and Parpura-V. *et al* (1994) has established that glial cells behaviour can directly influence neuronal signalling by altering neuronal $[Ca^{2+}]i$ levels.

The neuro-glial relationship appears to be a tightly controlled bi-directional partnership *in vitro*. However work by (Juurlink-B.H.J. & Hertz-L. 1986 ; Barres-B.A. *et al* 1989) has always cast some doubt on the reliability of these results due to the changed properties of astrocytes in culture. The questions must ultimately be addressed *in situ* and *in vivo* with intact mammalian CNS tissue (Muller-T. *et al* 1992; Muller-T. 1996; Verkhratsky-A. *et al* 1998).

5.1 Rat cerebellum

The anatomy of the cerebellum is summarised in figure 5.1.1. The dendritic tree of Purkinje neurones and filamentous processes of the Bergmann glia remained intact in saggital sections. The climbing fibre input to the Purkinje neurone soma and dendritic tree was also preserved in this orientation, but parallel fibres were cut in saggital slices and would be stimulated locally. The experiments reported in this section attempted to show the effect of climbing fibre stimulation on Purkinje neurone membranes and Bergmann glial $[Ca^{2+}]i$.

Figure 5.1.1 Cerebellar Organisation.

This illustration originates from Palay and Palay "Cerebellar Cortex" (Palay-S. L., 1974). It shows a section of the cerebellar cortex, comprising from outside the pial surface, the molecular layer, Purkinje cell layer, granular cell layer and the white matter in saggital and transverse orientations. The neurones were labelled Golgi cells, granule cell, Purkinje cell, basket cell, stellate cell, Lugaro cell. In black Bergmann glial cells and granular cell layer protoplasmic astrocytes have been superimposed. The climbing fibres, parallel fibres and mossy fibres are clearly labelled. The image shows the appearance of cells in the two orientations. In the transverse section Purkinje cells show a narrow outline. The parallel fibres in this section run parallel to the plane of the slice. In the saggital section, however, the parallel fibres run vertically. Bergmann glial cells are small and have a "candelabra" like filamentous projection, which remains homologous despite the slice orientation. This was true for the protoplasmic astrocytes, which were small and projected in all dimensions.

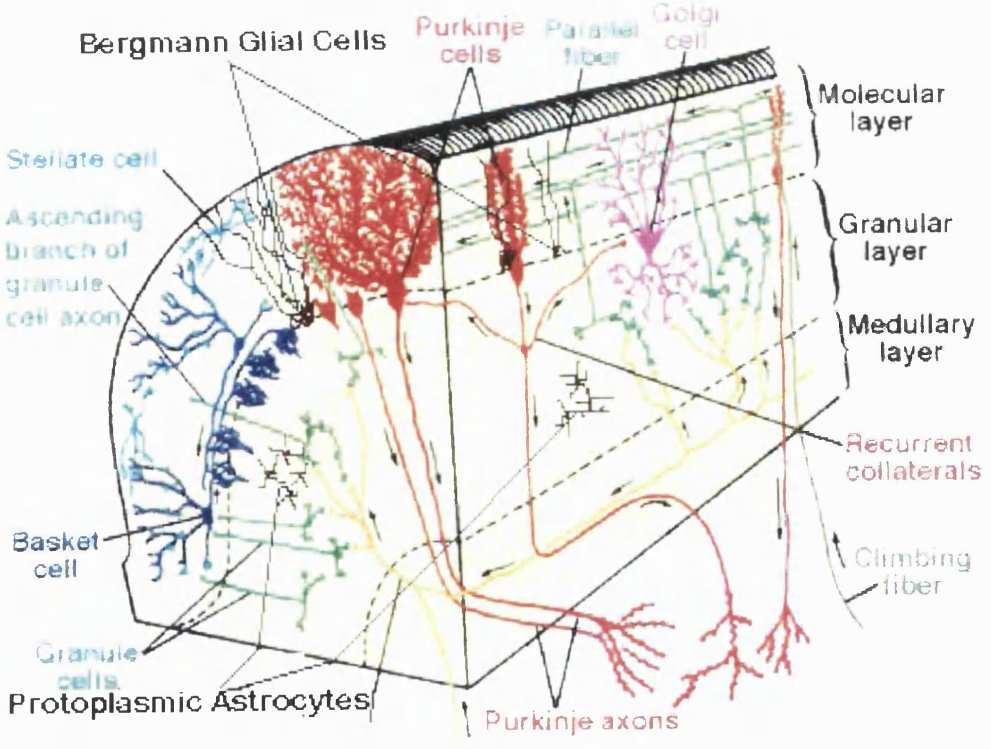

5.1.1 Glial cells in the Cerebellum

Within the cerebellum glial cells take on two main forms, long radial Bergmann glial cells and round smaller protoplasmic astrocytes (Chapter 3). Bergmann glial cells are unlike other radial glial cells in that after development they are still present in rat adult cerebellum. Their persistence implies that they are responsible for other functions. The adult Bergmann glial cells have a slightly different cell morphology from their younger counterparts. Their filaments thicken and have arborizations which appear to form intimate complexes with the synapses of predominantly Purkinje neuronal dendrites within the molecular layer (see figure 5.1.2 A). The cell somas of the Bergmann glial cells can be identified with practice on and in around Purkinje cell somas (Chapter 4 figure 4.5.1) and were studied further here.

The rounder "type 1 like" astrocytes are located in both grey and white matter. The velate protoplasmic astrocytes cells located in grey matter have fine inter projections which encompass and enclose many granule cells (chapter 3 Figure 3.4.A). When viewed with transmitted light these astrocytes were very difficult to identify. The astrocytes found in the white matter tracts are fibrous astrocytes and appear "star" like. These cells have finer projections and appear to contain more internal filaments (Palay-S. L. & Chan-Palay-V. 1974). Once again these cells were difficult to differentiate within a bright field illuminated slice (figure 5.1.2.B).

Figure 5.1.2: Neuro-glial Morphological Interactions

Image A illustrates a saggital cerebellar section loaded with furaptra-AM. The section shows a Purkinje cell layer (running middle top to bottom right) and was recorded with excitation >420nm emission using the T.I.L.L Photonics THETA camera and IDEA software. The Bergmann glial cells were filled with the calcium indicator, so appeared bright. Notice the tear shaped Bergmann glial somas located near the large black holes of the Purkinje cell somas which have not absorbed the indicator. Leaving the Bergmann glial somas are fine linear structures of their filaments. These were interspersed with small spots. The spots were the granule cells that migrate along Bergmann glial cells at this stage of development P12. Through this molecular layer other small parallel fibres were distinguished (top left to middle bottom). The indicator shows the small fine structures that form the glial-neuronal mesh.

Image B represents a section through the molecular layer in a saggital orientation. The bright field section was recorded using the T.I.L.L imaging system and Vision software (IMAGO camera). The Purkinje cell layer (top left to right side) was identified by the large somas (10-15μm) with a round shape and bifurcating dendrites. However it was difficult to identify the Bergmann glial cells which were located in around the cells somas.

Scale bar is 20μm.

A)

B)

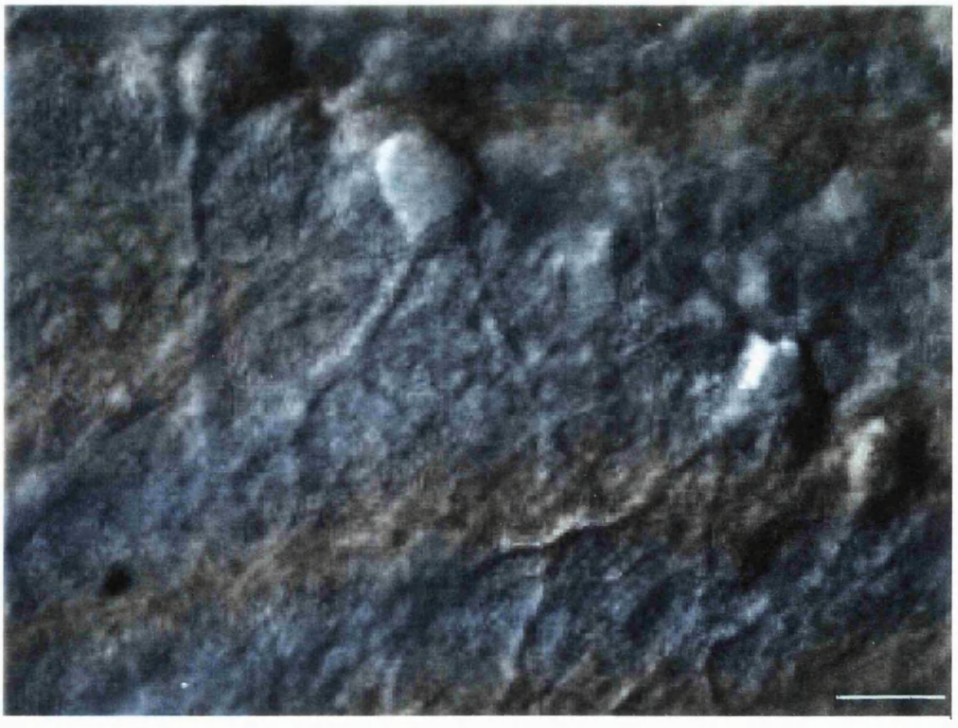

5.2 Measurement of $[Ca^{2+}]i$ from multiple Bergmann Glial cells

5.2.1 Calcium Imaging System

A T.I.L.L Photonics imaging system with fast switching monochromator recorded $[Ca^{2+}]i$ changes from Bergmann glial cells. The fast switching monochromator allowed dual wavelengths to be recorded at 100 millisecond intervals. Even when loaded with fluorescent indicators Bergmann glial cells in slices are small fine cells and difficult to identify. Standard CCD cameras create images of poor quality therefore distinguishing these cells intricate filaments has previously been difficult. New cooled CCD cameras have improved resolution which aids in recording $[Ca^{2+}]i$ levels from Bergmann glial cells.

5.2.2 Selective loading of Bergmann glial cells by local perfusion.

Acetoxymethyl (AM) forms of the calcium sensitive indicators were lipophilic and readily diffused through the cell membrane. Once inside the cell the indicator was released from the AM group by intracellular esterase activity and became lipophobic remaining inside the cell. Bergmann glial cells within a cerebellar slice were selectively loaded by perfusion of the pial surface as described in chapter 2 section 2.9.

An initial problem associated with this technique of selectively loading Bergmann glial cells *in situ* was the isolation of their fluorescent signal. The lipophilic dyes are not cell specific, so will enter other cells. At P12 the rat cerebellum is still undergoing development and Purkinje cells have not developed fully a dendritic tree. The top half of the molecular layer, closest to the pial surface consists of mainly Bergmann glial cells with a few stellate cells, migrating granule cells and parallel fibres. Ca^{2+} indicators were selectively applied to this area (figure 5.2.2.A) Within the first 5-10 minutes the Bergmann glia take up the indicator via their end feet and dendrites. The indicator travels through the length of the cells. As the AM indicator was washed over the area other small cells and fibres take up the indicator. The smaller granule and stellate cells

were distinguishable from the glial by their morphology. Purkinje cells within a thirty minute period did not take up the indicator. When the indicator was applied for longer it seeped up to the Purkinje cell dendritic tree ends and penetrated the cell. Once loaded a curtain of Bergmann glial cells were clearly identified. When loaded correctly the Purkinje cell somas were seen as black holes in the molecular layer. If the indicator was applied in this way to the molecular layer of older animals (P16-20) then the Purkinje cells, Bergmann glial cells, stellate cells granule cells, blood vessels erythrocytes and fibres all become labelled by the indicator (see figure 5.2.2 B).

To determine the slices orientation images were taken at the start of the experiment with transmitted light, then images at 420nm excitation light (for furaptra) prior to and after loading to ensure the glia were loaded correctly.

Figure 5.2.2 Loading Technique for Bergmann glial cells

Image A demonstrates the technique of Bergmann glial cell selective loading. The phase bright image shows an application microelectrode placed in between two pial surfaces of rat cerebellar folium. Notice how the folds are separated due to the positive pressure which forces the furaptra-AM out over the section.

Image B shows that Purkinje cells were filled with AM-indicators when the animal was older than P12 This pattern of loading was also seen when the AM-indicator was applied for over one hour to younger animals.

Scale bar is 20μm.

A)

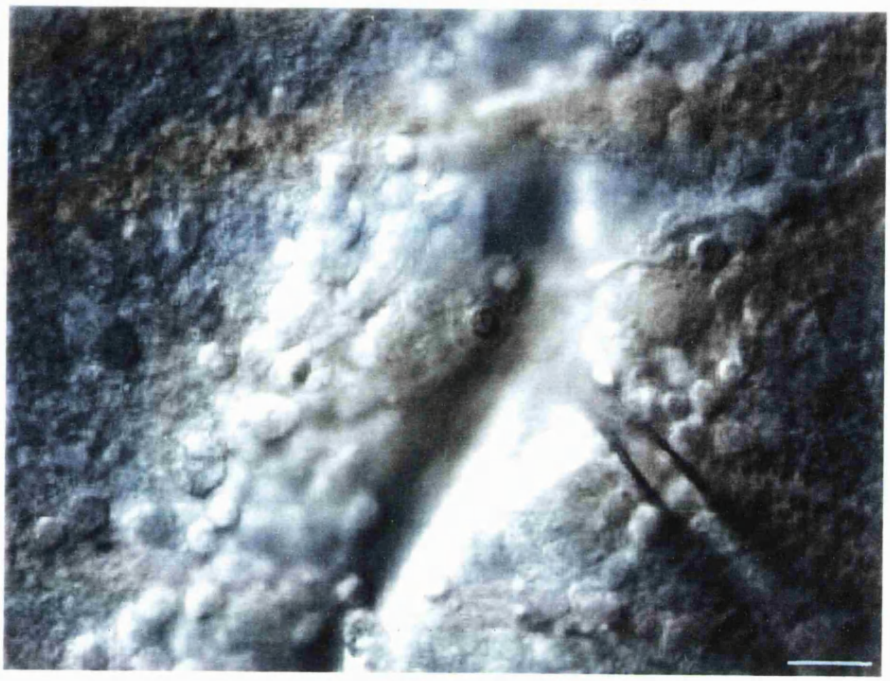

B)

Bergmann glial cells in slices were successfully loaded in 16 out 31 experiments with furaptra-AM. Other dyes were used unsuccessfully, fura-AM n=3, fluo-3-AM n=3, fura-red-AM n=2, indo-1-AM n=1. Furaptra had the advantage of being brightly fluorescent at low resting $[Ca^{2+}]i$ when excited at 420nm wavelength. This was important for these experiments to ensure that before the start the indicator was present in the Bergmann glial cells. With high affinity indicators low fluorescent signals at low Ca^{2+} made glial cell identification difficult. The indicators do not appear to form adequate emulsions after sonication with the DMSO and pluronic mix making absorption into cells difficult. The rate of external solution perfusion was also an important factor in indicator absorption. If the flow rate was too fast then the indicator washed away before coming into adequate contact with the cells (figure 5.2.3 A & B). This may be related to the ease with which they are dispersed in aqueous solution.

Figure 5.2.3. Bergmann glial cells $[Ca^{2+}]i$ responses from Purkinje cell stimulation.

Panel A shows a typical control transmitted image, recorded with a T.I.L.L photonic system and IDEA software. In the central region towards the top of the image the Purkinje cell layer runs from left to right. The dendrites were descending towards the bottom of the frame.

Panel B depicts the same frame as above recorded with 420nm wavelength excitation light after loading with 163μM furaptra-AM. Notice the central area towards the top of the image which was the unloaded Purkinje cell body layer. The round cells fanning across the top were within the granule layer. The Bergmann glial cells were the linear structures running down through the molecular layer. The glial filaments have arborizations along their length.

Panel C was a Purkinje cell that after electrical stimulation was re-patched with fluo-3. The image was recorded under excitation light wavelength 480nm. The Purkinje cell bifurcating dendrite descended towards the bottom right through the filaments of Bergmann glial cells. The pipette and the Purkinje neurone soma are bright and thus the fluorescence signal is saturating the CCD. The experiments were carried out at room temperature 23°C.

Scale bar for all images is 20μm.

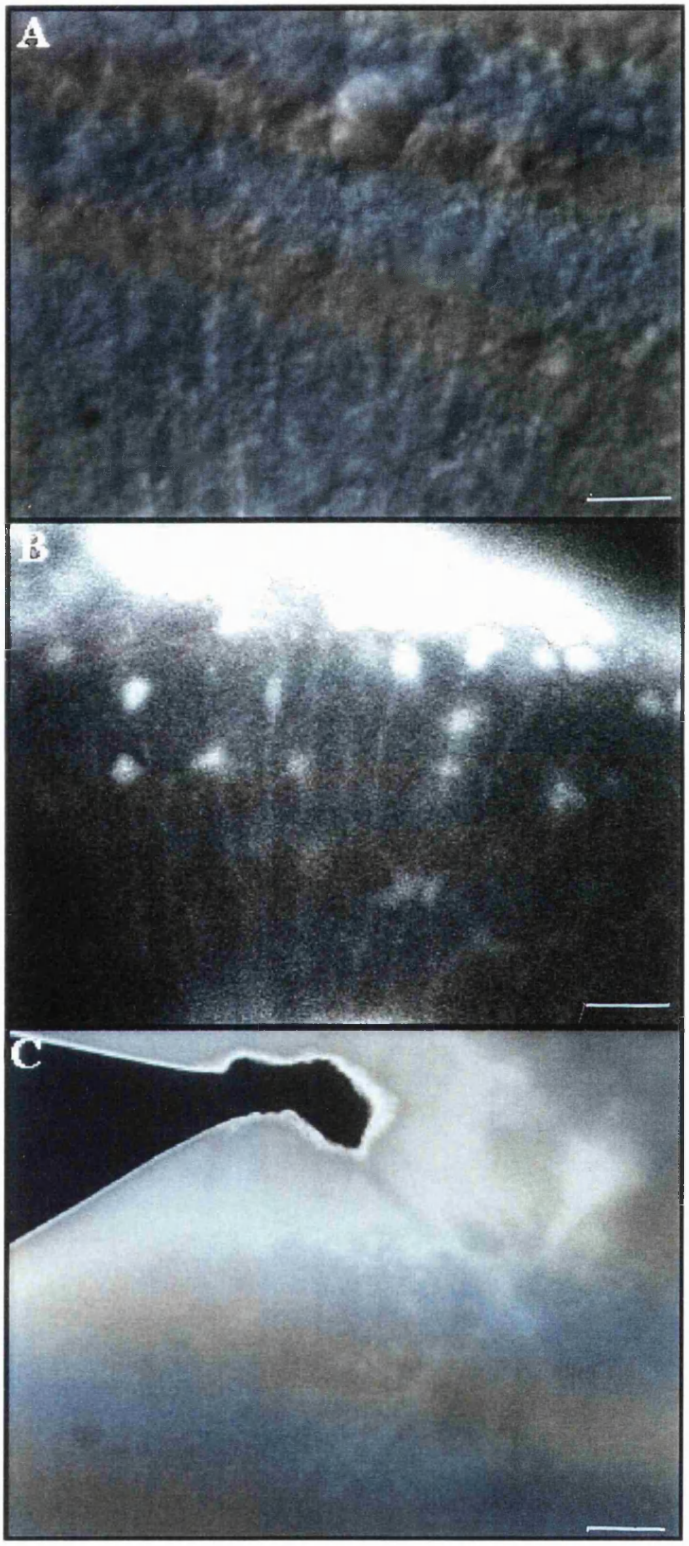
A
B
C

5.3 What does glial cell Ca^{2+} do during neuronal electrical behaviour?

5.3.1 Neurones of the Rat Cerebellum

Throughout the molecular layer there are many neural projections and synapses. The Purkinje cells and hence the dendrites located in the molecular layer have three main afferent inputs. (i) The first afferent input into the molecular layer comes from granule cells which project axons to the molecular layer as parallel fibres. The parallel fibres form connections via excitatory synapses directly onto the Purkinje cell dendrites. The mossy fibres, which are axons whose cell bodies originate in the spinal cord (the pontine nuclei), have synaptic connections with granule cells and their dendritic complexes (cerebellar glomeruli). (ii) The second afferent input are climbing fibres (which are the axons of inferior olivary neurones located in the brain stem). The climbing fibres synapse directly with multiple sites onto individual Purkinje cells (see figure 5.3.1). Each Purkinje cell has a climbing fibre input (iii) Finally the third input arises from the monoaminergic neurones (from the locus coeruleus and the raphe nuclei) which also terminate on the Purkinje cells.

The Purkinje cell layer within saggital sections has a dendritic tree which sits in this plane. The Purkinje cell axons form the only cerebellar output. The axons descend through the cerebellar cortex granule cell layer, to the central regions of the folium and towards the deep cerebellar nuclei of the brain stem where they end in synaptic boutons (figure 5.3.1).

5.3.2 Physiology of the cerebellum.

It has been hypothesised that pre and post synaptic activity underlies learning and that synaptic plasticity plays a fundamental role in memory (Hebb-D.O. 1949). One cellular model thought to induce motor learning within the cerebellum is long term depression (LTD). LTD is caused by the co-activation of climbing and parallel fibre inputs (1-4Hz for 4-6 minutes) on the Purkinje cell, to cause a persistent reduction in the activity of the Purkinje neurone (Ito-M. *et al* 1982). Inhibition of Purkinje cell activity comes from interneurones, stellate and basket cells, which are present within the molecular layer, and Golgi type II cells located in the granule cell layer. The parallel fibres and climbing fibres stimulate stellate and basket cells, whereas Golgi type II cells, although influenced by parallel fibres, are also influenced by the mossy fibres. The function of the synapses may be modified according to the requirements of the system to control information patterning and hence learned motor response.

Figure 5.3.1: Neural Inputs and Outputs of the Rat Cerebellum

The schematic diagram represents the neuronal circuitry of the rat cerebellum. This figure is adapted from "The cerebellum and Cognition" edited by Jeremy D. Schmahmann. International Review of Neurobiology volume 41, page 87 and "Neurobiology" edited by Shephard page 461.

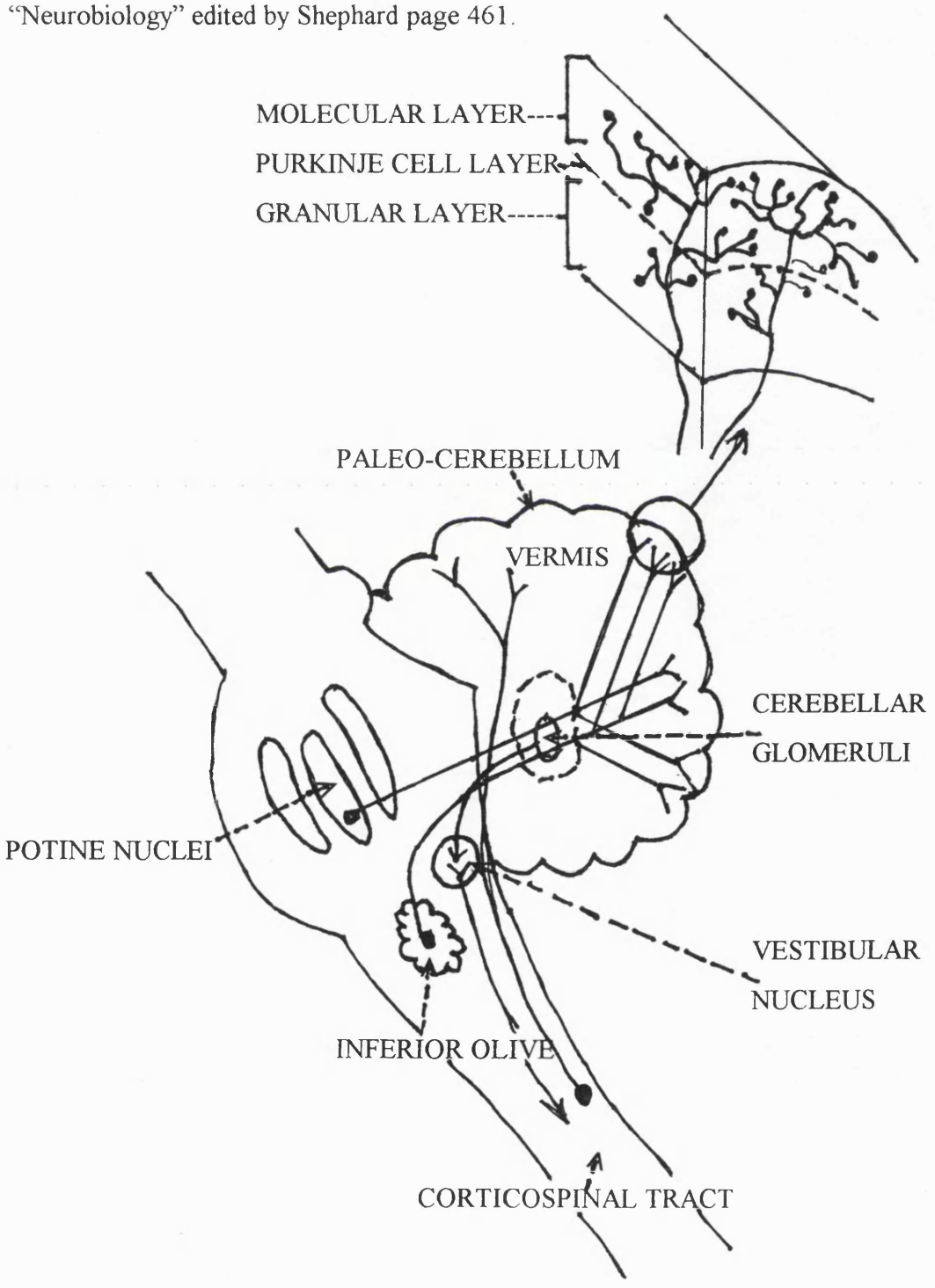

5.3.3 Stimulation of Purkinje cells

For neuronal stimulation excitatory post synaptic potentials (epsps) were induced by a stimulation electrode in the granule cell layer and recorded in a Purkinje cell soma, surrounded by the indicator loaded glial cell region (see figure 5.3.2). Several types of stimulating electrodes were tried. Bipolar tungsten electrodes, single tungsten electrodes and large patch pipettes filled with external solution. Large patch electrodes were the most successful. These electrodes were placed on the surface of the slice in the granule cell region to induce the climbing fibre epsps. The tungsten electrodes would have to be placed deep into the slice and only induce neuronal activity below the surface. This was not ideal when loaded glial cells are located at the slice surface. Purkinje cell somas were impaled with micro-pipettes to record electrical activity. This technique was not as efficient as the whole cell patch technique. Climbing fibre stimulation was at 1 3, 5, or 10Hz. When stimulation was induced above 10Hz the membrane potential of the Purkinje cell would become more positive and the cell condition would deteriorate. This was due to the climbing fibre input causing an increase in excitability, which when prolonged was toxic.

Climbing fibre epsps were identified by a sharp threshold. Occasionally the depolarisation fired groups of action potentials at their peak (n=8). There was some difficulty in inducing epsps via climbing fibre stimulation (43% success rate). However the same cells were electrically active and readily fired antidromic action potentials (12%) as a result of the stimulation, but no epsp (5.3.2.C).

Parallel fibre stimulation proved difficult in transverse sections and was not a successful means of activating neuronal activity.

Figure 5.3.2 Electrical Activity induced in Purkinje cells

Panel A shows typical examples of neuronal electrical activity. The first example shows a climbing fibre epsp. After the artefact there was a short delay followed by a sharp rise. In this instance action potentials were induced as the membrane potential was raised through the Purkinje cells threshold level. Vertical scale bar was 30mV.

Panel B illustrates a climbing fibre induced epsp which does not have induced action potentials. Vertical scale bar 15mV.

Panel C In some experiments climbing fibre stimulation did not elicit an epsp although the neurone repeatedly fired action potentials. On switching off the hyperpolarising current pulse caused action potentials to fire. The signal was attenuated due to the insufficient sample rate. Vertical bar was 30mV.

Panel D the fourth 5.3.2.D shows that when the current pulse was removed the Purkinje cells spontaneously fired action potentials illustrating that the cells were electrically active. Vertical scale bar 10mV.

All horizontal scale bars were 30 milliseconds.

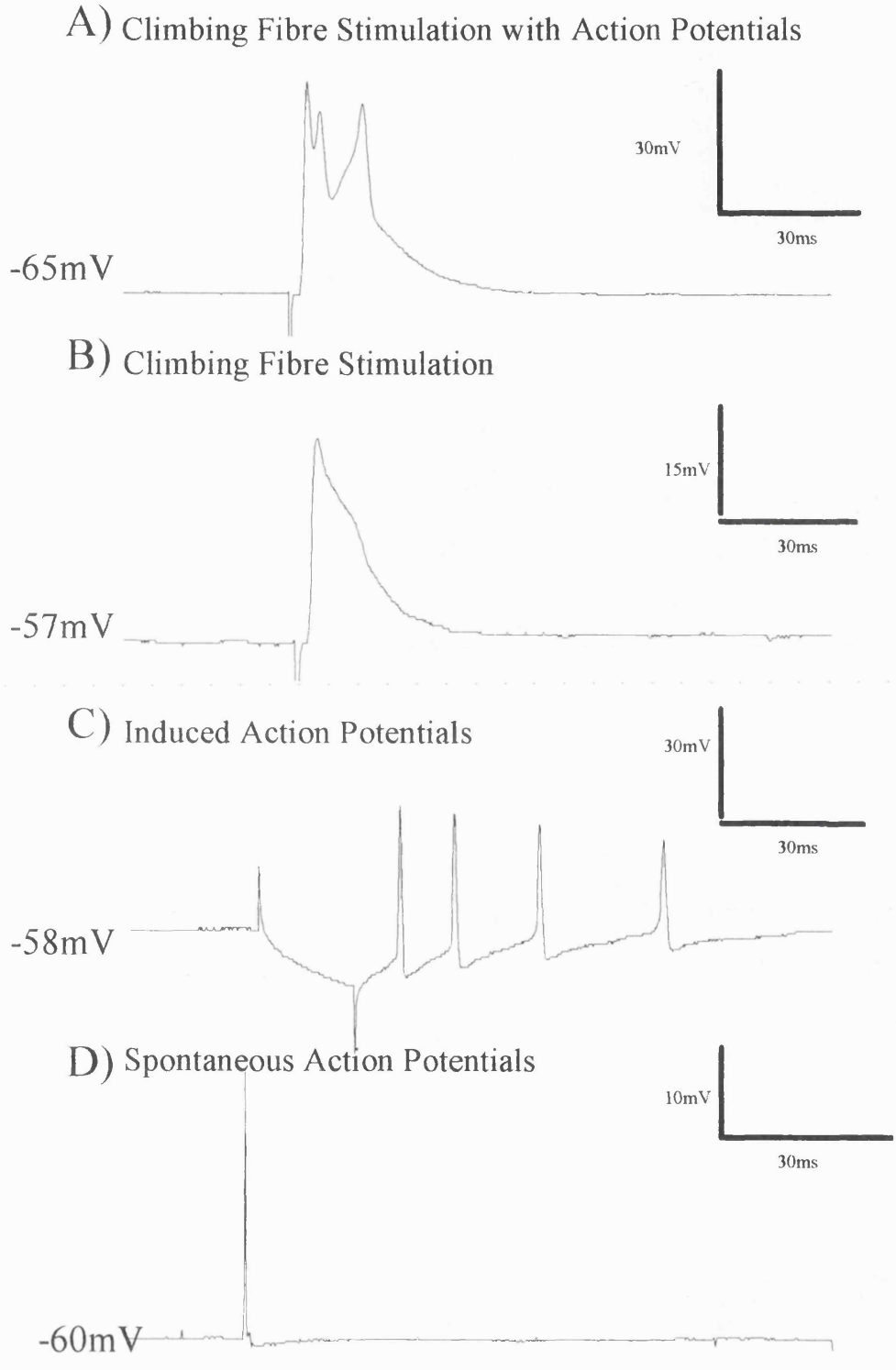
A) Climbing Fibre Stimulation with Action Potentials
30mV
30ms
-65mV
B) Climbing Fibre Stimulation
15mV
30ms
-57mV
C) Induced Action Potentials
30mV
30ms
-58mV
D) Spontaneous Action Potentials
10mV
30ms
-60mV

The dendritic trees of the activated Purkinje cells lay through the loaded Bergmann glial cells. At the end of the experiment if possible the patched Purkinje cell was loaded with a dye to distinguish the orientation of the bifurcated dendritic tree in relation to the imaged Bergmann glial cells (1 out of 6 successful experiments figure 5.2.3 C). Usually the control phase bright image was enough to identify the Purkinje cells dendrites (5.1.2). Bergmann glial cells were loaded and adequate neuronal stimulation was induced in 8 separate experiments out of n=33. Images of Bergmann glial cells were successfully recorded 4 times of the 8 (see figures 5.3.3 and 5.3.4 Below).

5.3.4 Fluorescent measurements recorded from Bergmann Glial cells *in situ*

The indicator used for each experiment was furaptra. Once the Bergmann glial cells in the slice had been loaded with furaptra and the climbing fibre Purkinje neurone stimulated separate pairs of frames were recorded at using excitation wavelengths of 420nm and 347nm. Stimulation was continual throughout the period marked by the bars in graphs 5.3.3.C and 5.3.4. The images recorded were taken as a ROI (region of interest) from the original image to ensure that the virtual disk of the computer did not saturate (chapter 2 section 2.91). Each image was recorded for 200ms exposure for a cycle time of 500ms. 50-100 images were collected. Data were collected as intensity profiles of fluorescence levels through each image. Each intensity line was exported as an ASCII file which was read in a spreadsheet program. The fluorescence intensity profiles were recorded through a series of Bergmann glial cells or along the length of individual cells (figure 5.3.3). Each fluorescence intensity line was mapped and displayed on the images.

Figure 5.3.3 Image analysis for selectively loaded Bergmann glial cells *in situ*

Panel A shows an example of an experimental recorded frame. The fluorescence intensity profiles were placed through the series of small round cells in the granular layer S1. The second line ran through a single Bergmann glial cell (S2). S3 was a section across the filaments of many glial cells. The cells were seen as points of interest and high fluorescence and were labelled on each profile.

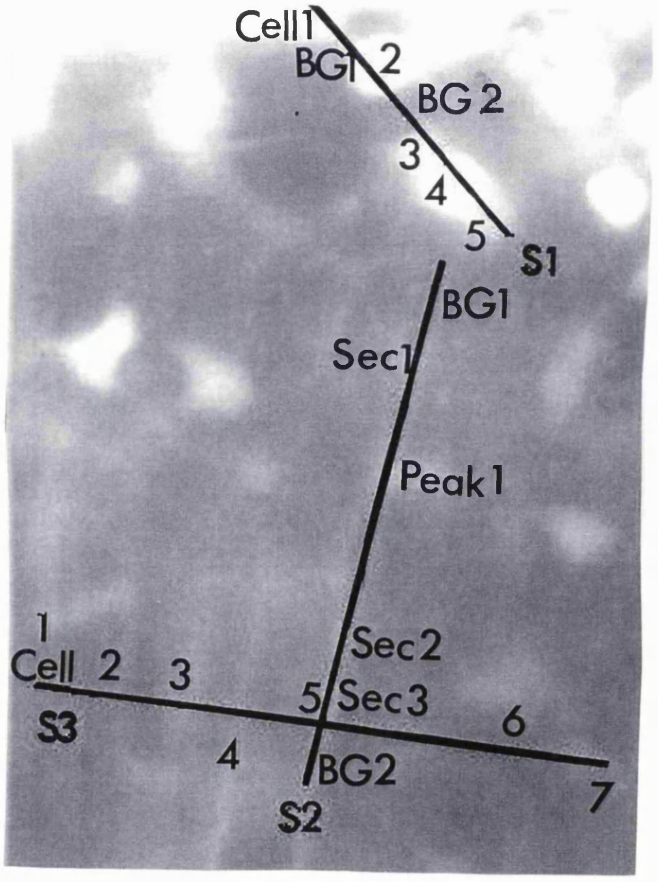

S1-Cells (1-5)

BG 1+2

S2-Sec1+2

Peak1

BG1+2

S3-Cells(1-7)

BG1

Figure 5.3.3: Continued

Panel B illustrates the corresponding line intensity profile recorded from image A. Each reference point labelled in A corresponded to the points indicated on the graph B. Graphs were plotted as pixel intensities (representing fluorescence) corresponding against the distance along the line profile (μm). Peak values of fluorescence intensity corresponded to cells of interest. Background (BG) levels were taken from the slice in areas where no indicator was present.

S1 dissected through the granular layer of the smaller cells. Each peak corresponded to the soma region of a cell. Each line profile was measured for each frame and exported as text files for fluorescence against position on line profile. Within spread sheets the corresponding values for cells were tracked as a function of time (frame number) from the series of images see figure 5.3.3.C.

S2 profile was split into sections of interest along the length of a single Bergmann glial cell. The cellular sections (corresponding to fluorescence peaks) were then measured over the period of the experiment see figure 5.3.3.C.

Finally S3 measures fluorescence levels over many filaments from Bergmann glial cells (fluorescence peaks) tracked within spreadsheet programs as a function of time throughout the series of images (see figure 5.3.3.C).

(B) S1 Cell Soma Region

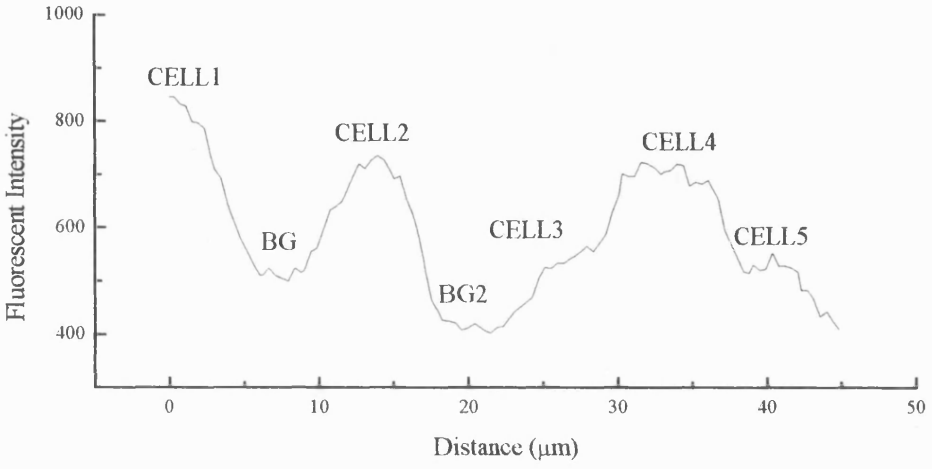

S2 Single Bergmann Glial Cell Filament

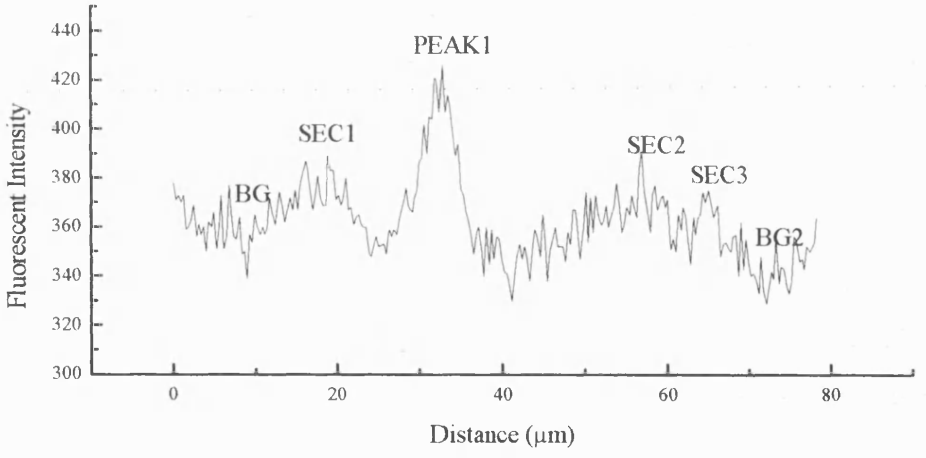

S3 Bergmann Glia Filaments

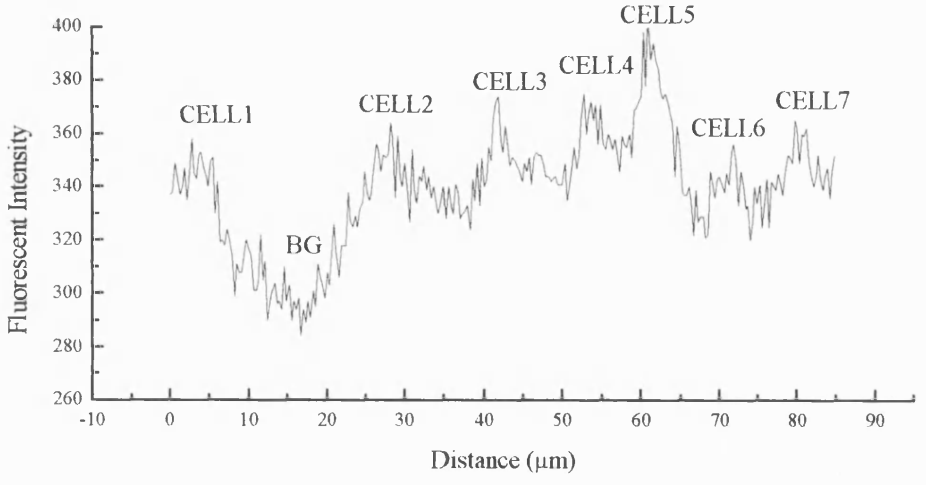

Figure 5.3.3 C Fluorescence measurements recorded from Bergmann Glia *in situ* using furaptra.

Section (i) Shows the intensity profile of line S1 tracked throughout the experiment. Y-axis pixel levels (arbitrary units) were plotted against frame number as a representation of time. Each frame consists of fluorescence recorded at 420nm excitation wavelength only. Due to technical problems (see section 5.4) the experiments were recorded as 4 separate files. The vertical lines represent the time breaks between different files. The first section was recorded during Purkinje cell stimulation, 10Hz via climbing fibres. The second section was measured during no stimulation. The third was during a further period of climbing fibre stimulation 1Hz Fourth a period of recovery.
Each line corresponds to either individual cells or cellular background regions.

Section (ii) S2 tracked over the same experiment as section (i). As above the fluorescence was plotted against frame number. Each line represents a different cell section area along its filament length from a single Bergmann glial cell. The four sections were separated as above.

Section (iii) was plotted as fluorescence against frame number for S3. The four sections correspond to four files as above. Each line in this panel represents individual Bergmann glial cell projecting filaments. Cellular background was labelled BG.

(C)

i) Profile S1Through Cell Somas

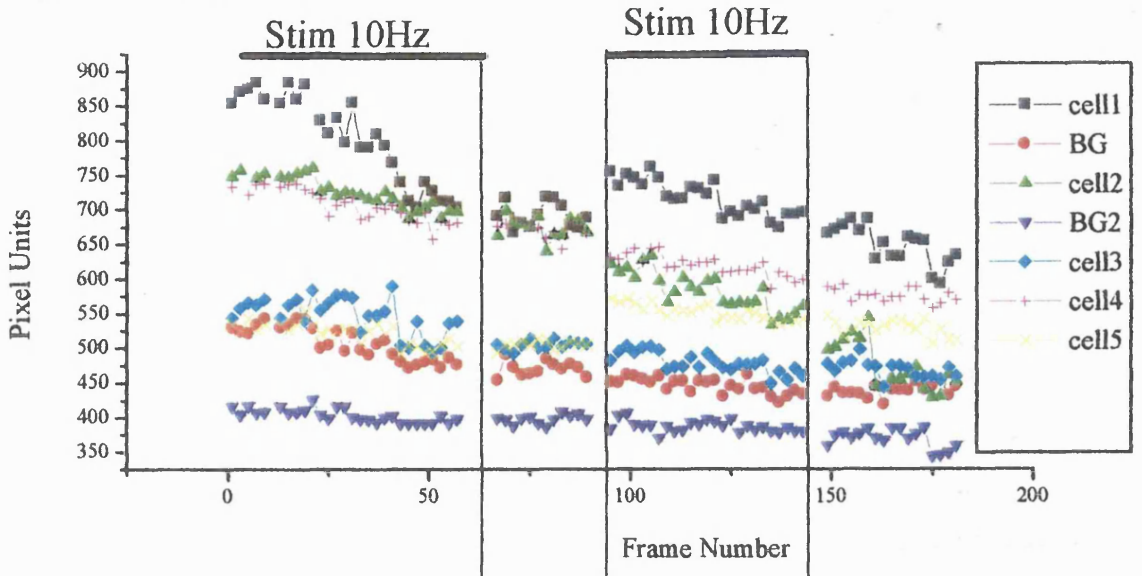

ii) Profile S2 Through Single Bergmann Glial Cell

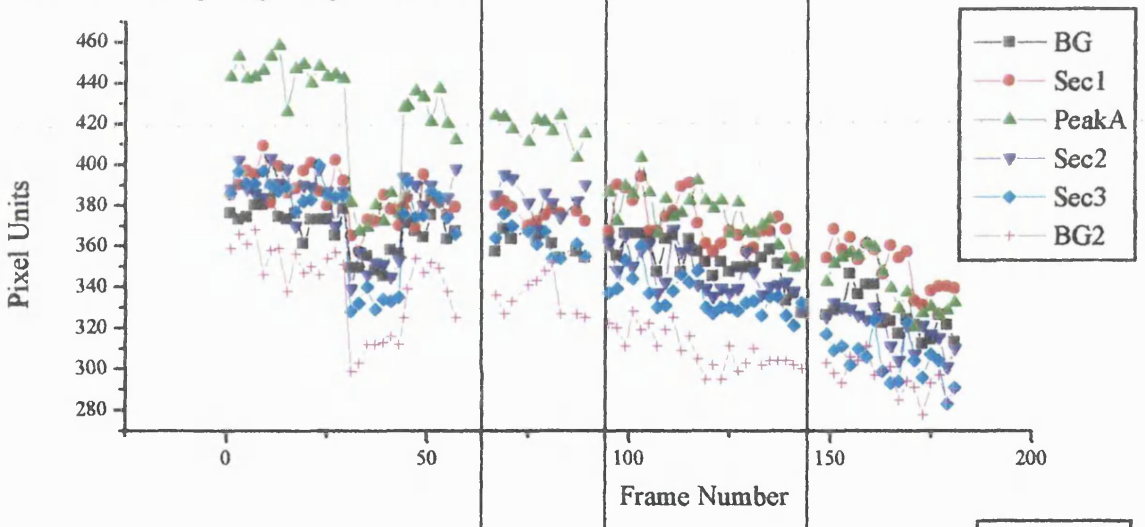

iii) Profile S3 Across Bergmann glial Cell Filaments

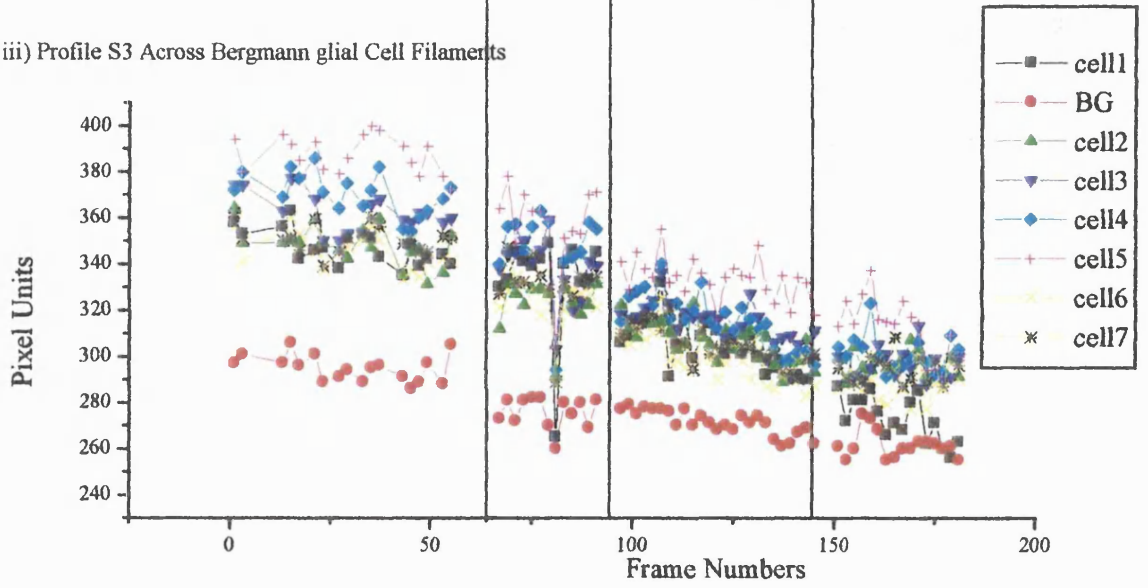

Figure 5.3.4 Calcium responses of Bergmann glial cells *in situ*

Figure 5.3.4 shows the fluorescence intensity profiles for the other 3 experiments (total n=4 figure 5.3.3.C). The intensities were measured as above. The fluorescence data comes from three separate slice preparations all loaded with furaptra-AM. The frames plotted were recorded with 420nm excitation light wavelength with T.I.L.L Photonics and IDEA software. The arrows indicate the regions of induced Purkinje cell electrical stimulation..

Panel(i) represents fluorescence line intensity profiles for frames 29 to 140. Each image was recorded at 420nm excitation wavelength light, with an exposure time of 200ms approximately every two seconds. The Ca^{2+} indicator used was furaptra-AM. Purkinje cell epsp stimulation lasted for 20 seconds (frame 29 to 39) at 1Hz. Each line represents individual cells.

Panel(ii) demonstrates fluorescence profile over 140 frames. Each line represents different Bergmann glial cells. The profile was split into three sections each representing three individual files from the same experiment. Stimulation (black line) was induced at 10Hz from frame 7-51(approximately 11 seconds). Each frame exposed for 200ms every 500ms. Third phase stimulation was 10Hz, frames 113-155 for cycles every 1 second.

Panel(iii) demonstrates Purkinje cell stimulation of 1 Hz from frames 7-105. Each image recorded at 420nm excitation light wavelength was exposed for 200ms every 2 seconds. The different lines represent different cells tracked through out the experiment.

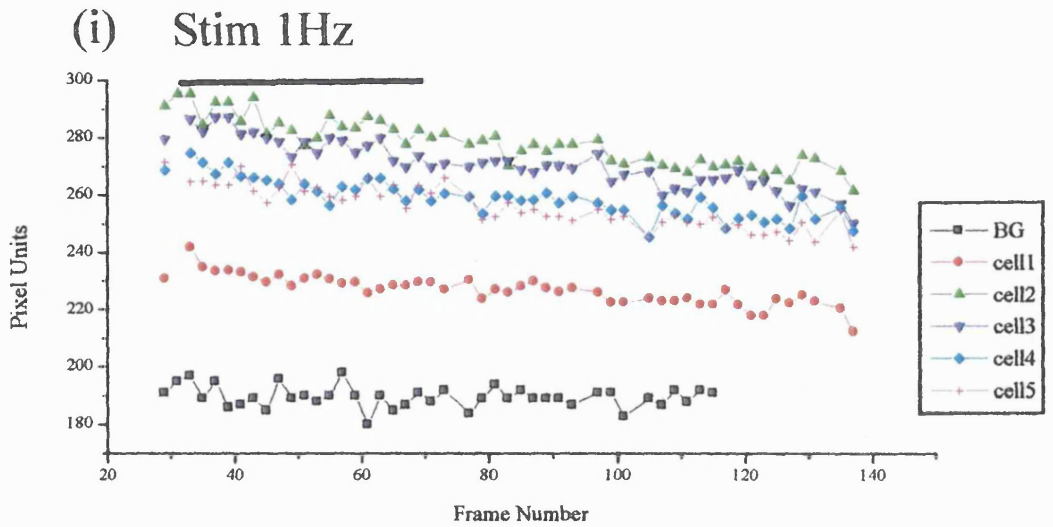
(i)
Stim 1Hz
Pixel Units
Frame Number
BG
cell1
cell2
cell3
cell4
cell5

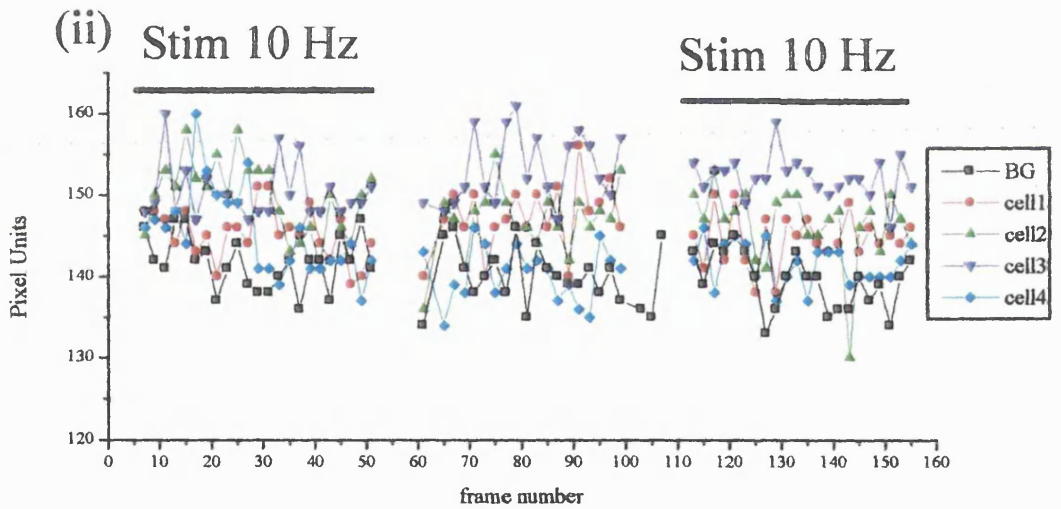
(ii)
Stim 10 Hz
Stim 10 Hz
Pixel Units
frame number
BG
cell1
cell2
cell3
cell4

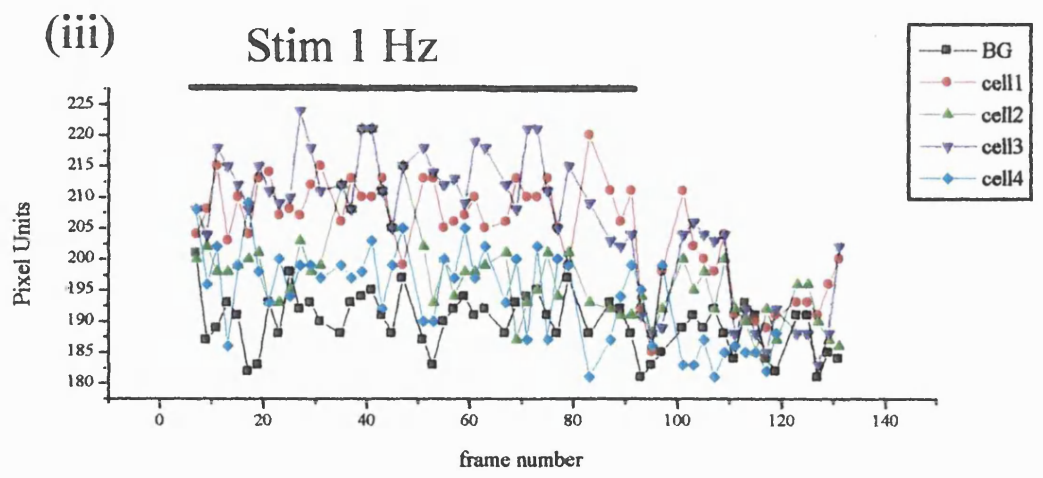
(iii)
Stim 1 Hz
Pixel Units
frame number
BG
cell1
cell2
cell3
cell4

5.3.5 Calcium responses of glia during electrical stimulation of Purkinje cells

As shown in figures 5.3.4, data was measured as line profiles of fluorescence intensity from calcium indicator mapped through several Bergmann glial cells. The timing co-ordination of the experimental protocol made the procedure difficult. The imaging system limited some of the analysis that could be performed and makes data interpretation difficult. The study was therefore preliminary (n=4). From the experiments completed it was difficult to determine any definite patterns of $[Ca^{2+}]i$ responses within Bergmann glial cells during Purkinje cell responses to climbing fibre stimulation.

The few results show that although the low affinity indicator furaptra was useful, in that its fluorescence was high at resting $[Ca^{2+}]i$ levels, its range of sensitivity to $[Ca^{2+}]i$ variation may be too low (Kd=48μM) for the Bergmann glial cells. Higher affinity indicators used were not loaded successfully as AM esters (see section 5.4).

The preliminary results showed that in the soma region the fluorescence fell indicating a rise in Bergmann glial $[Ca^{2+}]i$ levels during Purkinje cell electrical activity (background levels remained constant) {see 5.3.3.C (i), 5.3.4 (iii)}. However this region of somas consisted of many granule cells thus the fluorescent signal may be influenced by neuronal Ca^{2+} activity in these granular cells.

Interestingly the initial response taken along the length of a single Bergmann glial filament indicates that during the first stimulation the $[Ca^{2+}]i$ rises represented by the furaptra fluorescence fall (5.3.3.C (ii) S2 part 1). Unfortunately the same change was measured in the background signal.

In two other examples {5.3.4 (i) (ii)} the fluorescence levels remained unaffected by the Purkinje cell activity. A significant problem with the imaging system was the bleaching of the fluorescent signal. In all results fluorescence intensities fell during the experiment. In order to distinguish the small fine Bergmann glial cells, exposure times were long at 200 milliseconds and bleaching significant.

The gradual decline in the fluorescence signals was not due to increasing calcium concentrations, indicative of cell damage, because during the experiment Purkinje cells continued to respond to climbing fibre stimulation. This maintenance of activity indicates that the slice remained viable.

The *in vitro* studies using furaptra as the indicator showed that astrocytes had maximum peak free $[Ca^{2+}]i$ rises of up to 25μM for $InsP_3$ concentrations between 0.1-25μM. However, in these experiments this low affinity indicator would not detect any changes in free $[Ca^{2+}]i$ levels. Furaptra, with a Kd of 48μM, will not detect changes in $[Ca^{2+}]i$ that are smaller than 0.5μM. It is possible that the electrical activity of Purkinje cells produced by climbing fibre stimulation elicited either no change in free $[Ca^{2+}]i$ within Bergmann glial cells, or rises which were too small to be detected by furaptra. The development changes that have been described for Bergmann glial cells may account for $[Ca^{2+}]i$ changes not being detected. Bergmann glial cells during early development are involved in guiding neural projections as they pass through the molecular layer, and this may express only a low density of $InsP_3$ receptor proteins during this stage. At a later stage of development their physiological role changes, and the level of expression if $InsP_3$ may increase as a consequence.

5.4 Problems associated with this experimental technique

The main difficulty with this technique was co-ordinating all the different aspects of the procedures. The process was made easier by prior planning, having all four electrodes, (bath application of AM indicator electrode, dye removal suction electrode, stimulating micro-pipette and Purkinje whole cell micro-pipette) within the field of view before the experiment began. This was practically difficult as the working distance of the objective is only a couple of millimetres. Once all the background images of the slices were recorded great care had to be taken to ensure that the slice did not move. The slice was continually perfused with an external salt solution so a relatively slow rate was used.

5.4.1 Cell permeant indicators

The entry of the AM form of Ca^{2+} indicators into cells cannot be controlled, therefore the final indicator concentration is unknown. Indicators such as furaptra can become trapped within internal membranes and do not come into contact with esterases, therefore indicators remain in the AM form. The hydrolysis reaction of AM esters generates by-products such as acetate, protons and formaldehyde which could have deleterious effects. For that reason the indicator was usually used in small amounts (1μl). However as the indicators were bath applied to slices the concentration had to be higher (100-200μM). In aqueous solutions AM indicators, due to their lipophilic nature have poor solubility. If the indicator droplets were too large they washed straight over the cells. Bath applying indicators in slices means that they only come briefly into contact with the top layer of cells. Thus it was very important that the indicators were well dispersed in the pluronic, DMSO and external solution mixture.

5.4.2 Combining electrophysiology and fluorescence image data.

There was some difficulty in co-ordinating the electrical data from the Purkinje cells with the fluorescence data from the images. First a control set of images were recorded, with climbing fibre stimulation switched off. Then during a period of electrical activity the image acquisition occurred. This stimulation was stopped and a further cycle of images were recorded as a recovery period. The process of acquiring an image was governed by the computer parameters. Once the experimental protocol was set the computer controlled the camera. There was a time delay between activating the camera via the computer and writing the image. Once the image was recorded into the memory of the computer there was a further time delay. This was due to the processing and display time of the image. As the computer temporary (virtual) memory filled up the process of image acquisition slowed down. As the exact time of image acquisition was in some doubt the data were displayed as consecutive frames.

The T.I.L.L image system was being developed through out these experiments. It was essential to have some way of recording, via an analogue TTL pulse for example, the exact time of the image acquisition. If this was exported as an analogue signal the time patterns could be matched with the electrical data being recorded via the patch clamp amplifier. This was not possible. The imaging system made it difficult to measure exact $[Ca^{2+}]i$ kinetics of the Bergmann glial cells. These preliminary experiments were designed to give information on the trends in Ca^{2+} signalling within Bergmann glial cells during neuronal signalling. The data show that in this study there was no conclusive $[Ca^{2+}]i$ changes in Bergmann glial cells in response to induced electrical activity in Purkinje cells. However, the method has been developed to a point where physiological data can be obtained with a few minor changes of protocol and instrumentation.

5.5 Can the experimental techniques be improved?

5.5.1 Adapting the technique for use with caged neurotransmitters

For the reasons mentioned above some preliminary experiments were performed to see if the system could be adapted to perform flash photolysis experiments with cage photo-labile compounds. The system was calibrated with caged HPTS. The switching monochromator could be set to photolyse the caged compound at 340nm and record at 420nm (for furaptra). Once having loaded the glial cells with the Ca^{2+} indicator a caged neurotransmitter could be bath applied and released by photolysis with the U.V. lamp. However at 200ms exposures at excitation 420nm, the photolysis was already 2.8%. This level is enough to photolyse caged compounds continually during the recording phase. To overcome this the excitation wavelength could be made longer (e.g 440nm) even with furaptra, to reduce background photolysis, similarly a longer wavelength indicator used. The other option is to use a standard flash gun. This however may cause problems. During photolysis a large artefact exits. This would saturate light levels in the camera and so no image would be recorded

5.6 Summary

i) This chapter illustrates that it was possible to selectively load Bergmann glial cells *in situ* with furaptra-AM.

ii) Higher affinity indicators fura-red, fura-2, indo-1 and fluo-3 were used unsuccessfully. The indicators did not readily form emulsions and so penetration into the cells proved difficult.

iii) Stimulated climbing fibres induced epsps in patched Purkinje cells.

iv) The somal $[Ca^{2+}]i$ of furaptra loaded Bergmann glial cells did not change in response to Purkinje cell electrical stimulation.

v) Preliminary studies suggest that $[Ca^{2+}]i$ did not change in the filamentous region of the Bergmann glial cells. However these experiments need to be repeated and extended.

*vi)*Finally the experimental technique was being developed so technical improvements are discussed.

CHAPTER 6

DISCUSSION

6. Characterisation of cerebellar astrocytes and the $InsP_3$ receptor subtype *in vitro* and *in situ*.

6.1 Characterisation of cerebellar astrocytes

Chapter 3 described the immunocytochemical characterisation of cerebellar astrocytes both *in vitro* and in slices, using commercially available antibodies. Astrocytes *in vitro* showed the characteristic morphology of type 1 and 2 cells previously described, with both types being GFAP positive (see figure 3.1.1). Type 1 astrocytes were Gal C negative, A2B5 negative and 04 negative whereas type 2 astrocytes stained positive to A2B5. This confirms earlier characterisation studies (Bignami-A., & Dahl-D., 1974, 1976; Raff *et al* 1978, 1979, 1983a,b). The *in vitro* cerebellar astrocytes studied in this thesis were exclusively of the protoplasmic type 1 form, having a characteristic circular flat shape, with a raised nucleus.

Bergmann radial glial cells in cerebellar slices were GFAP positive and hence astrocytes. These cells had small round cell somas, which sat around Purkinje cell soma, with filaments radiating out to the pial surface. Interestingly these filaments were intertwined with the dendrites of the Purkinje cell, which might suggest a functional relevance to their location. The cerebellar saggital sections used in these studies were taken from rats at P12 stage of development. At this stage, the Purkinje cell dendritic tree is still developing and only occupies half of the molecular layer. Bergmann glial cells however cross the entire molecular layer, ending at the pial surface. This obvious anatomical separation was used to identify Bergmann glial cells unambiguously from Purkinje neurones.

6.1.1 Astrocytic $InsP_3$ receptor subtype

Type 1 astrocytes *in vitro* were shown to express the $InsP_3$ type 3 receptor protein because they stained positive for antibodies specific to the type 3 $InsP_3$ isoform (antibody KM1082, Sugiyama-T. *et al* 1994). However subcellular localisation of this isoform was not possible; the type 3 $InsP_3$ receptor has been proposed to be localised to the plasma membrane (DeLisle-S. *et al* 1996), but this was not evident in the present study. There was a low level of expression of the type 2 isoform (as assessed by the KM1083 antibody, Sugiyama-T. *et al* 1994). There was no immunoreactivity with antibody to the type 1 InsP3 receptor isoform (antibody 40, Dent-M. *et al* 1996) . These receptor isoforms have not been previously described in type 1 astrocytes *in vitro*. The $InsP_3$ receptor tetramer can exist as either a homotetramer (Mignery-G. *et al* 1989) or as a heteromultimeric complex of one or more of the three receptor subunit isoforms (Monkawa-T. *et al* 1995). It is possible, therefore, that the astrocytic isoform *in vitro* may exist as a heterotetramer composed of both type 2 and other subunit isoforms. Single cell reverse transcription polymerase chain reaction (RT-PCR) could be used to isolate mRNA message from astrocytes and hence determine the precise isoform present.

Experiments using P12 Wistar rat cerebellar saggital sections showed no detectable amounts of $InsP_3$ receptor type 1, 2 or 3 in Bergmann glial cells. However protoplasmic astrocytes located in the granular cell layer stained positive for the type 3 isoform. These results differ from a previous immunohistochemical study with the same antibody which demonstrated that Bergmann glial cells and protoplasmic astrocytes *in situ* only expressed the $InsP_3$ receptor isoform type 3 (Yamamoto-Hino-M. *et al* 1995). An important difference between the two studies is the age of the tissue used, with the latter study being performed on Wistar rat 8 weeks old. Bergmann glial cells undergo morphological changes, with filaments thickening and developing arborizations. It is possible that, as the function of glial cells changes from aiding neural development to being involved in cell signalling, there may be alterations in the levels of expression of the various $InsP_3$ receptors.

6.2 Kinetic studies of the $InsP_3$ evoked $[Ca^{2+}]i$ rise in astrocytes.

The results of chapter 4 demonstrate, for the first time, that release of $InsP_3$ (at concentrations between 0.1-25μM) can produce a rise in intracellular calcium in cerebellar astrocytes. These experiments were performed using a low affinity indicator (furaptra) to preserve kinetic information, with recordings being made from cerebellar astrocytes both *in vitro* and *in situ*. The $InsP_3$ evoked $[Ca^{2+}]i$ response comprised an initial delay, a fast rise in free $[Ca^{2+}]i$ due to $InsP_3$ evoked flux which reached a peak, where net flux is zero, and a slow decline to baseline. $InsP_3$ evoked $[Ca^{2+}]$ rises were quantified as the rate of change of free $[Ca^{2+}]i$ ($d[Ca^{2+}]i/dt$) in units of mole/litre of cytosol/second ($\mu M.s^{-1}$). The maximum rates of change of free $[Ca^{2+}]i$, and peak free $[Ca^{2+}]i$ in cultured astrocytes were $60\mu M.s^{-1}$ and 25μM respectively. A wide degree of cell to cell variability was evident at all $InsP_3$ concentrations, and within each cell it was not possible to normalise the results to a standard concentration. As discussed previously (see chapter 4) this variability could be due to different $InsP_3$ receptor density, different rates of endogenous Ca^{2+} buffering, or heterogeneity in $InsP_3$ receptor channel properties and subunit composition.

6.2.1 Delay between $InsP_3$ release and $[Ca^{2+}]i$ rise

The mean initial delay for type 1 astrocytes *in vitro* was 267±66ms at low concentrations (0.1-1μM), being decreased with increasing $InsP_3$ (10-25μM) concentrations to 111±15ms. The time delays for $InsP_3$ induced Ca^{2+} responses are about 200ms-30ms (for 0.1-10μM $InsP_3$ concentration) in hepatocytes (Ogden-D.C. & Capiod-T. 1997), and 430ms-30ms in endothelial cells (0.2-5μM $InsP_3$ concentration; Carter-T.D. & Ogden-D.C. 1997). These delays correspond well with those seen for cerebellar astrocytes (267-111ms for $InsP_3$ concentration 0.1-25μM). In contrast, Purkinje cells have much shorter delay times (85-<20ms for $InsP_3$ concentration 9-80μM; Khodakhah-K. & Ogden-D.C. 1995). Note that in Purkinje cells the concentrations of $InsP_3$ are much higher than the non-excitable cells (see below). In all

these studies, the time delay was dependent upon $InsP_3$ concentration such that delays were longer for lower $InsP_3$ concentrations.

The initial delay to the $InsP_3$ evoked $[Ca^{2+}]i$ rises could be due to either $InsP_3$ or calcium cooperativity in binding at their binding sites on the receptor. The structure of the $InsP_3$ receptor was characterised as being a tetramer, with a $InsP_3$ binding site on each subunit (Maeda-N. *et al* 1991), which would suggest that four $InsP_3$ molecules may be required for $InsP_3$ receptor activation. Previous studies in rat basophilic leukemia (RBL) cells (Meyer-T. *et al* 1988) and porcine endothelial cells (Carter-T., & Ogden-D.C., 1997) have demonstrated that 4 $InsP_3$ molecules were, in fact, required to activate the receptor, producing a conformational change in the protein to open the calcium channel. Thus $InsP_3$ cooperativity could account for the initial time delay at lower $InsP_3$ concentrations.

Cooperativity between $InsP_3$ and cytosolic calcium ions in binding to and activating the $InsP_3$ receptor protein, may cause a delay between the release of $InsP_3$ and the $InsP_3$ induced $[Ca^{2+}]i$ change. Calcium has been shown to promote $InsP_3$ binding to its receptor and subsequent activation (Iino-M. 1990; Bezprozvanny-I. *et al* 1991 ; Finch-E.A. *et al* 1991; Cardy-T.J.A. *et al* 1997; Yoneshima-H. *et al* 1997). A prior elevation of $[Ca^{2+}]i$ by hyperpolarisation abolished the delay of $[Ca^{2+}]i$ rise induced by low $InsP_3$ concentrations in hepatocytes (Ogden-D.C. & Capiod-T. 1997). However, in endothelial cells a prior calcium elevation only reduced the delay of $[Ca^{2+}]i$ rise by 30% (Carter-T.D. & Ogden-D.C. 1997). These results were interpreted in terms of a localised increase in $[Ca^{2+}]i$ around the calcium stores and $InsP_3$ receptors, with the $InsP_3$ receptor appearing to be primed by an increase in $[Ca^{2+}]i$, which caused $InsP_3$ to bind more efficiently to the receptor protein. Although this experiment was not performed in astrocytes, the resting glial cell $[Ca^{2+}]i$ of 100nm is within the concentration range reported to affect $InsP_3$ binding (see below).

6.2.2 Rates of rise and peak free $[Ca^{2+}]i$

There is a wide variation of the maximum $d[Ca^{2+}]i/dt$ and the maximal free peak $[Ca^{2+}]i$ evoked by $InsP_3$ in different cell types, especially between neuronal and astrocytic

calcium flux rates. For example, Purkinje cells have high maximum values for peak $[Ca^{2+}]i$ (80μM) with high flux rates (1400 $\mu M.s^{-1}$; Khodakhah-K. & Ogden-D.C. 1995); similarly, endothelial cells have high maximum values for peak $[Ca^{2+}]i$ (30μM) and flux rate (918$\mu M.s^{-1}$; Carter-T.& Ogden-D.C. 1997). In contrast to these high values, astrocytes have a maximal peak free $[Ca^{2+}]i$ of 25μM and maximal $d[Ca^{2+}]i/dt$ of 60$\mu M.s^{-1}$ values which are similar to those for hepatocytes, being 9.5μM and 52$\mu M.s^{-1}$ respectively (Ogden-D.C. & Capiod-T. 1997). One possible explanation for this difference is that the peak $[Ca^{2+}]i$ and flux rate are dependent upon the density of $InsP_3$ receptors. The $d[Ca^{2+}]i/dt$ would thus depend both on the flux of calcium into unit cytosolic volume (moles. $s^{-1}.liter^{-1}$) and on the proportion of calcium bound to buffers. To take the simplest case, if unitary calcium flux of each open $InsP_3$ gated channel was similar, then the size of $d[Ca^{2+}]i/dt$ would be dependent upon channel density per unit volume and its open probability (Bezprozvanny-I. *et al* 1991).

The data presented in chapter 3 demonstrated that the predominant isoform of $InsP_3$ receptor in astrocytes was type 3, whereas in Purkinje cells it is the type 1 isoform (Miyawaki-A. *et al* 1990). Interestingly, hepatocytes and endothelial cells express types 1 and 2 (De Smedt *et al* 1994 and Carter-T., unpublished), but have differing kinetic parameters. This provides evidence that channel density may account (in part) for the differences in the peak free $[Ca^{2+}]i$ and rate of flux. The density of the $InsP_3$ receptors in astrocytes is not known, but is clearly lower than that seen in Purkinje cells. The large cell to cell variability in the values of peak free $[Ca^{2+}]i$ and $d[Ca^{2+}]i/dt$ evident in each of these tissue types is probably due to differences in channel density. Alternatively the variations in kinetics may be due to the $InsP_3$ isoforms having different binding affinities and properties. For example, Purkinje cells have type 1 receptor protein, which are less sensitive to $InsP_3$ concentrations at resting $[Ca^{2+}]i$ compared to type 3 receptors, at least in microsomal experiments (Cardy-T.J.A. *et al* 1997; Yoneshima-H. *et al* 1997). For example, the Kd of the type 1 $InsP_3$ receptor protein for $InsP_3$ is 78.5nM at 3nM free calcium but 312nM with 1.4μM free calcium (Yoneshima-H. *et al* 1997).

The $d[Ca^{2+}]i/dt$ and peak free $[Ca^{2+}]i$ rise in astrocytes did not seem to be dependent on the $InsP_3$ concentration, at least in the range 0.1-25μM in separate cells (see chapter 4 section 4.1.2 and 4.1.3), in contrast to other cell types similarly studied. One possible explanation for this apparent lack of concentration-dependence in individual

cells is that these concentrations of $InsP_3$ are at the lower end of the $InsP_3$ concentration-dependence. This is unlikely as basal concentrations of $InsP_3$ are thought to be 0.1-3μM, rising to 20μM with agonist stimulation (Putney-J. 1990). Alternatively, astrocytic $InsP_3$ receptors may be highly sensitive to $InsP_3$, such that the concentrations used in this study were already maximal. Recent studies of the binding of ^{3}H-$InsP_3$ to type 3 $InsP_3$ receptor protein in microsomal preparations indicated that, at low calcium concentrations (3nM) the Kd was 116nM, whereas at higher calcium concentrations (1.4μM) the Kd had changed to 62.2nM (Yoneshima-H. *et al* 1997). Thus the affinity of the type 3 $InsP_3$ receptor protein to $InsP_3$ may be regulated by $[Ca^{2+}]$, at least in these biochemical studies. If the resting calcium levels in glial cells were low, then the sensitivity of the $InsP_3$ receptors would be reduced. However, the shift in the affinity of the receptor is not great enough to explain the lack of concentration-dependence seen in this study. Direct comparison of data obtained from biochemical measurements from microsomal preparations and that from photometric studies of astrocytes is problematic, especially as the experimental conditions are so different.

6.2.3 Termination rates

It was evident that if the flux rate ($d[Ca^{2+}]i/dt$) was high, then the duration of the fast $InsP_3$ evoked calcium rising phase was short (see chapter 4, section 4.2). The rate of termination of calcium efflux from the $InsP_3$ sensitive store was defined as the reciprocal of the 10-90% rise time and was plotted against the $d[Ca^{2+}]i/dt$. A correlation between these two parameters have been seen in other cell types; for example Purkinje cells have the highest range $d[Ca^{2+}]i/dt$ upto 1400 $\mu M.s^{-1}$ but the shortest rise times (10-20ms) of all cell types examined. A linear relationship between $d[Ca^{2+}]i/dt$ and termination rate ($duration^{-1}$, figure 4.2.1) exist for Purkinje cells, hepatocytes (Ogden-D.C & Capiod-T 1997), and endothelial cells (Carter-T.D. & Ogden-D.C 1997). A linear correlation was also seen for astrocytic responses, similar to the other cell types ($r=0.88$ compared to $r=0.91$) but was less well defined. As described in chapter 4 section 4.2.1, the data obtained from astrocytes lies on the same line as that from other cell types. However, Purkinje cells have a high channel density and hence, a large $d[Ca^{2+}]i/dt$ and more rapid

termination, whereas astrocytes, with a lower channel density, have slower termination rates, being similar to other non excitable cells.

There are a number of possible mechanisms underlying the termination of efflux from $InsP_3$-sensitive stores, including inactivation of the $InsP_3$ receptor by calcium, $InsP_3$ metabolism, or store depletion. Termination rates appear to be affected by the appearance of raised free cytosolic $[Ca^{2+}]i$. A prior elevation of $[Ca^{2+}]i$ in Purkinje cells (Khodakhah-K., & Ogden-D.C., 1995) hepatocytes (Ogden-D.C & Capiod-T. 1997) and endothelial cells (Carter-T., & Ogden-D.C., 1997) can reduce the $InsP_3$ evoked efflux, suggesting that calcium is involved in the termination of the response. This experiment was not tested on astrocytes. It is noteworthy that Purkinje cells, which have the shortest duration of response, have high calcium buffering capacity, compared to non excitable cells (2000; Fierro-L. & Llano-I. 1996, compared to approximately 100:1 in other cells; Neher-E. 1995). This supports the idea that it is the free cytosolic $[Ca^{2+}]i$, rather than total calcium flux, which is important in inhibiting the $InsP_3$ receptor. The free $[Ca^{2+}]i$ close to the open channels will be related to the calcium flux through the pore, and will rise very quickly in this region (within 10ms at 0.5μm from the pore; Stern-M.D., 1992; Roberts-W.M., 1994). The linear relationship for termination would be due to a first order reaction mechanism for inactivation of the $InsP_3$ receptor protein by binding calcium.

The termination of the $InsP_3$ evoked calcium rise could be explained by the metabolism of $InsP_3$ to $InsP_2$ by $InsP_3$ 5-phosphatase. However, as shown by the data in figure 4.2.3 in chapter 4, the calcium response evoked by a non-hydrolysable $InsP_3$ analogue, 5-thio-$InsP_3$, still terminated. Thus, even though the cytosolic $InsP_3$ concentration remains constant, the efflux of calcium from the store declines. Similar results using non-hydrolysable $InsP_3$ analogues have been previously reported (Khodakhah-K. & Ogden-D.C., 1995; Wootton-J.F. *et al* 1995; Ogden-D. & Capiod-T. 1997; Carter-T. & Ogden-D.C., 1997). Therefore termination of the $InsP_3$ evoked calcium rise is not due to $InsP_3$ metabolism.

If the termination of the efflux were be due to store depletion, a second photolytic release of $InsP_3$, given before the stores would have time to refill, would not be expected to elicit any further calcium efflux. Although not tested in this thesis, consecutive pulses of a low concentration of $InsP_3$, (with the second being given at the

peak of the response to the first) did not show a further increase in rate of change of free $[Ca^{2+}]i$ in endothelial cells (Carter-T.D. & Ogden-D. 1997) and hepatocytes (Ogden-D. & Capiod-T. 1997; Ogden-D.C. *et al* 1990). The finding that peak free was greater at high than at low $InsP_3$ concentrations in the same astrocyte (figure 4.1.4) implies that termination of efflux still occurred at low concentrations that did not deplete the store.

6.3 $InsP_3$ induced $[Ca^{2+}]i$ rises in astrocytes *in vitro* as a result of agonist activation

It has been hypothesised from studies *in vitro* that astrocytes of the CNS may communicate via an intracellular calcium signalling mechanism (Charles-A.C. *et al* 1993). Periodic "spiking" of intracellular free $[Ca^{2+}]$ have been seen in many other types of non-excitatory cells from peripheral systems and vascular tissues in response to hormone, neurotransmitter and mechanical stimulation. Cells such as hepatocytes (Capiod-T. & Ogden-D.C. 1989; Field-A.C. & Jenkinson-D.H. 1987; Woods-N.M. *et al* 1986), endothelial (Carter-T.D. *et al* 1991; Jacob-R. 1990), pancreatic acinar cells (Gray-P.T.A. 1988), ciliated tracheal epithelial cells (Sanderson-M.J. *et al* 1990) all respond by an elevation in $[Ca^{2+}]i$ as a result of $InsP_3$ release (Berridge-MJ 1993). The $[Ca^{2+}]i$ rise travels through adjacent cells at wave velocities between 5-200$\mu m.s^{-1}$ (Finkbeiner-S 1992). Cultured cerebellar type 1 astrocytes (3-7 DIV) displayed no $[Ca^{2+}]i$ oscillatory pattern, when recorded by patching single cells (chapter 4). However, in experiments where astrocytes were loaded by preincubation with the AM ester form indicator, propagating $[Ca^{2+}]i$ waves were detected in response to bath applied agonists. For example, in response to 100μM ATP type 1 astrocytes responded with synchronised calcium waves (15s peak intervals), which appeared to spread to adjacent cells (chapter 4 figure 4.4.2 part II). The most likely explanation for oscillatory behaviour not being seen in patched cells is probably due to loss of essential constituents, which were diluted out of the cell during exchange of the cytosol with the pipette solution.

It has been proposed that it is the $[Ca^{2+}]i$ spike frequency that controls the specificity of the induced signal (Andrea-P., & Grohovaz-F., 1995; Pasti-L. *et al* 1995: Pasti-L. *et al* 1997), and that $InsP_3$ receptors may be involved in controlling this rate.

Hence understanding the properties of the astrocytic $InsP_3$ receptor will provide information on the underlying mechanisms of calcium signalling. The time taken for the $InsP_3$ receptor to recover from calcium inhibition has been postulated to regulate the frequency of $[Ca^{2+}]i$ waves. For example, the half time for recovery of $InsP_3$ induced $[Ca^{2+}]i$ rises in hepatocytes and endothelial cells was 10-25s, with full response recovery at 60-120s (Carter-T.D. & Ogden-D. 1997; Ogden-D. & Capiod-T. 1997; Ogden-D.C. *et al* 1990). These time scales are similar to the $[Ca^{2+}]i$ spikes (peak intervals 15s) that have been described in the type 1 cerebellar astrocytes *in vitro* in response to ATP in chapter 4 section 4.4.1. However the studies in chapter 4 were preliminary and require more investigation.

6.3.1 How do $InsP_3$ evoked Ca^{2+} rises propagate to adjacent cells *in vitro*?

How do the $InsP_3$ evoked $[Ca^{2+}]i$ rises travel to adjacent cells in un-patched astrocytes? The $[Ca^{2+}]i$ communication system is thought to depend on gap junctions (Charles-A.C. *et al* 1993; Dermietzel-R. *et al* 1991; Finkbeiner-S. 1992; Venance-L. *et al* 1991). The gap junctions allow small molecules to diffuse readily from one cell to another throughout the glial syncitium. It is has been suggested that the second messengers $InsP_3$ and calcium are involved in initiating and mediating the $[Ca^{2+}]i$ wave in non-excitable cells (Berridge-M.J. 1993; Charles-A.C. *et al* 1993). In endothelial cells, which express gap junctions consisting of connexin 43, caged $InsP_3$ can diffuse across many cells within a confluent monolayer *in vitro* (Carter-T.D. *et al* 1996). The preliminary studies in chapter 4 section 4.3 suggested that is possible for caged $InsP_3$ to diffuse through astrocytic gap junctions (connexin 43). Thus $InsP_3$ molecules could act as diffusible second messenger agents in intercellular astrocytic calcium signalling. Although these experiments demonstrated that it was possible for the larger caged $InsP_3$ molecules to diffuse from one cell to another, some points should be noted. Gap junction selectivity is governed by molecule size, net charge and chemical structure (Elfgang-C. *et al* 1995). Caged $InsP_3$ is slightly larger than free $InsP_3$. Caged $InsP_3$ has a M_r of 635Da with a valency of 5^-, compared to free $InsP_3$ which has a M_r of 437Da and valency 6^-. The difference in size is due to the presence of the nitrophenyl group at the 5

phosphate site which constitutes the "cage". These factors have to be considered when making comparisons with free $InsP_3$ (Carter-T.D. *et al* 1996). The delay of initiation of $[Ca^{2+}]i$ rises seen in distant endothelial cells (i.e distant from the site of caged $InsP_3$ application) were too short to be accounted for by calcium diffusion (Allbritton-N.L. *et al* 1992). It was difficult to measure the delay of $[Ca^{2+}]i$ rises seen in patched paired astrocytes due to the phosphorescence artefact arising from the glass coverslips.

6.4 Investigating $InsP_3$ evoked $[Ca^{2+}]i$ signalling in astrocytes in situ

6.4.1 Studies of Bergmann glial $[Ca^{2+}]i$ rises in acute cerebellar slices.

The *in situ* experiments in this study examined the $InsP_3$ evoked $[Ca^{2+}]i$ rise in Bergmann glial cells for direct comparison to the *in vitro* single cell studies. The flash photolysis and microspectrofluorimetry experiments *in situ* of chapter 4 section 4.5 were preliminary. However early indications are that kinetic information gained from Bergmann glial cell responses to $InsP_3$ release *in situ* are similar to other non excitable cells *in vitro*. There was not enough data to determine the effects of varying $InsP_3$ concentrations on peak free $[Ca^{2+}]i$ or calcium flux rates. The few observations obtained suggest that flux rates are faster, and flux duration shorter compared to astrocytes in *in vitro* studies. More data is needed before any major conclusions are drawn.

In chapter 5 some attempt was made to measure the changes in $[Ca^{2+}]i$ of Bergmann glial cells *in situ* whilst electrically activating climbing fibres to stimulate surrounding Purkinje cells and their vast dendritic trees. A new method was developed to ensure that the $[Ca^{2+}]i$ changes could be recorded in many astrocytes *in situ* in saggital cerebellar slices. At the initial stage it was difficult to know exactly where along the Bergmann glial cell $[Ca^{2+}]i$ rises would occur. No $[Ca^{2+}]i$ changes were detected from the furaptra loaded Bergmann glial cells whilst stimulating Purkinje cells at physiological frequencies (1-10Hz for 25-100s). The fluorescence was measured along different sections of the Bergmann glial cells. The fluorescent signal in all experiments decreased due to bleaching. It is unlikely that the decay in fluorescence was due to an overall increase in free cytosolic $[Ca^{2+}]$ as continual electrical activity within the Purkinje cells

indicated that the slice tissue was viable. A possible explanation for the lack of detection of calcium rises was that a low affinity calcium indicator (furaptra) was used, which would not detect changes of less than 0.5μM above resting levels.

Furaptra was chosen an the calcium indicator in order to visualise cells at the start of the experiment, when the indicator would be bright at resting $[Ca^{2+}]i$ levels, and hence permit cell identification. Fura-2 would also have been suitable but was not taken up into the cells well in these experiments. Bergmann glial cells are small and so generate small fluorescent signals. The $[Ca^{2+}]i$ measurements may be improved by using a higher affinity indicator, which is bright at resting $[Ca^{2+}]i$ levels and capable of detecting smaller $[Ca^{2+}]i$ rises, e.g. Fura-2 Kd=200nM, Calcium green-1 Kd=390nM, or Oregan green-1 BAPTA-1 488 Kd=170nM.

The results presented in chapter 5 suggest that during physiological levels of Purkinje cell activity, any calcium changes in Bergmann glial cells are not detected by the low affinity indicator furaptra. Data from chapter 4 demonstrated that photolytic release of $InsP_3$ could elicit changes in free $[Ca^{2+}]i$ of up to 25μM. Thus, either these rises do not reflect those seen with physiological stimuli, or the magnitudes of calcium rises seen *in vitro* are artefactually high, possibly due to the limitations of the patch clamp technique. Other points to be considered are that the slices were taken from P12 rats, when Bergmann glial cells are undergoing morphological changes. It is possible that at this stage of development the Bergmann glial cells lack significant amounts of $InsP_3$ receptor proteins, as shown in chapter 3 section 3.5.4. Finally, the large changes in free cytosolic $[Ca^{2+}]i$ may only occur under extreme conditions, suggesting a neuroprotective role for Bergmann glial cells in vivo.

The advantage of selectively AM-loading Bergmann glial cells is that many cells can be visualised at once in a slice. Once identified, a cell could be patched and electrophysiological studies performed. In addition, caged neurotransmitters could be bath applied, with subsequent photolytic release, to further investigate $[Ca^{2+}]i$ signalling simultaneously in several Bergmann glial cells.

6.5 Conclusions

This thesis has described an investigation of $InsP_3$ evoked $[Ca^{2+}]i$ signalling in cerebellar astrocytes *in vitro* and *in situ*, by flash photolysis, microspectrofluorimetry and immunocytochemistry. Chapter 3 shows that cerebellar type 1 astrocytes *in vitro* and protoplasmic astrocytes *in situ*, located in the granular layer of cerebellar slices, express the type 3 $InsP_3$ receptor protein. The immunocytochemical studies also showed a low level expression of the type 2 receptor isoform but no type 1 $InsP_3$ receptor protein could be detected *in vitro*. Chapter 3 also shows that astrocytes *in vitro* possess connexin 43 which presumably constitute gap junctions.

The kinetic properties of astrocytic $InsP_3$ evoked $[Ca^{2+}]i$ changes described in chapter 4 are similar to those for $InsP_3$ receptor signalling in non excitable cells such as hepatocytes and endothelial cells, but unlike the changes seen in Purkinje neurones. However the magnitudes of astrocytic $InsP_3$ evoked $[Ca^{2+}]i$ fluxes and peak free $[Ca^{2+}]i$ did not depend on $InsP_3$ concentration in separate cells, unlike the responses in other tissues studied previously. The mechanism underlying termination of the $InsP_3$ induced $[Ca^{2+}]i$ rise was discussed in terms of calcium inactivation of the $InsP_3$ receptor, rather than store depletion or $InsP_3$ metabolism.

The demonstration that caged $InsP_3$ can diffuse between astrocytes coupled by gap junctions (also from chapter 4) suggests that $InsP_3$ may be important in intercellular signalling and propagating calcium waves. ATP and glutamate could evoke rises in astrocytic intracellular $[Ca^{2+}]$ *in vitro*. However propagating synchronised calcium waves could only be detected in AM loaded astrocytes, but not in whole cell voltage clamped cells.

Chapter 5 showed that no large changes in Bergmann glial cell $[Ca^{2+}]i$ were detected (under these experimental conditions) in response to physiological frequencies of climbing fibre stimulation of Purkinje cells. This observation would imply that if Bergmann glial cells do respond to Purkinje cell activity with a rise in $[Ca^{2+}]i$, this change must be small, at least at this stage of development.

CHAPTER 7

REFERENCES

AIRAKSINEN-MS; EILERS-J; GARASCHUK-O; THOENEN-H; KONNERTH-A; MEYER-M (1997) : Ataxia and altered dendritic calcium signalling in mice carrying a targeted null mutation of the calbindin D28k gene. : *Proceedings National Academy Science U S A* **94**: 1488-93

AITKEN, P. G., BREESE, G.R., DUDEK, F. F., EDWARDS, F., ESPANOL M.T., LARKMAN P.M., LIPTON P., NEWMAN G.C., NOWAK T.S., PANIZZON K.L., RALEY-SUSMAN, K.M., REID K.H., RICE, M.E., SARVEY J.M., SCHOEPP D.D., SEGAL M., TAYLOR, C.P., TEYLOR, T.J., VOULALAS. (1995) Preparative methods for brain slices: a discussion. *Journal of Neuroscience Methods* **59**: 139-149

AKOPIAN-G., KRESSIN-K., DEROUICHE-A., STEINHAUSER-C. (1996) Identified glial cells in the early postnatal mouse hippocampus display different types of Ca^{2+} currents. *Glia* **17**: 181-194

ALLBRITTON-N.L., MEYER-T., AND STRYER-L. (1992) Range of messenger action of calcium and inositol 1,4,5-trisphosphate. *Science* **258**: 1812-1815

ANDREA-P; GROHOVAZ-F (1995) : $[Ca^{2+}]i$ oscillations in rat chromaffin cells: frequency and amplitude modulation by Ca^{2+} and $InsP_3$. : *Cell Calcium* **17**: 367-74

BADING-H., GINTY-D.D., AND GREENBERG-M.E. (1993) Regulation of gene expression in hippocampal neurons by distinct calcium signalling pathways. *Science* **260**: 181-186

BAIMBRIDGE-K. G., CELIO-M.R., AND ROGERS-J.H. (1992) Calcium binding proteins in the nervous system. *Trends in Neuroscience* **15**: 303-308

BARRES-B.A. (1991) New roles for glia. *Journal of Neuroscience* **11**: 3685-3694

BARRES-B.A., CHUN-L.L.Y., AND COREY-D.P. (1989) Calcium currents in cortical astrocytes : induction by cAMP and neurotransmitters and permissive effect of serum factors. *Journal of Neuroscience* **9**: 3169-3175

BATTY-I.R., NAHORSKI-S.R., AND IRVINE-R.F. (1985) Rapid formation of inositol 1,3,4,5-tetrakisphosphate following muscarinic receptor stimulation of rat cerebral cortical slices. *Biochemical Journal* **232**: 211-215

BECKER, D. L., EVANS, W.H., GREEN, G., AND WARNER, A.,. (1995) : Functional analysis of amino acid sequences in Connexin 43 involved in intercellular communications through gap junctions. *: Journal of cell science* **108**: 1455-1467

BENNETT-M. V. L., BARRIO-L. C., BARGIELLO-T.A., SPRAY-D.C., HERTZBERG-E., AND SAEZ-PJ.C. (1991) Gap junctions : new tools, new answers new questions. *Neuron* **6**: 305-320

BERL-S., LAJTHA-A., WAELSCH-H. (1961) Amino acid and protein metabolism-IV cerebral compartments of glutamic acid metabolism. *Journal of Neurochemistry* **7**: 186-197

BERNSTEIN-M., LYONS-S.A., MOLLER-T., KETTENMANN-H. (1996) : Receptor-mediated calcium signalling in glial cells from mouse corpus callosum slices. *: Journal of Neuroscience Research* **46**: 152-163

BERRIDGE-M.J., IRVINE-R.F. (1989) Inositol phosphate and cell signalling. *Nature* **341**: 197-205

BERRIDGE-MJ. (1993) : Inositol trisphosphate and calcium signalling. *: Nature* **361**: 315-25

BEVAN-S., CHIU-S. Y., GRAY-P.T.A., RITCHIE-J.M. (1985) The presence of voltage-gated sodium, potassium and chloride channels in rat cultured astrocytes. *Proceedings of Royal Society London* **225**: 299-313

BEZPROZVANNY-I., EHRLICH-B. (1994) Inositol 1,4,5-trisphosphate gated Ca^{2+} channels from cerebellum: conductance properties for divalent cations and regulation by intraluminal calcium. *Journal of General Physiology* **104**: 821-856

BEZPROZVANNY-I., WATRAS-J., AND EHRLICH-B.E. (1991) Bell shaped calcium response curves of Ins(1,4,5) P3-gated and calcium-gated-channels from endoplasmic reticulum of cerebellum. *Nature (London)* **351**: 751-754

BIGNAMI, A., AND DAHL, D.,. (1974) Astrocyte-specific protein and neuroglial differentiation: An immunofluorescence study with antibodies to the glial fibrillary acidic protein. *Journal of Comparative neurology* **153**: 27-38

BIGNAMI-A., DAHL-D. (1976) The astroglial response to stabbing. Immunofluorescence study with antibodies to the glial fibrillary acidic protein. *Journal of comparative Neurology* **153**: 27-38

BIGNAMI-A., ENG-L.F., DAHL-D., AND UYEDA-C.T. (1972) Localisation of the glial fibrillary acidic protein in astrocytes by immunofluorescence. *Brain Research* **43:**: 429-435

CAJAL-R. Y. (1937) :Recollections of my life. *MIT Press, Cambridge Masachusetts*

CAPIOD-T., FIELD-A.C., OGDEN-D.C., SANDFORD-C.A. (1987) Internal perfusion of guinea-pig hepatocytes with buffered Ca^{2+} or inositol 1,4,5-trisphosphate mimics noradrenaline activation of K^+ and Cl^- conductances. *FEBS Letters* **217**: 247-252

CAPIOD-T., OGDEN-D.C. (1989) Properties of membrane ion conductances evoked by hormonal stimulation of guinea pig and rabbit isolated hepatocytes. *Proceedings of the Royal Society of London* **236**: 187-201

CARTER-T.D., BOGLE-R.G., AND BJAALAND-T. (1991) Spiking of intracellular calcium ion concentration in single porcine cultured endothelial cells stimulated with ATP or bradykinin. *Biochemical Journal* **278**: 697-704

CARTER-T.D., CHEN-X.Y., CARLILE-G., KALALPOTHAKIS-E., OGDEN-D.C., EVANS-W.H. (1996) Porcine aortic endothelial gap junctions: identification and permeation by caged $InsP_3$. *Journal of Cell Science* **109**: 1765-1773

CARTER-T.D., OGDEN-D. (1997) Kinetics of Ca^{2+} release by $InsP_3$ in pig single aortic endothelial cells: evidence for an inhibitory role of cytosolic Ca^{2+} in regulating hormonally evoked Ca^{2+} spikes. *Journal of Physiology* **504**: 17-33

CATALDO-A.M., BROADWELL-R.D. (1986a) Cytochemical identification of cerebral glycogen and glucose-6-phosphatase activity under normal and experimental conditions:Neurons and glia. *Journal of Electron Microscope Technology* **3**: 413-437

CHARLES-A.C., DIRKSEN-E.R., MERRILL-J.E., AND SANDERSON-M.J. (1993) Mechanisms of Intercellular calcium signalling in glial cells studied with Dantrolene and Thapsigargin. *Glia* **7**: 134-145

CHARLES-A.C., MERRILL-J.E., DIRKSEN-E.R., AND SANDERSON-M.J. (1991) Intercellular signalling in glial cells: calcium waves and oscillations in response to mechanical stimulation and glutamate. *Neuron* **6**: 983-992

CHIU-S.Y., SHRAGER-P., RITCHIE-J.M. (1984) Neuronal type Na^+ and K^+ channels in rabbit cultured Schwann cells. *Nature* **311**: 156-157

CLAPHAM-D.E. (1995) : Calcium signalling. *: Cell* **80**: 259-268

CLARK-B. A., BORBOUR-B. (1997) Currents evoked in Bergmann glial cells by parallel fibre stimulation in rat cerebellar slices. *Journal of Physiology* **502**: 335-350

COMBETTES-L., HANNAERT-MERAH-Z., COQUIL-J.F., ROUSSEAU-C., CLARET-M., SWILLENS-S., CHAMPEIL-P. (1994) Rapid filtration studies of the effect of cytosolic Ca^{2+} on inositol trisphosphate induced $^{45}Ca^{2+}$ release from cerebellar microsomes. *Journal of Biological Chemistry* **269**: 17561-17571

CORNELL-BELL-A. H., FINKBEINER-S. M., COOPER-M.S., SMITH-S.J. (1990) Glutamate induces calcium waves in cultured astrocytes: Long-range glial signalling. *Science* **247**: 470-473

DANI-JW, C.-A., & SMITH-SJ.,. (1992) Neuronal Activity triggers calcium waves in hippocampal astrocyte network. *Neuron* **8**: 1-20

DE BLAS-A.L. (1984) Monoclonal antibodies to specific astroglial and neuronal antigens reveal the cytoarchitecture of the Bergmann glial fibres in the cerebellum. *Journal of Neuroscience* **4**: 265-273

DE LA MONTE-S.M., HO-D.D., SCHOOLEY-R.T., HIRSCH-M.S., RICHARDSON-E.P. (1987) Sudacute enecephalomyelitis of AIDS and its relation to HTLV-III infection. *Neurology* **37**: 562-569

DENT-M.R., RAISMAN-G., LAI-F.A. (1996) : Expression of type1 inositol 1,4,5-trisphosphate receptor during axogenesis and synaptic contact in the central and peripheral system of developing rat. *: Development* **122**: 1029-1039

DERMIETZEL-R., SPRAY-D.C. (1993) Gap junctions in the brain: where, what type how many and why? *Trends in Neuroscience* **16**: 186-192

DERMIETZEL-R., HERTZBERG-E. L., KESSLER-J.A., AND SPRAY-D.C. (1991) Gap junctions between cultured astrocytes: immunocytochemical, molecular, and electrophysiological analysis. *Journal of Neuroscience* **11**: 1421-1432

DEROUICHE-A., RAUEN-T. (1995) Coincidence of L-glutamate/L-aspartate transporter (GLAST) and glutamine synthetase (GS) immunoreactions in retinal glial: evidence for coupling of GLAST and GS in transmitter clearance. *Journal of Neuroscience research* **42**: 131-143

DESMEDT, H., MISSIAEN, L., PARYS,J.B., BOOTMAN,M.D., MERTENS, L., VANDENBOSCH, L., AND CASTEELS, R.,. (1994) Determination of relative amounts of inositol trisphosphate receptor mRNA isoforms by ratio polymerase chain reaction. *Journal of Biological Chemistry* **269**: 21691-21698

DODT-H., ZIEGLGANSBERGER-W. (1990) Visualizing unstained neurons in living brain slices by Infrared DIC videomicroscopy. *Brain Research* **537**: 333-336

DRINGEN-R., GEBHARDT-R., HAMPRECHT-B. (1993a) Glycogen in astrocytes: possible function as lactate supply for neighbouring cells. *Brain Research* **623**: 208-214

DUFFY-S., MACVICAR-B.A. (1995) Adrenergic calcium signalling in astrocyte networks within the hippocampal slice. *Journal of Neuroscience* **15**: 5535-5550

DUNLAP-K., TAKEDA-K., AND BREHM-P. (1987) Activation of a calcium dependent photoprotein by chemical signalling through gap junctions. *Nature* **325**: 60-62

EDWARDS-F.A., GIBB-A.J. (1994) Patch clamp recording from cells in sliced tissues. *Microelectrodes techniques Plymouth Workshop Handbook* : 255-274

EDWARDS F.A., KONNERTH, A., SAKMANN B., AND TAKAHASHI, T. (1989) A thin slice preparation for patch clamp recordings from synaptically connected neurones of the mammalian central nervous system. *Pflugers Archives European Journal of Physiology* **414**: 600-612

EDWARDS-F.A., KONNERTH-A. (1992) Patch clamping cells in sliced tissue preparations. *Methods in enzymology* **207**: 208-222

EISENBARTH, G. S., WALSH, F.S., AND NIRENBERG, M.,. (1979) Monoclonal antibody to a plasma membrane antigen of neurons. *Proceedings of the National Academy of Science USA* **76**: 4913-4917

ELFGANG-C., ECKERT-R., LICHTENBERG-FRATE-H., BUTTERWECK-A., TRAUB-O., KLEIN-R.A., HULSER-D.F., WILECKE-K. (1995) Specific permeability and selective formation of gap junction channels in connexin-transfected HeLa cells. *Journal of Cell Biology* **129**: 805-817

ERECINSKA-M., SILVER-I.A. (1990) Metabolism and role of glutamate in the mammalian brain. *Programmes of Neurobiology* **35**: 245-296

FIELD-A.C., JENKINSON-D.H. (1987) The effect of noradrenaline on the ion permeability of isolated mammalian hepatocytes, studied by intracellular recording. *Journal of Physiology* **392**: 493-512

FINCH-E.A., TURNER-T.J., AND GOLDIN-S.M. (1991) Calcium as a coagonist of inositol 1,4,5-trsiphosphate induced calcium release. *Science* **252**: 443-446

FINKBEINER-S. (1992) Calcium waves in astrocytes-filling in the gaps. *Neuron* **8**: 1101-1108

FINKBEINER-SM. (1993) : Glial calcium. *: Glia* **9**: 83-104

FONNUM-F. (1993) Regulation of the synthesis of the transmitter glutamate pool. *Programmes of Biophysics Molecular Biology* **60**: 47-57

FRANK-G., GRISAR-T., MOONEN-G. (1983) Glial and neuronal Na^+, K^+ pump. *Advances in Neurobiology.* **4**: 133-159

FULTON-B.P., BURNE-J.F., RAFF-M.C. (1991) Glial cells in the rat optic nerve: The search for the type 2 astrocyte. *Annuals of the New York Academy of Sciences* **633**: 27-34

FURUICHI-T., FURUTAMA-D., HAKAMATA-Y., NAKAI-J., TAKESHIMA-H., MIKOSHIBA-K. (1989) Primary structure and functional expression of the inositol 1.4.5 bisphosphate-binding protein P400. *Nature* **342**: 32-38

GAJDUSEK-D.C. (1990) Subacute spongiform encephalopathies: transmissible cerebral amyloidoses caused by unconventional agents. *In Virology (eds Fields B. N., Knipe DM., et al) Raven Press New York* : 2289-2324

GALLO-V., GIOVANINNI-C., SUERGIU-R., AND LEVI- G. (1989) Expression of excitatory amino acid receptors by cerebellar cell of the type 2 astrocyte cell lineage. *Journal of Neurochemistry* **52**: 1-9

GIANNINI-G., CLEMENTI-E., CECI-R., MARZIALI-G., SORRENTINO-V. (1992) Expression of a Ryanodine receptor-Ca^{2+} channel that is regulated by TGF-B. *Science* **257**: 91-94

GRAY-P.T.A. (1988) Oscillations of free cytosolic calcium evoked by cholinergic and catecholaminergic agonists in rat parotid acinar cells. *Journal of Physiology* **406**: 35-53

GRYNKIEWICZ-G., P.-M., AND TSIEN-R.Y. (1985) A new generation of calcium indicators with greatly improved fluorescent properties. *Journal of Biological Chemistry* **260**: 3440-3450

HAMILL-O., P., MARTY, A., NEHER, E., SAKMANN, B., & SIGWORTH, F.J.,. (1981) Improved patch-clamp techniques for high resolution current recording from cells and cell-free membrane patches. *Pflugers Archives* **391**: 85-100

HEBB-D.O. (1949) The organisation of behaviour a neuropsychological theory.

HODGKIN-A.L., KEYNES-R.D. (1957) Movements of labelled calcium in squid giant axons. *Journal of Physiology* **138**: 253-281

HOLLINGWORTH-S., HARKINS-A.B., KUREBAYASHI-N., KONISHI-M., BAYLOR-S.M. (1992) : Excitation-contraction coupling in intact frog skeletal muscle fibers injected with mmolar concentrations of fura-2. *: Biophysical Journal* **63**: 224-234

HOLZWARTH-J.A., GIBBONS-S.J., BRORSON-J.R., PHILIPSON-L.H., MILLER-R.J. (1994) Glutamate receptor agonists stimulate diverse calcium responses in different types of cultured rat cortical glial cells. *Journal of Neuroscience* **14**: 1879-1891

IINO-M. (1990) : Biphasic Ca^{2+} dependence of inositol 1,4,5-trisphosphate-induced Ca^{2+} release in smooth muscle cells of the guinea pig taenia caeci. *: Journal of General Physiology* **95**: 1103-1122

INAGAKI-N;, WADA-H. (1994) : Histamine and prostanoid receptors on glial cells. *: Glia* **11**: 102-109

ITO-M. (1984) The cerebellum and Neural Control. *Raven Press*

ITO-M., Sakurai-M., Tongroach-P. (1982) Climbing fibre induced depression of both mossy fibre responsiveness and glutamate sensitivity of cerebellar Purkinje cells. *Journal of Physiology* **324**: 113-134

JACOB-R. (1990) Imaging cytoplasmic free calcium in histamine stimulated endothelial cells and in fMet-Leu-Phe stimulated neutrophils. *Cell Calcium* **11**: 241-249

JENSEN-A.M., CHIU-S.Y. (1990) : Fluorescence measurement of changes in intracellular calcium induced by excitatory amino acids in cultured cortical astrocytes. *: Journal of Neuroscience* **10**: 1165-75

JONES-B.W., FETTER-F.D., TEAR-G., GOODMAN-C.S. (1995) Glial cells missing: a genetic switch that controls glial versus neuronal fate. *Cell* **82**: 1013-1023

JUURLINK-B.H.J., HERTZ-L. (1986) Plasticity of astrocytes in primary cultures: an experimental tool and a reason for methodological caution. *Developmental Neuroscience* 7: 263-277

KANAI-Y., HEDIGER-M.A. (1992) Primary structure and functional characterisation of a high affinity glutamate transporter. *Nature* **360**: 467-471

KASTRITSIS-C.H., SALM-A.K., MCCARTHY-K. (1992) Stimulation of the P_{2Y} purinergic receptor on type1 astroglia results in inositol trisphosphate formation and calcium mobilisation. *Journal of Neurochemistry* **58**: 1277-1284

KHODAKHAH-K. AND OGDEN-D.,(1995) Fast activation and inactivation of inositol trisphosphate-evoked Ca^{2+} release in rat cerebellar Purkinje neurones. *Journal of Physiology* **487** 343-358.

KHODAKHAH-K., OGDEN-D. (1993) : Functional heterogeneity of calcium release by inositol trisphosphate in single Purkinje neurones, cultured cerebellar astrocytes, and peripheral tissues. *: Proceedings of National Academy of Science U S A* **90**: 4976-4980.

KIRISCHUK-S., TUSCHICK-S., VERKHRATSKY-A., KETTENMANN-H. (1996) : Calcium signalling in mouse Bergmann glial cells mediated by alpha1-adrenoreceptors and H1 histamine receptors. *: European Journal of Neuroscience* **8**: 1198-1208

KONISHI-M., HOLLINGWORTH-S., HARKINS-A.B., BAYLOR-S.M. (1991) : Myoplasmic calcium transients in intact frog skeletal muscle fibers monitored with the fluorescent indicator furaptra. *: Journal of General Physiology* **97**: 271-301

KRIEGLER-S., CHIU-S.Y. (1993) Calcium signalling of glial cells along mammalian axons. *Journal of Neuroscience* **13**: 4229-4245

KRISHTAL, O. A., PIDOPLICHKO V.I. (1980) A receptor for protons in the nerve cell membrane. *Neurosciences* **5**: 2325-2327

LAAKE-J.H., SLYNGSTAD-T.A., HAUG-F.M.S., OTTERSEN-O.P. (1995) Glutamine from glial cells is essential for the maintenance of the nerve terminal pool of glutamate: immunogold evidence from hippocampal slice cultures. *Journal of Neurochemistry* **65**: 871-881

LANGLEY-D., PEARCE-B. (1994) Ryanodine-induced intracellular calcium mobilisation in cultured astrocytes. *Glia* **12**: 128-134

LONDON, R. E., LEVY, L.A., MURPHY, E.,. (1996) 2-[2(5-carboxyethyl-oxazole)]-5-[2-(2-bis(carboxymethylmethyl)amino-5,6-difluorophenoxy)]ethoxy-6-bis(carboxymethyl-methyl)aminobenzofuran. *U.S Patent* **5,516,911**

MACVICAR-B.A., TSE-F.W. (1988) Norepinephrine and cyclic adenosine 3':5'-cyclic monophosphate enhance a nifedipine-sensitive calcium current in cultured rat astrocytes. *Glia* **1**: 359-365

MAGISTRETTI-P.J., HOF-P.R., MARTIN-J.L. (1986) Adenosine stimulates glycogenesis in mouse cerebral cortex: A possible coupling mechanisim between neuronal activity and energy metabolism. *Journal of Neuroscience* **6**: 2558-2562

MANGOURA-D., SOGOS-V., PELLETIERE-C., DAWSON-G. (1995) : Differential regulation of phospholipases C and D by phorbol esters and the physiological activators carbachol and glutamate in astrocytes from chicken embryo cerebrum and cerebellum. *: Brain Research Developmental Brain Research* **87**: 12-21

MARANTO-A.T. (1994) Primary structure, ligand binding, and localisation of the human type 3 inositol 1,4,5-trisphosphate receptor expressed in intestinal epithelium. *Journal of Biological Chemistry* **269**: 1222-1230

MASSA-P.T., AND MUGNAINI-E. (1985) Cell-cell junctional interactions and characteristic plasma membrane features of cultured rat glial cells. *Neuroscience* **14**: 695-709

MCCRAY-J.A., TRENTHAM-D.R. (1989) Properties and uses of photoreactive caged compounds. *Annual Review of Biophysics & Biochemistry* **18**: 239-270

MCNAUGHTON-L.A., LAGNADO-L., SOCOLOVSKY-M., HUNT-S.P., MCNAUGHTON-P.A. (1990a) Glutamate elevates free $[Ca^{2+}]i$ in type 1 astrocytes cultured from rat cerebral cortex. *Journal of Physiology* **424**: 48P

MCNAUGHTON-L.A., LAGNADO-L., SOCOLOVSKY-M., HUNT-S.P., MCNAUGHTON-P.A. (1990b) Use of the confocal microscope to measure changes in free $[Ca^{2+}]i$ in type 1 astrocytes cultured from rat cerebral cortex. *Journal of Physiology* **424**: 5P

MEADER-WOODRUFF-J.H., LEWIS-B.L., AND DEVRIES-G.H. (1984) Cyclic AMP and calcium as potential mediators of stimulation of cultured Schwann cell proliferation by axolemma-enriched and myelin-enriched membrane fractions. *Biochemistry Biophysics Research Communcications* **122**: 373-380

MERRILL-J.E., BENVENISTE-E.N. (1996) Cytokines in inflammatory brain lesions: helpful and harmful. *Trends in Neuroscience* **19**: 331-338

MEYER-FRANKE-A., KAPLAN-M.R., PFRIEGER-F.W., BARRES-B.A. (1995) Characterisation of the signalling interactions that promote the survival and growth of developing retinal ganglion cells in culture. *Neuron* **15**: 805-819

MIGNERY, G. A., SUDOF, T.C., TAKEI, K., DE CAMILLI, P.,. (1989) Putative receptor for inositol 1,4,5-trisphosphate similar to ryanodine receptor. *Nature* **342**: 192-195

MIGNERY-G.A., SUDHOF-T.C. (1990) The ligand binding site and transduction mechanism in the inositol 1,4,5-trisphosphate receptor. *EMBO* **9**: 3893-3898

MILLER-R.H., FFRENCH-CONSTANT-C., AND RAFF-M.C. (1989) The macroglial cells in the rat optic. *Annual Review of Neuroscience* **12**: 517-534

MINTA-A., GYZKIEWICZ-G., TSIEN-R.Y. (1989a) Fluorescent probes of cell signalling. *Annual Review of Neuroscience* **12**: 227-253

MINTA-A., KAO-J.P.Y., TSIEN-R.Y. (1989) Fluorescent indicators for cytosolic calcium based on rhodamine and fluorescein chromophores. *Journal of biological chemistry* **264**: 8171-8179

MITCHELL-P. (1961) Coupling of phosphorylation to electron and hydrogen transfer by a chemiosmotic type of mechanism. *Nature* **191**: 144-148

MONKAWA-T., MIYAWAKI-A., SUGIYAMA-T., YONESHIMA-H., YAMAMOTO-HINO-M., FURUICHI-T., SARUTA-T., HASEGAWA-M., MIKOSHIBA-K. (1995) Heterotetrameric complex formation of Inositol 1,4,5-trisphosphate receptor subunits. *The Journal of Biological Chemistry* **270**: 14700-14704

MOODY-W.J.JR., FUTAMACHI-K.J., PRINCE-D.A. (1974) Extracellular potassium activity during epileptogenesis. *Experimental Neurology* **42**: 248-263

MUGNAINI-E. (1986) Cell junctions of astrocytes, ependymal, and related cells in the mammalian central nervous system, with emphasis on the hypothesis of a generalised functional syncytium of supporting cells,. *Astrocytes. Academic press New York* **1**: 329-371

MULLER-T., MOLLER-T., BERGER-T., SCHNITZER-J., KETTENMANN-H. (1992) Calcium entry through Kainate receptors and resulting potassium-channel blockade in Bergmann glial cells. *Science* **256**: 1563-1566

MULLER-T., MOLLER-T., NEUHAUS-J., KETTENMANN-H.,(1996) Electrical coupling among Bergmann glial cells and its modulation by glutamate receptor activation. *Glia* **17**: 274-284

MURPHY-S., PEARCE-B. (1987) Functional receptors for neurotransmitters on astroglial cells. *Neuroscience* **22**: 381-394

NADAL-A., FUENTES-E., PASTOR-J., MCNAUGHTON-P.A. (1995) : Plasma albumin is a potent trigger of calcium signals and DNA synthesis in astrocytes. *: Proceedings of the National Academy of Science U S A* **92**: 1426-1430

NADAL-A., FUENTES-E., PASTOR-J., MCNAUGHTON-P.A. (1997) Plasma albumin induces calcium waves in rat cortical astrocytes. *Glia* **19**: 343-351

NAKADE-S., RHEE-S.K., HAMANAKA-H., MIKOSHIBA-K. (1994) : Cyclic AMP-dependent phosphorylation of an immunoaffinity-purified homotetrameric inositol 1,4,5-trisphosphate receptor (type 1) increases Ca^{2+}flux in reconstituted lipid vesicles. *: Journal of Biological Chemistry* **269**: 6735-6742

NAKAGAWA-T., SHIOTA-C., OKANO-H., MIKOSHIBA-K. (1991) : Differential localization of alternative spliced transcripts encoding inositol 1,4,5-trisphosphate receptors in mouse cerebellum and hippocampus: *in situ* hybridization study. *: Journal of Neurochemistry* **57**: 1807-1810

NEDERGAARD-M. (1994) Direct signalling from astrocytes to neurons in cultures of mammalian brain cells. *Science* **263**: 1768-1771

NISHIZUKA-Y. (1988) The molecular heterogenity of protein kinase C and its implications for cellular regulation. *Nature* **334**: 661-665

NORENBERG-M.D., MARTINEZ-HERNANDEZ-A. (1979) Fine structural localisation of glutamine synthetase in astrocytes of rat brain. *Brain Research* **161**: 303-310

OGDEN-D., AND CAPIOD-T. (1997) Regulation of calcium release by $InsP_3$ in single guinea pig hepatocytes and rat Purkinje neurones. *Journal of General Physiology* **109**: 741-756

OGDEN-D., KHODAKHAH- K., CARTER- T., THOMAS- M., CAPIOD-T. (1995) : Analogue computation of transient changes of intracellular free Ca^{2+}concentration with the low affinity indicator furaptra during whole-cell patch-clamp recording. *: Pflugers Archives* **429**: 587-591

OGDEN-D., KHODAKHAH-K. (1996) Intracellular Calcium release by $InsP_3$ in cerebellar Purkinje neurones. *Acta Physiological Scandinavian* **157**: 381-394

OGDEN-D.C., CAPIOD-T.C., WALKER-J.W., AND TRENTHAM-D.R. (1990) Kinetics of the conductance evoked by noradrenaline, inositol trisphosphate or calcium in guinea pig isolated hepatocytes. *Journal Of Physiology.* **422**: 585-602

OGDEN-D.C., KHODAKHAH-K., CARTER-T.D., GRAY-P.T.A., CAPIOD-T. (1993) Mechanisms of intracellular calcium release during hormone and neurotransmitter action investigated with flash photolysis. *Journal of Experimental Biology* 184 **105-127**

O'LAGUE-P.H., FURSCHPAN-E.J., POTTER-D.D. (1978) Studies on rat sympathetic neurons developing in cell culture. II. Synaptic mechanisms. *Development Biology* **67**: 404-423

OLNEY-J.W., SHARPE-L.G. (1969) Brain lesions in an infant rhesus monkey treated with monosodium glutamate. *Science* **166**: 386-388

ORKAND-R.K., NICHOLLS-J.G., KUFFLER-S.W. (1966) Effect of nerve impulses on the membrane potential of glial cells in the central nervous system of amphibia. *Journal of Neuro Physiology* **29**: 788-806

PALAY-S. L., AND CHAN-PALAY-V. (1974) Cerebellar Cortex. *Springer-Verlag New York*

PARPURA-V., BASARSKY-T.A., LIU-F., KSENIJA-J., JEFTINIJA-S., HAYDON-P.G. (1994) Glutamate-mediated astrocyte-neuron signalling. *Nature* **369**: 744-747

PASTI-L., POZZAN-T., CARMIGNOTO-G. (1995) : Long-lasting changes of calcium oscillations in astrocytes. A new form of glutamate-mediated plasticity. *: Journal of Biological Chemistry* **270**: 15203-15210

PASTI-L., VOLTERRA-A., POZZAN-T., CARMIGNOTO-G. (1997) Intracellular calcium oscillations in astrocytes: A highly plastic, bidirectional form of communication between neurones and astrocytes *in situ*. *The Journal of Neuroscience* **17**: 7817-7830

PAULSEN-R.E., FONNUM-F. (1989) Role of glial cells for the basal and Ca^{2+} dependent K^{+} evoked release of transmitter amino acids investigated by microdialysis. *Journal of Neurochemistry* **52**: 1823-1829

PAYNE-J., MAHER-F., SIMPSON-I.A., MATTICE-L.A., DAVIES-P. (1997) Glucose transporter GLUT5 expression in microglial cells. *Glia* **21**: 327-331

PEARCE-B., ALBRECHT-J., MORROW-L., AND MURPHY-S. (1986) Astrocyte glutamate receptor activation promotes inositol phospholipid turnover and calcium flux. *Neuroscience Letters* **72**: 335-340

PELLERIN-L., MAGISTRETTI-P.J. (1994) Glutamate uptake into astrocytes stimulates aerobic glycolysis: a mechanism coupling neuronal activity to glucose utilization. *Proceedings National Academy of Science USA* **91**: 10625-10629

PESSIN-J.E., BELL-G.I. (1992) Mammalian facilitative glucose transporter family: structure and molecular regulation. *Annual Review Physiology* **54**: 911-930

PINES-G., DANBOLT-N.C., BJORAS-M., ZHANG-Y., BENDAHAN-A., EIDE-L., KOEPSELL-H., STORM-MATHISEN-J., SEEBERG-E., KANNER-B.I. (1992) Cloning and expression of a rat brain L-glutamate transporter. *Nature* **360**: 464-467

POITRY-YAMATE-C., L., POITRY-S., TSACOPOULOS-M. (1995) Lactate released by Muller cells is metabolised by photoreceptors from mammalian retina. *Journal of Neuroscience* **15**: 5179-5191

PORTER-J.T., MCCARTHY-K.D. (1996) Hippocampal astrocytes *in situ* respond to glutamate released from synaptic terminals. *The Journal of Neuroscience* **16**: 5073-5081

RAFF, M. C., ABNEY, E. R., COHEN, J., LINDSAY, R., AND NOBLE, M. (1983a) :Two types of astrocyte in cultures of developing white matter: Differences in morphology, surface gangliosides and growth characteristics. *Journal of Neuroscience* **3**: 1289-1300

RAFF, M. C., FIELDS, K. L., HAKOMORI, S., MIRSKY, R., PRUSS, R. M., AND WINTER, J. (1979) Cell type markers for distinguishing and studying neurons and the major classes of glial cells in culture. *Brain Research* **170**: 283-308

RAFF, M. C., MILLER, R. H., AND NOBLE, M. (1983b) A glial progenitor cell that develops *in vitro* into an astrocyte or an oligodendrocyte depending on the culture medium. *Nature* **274**: 813-816

RAFF, M. C., MIRSKY, R., FIELDS, K. L., LISAK, R. P., DORFMAN, S. H., SILBERBERG, D. H., GREGSON, N. A., LIEBOWITZ, S., AND KENNEDY, M. C. (1978) Galactocerebroside is a specific cell surface antigenic marker for oligodendrocytes in culture. *Nature* **274**: 813-816

RAJU, B., MURPHY, E., LEVY, L.A., HALL, R.D., LONDON R.E.,. (1989) A fluorescent indicator for measuring cytosolic free magnesium. *American journal of physiology* **256**: C540-C548

RAPP-G., GUTH-K. (1988) A high intensity xenon flashlamp suitable for cell physiology. *Pflugers Archives* **411**: 200-203

REETZ-G., REISER-G. (1996) [Ca^{2+}]i oscillations induced by bradykinin in rat glioma cells associated with Ca^{2+} store-dependent Ca^{2+} influx are controlled by cell volume and by membrane potential. *Cell Calcium* **19**: 143-156

REGEHR-W.G., AND TANK-D.W. (1991) : Selective fura-2 loading of presynaptic terminals and nerve cell processes by local perfusion in mammalian brain slice. *:Journal of Neuroscience methods* **37**: 111-119

RIZZUTO-R., BRINI-M., MURGIA-M., POZZAN-T. (1993) Microdomains with high Ca^{2+} close IP_3-sensitive channels that are sensed by neighbouring mitochondria. *Science. Washington DC* **262**: 744-747

ROBB-GASPERS-LD:, THOMAS-A.P. (1995) Coordination of Ca^{2+} signalling by intercellular propagation of Ca^{2+} waves in the intact liver. *Journal of Biological Chemistry* **270**: 8102-8107

ROBERTS-W.M. (1994) Localisation of calcium signals by a mobile calcium buffer in frog saccular hair cells. *Journal of Neuroscience* **14**: 3246-3262

ROTHSTEIN-J.D., DYKES-HOBERG-M., PARDO-C.A., BRISTOL-L.A., JIN-L., KUNCL-R., KANAI-Y., HEDIGER-M.A., WANG-Y., SCHIELKE-J.P., WELTY-D.F. (1996) Knockout of glutamate transporters reveals a major role of astroglial transport in excitoxicity and clearance of glutamate. *Neuron* **16**: 675-686

ROTHSTEIN-J.D., MARTIN-L., LEVEY-A.I., DYKES-HOBERG M., JIN-L., WU-D., NASH-N., KUNCL-R.W. (1994) Localisation of neuronal and glial glutamate transporters. *Neuron* **13**: 713-725

ROTHSTEIN-J.D., TABAKOFF-B. (1984) Alteration of striatal glutamate release after glutamate synthetase inhibition. *Journal of Neurochemistry* **43**: 1438-1446

SAFRANY-S.T., WOJCIKIEWICZ-R.J.H., STRUPISH-J., MCBAIN-J., COOKE-A.M., POTTER-B.V.L., AND NAHORSKI-S.R. (1991) Synthetic phosphorothioate-containing analogues of inositol 1,4,5-trisphosphate mobilise intracellular calcium stores and interact differentially with inositol 1,4,5-trisphosphate 5-phosphatase and 3-kinase. *Molecular Pharmacology* **39**: 754-761

SANDERSON-M.J., CHARLES-A.C., AND DIRKSEN-E.R. (1990) Mechanical stimulation and intercellular communication increases intracellular Ca^{2+} in epithelial cells. *Cell Regulation* **1**: 585-596

SAUNDERS-R.D., DEVRIES-G.H. (1988) 1-oleoyl--2-acetylglycerol and A23187 potentiate axolemma- and myelin-induced Schwann cell proliferation. *Journal of Neurochemistry* **51**: 1760-1764

SIEBER-F.E., TRAYSTMAN-R.J. (1992) Glucose and the brain. *Critical care medicine* **20**: 104-114.

SKOFF-R.P. (1990) Gliogenesis in rat optic nerve: astrocytes are generated in a single wave before oligodendrocytes. *Developmental Biology* **139**: 149-168

SOMMER, I., AND SCHNANCHNER, M. (1981) Monoclonal antibodies (01and 04) to oligodendrocytes cell surfaces an immunocytological study in the central nervous system. *Development Biology* **83**: 311-327

SONTHEIMER-H. (1994) Voltage Dependent Ion Channels in Glial Cells. *Glia* **11**: 156-172

Sorrentino-V., Volpe-P. (1993) Ryanodine receptors: How many where and why? *Trends in Neuroscience* **14**: 98-103

STANIMIROVIC-D.B., BALL-R., MEALING-G., MORLEY-P., DURKIN-J.P. (1997) The role of intracellular calcium and protein kinase C in endothelin-stimulated proliferation of rat type 1 astrocytes. *Glia* **15**: 119-130

STERN-M.D. (1992) Buffering of calcium in the vicinity of a channel pore. *Cell Calcium* **13**: 183-192

STORCK-T., SCHULTE-S., HOFMANN-K., STOFFEL-W. (1992) Structure, expression and functional analysis of a Na^+ dependent glutamate/aspartate transporter from rat brain. *Proceedings National Academy Science USA* **89**: 10955-10959

SUDHOF-T.C., NEWTON-C.L., ARCHER-B.T. III, USHKAROV-Y.A., MIGNERY-G.A. (1991) Structure of a novel $InsP_3$ receptor. *EMBO Journal* **10**: 3199-3206

SUGIYAMA-T., YAMAMOTO--HINO-M., MIYAWAKI-A., FURUICHI-T., MIKOSHIBA-K., HASEGAWA-M. (1994) Subtypes of inositol 1,4,5-trisphosphate receptor in human hematopoietic cell lines: dynamic aspects of their cell-type specific expression. *FEBS Letters* **349**: 191-196

SUPATTAPONE-S., SIMPSON-A.W.M., ASHLEY-C.C. (1989) Free calcium rise and mitogenesis in glial-cells caused by endothelin. *Biochemical and Biophysical research communications.* **165**: 1115-1122

SUPATTAPONE-S., WORLEY-P.F., BARABAN-J.M., SYNDER-S.H. (1988) Solublisation, purification and characterisation of an inositol trisphosphate receptor. *Journal of Biological Chemisrty* **263**: 1530-1538

SWANSON-R.A., YU-A.C.H., CHAN-P.H., SHARP-F.R. (1990) Glutamate increases glycogen content and reduces glucose utilisation in primary astrocyte culture. *Journal of Neurochemistry* **54**: 490-496

TOMIMOTO-H., AKIGUCHI-I., SUENAGA-T., NISHIMURA-M., WAKITA-H., NAKAMURA-S., KIMURA-J. (1996) Alterations of the BBB and glial cells in white matter lesions in cerebrovascular and Alzehimer's disease patients. *Stroke* **27**: 2069-2074

TSACOPOULOS-M., MAGISTRETTI-P.J. (1996) Metabolic coupling between glia and neurons. *Journal of Neuroscience* **16**: 877-885

UBL-J.J., REISER-G. (1997) Characteristics of thrombin induced calcium signals in rat astrocytes. *Glia* **21**: 361-369

VAN DEN BERG-C.J., GARFINKEL-D. (1971) A stimulation study of brain compartments. Metabolism of glutamate and related substances in mouse brain. *Biochemistry Journal* **123**: 211-218

VANNUCCI-S.J., MAHER-F., SIMPSON-I.A. (1997) Glucose Transporter Proteins in Brain: Delivery of Glucose to Neurons and Glia. *Glia* **21**: 2-21

VENANCE-L., PIOMELI-D., GLOWINSKI-J., GIAUME-C. (1991) Inhibition by anandamide of gap junctions and intercellular calcium signalling in striatal astrocytes. *Nature* **376**: 590-595

VERKHRATSKY-A., KETTENMANN-H. (1996) : Calcium signalling in glial cells. *: Trends in Neuroscience* **19**: 346-352

VERKHRATSKY-A., ORKAND-R., KETTENMANN-H. (1998) Glial Calcium: Homeostasis and signalling function. *Physiological Reviews* **78**: 99-141

VERVERKEN-D., VAN VELDHOVEN-P., PROOST-C., CARTON-H., DE WULF-H. (1982) On the role of calcium ions in the regulation of glycogenolysis in mouse brain cortical slices. *Journal of Neurochemistry* **38**: 1286-1295

WALKER, J. W., FEENY, J., AND TRENTHAM, D.R.,. (1989) Photolabile precursors of inositol phosphates . Preparation and properties of 1-(2-nitrophenyl)ethyl esters of myo-inositol 1,4,5-trissphosphate. *Biochemistry, N.Y* **28**: 3272-3280

WALKER-J.W, MCCRAY-J, TRENTHAM-D,R (1989) The synthesis of caged phosphates. *Methods in Enzymology* **172**: 288-301

WHITTINGHAM, T. S., LUST, W. D., CHRISTAKIS, D. A., AND PASSONNEAU, J. V. (1984) Metabolic activity of hippocampal slice preparations during prolonged incubation. *Journal of Neurochemistry* **34**: 689-696

WIESINGER-H., HAMPRECHT-B., DRINGEN-R. (1997) Metabolic pathways for glucose in astrocytes. *Glia* **21**: 22-34

WINTER-WOLPAW E., MARTIN-D.L. (1984) Cl^- transport in glioma cell line: evidence for two transport mechanism. *Brain Research* **297**: 317-327

WOODS-N.M., CUTHBERTSON-K.S.R., COBBOLD-P.H. (1986) Repetitive transient rises in cytoplasmic free calcium in hormone-stimulated hepatocytes. *Nature* **319**: 600-602

WOOTTON-J.F.; CORRIE-J.E., CAPIOD-T., FEENEY-J., TRENTHAM-D.R., OGDEN-D.C, (1995) : Kinetics of cytosolic Ca^{2+} concentration after photolytic release of 1-D-myo-inositol 1,4-bisphosphate 5-phosphorothioate from a caged derivative in guinea pig hepatocytes. *: Biophysical Journal* **68**: 2601-2607

YAMAMOTO-HINO, M., MIYAWAKI, A., KAWANO, H., SUGIYAMA, T., FURUICHI, T., HASEGAWA, M., MIKOSHIBA, K.,. (1995) : Immunohistochemical study of inositol 1,4,5-trisphosphate receptor type 3 in rat central nervous system. *: Neuroreport* **6**: 273-276

YANG-Z.W., KONG-C.F. (1988) Characterisation and location of divalent cation binding sites in bovine glial fibrillary acidic protein. *Biochemistry* **27**: 7045-7050

ZHANG-W., SAKAI-N., YAMADA-H., FU-T., NOZAWA-Y.,(1990) Endothelin-1 induces intracellular calcium rise and inositol 1,4,5-trisphosphate formation in cultured rat and human glioma cells. *Neuroscience Letters* **112**; 199-204

ZHOU-Z., NEHER-E. (1993) Mobile and immobile calcium buffers in bovine adrenal chromaffin cells. *Journal of Physiology (London)* **469**: 245-273

ZLOTNIK-I. (1968) The reaction of astrocytes to acute virus infections of the central nervous system. *British Journal of Experimental Pathology* **49**: 555-564

CARDY-T.J.A., TRAYNOR-D., TAYLOR-C.W., (1997) Differential regulation of types 1 and 3 inositol trisphosphate receptors by cytosolic calcium. *Biochemical Journal* **328**: 785-793.

DELISLE-S., BLONDEL-O., LONGO-F., (1996) Expression of inositol 1,4,5-trisphosphate receptors changes the calcium signal of Xenopus oocytes. *American Journal of Physiology*. **270**:C1255-C1261.

FIERRO-L., AND LLANO-I., (1996) High endogenous calcium buffering in Purkinje cells from rat cerebellar slices. *Journal of Physiology (London)*. **496**: 617-625.

FINCH-E.A., TURNER-T.J., AND GOLDIN-S.M., (1991) calcium as a coagonist of inositol 1,4,5-trisphosphate induced calcium release. *Science (Washington D.C.)* **252**:443-446.

ILYIN-V., & PARKER-I., (1994) Role of cytosolic Ca^{2+} in inhibition of $InsP_3$ evoked Ca^{2+} release in Xenopus oocytes. *Journal of Physiology* **477**, 503-509.

IINO-M., (1990) Biphasic calcium dependence of inositol 1,4,5-trisphosphate-induced calcium release in smooth muscle cells of the guinea pig Taenia Caeci. *Journal of General Physiology* **52**: 1103-1122.

MAEDA-N., KAWASAKI-T., NAKADE-S., YOKOTA-N., TAGUCHI-T., KASAI-M., MIKOSHIBA-K., (1991) Structural and functional characterisation of inositol 1,4,5-trisphosphate receptor channel from mouse cerebellum. *Journal of Biological Chemistry* **266**: 1109-1116.

MEYER-T., HOLOWKA-D AND STRYER-L. (1988) Highly cooperative opening of calcium channels by inositol 1,4,5-trisphosphate. *Science (Washington D.C.)* **240**: 653-656.

MIGNERY-G.A., SUDHOF-T.C., (1990) The ligand binding site and transduction mechanism in the inositol 1,4,5-trisphosphate receptor. *EMBO* 9: 3893-3898.

MIYAWAKI-A., FURUICHI-T., MAEDA-N., AND MIKOSHIBA-K., (1990) Expressed cerebellar type 1 inositol 1,4,5 trisphosphate receptor, P400 has calcium release activity in a fibroblast L cell line. *Neuron* **5** (1) 11-18.

NEHER-E., (1995) The use of Fura-2 for estimating calcium buffers and calcium fluxes. *Neuropharmacology* **34**: 1423-1442.

PUTNEY-J.JR (1990) The integration of receptor regulated intracellular calcium release and calcium entry across the plasma membrane. *Current Opinions in Cellular Regulation* **31**:111-127.

SUGIYAMA-T., FURUYA-A., MONKAWA-T., YANAMOTO-HINO-M., SATOH-S., OHMORI-K., MIYAWAKI-A., HANAI-N., MIKOSHIBA-K., HASEGAWA-M., (1994) Monoclonal antibodies distinctively recognising the subtypes of inositol 1,4,5-trisphosphate receptor: Application to the studies on inflammatory cells. *FEBS letters* **354:** 149-154.

YONESHIMA-H., MIYAWAKI-A., MICHIKAWA-T., FURUICHI-T.,MIKOSHIBA-K., (1997) calcium differentially regulates the ligand affinity states of type 1 and type 3 inositol 1,4,5-trisphosphate receptors. *Biochemical Journal* **332**:591-596.